Origin and Control of Anisotropy in Three Dimensional Printing of Structural Ceramics

by

Satbir Singh Khanuja

B.S. Metallurgical Engineering, Indian Institute of Technology, Bombay, 1989

M.S. Materials Science and Engineering, University of Washington, Seattle, 1991

Submitted to the Department of
Materials Science and Engineering in
Partial Fulfillment of the Requirements for the
Degree of

DOCTOR OF PHILOSOPHY
in Ceramics

at the

Massachusetts Institute of Technology

February, 1996

Signature of Author_____
Department of Materials Science and Engineering
January 12, 1996

Certified by_____
Professor Michael J. Cima
Norton Professor of Ceramics
Thesis Supervisor

Accepted by_____
Professor Michael F. Rubner
TDK Professor of Materials Science and Engineering
Chairman, Departmental Committee on Graduate Students

Origin and Control of Anisotropy in Three Dimensional Printing of Structural Ceramics

Satbir Singh Khanuja

Submitted to the Department of Materials Science and Engineering
on January 12, 1996
in partial fulfillment of the requirements for the degree of
Doctor of Philosophy in Ceramics

ABSTRACT

The overall objective of this research was to develop a process to fabricate fully dense and distortion free structural ceramic parts via three dimensional printing (3DP). The development of this application requires the fabrication of high packing density fine ceramic components with uniform microstructure. 3DP consists of many repetitive processes, each of which can potentially produce anisotropy and non-uniformity in the component. The basic 3DP microstructural unit, consisting of a printed layer, is not only anisotropic because it is formed from sheets, but is also anisotropic because the binder is printed in lines along a certain direction and the top and bottom of the layers have different processing histories. This study focusses on the origin and control of anisotropy in three dimensional printing of structural ceramics.

Fine powder agglomerates in the dry state due to Van der Waal's force. The presence of these irregular shaped agglomerates not only reduces the flowability of fine powder but also results in non-uniform microstructure in the powder layer during the spreading stage. The uniformity of the spread powder layer was successfully improved by the use of highly flowable spray dried (SD) porous granules. The parts made out of SD granules, however, exhibited extensive warpage during the build stage. The parts made out of coarse dense particles for investment casting and tooling applications, in comparison, had never shown such warpage behavior.

The dissolution of SD granules by printed binder and interlayer liquid migration due to the fine pores of SD granules were found to be the key mechanisms introducing asymmetry in the build process and resulting in excessive warpage of SD parts. Processing strategies have been devised to minimize the anisotropy during the printing stage and has been successfully used to build distortion free SD green alumina parts. The green density of the SD parts is ~ 30 vol%. The SD parts also have interlaminar defects, thereby reducing the isotropy along the z-axis. Additional post processing, such as isopressing, is required to increase the packing density to ~ 60 vol% and to heal the interlayer defects before the SD parts can be consolidated to full density upon firing.

Two different processes were developed to fabricate high green density fine ceramic components directly out of 3DP machine. The first approach consisted of increasing the packing density by printing the colloidal slurries into a SD granule powder bed. The printed parts showed segregation of the printed slurry on the top half of spread powder layers. Such non-uniformity in microstructure was not observed in parts made out of dense particles and is unacceptable for fabricating defect free structural ceramic components. Slip casting of the slurry on the SD granules was found to be the mechanism producing the segregation.

A novel wet deposition technique has been developed to build high and uniform packing density and isotropic powder beds out of fine powder. The high cohesive strength of the powder bed, however, made the conventional method of removing powder, such as brushing, ineffective to retrieve the printed part from the sprayed powder bed. A chemical method has been developed to disperse the alumina powder bed and leave the printed part intact. The use of electrostatically stabilized alumina slurry for the powder bed allowed for easy redispersion in water during the cleaning process. The printed binder was chosen so as to chemically bond with the surface of the particles and provide a strong printed part insoluble in water. Alumina was successfully chemically bonded with a polyacrylic acid (PAA) binder. The results of this research has been used successfully to fabricate 56% dense structural ceramic parts directly by 3DP, which achieved almost full density upon firing.

Thesis Supervisor: Michael J. Cima
Title: Norton Professor of Ceramics

TABLE OF CONTENTS

		Page #
	TITLE PAGE	1
	ABSTRACT	2
	TABLE OF CONTENTS	4
	LIST OF FIGURES	9
	LIST OF TABLES	15
	ACKNOWLEDGEMENTS	17
	EXECUTIVE SUMMARY	19
Chapter 1:	INTRODUCTION	25
Chapter 2:	BACKGROUND AND LITERATURE REVIEW	29
	2.1 Introduction	29
	2.2 Traditional forming technologies: Advantages and limitations	29
	2.2.1 Pressing	29
	2.2.1.1 Dry pressing	29
	2.2.1.2 Hot pressing	31
	2.2.2 Slip casting	31
	2.2.3 Plastic forming	32
	2.3 SFF technologies	34
	2.3.1 Stereolithography	34
	2.3.2 Selective laser sintering	35
	2.3.3 Three dimensional printing	37
	2.3.4 Laminated object manufacturing	39
	2.3.5 Fused deposition modeling	39
	2.4 Factors controlling warpage of fine ceramic components	41
	2.4.1 Warpage during drying	41
	2.4.2 Strategies to reduce warpage during drying	43
	2.4.3 Warpage during firing	43
	2.4.4 Warpage in SFF process	44
	2.4.5 Sterelithography: Case study of warpage in a SFF technique	44

Page #

2.5 Properties required in green preforms for making defect free fully dense ceramic parts 46
2.5.1 Use of fine powder 46
2.5.2 High green density 48
2.5.3 Uniform green density and microstructure 50

Chapter 3: PRESS ROLLING OF FINE POWDER 53
3.1 Introduction 53
3.2 Description of the 'Press-rolling' process 53
3.3 Properties of green parts 55
3.4 Distortion during isopressing 58
3.4.1 Shear distortion 58
3.4.1.1 Characterization 58
3.4.1.2 Results and discussions 58
3.4.1.3 Strategies to avoid shear distortion 61
3.4.2 Z-axis distortion 65
3.4.2.1 Characterization 65
3.4.2.2 Results and discussions 65
3.5 Conclusions 67

Chapter 4: PRINTING ON SPRAY DRIED GRANULES 69
4.1 Introduction 69
4.2 SD granules preparation 70
4.3 SD granules properties 72
4.3.1 Interaction between ceramic and organic additive 72
4.3.2 Flowability 76
4.3.3 Bulk density and pore size distribution 78
4.4 Distortion during printing 80
4.4.1 Possible mechanisms for shrinkage in 3DP process 80
4.4.2 Distortion due to chemical dissolution 81
4.4.2.1 Experimental methods 81
4.4.2.2 Results and discussions 81
4.4.3 Distortion due to liquid redistribution 88
4.4.3.1 Experimental procedure 88

Page #

4.4.3.2 Results and discussions 88
4.4.3.2.1 Effect of saturation on distortion 90
4.4.3.2.2 Effect of SD granules-binder interaction on distortion 98
4.4.3.2.3 Effect of binder on distortion 101
4.5 Strategies to reduce shrinkage 103
4.5.1 Avoid physical ejection or physical rearrangement during printing 103
4.5.1.1 Vacuum deposition of powder 103
4.5.1.2 Use of PEG/water mist to increase the strength of the powder bed 104
4.5.2 Avoid moisture migration 106
4.5.2.1 Intermediate drying of printed layers 106
4.5.2.2 Adding gelling additives to the powder bed 106
4.5.2.3 Coating granules to seal the intragranular pores 106
4.5.3 Decrease the strength of polymer binder 107
4.6 Properties of green bodies 107
4.7 Post processing of green parts 109
4.8 Conclusion 109

Chapter 5: PRINTING SLURRIES ON SPRAY DRIED GRANULES 113
5.1 Introduction 113
5.2 Process concept
5.3 Printing slurries 115
5.3.1 Slurry preparation 115
5.3.1.1 Requirement 115
5.3.1.2 Preparation and characterization 116
5.3.2 Selection of nozzle 116
5.3.2.1 Requirements 116
5.3.2.2 Results and discussions 119
5.3.3 Filtration optimization 119
5.3.3.1 Requirements 119

Page #

5.3.3.2 Results and discussions 124
5.3.4 Droplet formation characteristics of slurries 128
5.3.4.1 Requirements 128
5.3.4.2 Results and discussions 130
5.4 Green body formation 133
5.4.1 Experimental procedure 133
5.4.2 Properties of green parts 133
5.5 Conclusions 138

Chapter 6: PRESS-COMPACTION 139
6.1 Introduction 139
6.2 Process concept 140
6.3 Design of set-up to do repeated pressing operation 143
6.4 Powder bed properties 143
6.4.1 Packing density of powder bed 145
6.4.2 Inter-layer stitching 148
6.4.3 Pore size distribution of powder bed 148
6.4.4 Fired density and shrinkage 148
6.5 Printing Stage 152
6.5.1 Selection of binder and powder packing density for printing 152
6.5.2 Shape change of printed region upon further compaction 152
6.5.2.1 Experimental procedure 152
6.5.2.2 Results and discussions 153
6.6 Part retrieval stage 153
6.6.1 Selection of cleaning solution 153
6.6.2 Part retrieval: observations and analysis 157
6.7 Conclusions 157

Chapter 7: SPRAY DEPOSITION 158
7.1 Introduction 158
7.2 Criteria for making crack-free powder beds 158
7.3 Methods for we: deposition of fine powder 160

Page #

7.4 Process concept 162
7.5 Powder bed generation 162
7.5.1 Repeated layer formation by spraying slurry 164
7.5.2 Packing density 173
7.5.3 Inter layer stitching 175
7.5.4 Permeability of the powder bed 175
7.6 Printing 178
7.6.1 Identification of critical process variables using aqueous PVA/alumina powder bed and methyl cyano-acrylate 178
7.6.1.1 Printing of binder and infiltration stage: observations and analysis 178
7.6.1.2 Binder and powder bed interaction: observations and analysis 179
7.6.1.3 Lessons learned 181
7.6.2 IPA/HBA/alumina powder bed 181
7.6.2.1 Selection of binder 181
7.6.2.1.1 Monomer approach 181
7.6.2.1.2 Solution approach 183
7.6.2.1.3 Lessons learned 185
7.7 Part retrieval stage 185
7.7.1 Initial observations and analysis 185
7.7.2 Theory of cracking during part retrieval 186
7.7.3 Strategies to improve the part retrieval 191
7.8 Properties of printed green part 192
7.9 Conclusions 192

BIBLIOGRAPHY 197

LIST OF FIGURES

Figure #		Page #
	CHAPTER 2	
2.1	Stereolithography process.	36
2.2	Selective lase sintering process.	36
2.3	Three dimensional printing process.	38
2.4	Three dimensional machine.	38
2.5	Laminated object manufacturing process.	40
2.6	Fused deposition process.	40
2.7	Schematic illustrating the mechanics of warpage behavior for a SFF process.	45
2.8	Bruch's sub-normal and normal sintering regimes in green density and temperature space.	49
	CHAPTER 3	
3.1	Schematic of the counter-rolling sequence.	54
3.2	Schematic of the press-rolling sequence.	56
3.3	SEM micrograph showing the polished cross-section of a green part made by the press-rolling process.	57
3.4	Measured shrinkage values of green parts after isopressing and firing step in various directions.	57
3.5	Schematic of shear distortion and z-axis warpage.	59
3.6	Optical micrographs showing the polished cross-section of a wipped part.	60
3.7	Shear angle distortion values of a green, wiped and fired press-rolled bars.	60
3.8	Micro and macro-mechanics of pore collapse model.	62
3.9	Schematic of bi-directional press-compaction technique involving press-rolling in opposite direction in subsequent layers.	63
3.10	SEM micrograph showing the polished cross-section of a green part made by the bi-directional press-rolling process.	64

Figure #		Page #
3.11	Optical micrograph showing the polished cross-section of a green part made by the bi-directional press-rolling process.	64
3.12	Measured z-axis warpage of a green and wiped press-rolled bar.	66
3.13	Packing density of the press-rolled powder bed as a function of built thickness.	66
3.14	Variation in z-axis warpage exhibited by the green samples, built at various locations within the same powder bed, during isopressing.	68

CHAPTER 4

4.1	TGA of SDPEG/alumina.	71
4.2	TGA of SDPAA/alumina granules.	71
4.3	TGA of SDPEG/alumina granulesafter being washed in water and dried.	73
4.4	TGA of SDPAA/alumina granules after being washed in water and dried.	73
4.5	DRIFTS spectrum of neat PAA polymer.	74
4.6	DRIFTS spectrum of PAA polymer heated to 120 C.	74
4.7	DRIFTS spectrum of SDPAA/alumina granules.	75
4.8	Pore size distribution of SD granule powder bed.	79
4.9	Pore size distribution of 30 μm dense alumina powder bed.	79
4.10	Photographs of single layers made by printing water on SDPEG, SDPVA and SDPAA alumina granules powder bed.	82
4.11	Photographs of single layers made by printing water on debound SDPEG, SDPVA and SDPAA alumina granules powder bed.	83
4.12	Photographs of single layers made by printing water on 30 μm dense spherical powder bed.	84
4.13	SEM micrographs of the top surface of single layers made by printing water on SDPEG, SDPVA and SDPAA alumina granules powder bed.	85
4.14	Warpage behavior of parts made by printing 7 vol% alumina slurries on debound SD granules.	91

Figure #		Page #
4.15	Micro and macro-mechanics of interlayer liquid migration.	94
4.16	Effect of intermediate drying on warpage of SD parts.	96
4.17	Schematic of intermediate dryir g of layers	97
4.18	Warpage: Debound and non-debound granules.	99
4.19	Schematic of warpage behavior in parts made out of debound granules.	100
4.20	Warpage: effect of concentration of the printed binders.	102
4.21	Warpage: effect of nature of the printed binder.	102
4.22	Schematic of vacuum piston.	105
4.23	Effect of plasticizer in the binder on warpage of SDPAA/alumina parts.	108
4.24	SEM of the fired cross-section of theSD part fired to 1650 C (no cipping).	108
4.25	Packing density of isopressed and fired part as a function of isopressing temperature.	110
4.26	Shrinkage of SD granule parts.	110
4.27	Optical micrograph of SD part after wipping showing no shear distortion.	111
4.28	Measured z axis coordinates for the press-rolled and the SD parts after wipping.	111

CHAPTER 5

5.1	Schematic of printing slurries on spray dried granules powder bed	114
5.2	Calculated increase in green density of a 30 vol% SD granules powder bed as a function of solids volume concentration in the printed slurry.	114
5.3	Particle size distribution of classified slurry.	117
5.4	Plot of viscosity vs shear rate for 30 vol% alumina slurry.	118
5.5	Measured flow-rate of 32.88 vol% alumina slurry through a nickel orifice plate.	120
5.6	Ni orifice before and after printing 32.8 vol% alumina slurry.	121
5.7	Ni orifice before and after printing water at pH 3.5.	122

Figure #		Page #
5.8	Schematic of filtration set-up.	125
5.9	Measured concentration and flowrate profile for slurries introduced into filters filled with water.	126
5.10	Measured concentration and flowrate profile for slurries introduced into empty filters (filtration felt contains water).	127
5.11	Measured concentration and flowrate profile for slurries introduced into filters which are washed with slurry once to get rid of water from the felt.	129
5.12	Break-off lengths as a function of applied frequency and amplitude for a 19.4 vol% alumina slurry.	131
5.13	Cumulative intrusion volume of SD part printed with 7 and 26 vol% alumina slurry.	135
5.14	SEM micrographs of polished cross-sections of parts made by printing 7 and 26 vol% alumina slurry on SD granule powder bed.	136
5.15	SEM micrographs of polished cross-sections of parts made by printing 30 vol% alumina slurry on 30 μm dense platelet alumina powder bed.	137

CHAPTER 6

6.1	Latex binder droplet on top of ~55% dense SDPAA/alumina compact.	141
6.2	Schematic of the press compaction technique.	142
6.3	Schematic of the ram design.	144
6.4	Packing density of single layers.	147
6.5	Packing density of single and multipl-layered parts.	147
6.6	SEM micrographs showing the cross-section of SDPEG/alumina pressed at 127 psi and SDPAA/alumina pressed at 637 psi. Both the samples were fired at 1500 C for for 4 hours.	149
6.7	SEM micrographs showing the cross-section of SDPEG/alumina pressed at 2546 psi and SDPAA/alumina pressed at 6367 psi. Both the samples were fired at 1500 C for for 4 hours.	150

Figure #		Page #
6.8	Pore size distribution of SDPEG/alumina compacts at various compaction pressures.	151
6.9	Pore size distribution of SDPAA/alumina compacts at various compaction pressures.	151
6.10	Effect of shift error on the shape of the printed region	154
6.11	DRIFTS spectrum of SDPAA/alumina powder after being washed in KOH solution at pH 10.	155
6.12	DRIFTS spectrum of SDPAA/alumina powder after being washed in KOH solution at pH 13.	155
6.12	SEM micrograph showing the top surface of SD alumina powder bed printed with 30 vol% rhoplex once and twice respectively.	156

CHAPTER 7

7.1	CCT of alumina granular film as a function of wt% PVA.	161
7.2	Schematic of the spray deposition process.	163
7.3	DRIFTS spectrum of 0.5 wt% HBA/alumina powder bed.	166
7.4	Spray machine set-up.	168
7.5	Measured flow-rate as a function of time when the slurry was gravity fed.	169
7.6	Measured flow-rate as a function of time when the slurry was pressurized.	169
7.7	Drying stress as a function of saturation ofthe wet film. The film was 60 μm thick and the average particle size was 0.4 μm. The drying rate was $7.2 * 10^{-6}$ $Kg/m^2.s$.	171
7.8	SEM micrograph showing the polished cross-sections of HBA/alumina powder beds fired at 1650 C for 2 hours.	176
7.9	Pore size distribution of PVA/alumina and HBA/alumina powder beds.	177
7.10	SEM micrographs of polished cross-sections of parts made by printing 8 wt% PMMA/acetone solution once and thrice on HBA/alumina powder bed. Both the samples were fired at 1650 C for 2 hours.	184

Figure #		Page #
7.11	Penetration of liquid in capillary of non-uniform size.	189
7.12	Three stages in the escape of air from a capillary.	189
7.13	Part made by printing 10 wt% PAA solution in water on aqueous alumina powder bed.	193
7.14	DRIFTS spectrum of a part made by printing 10 wt% PAA solution on aqueous alumina powder bed.	194
7.15	TGA of the part made by printing 10 wt% PAA solution on aqueous alumina powder bed.	195
7.16	TGA of the part made by printing 10 wt% PAA solution on aqueous alumina powder bed after being washed for 20 hours.	195

LIST OF TABLES

Table #		Page #
	CHAPTER 2	
2.1	Calculated absolute and relative shrinkages for 30 and 50 vol% dense green body with a non-uniformity of 1vol% each.	49
	CHAPTER 3	
3.1	Machine parameters for counter-rolling and press-rolling spreading technique.	56
	CHAPTER 4	
4.1	Physical properties of spray dried granules.	77
4.2	Extent of warpage for various SD granules-binder systems.	89
	CHAPTER 5	
5.1	Operating parameters for classifying alumina slurries.	117
5.2	Erosion and corrosion rate of nickel orifice plate with various binder sytems.	123
5.3	Calculated break-off lengths for a 19.4 vol% alumina slurry.	132
	CHAPTER 6	
6.1	Major and minor axis of the elliptical printed region right after printing and after high pressure compaction step.	154
	CHAPTER 7	
7.1	Width of spray pattern deposited on the glass slide as a function of working distance and fast axis speed.	171

Table #		Page #
7.2	Extent of drying during spraying for aqueous and non-aqueous alumina slurries.	172
7.3	Measured packing density for various slurry systems.	174
7.4	Disintegration experiments.	187

Acknowledgements

I would like to thank a lot of people for making my stay at MIT a great and a memorable experience. First, I would like to thank my thesis advisor, Prof. Michael Cima, for his excellent guidance and brilliant suggestions through out my thesis research. I would also like to thank Profesor Ely Sachs for his thoughtful suggestions for my experiments. I have grown personally and professionally working with both of you. I would also like to thank: Professor Sam Allen for pushing me to come up with a new and better title for my thesis (Previous title: "Packing density and distortion control of structural ceramic components fabricated by 3DP". The new thesis title, " Origin and control of ansiotropy in three dimensional printing of structural ceramics," definitely sounds more profound and esoteric!), Wendell Rhine for answering all my trivial and vague questions related to chemsitry, Jack and Dick Pober for being patient with all those odd questions I did not know who to turn to, John Centerino and Lenny Rigione for entertaining and keeping me sane during those long spray drying and continuous classification experiments, Barbara Layne for providing me with white envelopes and other office supplies on numerous occasions when I did not feel like dragging myself to the Lab Supplies.

The people @ CPRL and 3DP lab constantly provided the support, friendship and fun throughout my tenure at MIT. Thank you one and all.

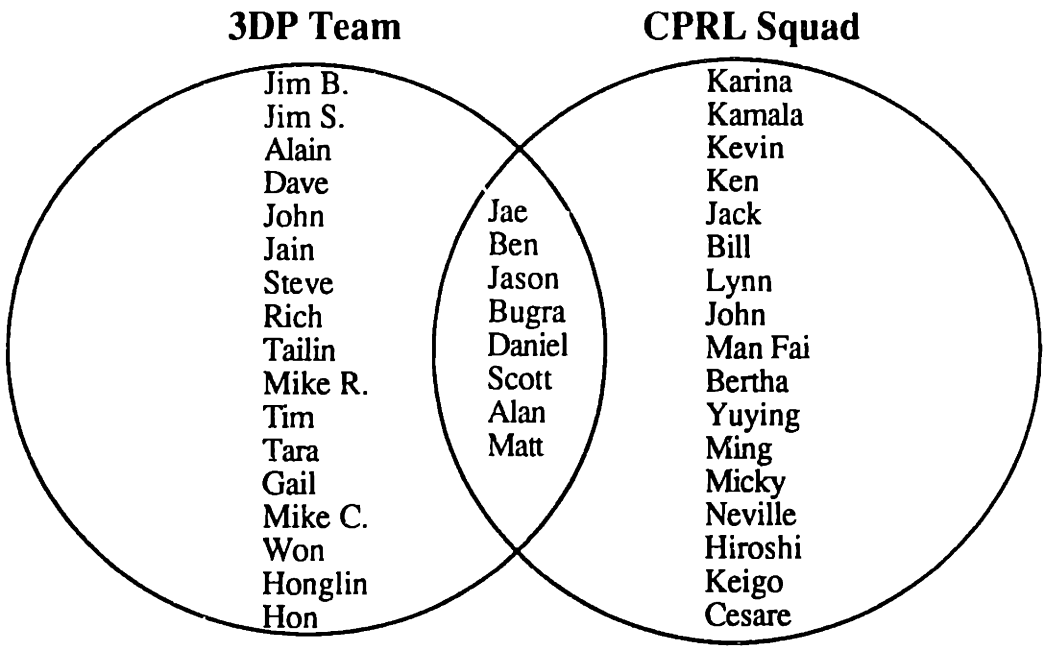

I am obliged to students working in the 3DP project for their help with my experiments. This thesis would not have existed without their help and suggestions. I am

especially grateful to the 3DP materials science team for their advice, wise cracks and jokes during the long printing sessions. They always tried to show me the silver lining in desperate situations.

Special thanks go to my apartmentmates: Nikhil, Hitesh, Vishnu, Geeta and Maria for fun filled activities over the weekends and encouragement throughout my thesis research. I would also like to thank my squash partners, Mitesh and Vishal, for providing a wonderful outlet outside research.

Finally, I would like to thank my father, Balwant, my mother, Raj, my brothers, Jasbir and Tanbir for their constant support and encouragement throughout my life.

EXECUTIVE SUMMARY

The overall objective of this research was to develop a process to fabricate fully dense and distortion free structural ceramic parts via three dimensional printing (3DP). The development of this application requires the fabrication of high packing density fine ceramic components with uniform microstructure. 3DP consists of many repetitive processes, each of which can potentially produce anisotropy in the component. Indeed, all laminated building processes are inherently anisotropic since the build direction is necessarily different from directions in the plane of lamination. The basic 3DP microstructural unit, consisting of a printed layer, is not only anisotropic because it is formed from thin spread powder layers, but is also anisotropic because the binder is printed in lines along a certain direction and the top and bottom of the layers have different processing histories. The fast axis is different from the slow axis and the top is different from the bottom. Therefore, the basic microstructural unit in a 3DP process has very little inherent symmetry. In this study, we have focused on the origin and control of anisotropy within each of the process elements that comprise 3DP.

Anisotropy was created in the powder bed during the powder spreading stage of the press-rolling technique. The fine powder used in the press-rolling process consisted of non-uniform agglomerates and resulted in inhomogeneities in the powder bed. The uni-directional press-rolling of fine powder introduced elongated trapezoidal pores (figure 1) in the spread powder layer. The basic microstructural unit of such a layer is highly anisotropic. The microstructure of the spread layer was modified by bi-directional press-rolling which introduced trapezoidal pores in opposite directions in subsequent layers (figure 1).

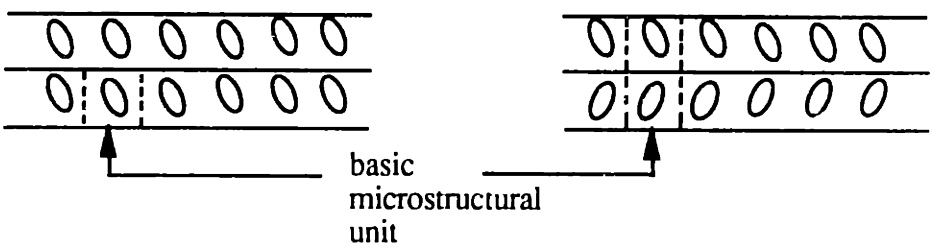

Uni-directional press-rolling Bi-directional press-rolling

Figure 1: Microstructure of parts made with uni- and bi-directional press-rolling of fine powder.

The packing density of the printed part was measured as ~ 40 vol%, not sufficient to achieve full densification by pressureless sintering. Individual layers were easily distinguishable in the printed part. Interlayer defects, therefore, introduced an anisotropy in the printed parts along the z-axis. A post-printing step, isopressing, was employed to achieve high and uniform packing density. Isopressing was also found to heal the interlayer defects, thereby increasing the uniformity within the pressed part. The green uni-directional press-rolled body exhibited shear distortion during the isostatic pressing operation. The anisotropic deformation behavior of the volume element around the trapezoidal pore in a uni-directional press-rolled body resulted in shear distortion. The shear distortion of press-rolled components was corrected by modifying the microstructure of the press-rolled spread powder layers using bi-directional press-rolling. The shear produced in layers with trapezoidal pores along one direction is cancelled by the shear produced in alternate layers with pores in the opposite direction. The uni- and bi-directional press-rolled components were shown to have intrinsic packing density variation within the printed part which resulted in differential shrinkage during isopressing.

The uniformity of the spread powder layer was successfully improved by the use of highly flowable spray dried (SD) granules. SD granules have a high flowability and can be spread easily with a counter-rolling spreading technique. The angle of repose of SD granules was measured as ~ 20°, significantly lower than the corresponding value of 38.3° for fine powder. The basic microstructural unit in the SD granular powder bed is more isotropic than the press-rolled powder bed (figure 2). The individual pores do not have any preferential orientation along the axis of the layer The use of SD granules, however, did not eliminate interlayer defects.

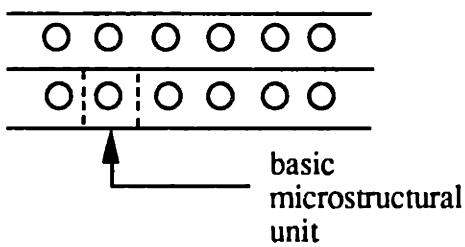

Figure 2: Microstructure of parts made with SD granules.

The ceramic parts made from SD granules, however, exhibited extensive warpage during the printing stage. The ceramic parts made out of coarse dense particles for investment casting and metal parts for tooling applications had never shown such unusual warpage behavior. Printing of individual lines in 3DP is an anisotropic process; one side of a new printed line is printed region while the other side consists of dry spread powder.

The relative shrinkage between the printed elements in earlier 3DP applications is negligible. The extensive shrinkage produced in the SD parts during printing stage creates an additional anisotropy in the build process; the new printed element undergoes a relative shrinkage with respect to the existing printed region.

Two different factors; dissolution of SD granules in the printed binder and interlayer liquid migration due to the fine pores of SD granules, were found to be responsible for introducing excessive shrinkage in the SD granule parts during the printing stage. SD granules containing a water soluble organic additive, such as poly ethylene glycol (PEG), disintegrated during printing and shrank upon drying to high packing density. The relative shrinkage between the two printed lines was inferred from warpage as 7.9%. This shrinkage resulted in warpage of the printed layer, as the lines are built sequentially and bonded to each other (figure 3).

Figure 3: Schematic illustrating the mechanics of warpage of a single layer due to relative shrinkage between the printed lines.

Shrinkage due to SD granule dissolution was avoided by the use of SD granules containing 2 wt% polyacrylic acid (PAA) as an additive. PAA was shown to be completely chemisorbed to the alumina surface and as a result the SDPAA granules were insoluble in water. Therefore, SDPAA granules did not disintegrate upon printing.

The parts made with SDPAA granules, however, warped when a powder layer was spread on top of a printed layer. Fine pores (~ 0.1 μm) in the spread layer can absorb liquid from the larger inter-granular pores (~ 6 μm) of the printed layer. Spreading of a new powder layer created an anisotropic liquid migration condition with respect to the printed layer below (figure 4). This introduced an asymmetry in the build process. The mass flux of liquid migration due to intragranular (fine) pores of SD granules was calculated as 1.1 g/cm^2-s. The mass flux due to water evaporation to atmosphere, in comparison, is in the order of 10^{-4} g/cm^2-s. The top surface of a printed layer lost liquid, while the interior portion stayed saturated. The anisotropic interlayer liquid redistribution introduced a compressive force on the top surface of the printed region and therefore resulted in warpage of the printed region. The extent of asymmetry and as a result warpage was shown to be strongly dependent on the saturation of the printed part

and on the strength of the printed binder. Higher saturations and higher strength binders resulted in increased warpage.

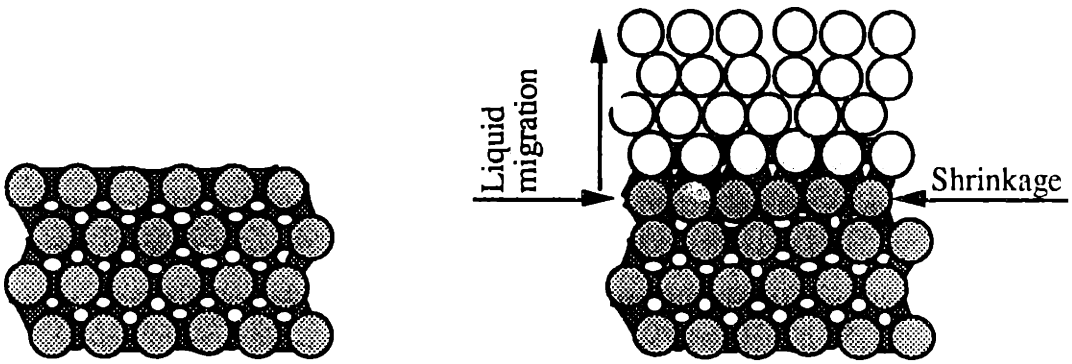

Printed layer

Inter-layer liquid migration from printed to spread powder layer

Figure 4: Warpage due to anisotropic liquid migration from the printed layer.

The asymmetry in the build process due to interlayer liquid migration has been reduced by employing an intermediate drying of the printed layers with a heat lamp. Heating of a printed layer with long wavelength light ensured uniform drying and avoided the anisotropic interlayer liquid migration during spreading of a subsequent powder layer. The response to anisotropic interlayer liquid was reduced by an addition of a plasticizer in the printed binder. The addition of a plasticizer (PEG, Molecular weight 1000) decreased the strength of the acrysol binder and therefore reduced the warpage. The above strategies have been used to successfully fabricate complex shaped parts from SD alumina and silicon nitride powder.

The parts made out of SD granules are ~30% dense and require an intermediate isopressing step to achieve the critical packing density, before they can be sintered to full density. The SD parts did not exhibit distortion problems during the isopressing step, thus indicating uniform packing density.

Two different approaches were investigated to fabricate high green density fine ceramic parts directly from the 3DP machine. The first approach consisted of adding matter by printing alumina slurries into a powder bed made out of SD granules. Anisotropy was introduced in the green part built with 26 vol% alumina slurry due to segregation of the printed slurry on the top half of a spread powder layer (figure 5). Segregation of the printed slurry, therefore, created anisotropy along the z-axis of the printed part. Such non-uniformity in microstructure was not observed in parts made out of

dense particles and is unacceptable for fabricating defect-free structural ceramic components. An interaction of the printed slurry droplet with SD granules powder bed was shown to involve two competing phenomenon: slip casting of the slurry on the SD granules (intragranular pores) versus infiltration of the slurry droplet into the powder layer. The time required by water to infiltrate a SD granule was calculated as to be the order of 1 millisecond; this is comparable to the measured time taken by a slurry droplet to infiltrate a powder layer thickness.

Figure 5: Segregation due to slip casting of the printed slurries (26 vol%) on the SD granule powder bed.

The anisotropy due to slurry segregation was reduced by printing dilute slurries (7 vol%) into SD granule powder bed.

The anisotropy in the printed fine ceramic part; therefore, was introduced during spreading and/or printing stage. Relative shrinkage between printed elements and binder segregation within the spread powder layer are the key mechanisms responsible for introducing undesirable asymmetry during the printing stage. The interlayer defects are intrinsic in the green parts fabricated by conventional 3DP process. The above factors which created anisotropy in the printed parts have been successfully eliminated in the spray deposition approach.

Figure 6 compares the powder generation step of spray deposition process with the conventional counter-rolling method of powder spreading. The leveling process of counter-rolling introduces asymmetry within the plane of a spread powder layer and generates particle size segregation along the z-axis. The spray deposition step eliminates this anisotropy.

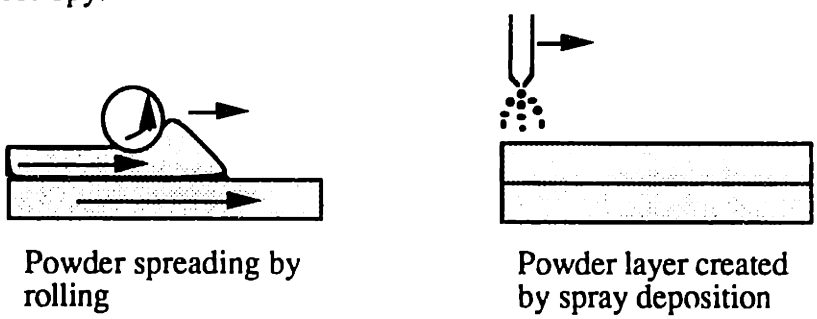

Figure 6: Powder generation step: counter-rolling method and spray deposition process.

The packing density of a crack free powder bed created by spraying electrostatically stabilized alumina slurry was measured as ~56%. The powder beds prepared by spray deposition develop a fairly high cohesive strength during drying. The high packing density and cohesive strength of the powder bed eliminated the shrinkage during printing. Therefore, no warpage was observed in the printed part. The concentration of polymer binder solutions were selected to avoid segregation of the printed binder within the powder layer. The individual printed layers were dried to avoid the anisotropy created due to interlayer liquid migration. The printed part does not show any interlayer defects. Therefore, the spray deposition process eliminates the anisotropy due to inter-laminar defects along the z-axis. Thus, a highly symmetric and uniform packing density parts can be made with the 3DP spray deposition process.

The high cohesive strength of the powder bed, however, made the conventional method of removing powder, such as brushing, ineffective to retrieve the printed part from the sprayed powder bed. A chemical method has been developed to disperse the alumina powder bed and leave the printed part intact. The use of electrostatically stabilized alumina slurry for powder bed allowed for an easy redispersion in water during the cleaning process. The printed binder was chosen so as to chemically bond with the surface of the particles and provide a strong printed part insoluble in water. Alumina was successfully chemically bonded with a polyacrylic acid (PAA) binder. The result of this research work has been successfully used to fabricate 56% dense structural ceramic parts directly by 3DP, which achieved full density upon firing.

CHAPTER 1
INTRODUCTION

The market for advanced ceramics is large and growing. According to T. Abraham from Business Communications Company, the total value of advanced ceramics components market in U.S for 1994 was $4.9 billion. The market share of structural ceramic components is 9.8% while electronic ceramic segment is 79.4%. The overall advanced ceramics market is expected to increase to $8.5 billion by 2000 at an annual growth rate of 9.8% [1]. However, one of the difficulties to be overcome before these markets can be fully exploited concerns the fabrication of shapes from ceramic powders. Powder packing and densification via heat treatment is still the most efficient and economical method of organizing ceramic matter to form engineering shapes.

The current methods of transforming powder into commercial ceramic product are almost no different to those used more than a century ago. New approaches are required as traditional processing imposes severe limitations on the shape, size and reliability of the products. Currently available forming techniques can be divided into three main themes: pressing, casting and plastic forming. Dry pressing and isostatic pressing are the most popular dry forming methods. Slip casting, injection molding and extrusion are the most common wet forming methods for the macro-components and tape casting for thin parts. All the current ceramic forming techniques need tools to define the shape and cannot change the composition locally. The development of tooling is not only very expensive but also very time consuming [2,3].

Pujari from Saint Gobain - Norton company emphasized an urgent need for developing robust forming technologies for advanced ceramics in the session entitled, "Commercialization of powder synthesis and shape forming processes," during 97th American Ceramic Society Meeting [4]. According to him, the requirements for ideal forming technology for advanced ceramics should include:

1. Reliability and reproducibility.
2. Complex shape capability.
3. Fast cycle times.
4. High yields.
5. Dimensional control.
6. Adequate as-processed strength.
7. Low-cost machining.
9. Automation and standardization and applicability to a wide variety of materials.

Several of the requirements above have become necessary requirements for the manufacturing industry as a whole and are the key technological drivers for the recent developments in the prototyping, investment casting and tooling industry. The demand to reduce the time between conception to implementation of a product design has lead to the emergence of a new class of manufacturing technology called Solid Freeform Fabrication (SFF). The SFF processes provide an ideal manufacturing method of satisfying industrial demand of shortening production cycle and improving design quality [5,6,7,8]. Most of these techniques create part on a layer by layer basis. Slicing algorithms are used to produce the two dimensional cross-section of the object to be made from its CAD representation. This information is then downloaded to the SFF machine to guide the fabrication process. Three Dimensional Printing (3DP) is a SFF technique which constructs parts by spreading powders in thin layers and then subsequently binding it with appropriate binder. 3DP processes build components on a point by point basis and therefore make it possible to vary the microstructure of a component locally. Refractory ceramics for investment casting tooling were the first materials to be constructed by 3DP. The parts were constructed by spreading 10-30 μm alumina powder and printing solutions of colloidal silica [9,10].

3DP is potentially a very useful tool for the advanced ceramics industry [11]. The motivations for its use are numerous: a) applications where complex shape is a premium, b) where properties of the final material need to be evaluated in environments that the component will be used, c) fabricating composite materials with internal structure that cannot be made by traditional forming methods and d) small batch manufacturing of ceramic components which will be too expensive to be made by traditional methods.

Fine powder, high and uniform packing density are the most important attributes required in a green ceramic part to achieve full density upon firing. The uniformity of packing is crucial for shrinkage control and to prevent the distortion and formation of defects in the final component [12,13]. 3DP of refractory body formation involved spreading of particles in the range of 10-30 μm. The use of coarse particles is acceptable for investment casting and tooling, however, fine particles are required for structural ceramics applications. Therefore, processing strategies will have to be developed to meet the challenges imposed by processing of fine powders.

Scope of thesis

This dissertation addresses the issues involved in the freeform fabrication of fine ceramic components via three dimensional printing technique. The main challenge is to

devise processing strategies to deposit fine powders via 3DP and construct high and uniform packing density green bodies.

Three Dimensional Printing (3DP) consists of many repetitive processes, each of which can potentially produce anisotropy and non-uniformity in the component. The basic 3DP microstructural unit, consisting of a printed layer, is not only anisotropic because it is formed from sheets, but is also anisotropic because the binder is printed in lines along a certain direction and the top and bottom of the layers have different processing histories. Therefore, the basic 3DP microstructural unit has very little inherent symmetery. This study focuses on the origin and control of anisotropy in three dimensional printing of structural ceramics.

Fine powders in the dry state tend to agglomerate due to Van der Waal's attractive force [14]. The presence of these irregular shaped agglomerates, as will be shown in the thesis, not only reduce the flowability of the powder but also result in non-uniform microstructure in the powder layers during the spreading stage. The uniformity of the spread powder layers was successfully improved by the use of highly flowable spray dried (SD) granules. The parts made from SD granules, however, exhibited extensive warpage during the build stage. The parts made out of coarse dense particles for investment casting and tooling applications, in comparison, had never shown such warpage behavior. The dissolution of SD granules by the printed binder and the interlayer liquid migration due to the fine pores of SD granules were found to be the key mechanisms introducing asymmetry in the build process and resulting in excessive warpage of SD parts. Processing strategies have been devised to minimize the anisotropy during the printing stage and have been successfully used to build distortion free SD green alumina parts. The green density of the SD parts is ~ 30 vol%. The parts made by spreading dry powder also have interlaminar defects, thereby reducing the isotropy along the z-axis. Additional post processing, such as isopressing, is required to increase the packing density to ~ 60 vol% and to heal the interlayer defects before the SD parts can be consolidated to full density upon firing.

A novel wet deposition technique has been developed to build high packing density and isotropic powder beds out of fine powder. Conventional 3DP process has so far employed only dry methods for spreading powders. The powder beds prepared by the wet deposition technique have fairly high cohesive strength and conventional methods of powder removal can not be employed. The main challenge in the development of spray deposition process is, therefore, to retrieve the printed part from the powder bed. The chemical interaction between the powder and the polymer, as will be shown in this work, is the key for a successful part retrieval. The results of this research have been used

successfully to fabricate 56% dense alumina structural ceramic parts directly by 3DP, which achieved almost full density upon firing.

Thesis organization

The second chapter of this thesis describes the pertinent literature. The first section briefly discusses the advantages and limitations of the conventional manufacturing techniques such as pressing, casting and plastic forming methods used for making advanced ceramics components. It also evaluates the current status of various SFF technologies in the context of manufacturing structural ceramics. The last section describes the literature pertaining to the desired properties required in a green body and factors responsible for distortion during processing of these components. In the following chapters, other topics that are relevant to the discussion of the experimental results or theoretical aspects of the work are reviewed. Chapters 3 and 4 describe the experimental techniques and critical processing variables necessary to fabricate ceramic components via 3DP by printing organic latex emulsion on dry fine powder and SD granules respectively. Chapters 5, 6, and 7 describe different strategies to make high green density parts directly by 3DP. Chapter 5 discusses the processing issues involved in fabricating high green density parts by printing colloidal suspension into SD granules powder bed. Chapter 6 addresses the issues involved in fabricating high green density parts by uniaxial pressing each spread layer. Chapter 7 describes the wet deposition technique of fabricating high green density parts directly by 3DP. All the processing strategies are evaluated in terms of origin and control of anisotropy in green structural ceramic components fabricated by them. The major conclusions derived from this study and their general implications to 3DP technology are presented in the executive summary.

CHAPTER 2
BACKGROUND INFORMATION

2.1 Introduction

Section 2.2 briefly describes the traditional forming methods to make structural ceramics, their advantages and limitations. Section 2.3 describes various SFF technologies and their development efforts to fabricate structural ceramics components. In 3DP process, binder is added to the loose powder to define the printed region. Drying of the binder results in the shrinkage of the printed region. The factors controlling the shrinkage and warpage of a wet body during drying are discussed in section 2.4. Section 2.4 also describes the factors responsible for warpage of a green part during firing. Section 2.4.3 summarizes the case of warpage specific to SFF process. Finally section 2.5 summarizes the necessary properties required in a green body for making defect free fully dense ceramic parts.

2.2 Traditional ceramic forming technologies

2.2.1 Pressing

2.2.1.1 Dry pressing

Pressing consists of simultaneous compaction and shaping of a powder confined in a rigid or flexible mold [15-19]. Dry pressing consists of three distinct stages: filling of die with powder, compaction and shaping, and ejection of built parts. Pressing powder should be free flowing deformable granules with high bulk density, stable under ambient conditions, and should cause a minimum of die wear and not adhere to the punch. These requirements are met by forming granules with appropriate processing additives using spray drying or spray granulation technique. The binder content is usually as low as practicable to minimize the cost of higher binder cost and the amount of gas produced during binder burnout. Typical binder content is the range of 2 to 5 wt% of ceramic material, usually sufficient to provide enough strength to the pressed part to survive ejection and subsequent handling. The maximum pressing pressure used in dry-pressing is in the range of 20-100 MPa. Die set life may range upto several hundred thousand parts for a simple die and a low pressing pressures.

Friction between the powder particles and between powder and die walls causes a gradient in pressure through the thickness of the compact, resulting in density gradients in the part. The maximum densification occurs near the top surface of the part and diminishes towards the center of the thickness. These density variations cause warping or cracking during the sintering stage. Lubricants are usually pre-mixed into the ceramic

powders to enhance the redistribution of stress and minimize the density gradients. Dimensional tolerances are in the range of $\pm$ 0.02 mm in thickness, but shapes are usually limited because length to breadth aspect ratios should not exceed 3:1 in order to avoid non-uniform density gradients. Dimensional tolerances and the uniformity of the microstructure are more difficult to control when the part has several surface levels.

Elastic energy stored in the pressed part produces a volume expansion called elastic springback when the pressed part is ejected. Springback must be controlled to prevent laminations and microcracks in pressed products but yet cause separation of the product from the punch.

Dry pressing is widely used in fabricating a variety of magnetic and dielectric ceramic products, various fine grained technical alumina including chip carriers and spark plugs, engineering ceramics such as cutting tools and refractory sensors, ceramic tile and porcelain products, and coarse grained refractories, grinding wheels and structural clay products.

Dry pressing is the most widely used forming practice for high productivity and the ability to produce parts ranging widely in size and shape to close tolerances with essentially no drying shrinkages.

Isopressing is typically used to avoid the die wall friction of dry-pressing [15,20]. The powder is contained in a flexible mold and pressed by a fluid. There are two different kinds of isopressing techniques: wet bag and the dry bag process. In the wet bag process, a flexible rubber or polymer container is filled with the powder, the container is sealed and immersed in the liquid within the pressure vessel, the vessel is then sealed and liquid is pressurized in the range of 15-300 MPa. Dry bag pressing imitates dry-pressing except that the pressure is applied radially by means of the pressurized liquid medium contained between a flexible mold and rigid shell. Dry bag method can be automated easily to yield high production rates. Wet bag processing is used for pressing complicated shapes such as spark plugs. Sudden decompression must be avoided to allow air to escape slowly and to avoid a large differential air pressure. Slow decompression below 2 MPa is important when thick walled tooling that has a relatively high springback is in contact with the part. Springback must be controlled to prevent cracking of the pressed products. Isopressing equipment capital costs are high, and development work is always needed to design tools and avoid distortions. Design of rubber molds to produce good ware requires substantial empirical experience and is very time consuming and expensive. Components formed by isopressing are of uniform density, have no drying shrinkage, and lower firing shrinkage than that produced with other forming methods. Isostatic pressing has been used in

making shapes with one elongated dimension such as rods and tubes, and parts with thick cross-sections.

2.2.1.2 Hot pressing

Hot pressing densifies material by the simultaneous application of pressure and temperature. The application of applied stress at the sintering temperature not only improves the particle packing but also enhances the densification process by increasing the contact stress between the particles. The main advantage is that densification can be achieved at lower temperatures resulting in fine grained final part with superior mechanical properties. The hot pressing technique is restricted to making simple shapes and is also very expensive.

2.2.2 Slip Casting

Slurry is poured or pumped into a permeable mold having a particular shape in slip casting process. Capillary suction and filtration concentrate the solids into a cast adjacent to the wall of the mold. Excess slurry is drained from the mold after the desired wall thickness is achieved. Filtration continues in solid casting, until a nearly solid cast with a center pipe, having the shape of the cavity of the mold develops. Control parameters in slip casting are the slurry rheology during mold filling, the casting rate, the cast densities and yield strength, flow rheology on draining, the shrinkage and release of the cast from the mold, and the strength and plasticity of the piece during trimming and surface finishing. Processing strategies are designed to have a uniform distribution of both the liquid and the particle sizes throughout the cast in order to reduce stress and distortion upon drying and firing. Slip casting has been used to produce high packing density green bodies [15, 21-24].

Casting is a traditional process to produce a variety of porcelain products with complex shape such as bathroom fixtures, chemical porcelain components dense refractories that are of a complex shape or massive in cross-section. Some high performance ceramics with complex shapes are also produced by casting now. Capital investment for casting are relatively low. Slip cast pieces need trimming and surface finishing. Permeable molds for casting are commonly gypsum with 40-50% porosity. The casting time may range from few minutes for a porcelain product with a thin wall to about 1 hour for a thin but dense cast from a well dispersed slurry. The casting time for a dense solid cast refractory of fine particle size may range upto several weeks for thicknesses of 30 cm. Casting time can be reduced either by applying pressure to the

slurry (pressure casting) or by applying vacuum to the mold (vacuum assisted casting). Pressure casting, however, involves newer mold materials and higher capital costs.

Common defects in cast structure are: pinholes, wreathing, warped shapes, uneven thickness and cracks on drying. Wreathing is a wave like pattern on the drained surface and is caused by the variations in the casting rates in different regions of the cast. This problem is minimized by using a mold with uniform pore structure. Warping is caused by the differential shrinkage on drying due to a gradient in the liquid content or average particle size in the cast. An anisotropic drying shrinkage may occur where two surfaces of the cast meet at a sharp angle when using dispersed anisometric particles. The juncture is a potential site for crack on drying. Organic binders used in non-clay slip reduces the slip casting rate but improves the mechanical properties of the cast.

2.2.3 Plastic forming

The technology of plastic forming of ceramics was borrowed from polymer industry. Extrusion and injection molding are the most commonly used plastic forming technologies for shaping ceramic materials. Extrusion is the shaping of the cross-sections of a cohesive plastic material by forcing it through a rigid die. Products formed by extrusion include structural refractory products such as hollow furnace tubes, honeycomb catalyst support, electric porcelain products, flat substrates and tile products.

Thermoplastic polymer loaded ceramic paste is formed into a complex shape by injecting the heated material into a metal die in an injection molding process. Injection molding is used for fabricating complex shapes such as multivaned turbine rotors and small electronic components.

The selection of right raw materials is a critical factor in a successful extrusion and injection molding process. The raw material parameters are the particle size distribution and particle shape of the ceramic and the characteristics of the organic vehicle used to confer plasticity to the mix. Binder system for plastic forming consists of typically a potpourri of organics. Binder for injection molding has to fulfill a number of requirements, of them three are essential [25,26]:

1. Deliver the required flow properties of the mix at high solids loading.
2. Be chemically stable so that it does not degrade during mixing or molding and does not interact with the ceramic.
3. Be easily removed by some means from the molding without distortion.

Surface craters and blisters can be formed when the dissolved air migrates to the surface upon ejection. Proper de-airing of feed material therefore is an essential processing step. Injection molding defects may also originate at the mold filling stage or

during solidification in the cavity. The former include incomplete cavity filling and the incidence of weld or knit lines. The latter are defects which originate from volume shrinkage effects or from unrelieved polymer orientation and consist typically of voids, microcracks. Such defects can provide initiation for defects found in powder assemblies after polymer removal. Most cracks and lamination defects are caused by the differential springback and/or differential drying shrinkage.

The polymer removal stage of the process involves the extraction of typically 30-40 vol% of vehicle. In the first step of debonding some 5% of the volatile portion of binder gets removed from an impermeable body. This process clearly depends on the diffusion of the volatile component through the binder filling the capillaries between the particles of the ceramic. The first step takes 50 % of the debonding time. At the end of this period small interconnected porosity forms in the body and provides passageways for the decomposition products of the rest of the binder. The heating schedule is very specific to the binder system and is a slow process and may take typically 50-150 hours for objects 6 mm thick and may become decisive in the economic feasibility of the process. When the binder has been removed the strength of the body is very low as there is nothing to hold the particles together. Any internal stresses in this stage will bring about cracking. Such stresses can be generated by a small shrinkage frequently associated with the elimination of the binder.

Heating rates as low as 5 degree/hour are often necessary for debonding. Various other methods such as oxidative degradation, solvent washing, capillary extraction, and evaporation or sublimation have been employed to remove the polymer after forming.

A wide range of injection molding machines can be used for components of small cross-section but the real challenge to ceramic injection molding technology is the ability to produce thick sections which will survive solidification in the cavity and subsequent polymer removal without the incidence of defects. Solutions to the former problem include techniques for keeping the sprues and runners molten during the post injection stage to allow extended mold filling and thus control shrinkage stresses during solidification and cooling.

Dimensional precision for plastic formed bodies varies with shape and shrinkage but is generally lower than that of dry pressed products because of plastic deformation during handling and variable drying shrinkage. Injection molded parts may be formed with a high precision in size and shape, but this precision is not always maintained in parts with moderately thick cross-sections because of problems in thermally removing the resin. Defects in the products may occur owing to differential drying shrinkage or springback, entrapped air, discontinuities in particle orientation, and the incomplete bonding of material

separated and rejoined during flow. The major disadvantages of plastic forming are the binder removal process and tooling cost. The wear of ceramic molding machinery is extensive and replacements parts are very expensive. The major advantage of injection molding is its capability to fabricate complex shapes [27-32].

2.3 SFF technologies

The Solid Freeform Fabrication (SFF) processes provide an ideal manufacturing method of satisfying industrial demand of shortening production cycle and improving design quality. SFF refers to a new group of manufacturing techniques, in which the shape is produced by 'adding' rather than 'removing' or 'deforming' material. All commercial and evolving SFF processes have several features in common. A graphic workstation is used to represent a solid or surface CAD model of the object. Slicing algorithms are then used to electronically section the CAD representation of the object into thin layers of predetermined thickness. The sections collectively define the shape of the part. The information about these two dimensional cross-sections is stored as .STL format which is currently the industry defacto standard. Information about each section is then transmitted layer-by-layer to the SFF workstation. Material is processed only at "solid areas" of the section. Subsequent layers are sequentially processed until the part is complete. Following is a brief description of various SFF technologies which are currently being adapted and modified to make fully dense fine ceramic parts.

2.3.1 Stereolithography (SLA)

The enabling technology for stereolithography was the development of liquid photomonomers that solidify when exposed to ultraviolet (UV) radiation. In this process (Figure 2.1), a support platform is submerged in a vat of liquid photomonomers and held near the surface. A low power UV laser scans the surface of the liquid, partially or completely curing selected areas of the resin. The platform is lowered incrementally between scans to allow fresh resin to cover the previously solidified layer. The finished part is removed, cleaned, and postcured under UV actinic fluorescent lamps to solidify any uncured resin. The support structure and platform are then removed, and the part is subjected to minor sanding and/or glass bead blasting. The support structure consists of vertical members extending from the platform to the part. They are needed for parts having features such as horizontal overhangs, because the liquid cannot support isolated islands. Typical SLA resin (acrylates) undergoes about 5 to 7 % total volumetric shrinkage, of which 50 to 70 % occurs in the vat as a result of laser induced polymerization while the remaining shrinkage occurs during post curing step. Extensive

shrinkage creates problems of warpage and dimensional control in the built part. SLA has been quite successful in reducing the shrinkage by designing low shrinkage epoxy resins and using innovative build style. The epoxy resins are less reactive than acrylates and therefore increase the build time. WEAVE , STAR-WEAVE and QUICK-CAST print styles are used to compensate for the internal stresses created during the build process. Stereolithography, until very recently, was used to make polymers parts.

Research groups from University of Michigan and Princeton University are trying to adapt the current stereolithography process to make ceramic parts. The process consists of dispersing ceramic powders in UV curable monomer solution. A laser is then used to cure the ceramic slurry on a layer by layer basis to form a ceramic green body. The green body is subsequently fired to remove the binder and densify the ceramic. The main processing challenge has been to design the slurry so as to have a cure depth of ~ 200 μm, typical layer thickness. Addition of ceramic particles in photomonomer not only limit the cure depth by scattering of UV laser but also increases the viscosity of the solution and makes spreading difficult. Part construction by ceramic stereolithography is still in its infancy and exhibit warpage due to shrinkage during polymerization. Debinding process will create challenges very similar to injection molding since the built parts will contain ~ 50 vol% polymer. Binder removal in injection molding is usually accompanied by the formation of defects and adds considerably to the cycle time for component production [33,34].

2.3.2 Selective Laser Sintering (SLS)

SLS fabrication process starts with the deposition of a thin layer of powder under controlled temperature and atmosphere using a powder drum. The layer thickness ranges between 75 - 250 μm for various powders. A laser scans the powder layer (Figure 2.2), while its beam is modulated to sinter or melt powder only in areas defined by the geometry of the cross-section. Binding of the loose powder takes place by either partial melting or sintering. The layering process is repeated to produce a three dimensional object. The whole powder bed is heated to relieve the residual stresses generated within the built part due to rapid heating and cooling of a local region. Thermal stress created during part building is a major bottleneck of this process. The laser beam diameter is on the order of 0.5 mm, and working output power ranges between 5W and 50W. The surface scan rate is on the order of 100 cm/sec for polymers and waxes and from 2 - 6 cm/sec for metals and ceramics for the low power laser. Various glass compositions (ammonium dihydrogen phosphate) and polymer (styrene-methylmethacrylate copolymer) have been used as binders for ceramic components. Commercial SLS machines are configured to

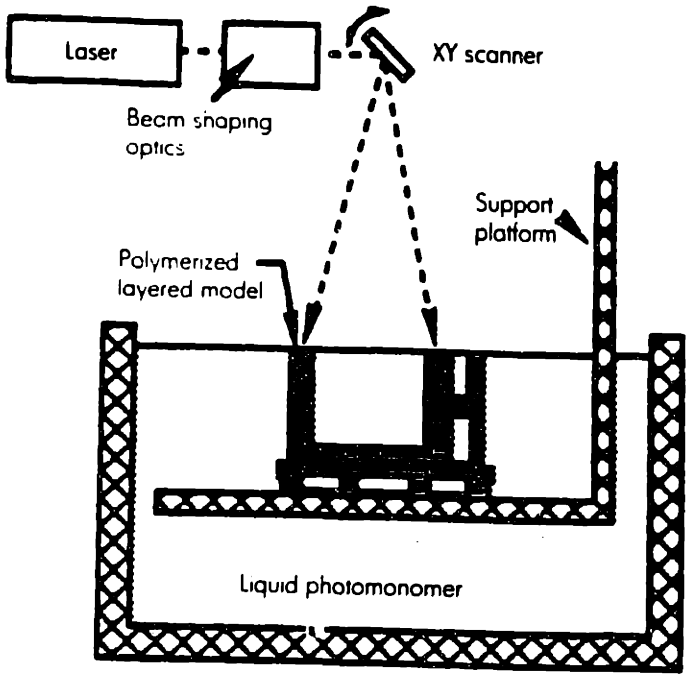

Figure 2.1: Stereolithography process.

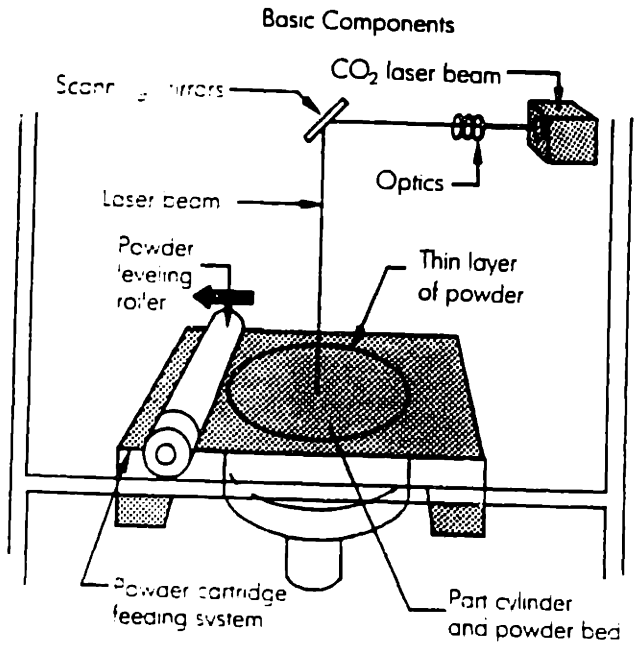

Figure 2.2: Selective laser sintering process.

use investment casting wax and various thermoplastics. Ceramic and metal powder coated with polymeric binder are still under development stage. Researchers have not yet reported the use of conventional SLS to make bulk parts out of fine ceramics [35,36].

Selected area laser deposition: The process consists of scanning a laser over a powder substrate in the presence of gas precursors. Laser pyrolytically decomposes the gas and the products of decomposition locally infiltrate and bond the particles together. Parts have been made out of silicon carbide, tetramethyl silane was used as the gas precursor. A major issue in this process is the reflectivity of the laser by the powder. The reflected laser decreases the efficiency of the precursor to infiltrate and bond the particles together. This technique is still very new and lot of improvements may be made in the future.

2.3.3 Three dimensional printing (3DP)

3DP process involves spreading powders in thin layers and then binding it with an appropriate binder. Printing is accomplished by moving the print-head in a raster pattern. Layers are added sequentially to complete a part. Figures 2.3 & 2.4 show the schematic of sequence of operations in a 3DP process and 3DP machine respectively. Following a heat treatment, the loose powder is removed, leaving the fabricated component. The modulation of very small binder droplets at high rates is controlled by the implementation of continuous-jet ink-jet printing. A continuous stream of liquid is forced to break into regular sized droplets (~ 80 μm) by applying an electric impulse (50 - 60 khz) to piezo-disk mounted on the nozzle. The binder droplets are allowed to fall in areas where the powder is to be joined. In areas that are not to be joined, the droplets are electrostatically charged and deflected and are collected in a catcher. Typical print-head speed is 1.65 m/s, line and layer spacing are ~ 180 μm. 3DP is currently used to make metal and ceramic parts. Colloidal silica and polymer latex emulsions are the commonly employed binders. Much less binder is used in 3DP, as the binder is used only to hold the green part together rather than plasticize the powder mass. Since the 'glue' is dispensed through an ink-jet, parts have been constructed with very small amounts of binder in the final part (4-6 vol%) and this makes binder burnout very easy, in case of an organic binder. Further different binders can be dispensed through different printheads thus allowing to control the composition on a local scale. Yoo has successfully used this capability of 3DP technology to make ZTA parts with complex compositional profiles. Glass-ceramic parts have also been made [37-43].

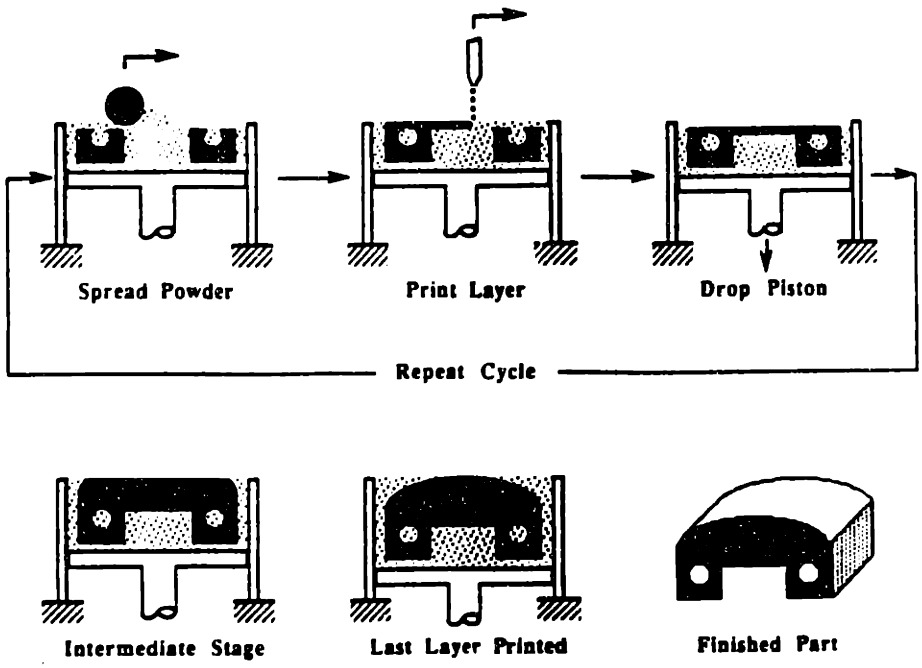

Figure 2.3: Three dimensional printing process.

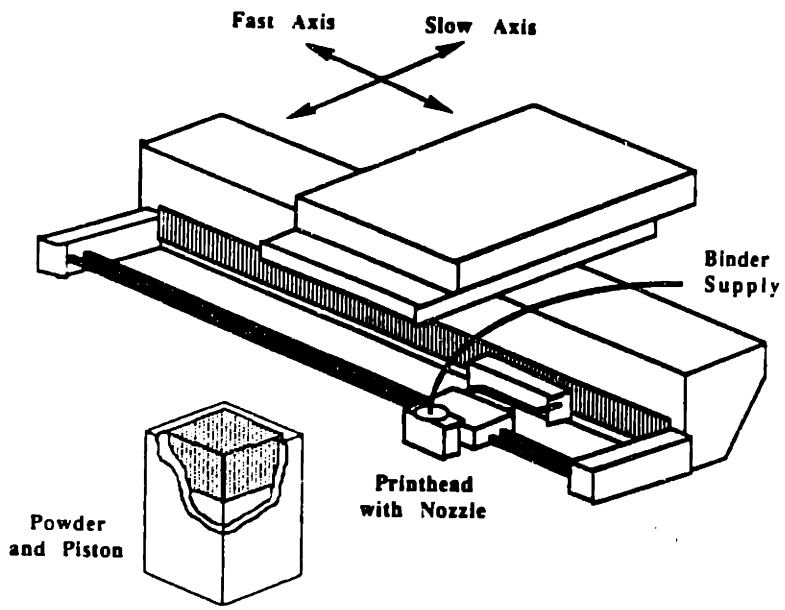

Figure 2.4: Three dimensional printing machine.

2.3.4 Laminated Object Manufacturing (LOM)

Unlike SLS and 3DP, which use powder, LOM uses thin sheets of material to build a component. Each layer is first glued to a stack and then a focused laser beam, positioned by an X-Y system, cuts around the peripheries of the cross-sections according to geometrical information provided by the computer. The velocity and focus of the laser beam is adjusted so that the cutting depth exactly corresponds to the thickness of the layer without damaging the previous layer. The material surrounding the cross-section is generally cross-hatched to facilitate separation of the built part. Figure 2.5 shows the configuration of a LOM machine. Currently used material include plastic, paper, composite sheet with a heat activated adhesive and ceramic green sheets.

Part buildup by LOM is rapid, particularly for large parts, because only contours are scanned. The major advantage of this technique is the absence of drying shrinkage. Currently, the technology is not capable of making thin wall sections, powder removal is a major problem. Since the final part contains ~ 40 vol% organic, binder burnout will have issues similar to injection molding.

LOM has successfully made parts out of fine ceramic. Ceramic tapes were fabricated out of slurry consisting of Alumina (A-16SG, Alcoa) powder and an organic binder. The tape thickness was ~ 15 μm. Pieces, 10 cm by 15 cm, were cut from the tape cast roll. These tapes were manually applied using a small amount of pressure. The initial sheet was placed onto a glass plate while the subsequent layers were placed onto the previous layers. The lamination temperature was 45^0C and the lamination time was ~ 1 minute. The power and speed of the laser was adjusted so as to cut only the top layer. These LOMed parts were fired at 1550°C for 2 hours. The fired density of parts was measured by an immersion technique as ~3.88 g/cc. The sintered bars were ground by a 320 grit diamond wheel. Some of the ground bars were polished to a 1 mm finish. Flexural strength of LOMed parts were measured, both in parallel and perpendicular direction with respect to the lamination, using a four point bending technique. The average strength of the parts was measured as ~314 MPa in both the testing modes. According to the authors, there were no lamination defects [44-46].

2.3.5 Fused deposition modeling (FDM)

FDM process builds up parts by deposition of molten material onto a base plate or onto previously solidified material. Solidification occurs by the cooling of molten material, which is kept at temperatures just above the melting point. Parts have been built out of thermoplastics polymers so far. The material to be deposited is fed in the form of a filament to an extrusion head with a built in heater. The flow rate of the molten material is

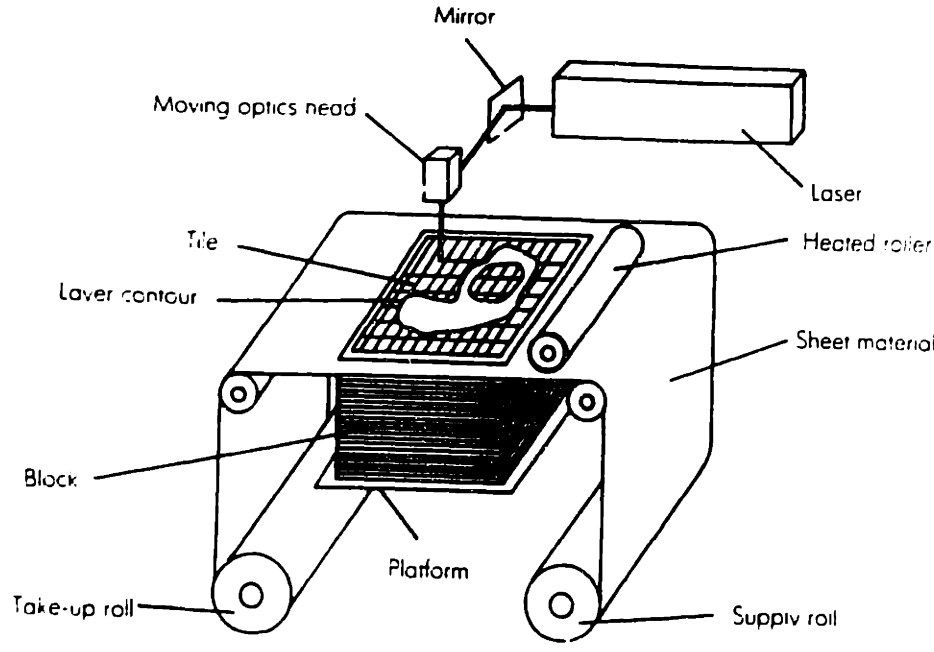

Figure 2.5: Laminated object manufacturing process.

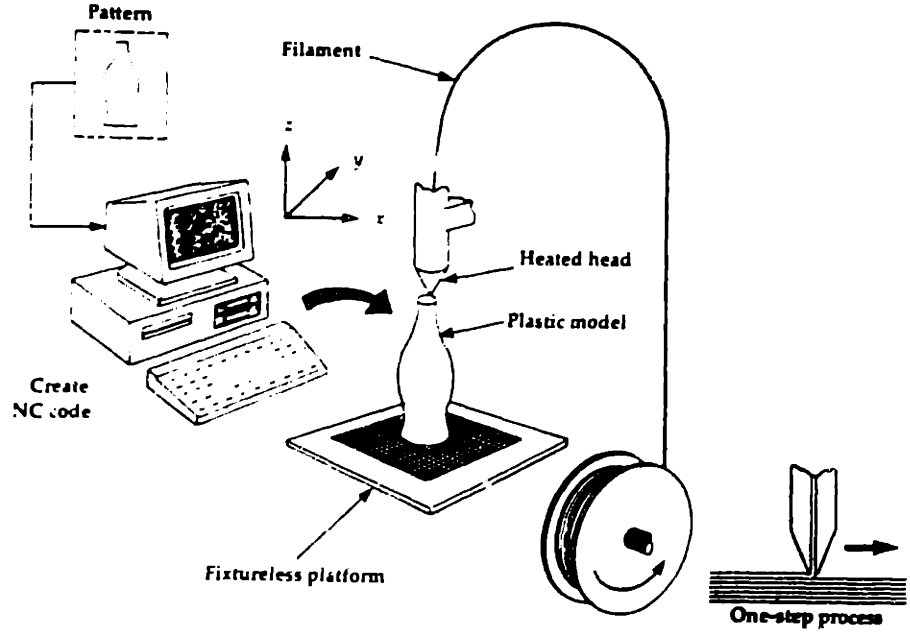

Figure 2.6: Fused deposition process.

controlled accurately by precision volumetric pumps. Figure 2.6 shows a schematic of a FDM system. A similar process, called Shape Melting (CMU process), produces near net shape metal parts [47,48].

Researchers (Danforth) at Rutgers university are currently trying to adapt FDM technology to make fine ceramic components. The process consists of loading ceramic particles in polymers. The paste is then extruded as in the normal process to define shape. Process is still in its infancy and no data is available about the current capabilities of the ceramic FDM process. The built parts will be loaded with polymer and binder burnout will create a challenge similar to injection molding.

2.4 Factors controlling warpage of fine ceramic components

2.4.1 Warpage during drying

Shrinkage occurs during drying as the liquid between the particles is removed and the interparticle separation decreases. For granular ceramic systems, the shrinkage is attributed to the elimination of the electrostatic or electrosteric repulsion layer between dispersed particles upon drying.

The first stage of drying is called the constant rate period as the rate of evaporation per unit area of the drying surface is independent of time. The evaporation rate is close to that from an open dish of liquid. The rate of evaporation V_E is proportional to the difference between vapor pressure of liquid p_v and the ambient vapor pressure p_a and is expressed as:

$$V_E = k\,(p_v - p_a)$$

where k is a factor that depends on the temperature, airflow and geometry of the drying system. Drying continues as long as the vapor pressure of liquid exceeds the ambient partial pressure.

The capillary redistribution pressure draws liquid from the interior to the surface of the wet body during drying and thereby exerts a tensile force on the liquid. The tension in the liquid is supported by the solid phase which therefore goes into compression. In effect, the capillary forces act to shrink the green body during drying. The network becomes increasingly stiffer as drying proceeds. The liquid exerts the maximum possible force once the radius of the meniscus becomes equal to the radius of the pores in the network. The tension in the liquid cannot overcome further stiffening of the network so the meniscus recedes into the pores, leaving air-filled pores on the surface. The end of constant rate period is called the critical point and it is at this point that shrinkage stops. The amount of shrinkage that precedes the critical point depends on the magnitude of the maximum capillary stress P expressed as:

$$P = \frac{\gamma_{lv}\cos\theta}{r}$$

where r is the pore radius, γ_{lv} is the liquid surface tension and θ is the contact angle. Fine pore size and high surface tension result in high capillary stress and therefore higher shrinkage.

Differential shrinkages occur during drying and result in warping and cracking of a green body. The development of differential stress in a green body during drying can be due to:

1. Presence of moisture gradient through the piece when it is formed. When dried the wetter side will shrink more than the other and the piece will distort.
2. Anisotropy in shrinkage due to non uniform distribution of granular particles. Non-uniformity could be introduced in the product due to binder and particle migration during drying which can result in non-uniform surface permeability. Another factor for anisotropic shrinkage is the preferred orientation of high aspect ratio particles during shaping. Objects made out of clay by extrusion have oriented clay plates near the mold surface but have randomly distributed plates away from the mold surface. As the shrinkage results due to the elimination of water film, the face towards the mold surface shrinks less, because there are fewer films per unit length. The dried body curls away from the mold.
3. Non-uniform drying, where a body is dried more rapidly from one side than on the other. The body curls up towards the drier side.
4. External mechanical restraint, frictional forces at the resting surface mechanically restrain the surface in its contact to shrink.

Moisture gradients set up within a body during drying are the most common cause of warping and cracking in big ceramic green wares. The drying stress developed in the green body as a result of pressure gradient is derived by Scherer [51] as a function of position along the thickness as:

$$\sigma_x = \left(\frac{L\eta_L \dot{V}_E}{2D}\right)\left(\frac{z^2}{L^2} - \frac{1}{3}\right)$$

where L is the thickness of the drying body, V_E is the drying rate, D is the permeability and η_L is the viscosity of the liquid. The stress increases in proportion to the thickness of the plate, the rate of evaporation, and the viscosity of the fluid and in inverse proportion to the permeability. Therefore stress is increased by those factors that steepen the pressure gradient within the drying body. Maximum drying stress will be equal to the maximum capillary stress. The results derived by Scherer apply only when the pores remain filled

and the mechanical properties remain constant. The permeability varies as soon as the pores start to empty [49-53].

2.4.2 Strategies to reduce warpage during drying

Warpage can be reduced by increasing the uniformity of drying and/or by reducing the average drying shrinkage of the body. Uniform drying is desirable to avoid a sharp moisture gradient in the drying body. Temperature, flowrate and humidity of the drying air is controlled to reduce the rate of drying in commercial operations.

The drying shrinkage is minimized by reducing the capillary pressure. The maximum capillary pressure can be reduced by increasing the pore size and/or decreasing the surface tension of the liquid. Increase in pore size is not be a viable solution for fine structural ceramics parts, as it may inhibit the densification kinetics during firing. The surface tension of the liquid can be reduced by using an appropriate surfactant.

Capillary tension can be completely avoided by using super critical drying. The wet body is isothermally pressurized in super critical drying until the liquid becomes a supercritical fluid. This stage eliminates the tension due to liquid-vapor interface and ensures negligible stress during drying. Super critical drying involves high temperatures and pressures and therefore is fairly expensive process.

Each of the above approaches involve trade-offs in terms of processing time, cost and sintering temperature. The right strategy should be chosen by considering the process as a whole.

2.4.3 Warpage during firing

The development of warpage during firing can be a result of one or several of the following factors:

1. Non-uniform packing density within a green preform. Density differences in the green ware may occur either due to the presence of agglomerates in the starting powder or during shaping process. Shrinkage during firing varies with the packing density. The lower packing density parts will always shrink more than the higher packing density parts for the same final fired density. On the other hand, if densification is not complete, the denser portion may have the higher shrinkage due to more rapid densification. Any differential shrinkage will cause warpage. Warpage in this situation can be corrected only by solving the problem in an earlier processing step that caused the inhomogeneity.
2. Non-uniform temperature gradients during firing step will result in differential shrinkage and can cause warpage.

3. Friction forces effect warpage. The bottom surface of a part during firing can be constrained by the substrate resulting in lesser shrinkage than the top surface. This differentiai shrinkage would result in warpage.
4. Warpage during sintering can also result from inadequate support during sintering. The former can be corrected by shifting the orientation of the part in the furnace or by supporting the part with the saggers, a refractory nonreactive ceramic pieces which restrict the component from deforming during sintering [2,54].

2.4.4 Warpage in SFF processes

Differential shrinkages are produced in the components after they are formed in conventional ceramic manufacturing methods. The components are assembled on a layer-by-layer basis in a SFF process and differential shrinkage can be produced while the part is getting built. Presence of differential shrinkage will manifest itself as warpage of the component as it is getting built. A simple model illustrating the mechanics of warpage behavior for a SFF process is shown in Figure 2.7. The entire single layer is assumed to shrink after it gets built and also the successive layers are bonded with each other. The first layer is free to shrink without introducing any distortion stresses. However, the successive layers are bonded to the previous layers and thereby introduce an upward bending moment upon shrinking and thus result in warpage. The radius of curvature 'R' of the warped layer can be approximated by an expression for a straight elastic beam subjected to constant bending moment as:

$$R = EI/M$$

where M is the bending moment, I is the moment of inertia and E is the Elastic modulus of the beam. A large radius of curvature implies a lesser curling problem. Therefore, the bending moment and thereby shrinking stresses should be reduced in order to minimize warpage. For a straight elastic beam, radius of curvature is also related to shrinkage as [33]:

$$R= c/2s$$

where C is the layer thickness and s is the layer strain. Larger strains will result in smaller radii of curvature and therefore larger curling. For the same radius of curvature, absolute curling amount increases as the dimensions of the parts are increased.

2.4.5 Stereolithography: Case study of warpage in a SFF technique

Stereolithography, one of the earliest SFF technology exhibited the problem of warpage during the part building process. SLA uses resin which undergo 5 to 7 vol% total volumetric shrinkage, of which 50 to 70 % occurs in the vat as a result of laser

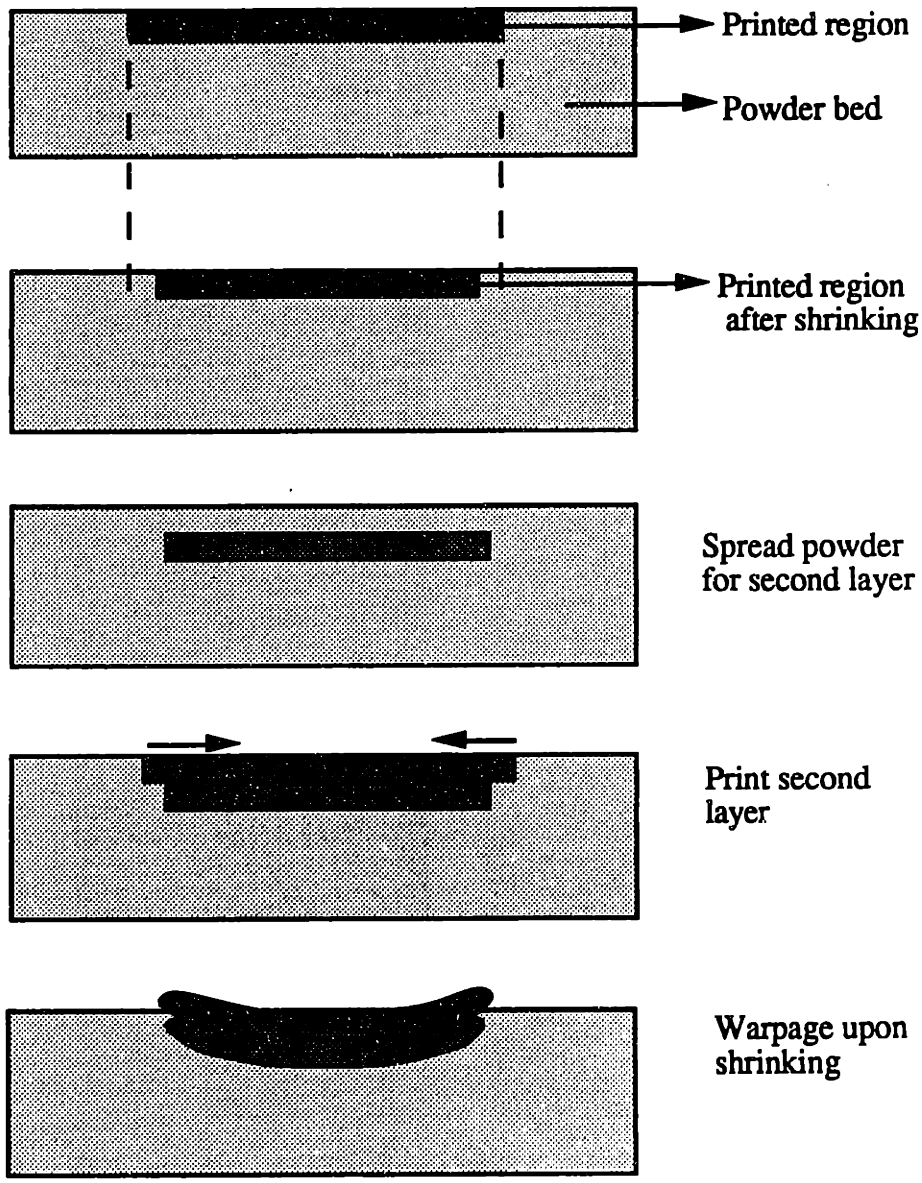

Figure 2.7: Schematic illustrating the mechanics of warpage behavior for a SFF process.

induced polymerization, while the remaining shrinkage occur during post curing step. The first layer shrinks without any distortion. The second shrinking layer induces an upward bending moment on the part and result in warpage. A new printing technique WEAVE™ was developed to reduce the warpage problem in stereolithography components [33,34]. The lines are cured at a spacing of 10 mils along y-axis, followed by a similar pattern filling in the orthogonal direction (x-axis). The lines along y-axis are neither connected to each other nor are they attached to the previous layers. The cured lines therefore undergo majority of shrinkage independently, before getting bonded to the previous layers during the x-axis scan at the intersection point. Efforts are also being made to develop new types of epoxy resins to minimize shrinkage upon polymerization .

2.5 Properties required in green preforms for making defect free fully dense ceramic parts

The ultimate objective of 3DP fine ceramics process is to make fully dense defect free parts. Fine grain microstructure is desirable for high performance and reliability. Researchers have evaluated the effect of various properties of the green body on their subsequent densification and distortion behavior during firing. This section summarizes the role of various attributes desirable in a green body to fabricate fully dense parts upon firing. The properties of an ideal green body will be used as a benchmark during the fine ceramics 3DP process development.

2.5.1 Use of fine powder

The densification of a particulate ceramic compact is referred to as sintering. Sintering is essentially a removal of the pores between the starting particles accompanied by the shrinkage of the component. The primary driving force for densification of compacted powder at high temperatures is the change in surface energy. Herring's [55] scaling laws are very useful to understand the particle size dependence of the sintering mechanism. The laws can be written in the following general form:

$$\left(\frac{\Delta t_2}{\Delta t_1}\right) = \left(\frac{R_2}{R_1}\right)^m$$

where Δt_1 is the time taken to produce a microstructural change in system 1, Δt_2 is the time taken to produce similar microstructural change in system 2, R_1 and R_2 are the radii of the particle sizes in systems 1 and 2 and 'm' depends on the mechanism of sintering. Lattice diffusion and grain boundary diffusion are the two main mechanisms of densification in polycrystalline ceramics. The value of 'm' is 3 for lattice diffusion and 4

for grain boundary diffusion. According to Herring's scaling law, the time taken to densify by a lattice diffusion mechanism increases as the cube of the particle size.

Kingery [57] derived the following equation for the mechanism of transport by lattice diffusion from the line of contact between two particles to the neck region:

$$\frac{\Delta L}{L_0} = \left(\frac{20\gamma a^3 D^{2/5}}{\sqrt{2}kT} \right) r^{-6/5} t^{2/5}$$

where $\Delta L/L_0$ is the linear shrinkage (equivalent to the sintering rate), γ is the surface energy, a^3 atomic volume of diffusing vacancy, D the self diffusion coefficient, k the Boltzmann constant, T the temperature, r the particle radius and t is the time. Therefore, finer particles can be sintered more rapidly and at a lower temperatures than coarser particles.

The densification of polycrystalline ceramic powder is normally accompanied by a coarsening of microstructure: the average size of the grains and average size of the pores become larger. Coarsening is more pronounced during the final stages of the sintering. Grain growth is either normal or abnormal. The grain sizes and shapes in normal grain growth are within a fairly narrow range. The distribution in grain sizes at a later stage during sintering is fairly similar to that at an early stage except for a magnification factor. Abnormal grain growth is characterized by the rapid growth of a few larger grains at the expense of the smaller ones. Rapid grain growth causes a drastic reduction in the densification rate. Prolonged firing times are therefore needed to achieve the required density, and this increases the possibility of for abnormal grain growth to occur. When abnormal grain growth occurs, the pores become trapped inside the the grains and become difficult or impossible to remove. Fine grain size is desirable as the fracture strength of many ceramics is found to vary as inverse square root of grain size. The presence of trace amounts of dopants can reduce the abnormal grain growth. Small amounts of MgO is added to alumina to reduce the abnormal grain growth [58,59].

Impurities in the form of inorganic inclusions can limit the powder densification and produce microcracks during cooling from the densification temperature or upon subsequent stressing. Impurities present as inclusions act as strength limiting flaws. The effect on strength will depend on the size of the inclusion compared to the grain size of the ceramic and on the relative thermal expansion and elastic properties of the matrix and inclusions. Elimination of agglomerates and inclusions will therefore improve the reliability of the ceramic products. Currently, the same 3DP machine set-up is used to fabricate parts out of a variety of different materials for investment casting, tooling and

structural ceramics applications. Extreme care should be practiced to avoid the contamination of one class of materials by another [60].

Binders are usually added to the ceramic powder to improve their processing and forming capabilities. Binders are usually organic and can leave a carbon residue if the temperature/time and atmosphere parameters are not properly controlled. The presence of residue affects the yield, performance and properties of advanced ceramics [56].

2.5.2 High green density

High green density ensures lower sintering temperature. A high green density means an increased number of particle contacts which in turn provides a greater driving force for sintering. This will result in faster sintering and at lower temperatures. A part with a low green density may not densify to full density even at very high temperatures. The big pores, as a result of low packing density, are more difficult to remove due to the kinetics to fill a larger pore by diffusion [61-63].

Bruch [62] studied the effect of green density on the densification rate. He proposed two different regimes of sintering: normal and subnormal as shown schematically in figure 2.8. Higher green density and higher firing temperature ensure densification in the normal regimes. He also reported that within the sub normal regime, sintering rate increased with increasing green density whereas within the normal regime, sintering rates decreased with increasing rates. The presence of non-uniform green density therefore would result in differential strain during densification.

The sintering kinetics is given by the following equation (Bruch):

$$P = C.t^{-n}$$

where P is the percent porosity after sintering, t is the sintering time, and C and n are constants for constant temperature and green density. The magnitude of 'n' within the subnormal regime, was experimentally observed to decrease with decreasing temperature and/or temperature, resulting in lower sintering kinetics than for compacts within the normal regime. The above observation is very well justified by the fact that loose powders exhibit little or no densification.

Increased density also statistically reduces the likelihood of defects. A uniform green compact leads to a uniform sintered piece with few defects and little susceptibility to cracking.

A low relative shrinkage is desirable to avoid warpage during firing. Table 2.1 shows the calculated values of relative shrinkage in green bodies with initial packing densities of 30 and 50 vol%. Both the samples were assumed to have a non-uniformity of

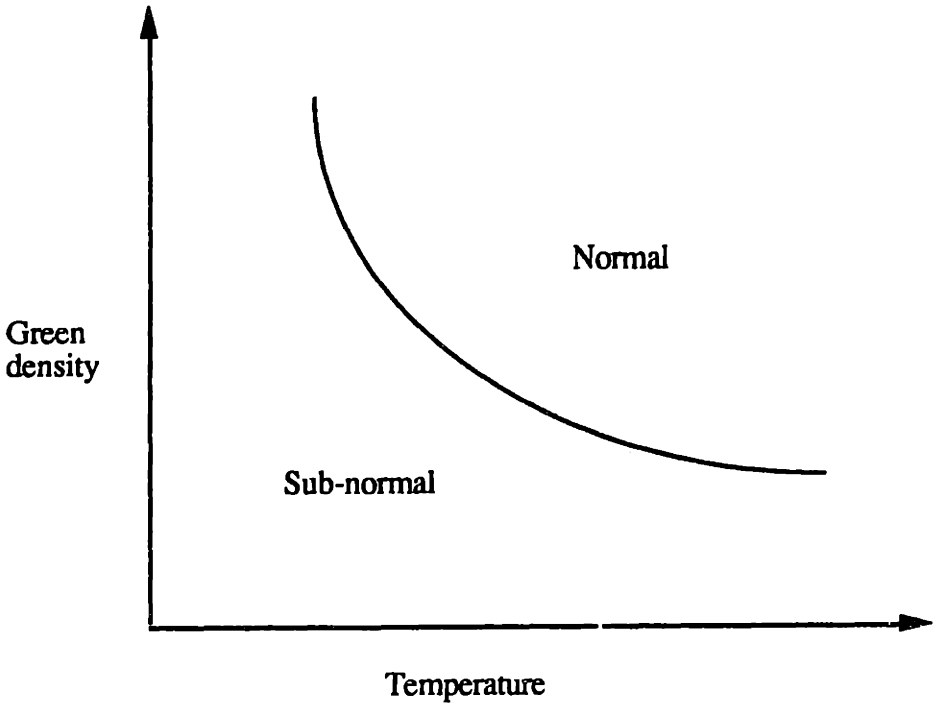

Figure 2.8: Bruch's sub-normal and normal sintering regimes in green density and temperature space.

Table 2.1: Calculated absolute and relative shrinkages for 30 and 50 vol% dense green bodies with a non-uniformity of 1 vol% each.

Initial density (vol%)	Final density (vol%)	Absolute shrinkage (linear %)	Relative shrinkage (linear%)
30 (non-uniformity 1vol%)	60	20	0.87
50 (non-uniformity 1vol%)	60	5.5	0.62

1% and densified to the same final density. The samples with higher packing density exhibit not only lower absolute shrinkages but also lower relative shrinkages.

The selection of particle size and its distribution and particle shape will affect the packing density and the pore size of the green body. M. Sachs [64] has studied the effect of particle size distribution on the sintering of alumina. Two sets of powders with an average particle size of 0.4 μm were used. Both the powder batches had log normal distribution, one with standard deviation of 1.3 while the other one at 2.4. The slip cast samples with broad size distribution (BSD) resulted in higher relative density (73%) and smaller median pore channel radius (29 nm) as compared to the narrow size pore distribution (green density ~65% and pore channel radius ~50 nm). These results indicate that finer particles are filling the interstices formed by larger particles in the sample with broad size distribution. Both the batches achieved the same final density, but the one with BSD had an advantage of less total shrinkage during densification. Similar grain sizes were reported for both the samples. A reduction in the overall shrinkage is helpful in achieving dimensional tolerances and minimizing differential shrinkage in large bodies.

It is experimentally well established that compacts with fine and homogenous pores sinter best. Harmer [65] have extensively studied the role of pore size distribution on the microstructural development during sintering. Narrowing the pore size distribution have been reported to inhibit the grain growth and also increase the densification rate. Mercury porosimetry studies have shown that the pore size distribution in a sintered compact is predetermined to a large degree by the original particle packing arrangement in the powder compact. It has been shown for alumina that increasing the packing density narrows the pore size distribution and therefore increase the densification rate.

Particle shape can also be important. A high concentration of elongated or flattened particles can result in bridging during forming, producing a large or irregularly shaped pore that is difficult to remove during sintering.

2.5.3 Uniform green density and microstructure

It is experimentally very well established that the presence of non-uniform packing density within a green preform would result in defects upon firing. These defects affect the reliability of the components. Non-uniformity could be introduced in the part either due to the presence of agglomerates in the starting material or during shape forming process [12,60,63,66].

Fine powders tend to agglomerate due to Van der Waals's force. Rumpf [14] has shown that the presence of adsorbed moisture also increases the cohesiveness of the fine

powder due to capillary forces. The presence of these agglomerates introduce non-uniformity in the part.

The green bodies formed by dry pressing have non uniform density due to the pressure gradients generated by frictional forces between the powder and dies. Gas entrapment in the ceramic paste and the presence of lamination and fold lines result in non-uniform microstructure during injection molding and extrusion. Particle segregation during casting due to settling result in variable density regions in the green body.

Lange [12] had shown that the presence of an agglomerate or a region with a packing density different than the bulk of the body (matrix) could potentially result in defects upon firing. Specimens containing low-green density agglomerates produced circumferential crack like voids at the agglomerate/matrix interface. Agglomerates with a higher density than the matrix are subjected to tangential tensile stress resulting in radial cracks. The presence of crack like voids due to differential sintering not only produce less than fully dense bodies but are also a potential source of fracture. The fracture strength is inversely proportional to the square root of the crack length and the crack size is proportional to the agglomerate size. The fracture strength therefore would be inversely proportional to the square root of the agglomerate size.

Non-uniform packing density also results in undesirable abnormal grain growth. However, a combination of high purity and doping can make grain growth independent of the density.

Many of the heterogeneities including agglomerates can be removed by colloidal approaches to powder preparation [67-69]. Repulsive interparticle forces are used to overcome the long range London - Van der Waals force holding the fine particles as agglomerates. As received dry powders are dispersed in an appropriate fluid that produces interparticle repulsive forces. There are two general ways of stabilizing a colloidal suspension: electrostatic stabilization and steric stabilization. The particles are charged in the electrostatic stabilization method to provide electrostatic repulsion between particles. Colloidal particles when placed in an aqueous or other highly polar medium attract counter-ions from the fluid to the particle surface. It results in an increased concentration of counter-ions next to the particle surface relative to that in the bulk of the solvent. This arrangement is known as diffuse double layer. As particles with extended double layers approach each other, net repulsion occurs between the similarly charged particles.

In non-polar organic solvents, the colloidal particles are stabilized by attaching macromolecules to the surfaces of the particles. Steric hinderance provided by the attached macromolecules create the repulsive force necessary to overcome the attractive VDW

force. The steric repulsion is proportional to the thickness of the adsorbed layer and the chemical nature and concentration of the adsorbed chain.

These repulsive forces keep the particles apart once shearing forces break the weak agglomerate. Partially sintered and other hard agglomerates which can not be broken apart can be separated by sedimentation or centrifugation. Both electrostatic and steric stabilization techniques were used to prepare colloidal alumina suspensions for this research (chapters 5 & 7).

CHAPTER 3
PRESS-ROLLING OF FINE POWDER

3.1 Introduction

3DP has successfully demonstrated the fabrication of complex parts for investment casting and tooling industry. All these earlier applications made use of coarser particles which could be easily spread into a uniform and defect free layers. One of the main challenges in adapting 3DP technology to fabricate structural ceramics components was to devise a process to deposit fine powders via 3DP. The use of fine powders in making fully dense ceramics is desirable for its high sinterability. The densification of the fine ceramics is governed by solid state diffusion and is accelerated by the use of high surface area fine ceramic particles. Fine powders not only reduce the sintering temperatures but also result in fine grained microstructures necessary for superior mechanical properties.

Fine powders in the dry state tend to agglomerate due to Van der Waal's attractive force. As a result, when these agglomerated units are used as the building blocks of a green compact, wide variations in the pore size distribution are inevitably introduced into the compact. The advantage of using submicrometer sized particles is then lost, since these inhomogeneities introduced into the powder compact, in much larger scale than the primary particles themselves will control the evolution of the microstructure during sintering [12, 13, 14]. In addition, the presence of these rough irregular shaped agglomerates also reduces the flowability of fine powders and will make the powder spreading step of 3DP process a difficult operation. Therefore, in order to take advantage of these fine particles, techniques must be developed to pack these particles without any agglomeration. The first-generation process, termed as 'Press-Rolling process', used dry powder processing since minimal modification of the existing 3DP process was required. The purpose of the first-generation process, developed by Yoo et. al. [42], was to demonstrate the feasibility of fabricating structural ceramic components by 3DP.

The first section of this chapter briefly describes the press-rolling process and evaluates the microstructural uniformity of the green parts made by using this process. The latter half of the chapter correlates the microstructure and deformation behavior of the green parts during isopressing operation. It also describes strategies to minimize the anisotropy in structural ceramic parts built by press-rolling process.

3.2 Description of the 'Press-Rolling' process

Figure 3.1 shows a typical powder spreading sequence, termed as 'Counter-Rolling process', used by the 3DP process for the earlier applications. Powder is poured

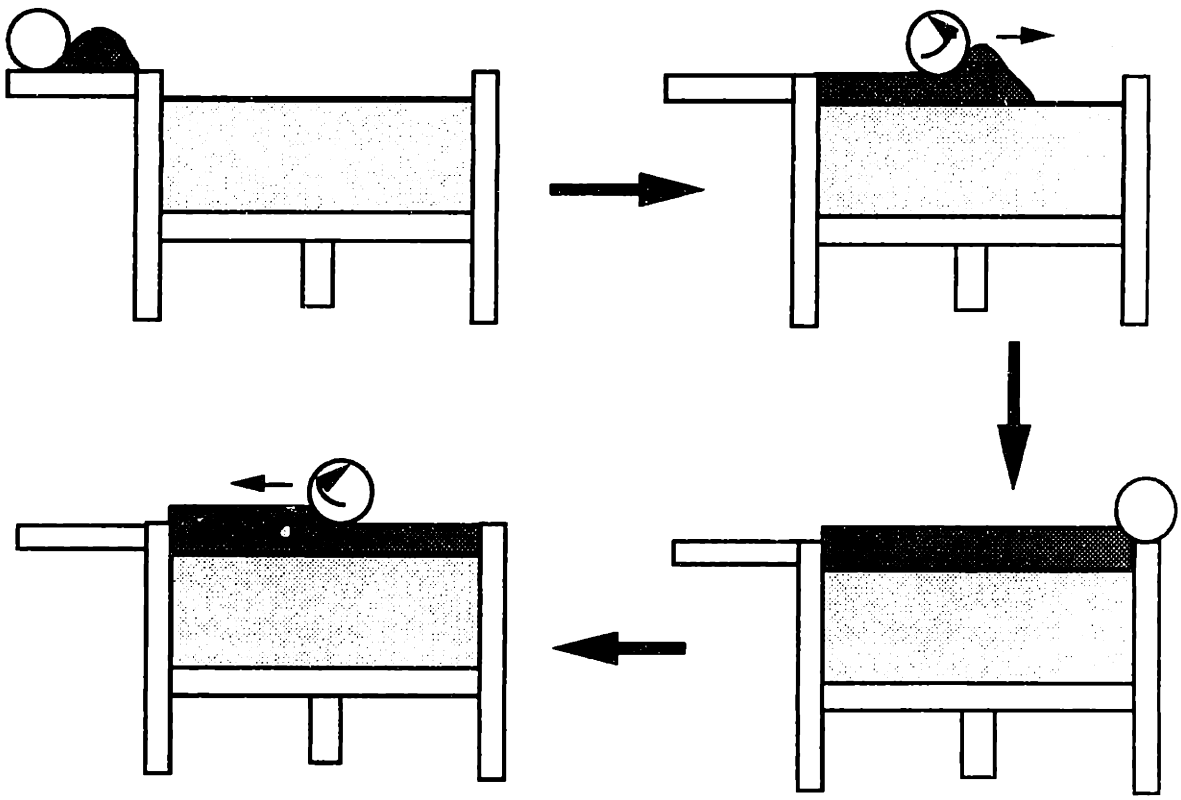

Figure 3.1: Schematic of the counter-rolling sequence.

in the form of a thin bead at one corner of the piston and the piston is dropped by 238 μm. The spreader rod which consists of a roller rotating counter-clockwise is then used to spread the powder across the piston. The piston is raised by 63 μm in the reverse pass, and the roller rotating counter-clockwise is used to do the final leveling of the powder bed. The resulting layer thickness is ~ 175 μm. Fine powders did not flow well enough to spread into defect- free layers with the conventional spreading technique. The defect consisted of big craters formed on the powder surface as a result of poor flowability of the powder. The low flowability also resulted in low packing density (28%) of the powder bed.

A press-rolling technique was devised by Yoo et. al. [42] to address the above-mentioned problems. Yoo sieved the as-received alumina powder and selected the agglomerates between the size range of 75 and 100 μm for the spreading experiments. The technique, as shown in Figure 3.2, consists of spreading fine agglomerates via counter-rolling in the front pass. The piston is then raised to partly expose the loose packed powder layer. On the return pass, the load is applied by press-rolling to compact the agglomerates. The layer thickness of the compacted layer was 127μm. This technique appeared to produce defect-free layers with a powder packing density of ~ 40%. Table 3.1 describes the machine parameters used by conventional counter-rolling and press-rolling spreading techniques.

3.3 Properties of green part

J. Yoo successfully fabricated parts out of fine powder by printing 6 vol% acrysol, a latex emulsion, into the powder bed. The cohesive strength of the powder bed was remarkably high and did not exhibit any powder ejection during printing. The packing density of the printed part was ~ 40%, not high enough to achieve full densification by pressureless sintering. Figure 3.3 shows the SEM of a polished cross-section of a green part made by press-rolling technique. The micrograph clearly shows the presence of large agglomerates and big pores detrimental to the densification process. Individual layers were easily distinguishable in the printed part. Interlayer defects, therefore, reduce the isotropy of the printed part along the z-axis. A post-densification step in the form of iso-pressing was therefore necessary not only to increase the packing density to a critical value but also to break all the agglomerates to achieve a uniform packing density before the firing step. Isopressing was also found to heal the interlayer defects, thereby increasing the uniformity within the pressed parts. Figure 3.4 shows the overall linear shrinkage of the parts made by the press-rolling technique between the green and the fired state in various directions. The average linear shrinkage is in the order of ~ 30%. The number

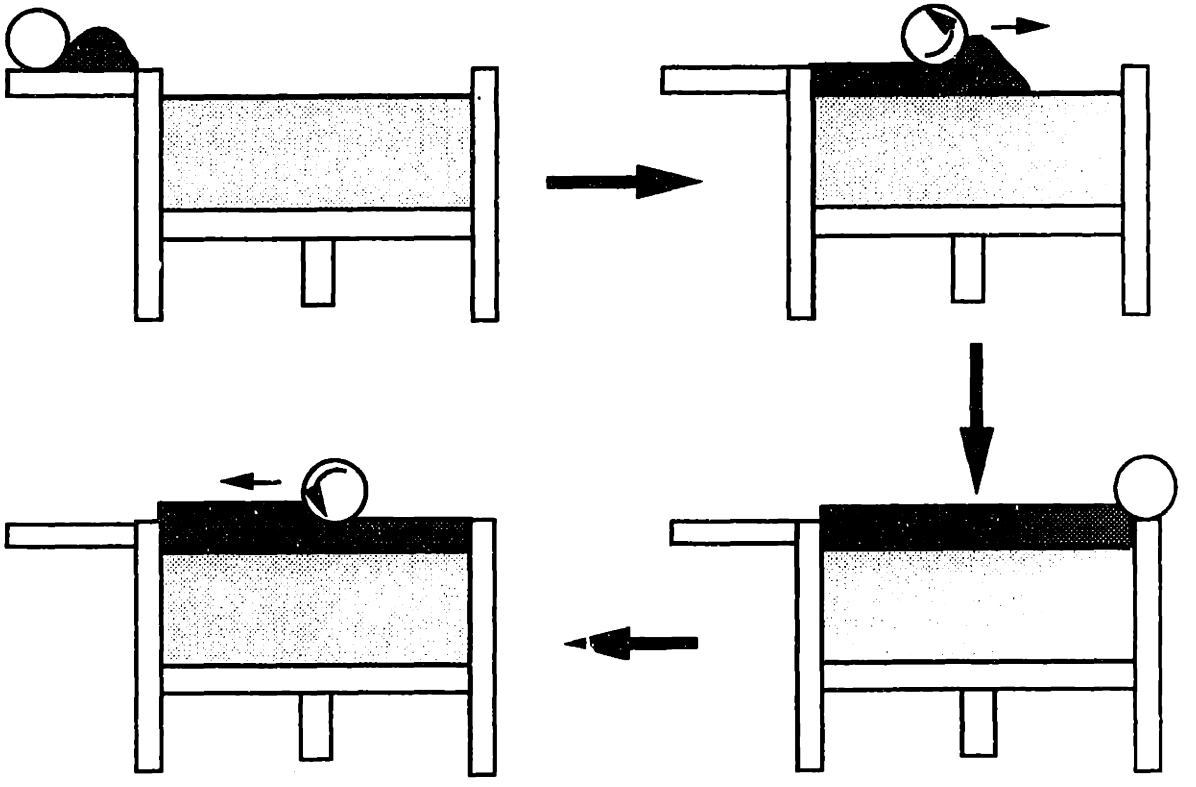

Figure 3.2: Schematic of the press-rolling sequence.

Table 3.1: Machine parameters for the counter-rolling and the press-rolling spreading techniques.

Machine parameters	Counter-rolling technique	Press-rolling technique
Traverse speed (Slow-axis speed)	50 mm/sec	25 mm/sec
Roller speed	45 mm/sec	15 mm/sec
Roller vibration frequency	400 hz	400 hz

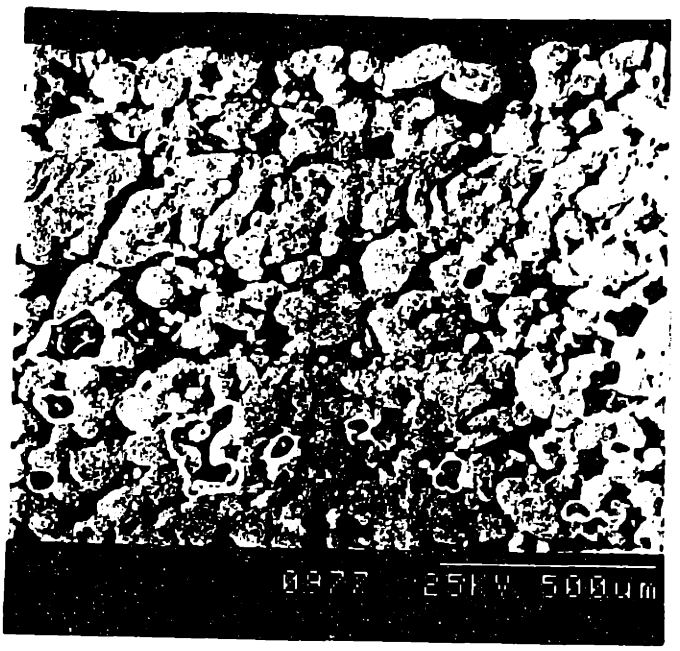

Figure 3.3: SEM micrograph showing the polished cross-section of a green part made by the press-rolling process.

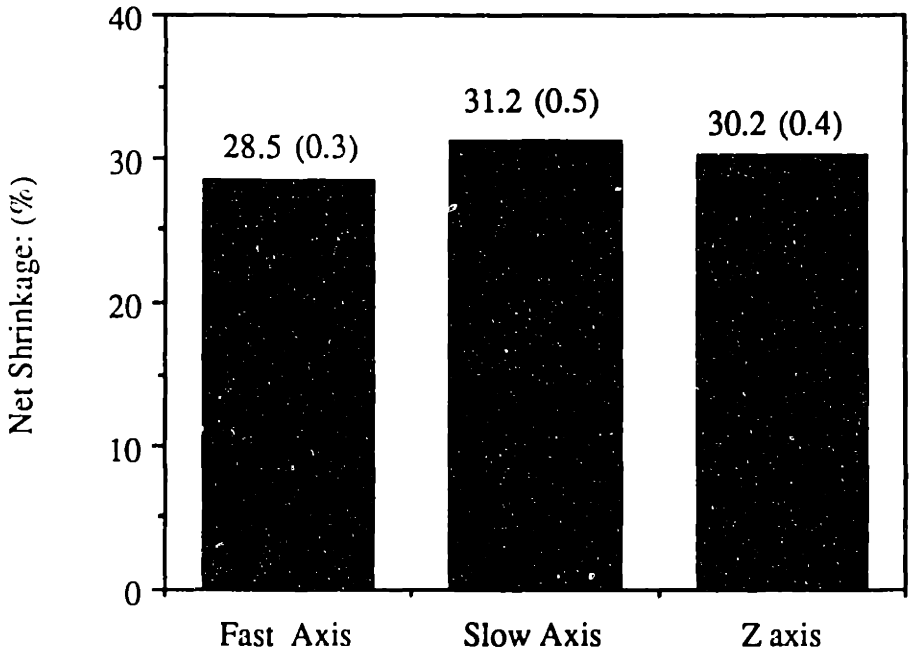

Figure 3.4: Measured shrinkage values of green part after isopressing and firing step in various directions. (Yoo)

within the brackets indicate the standard deviation values. The low deviation values indicate fairly reproducible shrinkage.

Compaction of ceramic powders depends on the strength and the nature of the agglomerates. Hard agglomerates are detrimental to the compaction process [13,59]. The presence of unbroken agglomerates not only reduces the green density of the compact but also acts as strength limiting flaws. The sinterability of the fine powders is destroyed if they are bound together as agglomerates. Agglomerates introduce inhomogeneity in the green parts and result in non-uniform microstructure, upon firing, in the finished parts. Microstresses develop within a shrinking body with a non-uniform green density distribution, resulting in cavities and cracks within the sintered part [12].

3.4 Distortion during isopressing

During the isostatic pressing operation, the green bodies prepared by the press-rolling process showed (Figure 3.5) two generic types of distortion: shear distortion and z-axis warpage. Systematic experiments were conducted to determine the factors responsible for these distortions and the understanding was then subsequently used to improve the processing steps so as to eliminate them.

3.4.1 Shear distortion

3.4.1.1 Characterization

Rectangular bars (length: 37 mm, width: 5 mm, thickness: 5 mm) were made by printing 6 wt% acrysol on press-rolled alumina powder to quantify the distortion behavior. The printed bars were warm isostatically pressed (WIP ~ 80 C) at 40,000 psi for 10 minutes. The parts were subsequently fired to 1650 C for 4 hours.

The shear angle of green, wipped and fired parts were measured by taking photomicrographs of the corresponding polished cross-sections. Figure 3.6 shows the optical micrograph of a polished cross-sections of a wipped part.

3.4.1.2 Results and discussions

The shear angle measurements for green, wipped and fired bars are shown in Figure 3.7. The green bars show a slight shear after the build process, in the order of 1^{o}. However, upon wipping, the shear angle accentuates to an average of 7.5^{o} (standard deviation of 1.87^{o} for 6 samples). The topmost layer of the part shows the maximum absolute shear displacement. The shear angle stays constant at 7.5^{o} after firing.

The anisotropic deformation response is due to the non-uniform microstructure of the preform, since the deforming pressure is isotropic. The microstructure of a green

1. Shear distortion

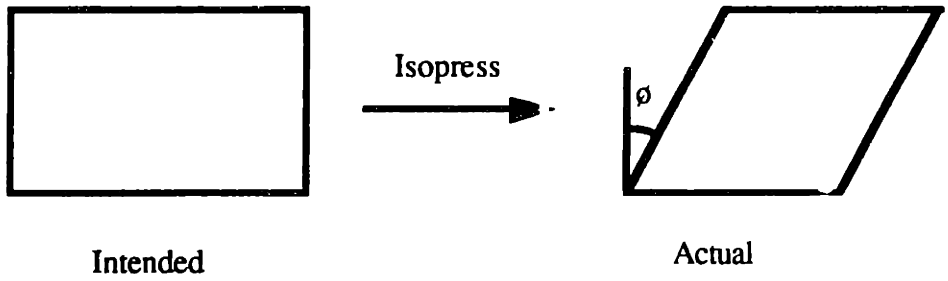

2. Z-axis warpage

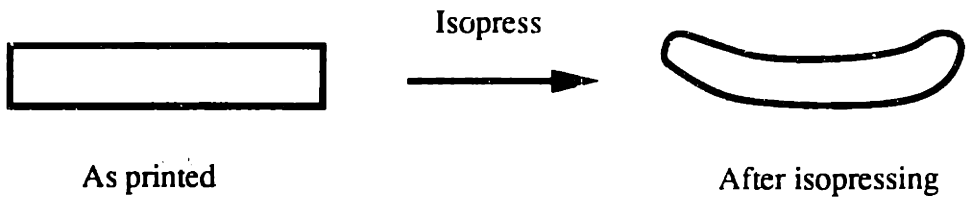

Figure 3.5: Schematic of shear distortion and z-axis warpage.

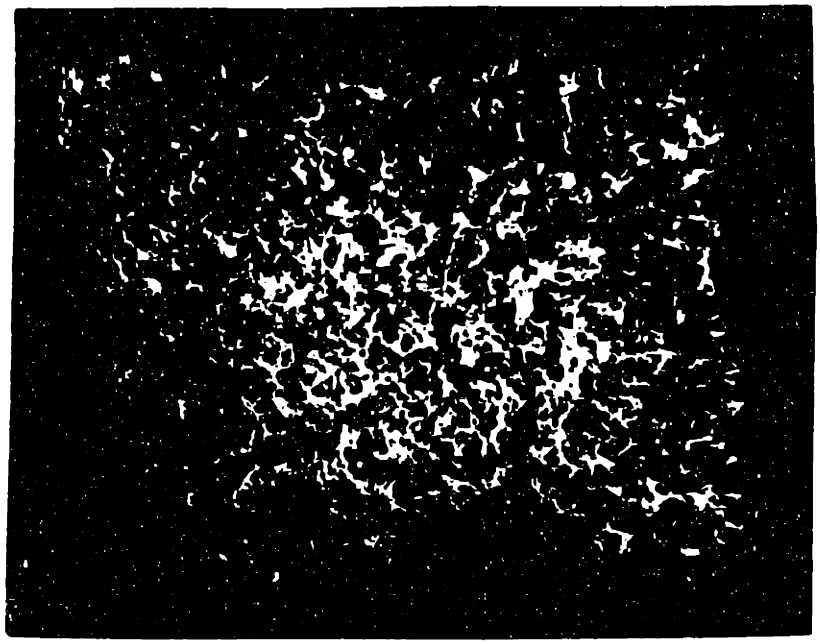

Figure 3.6: Optical micrographs showing the polished cross-section of a wiped part.

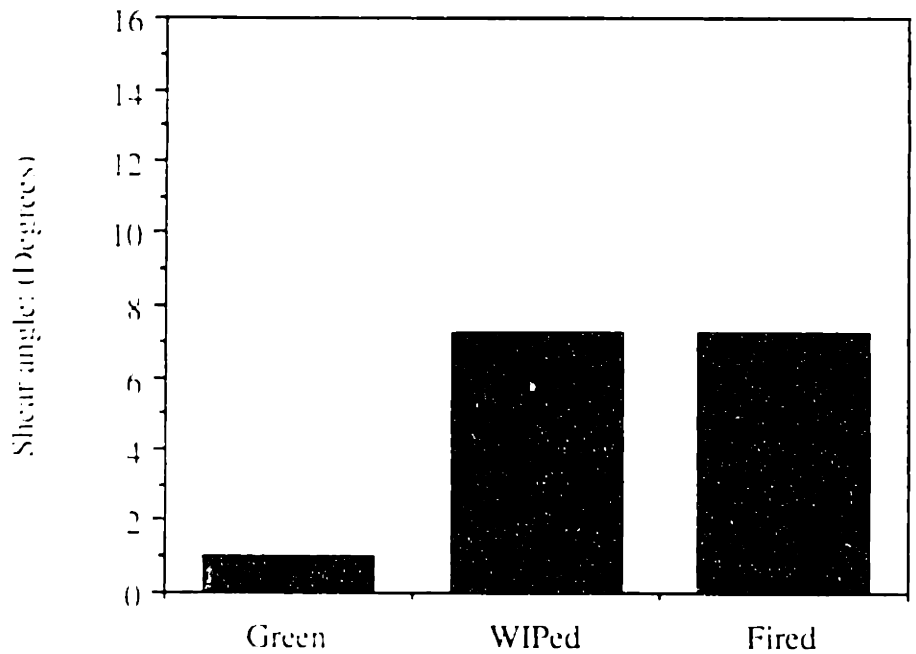

Figure 3.7: Shear angle distortion values of a green, wiped and fired press-rolled [illegible]

press-rolled part is shown in Figure 3.3. It shows the presence of elongated trapezoidal pores in the spread powder layers along the direction of press-rolling. The basic microstructural unit of spread powder layers, therefore, is highly anisotropic. The transverse roller speed is 25 mm/sec while the linear speed of the roller at the point of contact with the powder is 15 mm/sec in a press-rolling operation. This will provide a net downward shear force in the transverse direction to deform the agglomerates creating elongated pore-structure in the green preforms.

The response of these anisotropic elongated trapezoidal pores to isostatic pressure is shown schematically in Figure 3.8. The applied pressure on the volume elements enclosing the trapezoidal pores during isopressing is equal in all the directions. However, if the mechanical strength of the volume elements is different in slow and 'z' axis, then one side can preferentially fail before the other, even with the isostatic pressure. Giritloglu [70] and Bang [71] have shown that the parts made by conventional 3DP process exhibit anisotropic mechanical behavior. Therefore, even though the applied pressure is isostatic, the anisotropic mechanical properties of the part will allow one side of the trapezoidal volume element to fail preferentially before the other during isopressing. The collapse of the pore, as a result, will introduce a relative shear between the volume element on the top and the bottom of the trapezoid. Figure 3.8 shows schematically the effect of the deformation behavior of trapezoidal pores on the bulk deformation response. The trapezoidal pores are lined up next to each other within the same layer. The collapse of individual pores within layer 1 will therefore shear the corresponding volume element located right above in layer 2. The net result will appear as a bulk shear between the two layers. Layer 3 will shear when the pores in layer 2 collapse. Since layer 2 has already sheared due to the collapse of pores in layer 1, layer 3 will in effect undergo a cumulative shear of layer 1 and 2. The topmost layer of the part will therfore exhibit the maximum amount of absolute shear since it is riding on the largest number of layers with elongated pores.

3.4.1.3 Strategies to avoid shear distortion

The microstructure of the spread press-rolled layers was made more isotropic by bi-directional press-rolling, which introduced trapezoidal pores in opposite directions in subsequent layers. Figure 3.9 shows the schematic of the new bi-directional press-rolling spreading sequence. Figure 3.10 shows the microstructure of a green compact made with the bi-directional press-rolling sequence. The basic microstructural unit of the powder bed prepared by bi-directional pressing consists of two layers with trapezoidal pores in opposite directions. Figure 3.11 shows the polished cross-section of a part made by this

Micromechanics : Weakest link failure

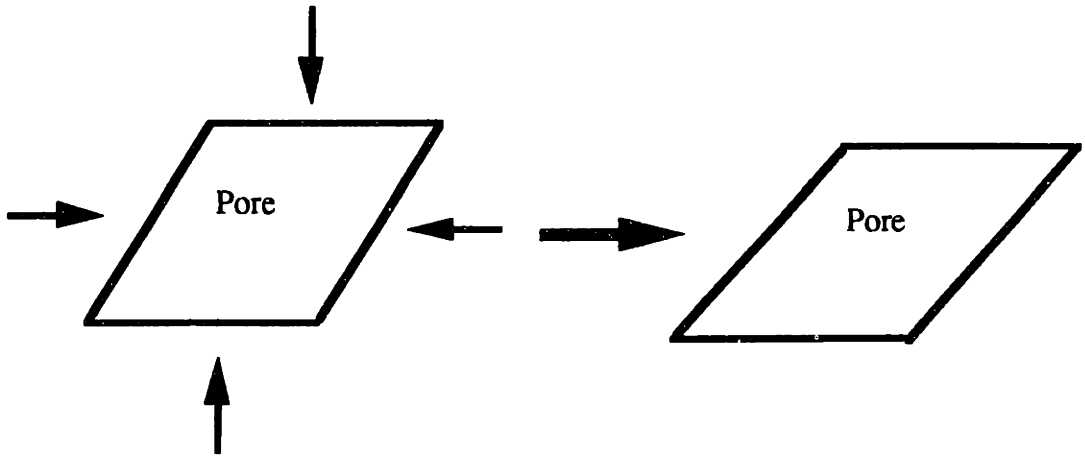

Macro-mechanics: Shear angle accentuation upon WIPing

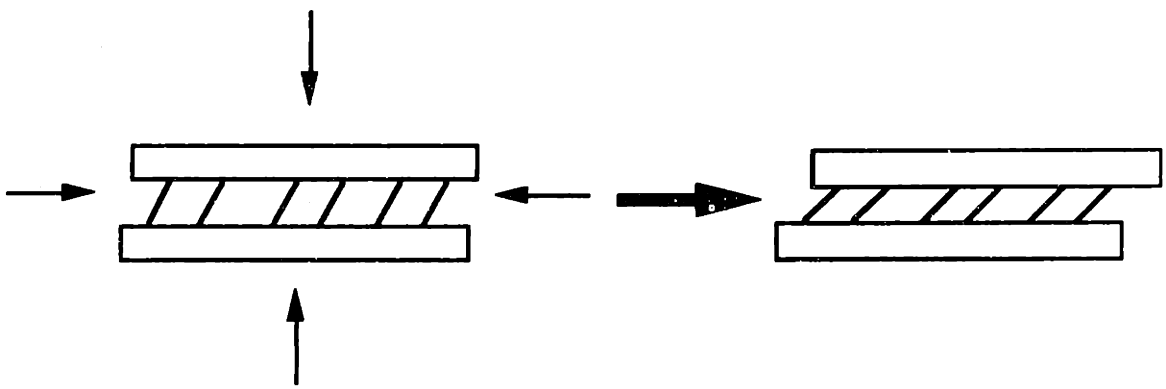

Figure 3.8: Micro and macro-mechanics of the pore collapse model.

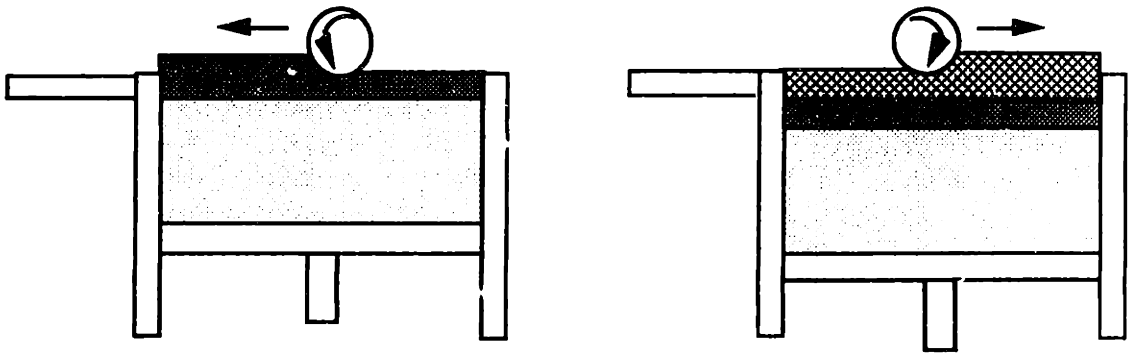

Figure 3.9: Schematic of the bi-directional press-compaction technique involving press-rolling in opposite directions in subsequent layers.

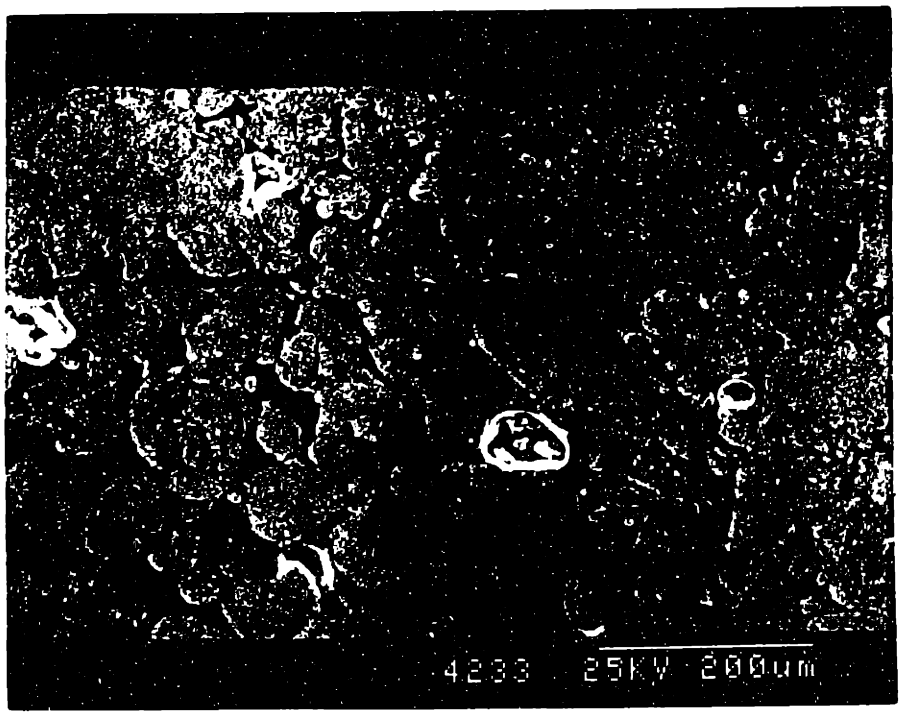

Figure 3.10: SEM micrograph showing the polished cross-section of a green part made by the bi-directional press-rolling process.

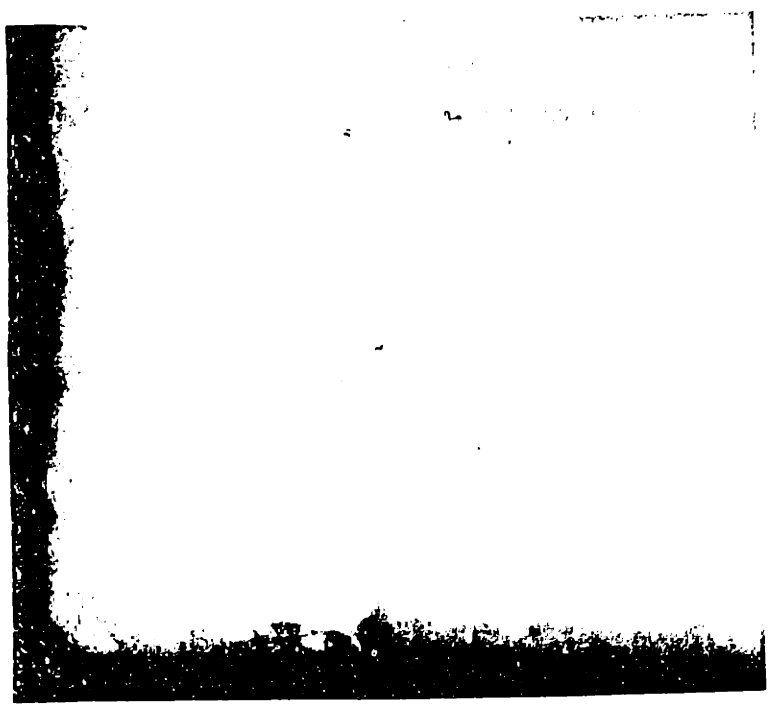

Figure 3.11: Optical micrograph showing the polished cross-section of a green part made by the bi-directional press-rolling process.

method and wipped at 40,000 psi for 10 minutes. The micrograph clearly shows the absence of shear distortion in the wipped part. The shear produced in layers with trapezoidal pores along one direction is cancelled by the shear produced in alternate layers with pores in the opposite direction. The net result is the elimination of shear distortion from the press-rolled parts.

3.4.2. Z-axis distortion

3.4.2.1 Characterization

The green printed part made by the press-rolling process did not show any z-axis warpage. However, upon wipping the parts warped along the top surface. The warpage was quantified using an optical microscope with a calibrated eye-piece. The top surface of the printed bar along the length direction was brought into focus with the optical microscope. The focusing knob position does not change over the entire length of an ideal flat surface. The focusing knob position, however, has to be changed to focus on the entire length of an undulated surface. Since the focusing knob is calibrated, the change in position of the knob can be effectively used to quantify the z position of any surface.

3.4.2.2 Results and discussions

Figure 3.12 shows the warpage behavior of a press-rolled bar upon wipping. The printed part bends towards the top surface upon wipping. The anisotropic response of the samples lead us to believe that the preforms were not uniform, since the applied stress during isopressing is isotropic. The bulk packing density of the green samples is 40% and that of the wipped samples is 60%. Theretore, the green samples shrink linearly by ~ 12.6% during wipping. The non-uniformity in the packing density of the printed parts could lead to warpage upon densification due to differential shrinkage [2, 12]. The press-rolled powder bed does not show any particle rearrangement during printing, therefore, the non-uniformity is introduced during the powder spreading stage. The packing density of the powder bed was measured as a function of their thickness to assess the uniformity along the z-axis. The data are shown in figure 3.13. The packing density of the lowermost layers of the powder bed have higher density than the top layers. The bottom few layers are pressed against the solid aluminum piston surface which can lead to better compaction than the top layers where the powder is being crushed against the press-compacted powder surface. However, the powder packing density stabilizes as the thickness of the powder bed increases. All the parts were printed after spreading seven foundation layers, therefore, there was a built in packing density variation within the printed part. The bottom layers have higher packing density than the top layers. The top

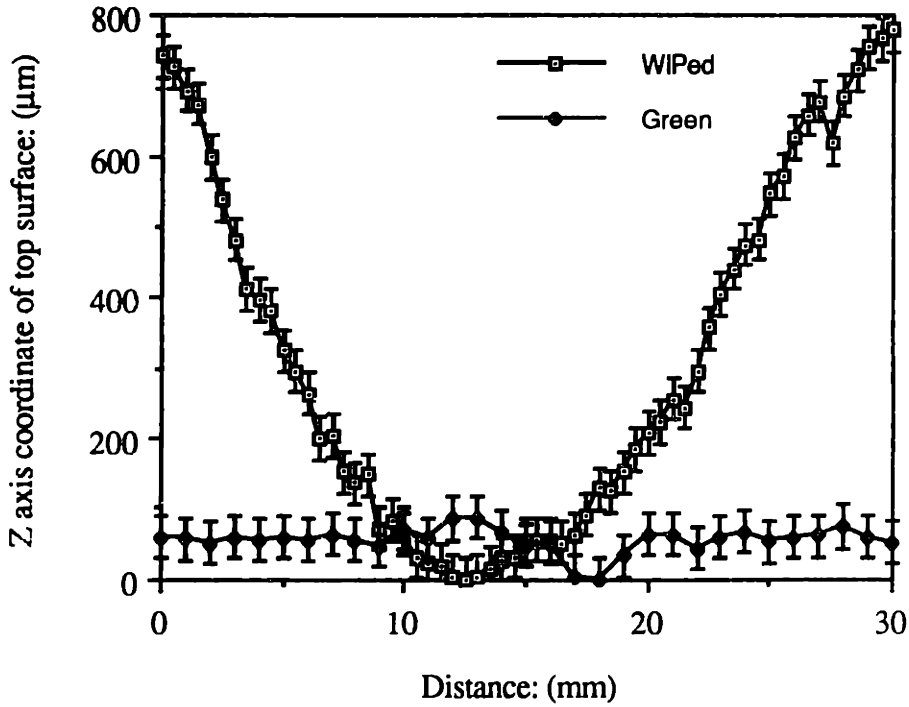

Figure 3.12: Measured z-axis warpage of a green and WIPed press-rolled bar.

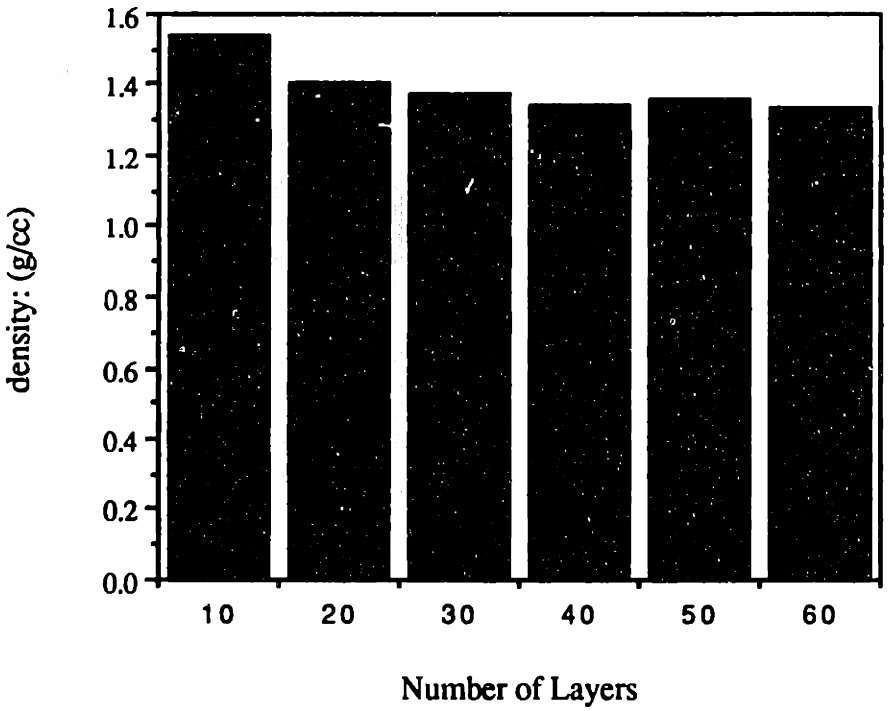

Figure 3.13: Packing density of the press-rolled powder bed as a function of built thickness.

layers shrink more than the bottom layers resulting in z-plane upward warpage upon wipping.

The parts made by the press-rolling method also showed a variable z-axis warpage behavior within the same printed batch as shown in Figure 3.14. This data indicate non-uniformity of packing density within the same spread powder layer. The press-rolled powder bed is also very cohesive and creates problems in removing loose powder from within the printed part. These issues were addressed in our second-generation process where the problems due to the poor flowability of the as-received fine powder were eliminated. Our strategy was borrowed from the dry-pressing industry where granulated spray dried powder is routinely used to improve the flowability of the fine powder for easy die-fill operation.

3.5 Conclusions

Anisotropy was created in the powder bed during the powder spreading stage of the press-rolling technique. The fine powder used in the press-rolling process consisted of non-uniform agglomerates and resulted in inhomogeneities in the powder bed. The uni-directional press-rolling of fine powder introduced elongated trapezoidal pores in the spread layer. The basic microstructral unit of such a layer has no symmetry. The microstructure of the spread layer was made more isotropic by bi-directional press-rolling which introduced trapezoidal pores in opposite directions in subsequent layers. The packing density of the printed part is ~40%, not sufficient to full densification by pressureless sintering. Individual layers were also easily distinguishable in the printed part. Interlayer defects, therefore, reduced the symmetry of the printed parts along the z-axis. A post-printing step, isopressing, was employed to achieve high and uniform packing density in the printed parts. Isopressing was also found to heal the interlayer defects, thereby increasing the uniformity within the pressed part. The anisotropic uni-directional press-rolled green parts exhibited shear distortion during the isostatic pressing operation while the more symmetric bi-directional press-rolled parts did not exhibit shear distortion. The anisotropic deformation behavior of the volume element around the trapezoidal pore was shown to explain the shear distortion phenomenon. The press-rolled components were also shown to have intrinsic packing density variation within the printed part which resulted in warpage during isopressing.

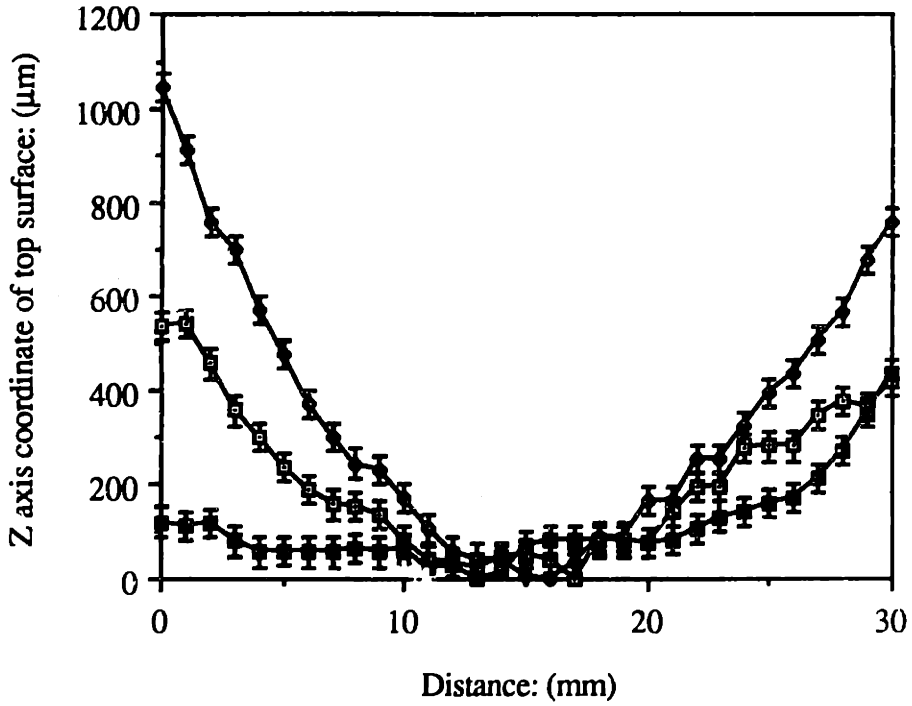

Figure 3.14: Variation in z-axis warpage exhibited by the green samples, built at various locations within the same powder bed, during isopressing.

CHAPTER 4
PRINTING ON SPRAY DRIED GRANULES

4.1 Introduction

One of the main problems of the press-rolling process is the poor flowability of fine powders which results in non-uniform density within the printed parts and creates an array of distortion problems during post-processing. The problems of poor flowability of fine powders have been solved by the use of spray dried granules in the dry-pressing industry [72,73]. Spray dried granules are porous spherical agglomerates that are bonded together with an organic phase.

Spray drying consists of atomizing a ceramic slurry into a turbulent heated stream inside an enclosed drying chamber where the droplets are dried quickly. Water evaporation takes place at an extremely rapid rate due to the large surface area of the droplets. The dried spherical droplets are collected in the bottom of the drying chamber, while the fines are carried out by the air stream and recovered in the cyclone collectors. Although, air inlet temperatures as high as 300 C are typically used, the particles being dried never attain these temperatures due to water evaporation and short flight times. These factors permit the use of many binders which are temperature sensitive since the product experiences moderate temperature for short times. Bulk density and physical characteristics of the granules are a strong function of the slurry properties such as surface tension, viscosity, solids content, binder type and spray drying operational conditions. Bulk density remains essentially constant for a powder lot. A lack of fines improves the flowability of the spray dried granules.

Alan Lauder [74] was the first 3DP researcher to use SD alumina granules as a feed stock for the powder bed. SD granules were spread with a counter-rolling technique and were reported to have an excellent flowability. Extensive warpage was reported as a major problem in the parts made by printing silica on SD alumina granules. The warpage was quoted to be so extensive that making multi-layered parts was almost impossible. No explanation was offered for this observation.

It is necessary to understand the factors controlling the warpage of SD printed parts in order to utilize the good flowability of the SD granules. Warpage is a manifestation of stresses created within the printed components due to shrinkage. These shrinkage stresses can distort, and in extreme cases, can delaminate the built parts, and are therefore undesirable in 3D printing process. SD granules have shown to accentuate the extent of warpage. SD granules, therefore, are ideal material systems to investigate the effect of various parameters controlling the shrinkage of the parts made by the 3DP

process. The results of this study will not only improve the current system and but will also help in developing new systems with minimal shrinkages.

This chapter first describes the preparation and the properties of SD alumina granules used for the warpage studies. The second half of the chapter discusses the key mechanisms controlling the shrinkage and subsequently warpage in 3DP components made out of spray dried granules. This understanding is then used to develop strategies to reduce distortion in SD granule parts. Finally, the properties of green body and the post processing necessary to achieve full density alumina parts are discussed.

4.2 SD granules preparation

Submicron alumina powder (RC-172 DBM),with an average primary particle size of 0.8 μm, was used as a starting material for spray dried granules (SD). Surface area of alumina powder was measured by nitrogen BET as 7.4 m^2/g. The three different organic systems; Polyethylene glycol (PEG, MWt. 4600), Polyvinyl alcohol (PVA, MWt. 9000 - 10,000) and Polyacrylic acid (PAA, MWt. 90,000) were chosen as binders for SD granules, with an objective of achieving a wide range of dissolution characteristics of organic additives in the printed solvent. The aqueous slurries (25 vol%) for spray drying were electrostatically stabilized at pH 3.5 with nitric acid for the binders PEG and PVA. Alumina slurry containing PAA did not require any pH adjustment as PAA acted as a dispersant as well as the binder. Organic additives were added at a concentration of 2% of the dry weight of the powder in the suspension. Low molecular weight PEG and atactic PAA dissolved easily in cold water. PVA does not disolve in cold water easily, therefore water had to be heated to 80^0C in order to dissolve PVA readily [75]. Octyl alcohol was used as a defoaming agent.

The powder was granulated by spray drying a 25 vol% alumina suspension at inlet temperatures ranging from 300 - 330^0C. The outlet temperature ranged from 100 - 130^0C and the volumetric feed rate was maintained at 45ml/min with a peristaltic pump. Thermogravimetric analysis (TGA) of spray dried granules shows no loss of organic phase during spray drying operation (figures 4.1 and 4.2). Granules were sieved through -270 mesh screens to remove the abnormally bigger agglomerates and flakes of granule crust originating from the wall of the dryer. The average particle size of the granules was determined from SEM micrographs. Agglomerate bulk densities were calculated using a mercury porosimeter. The packing density of the powder bed was calculated by spreading known volumes of different powders on the 3DP machine, using counter-rolling spreading parameters and then measuring its corresponding mass.

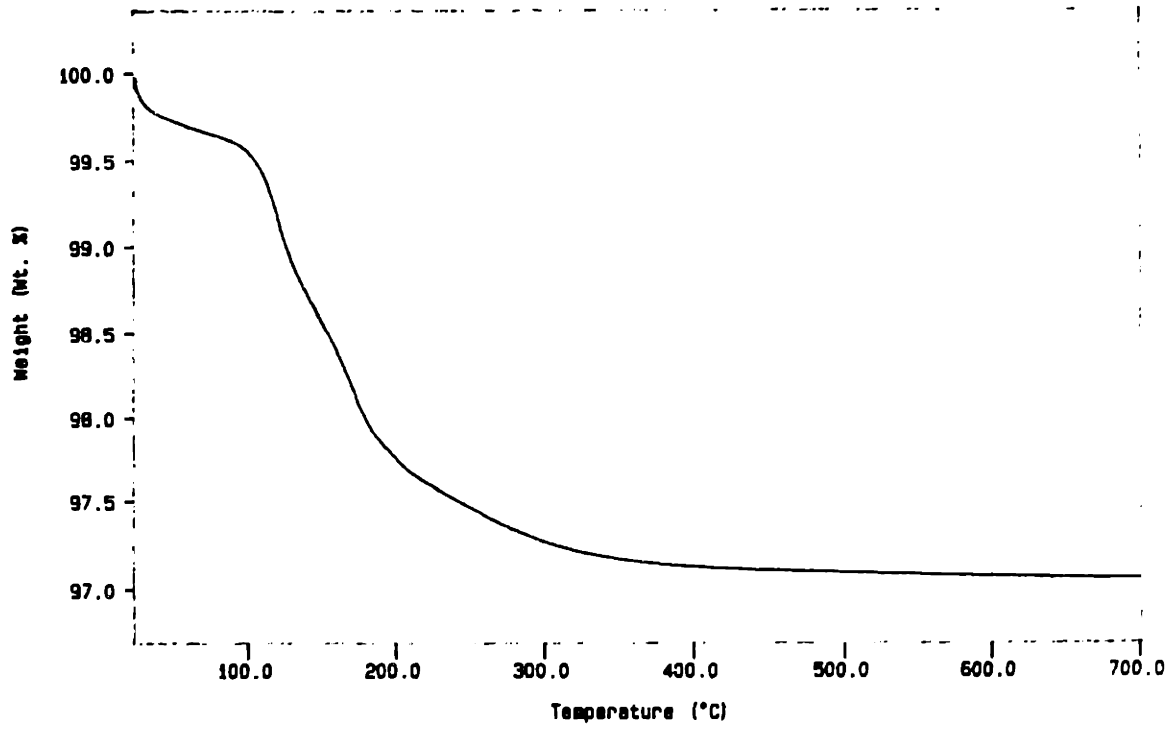

Figure 4.1: TGA of SDPEG/alumina granules.

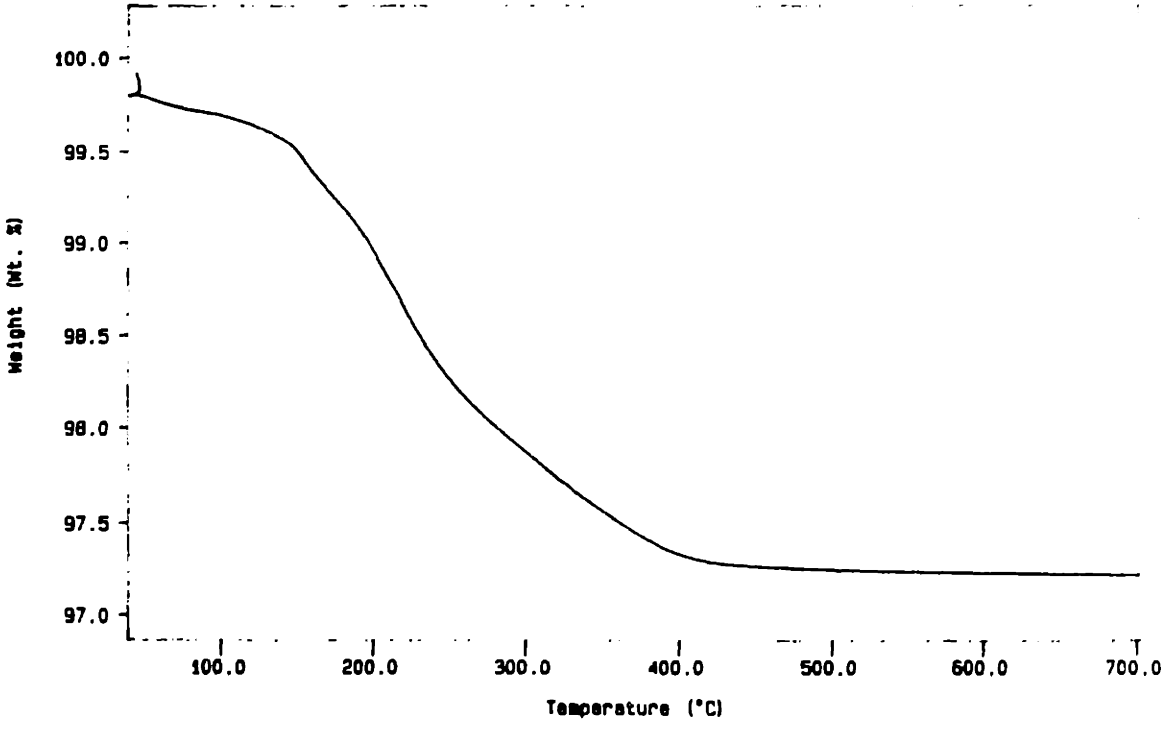

Figure 4.2: TGA of SDPAA/alumina granules.

4.3 SD granules properties

4.3.1. Interaction between ceramic and organic additive

The chemical nature of organic additive used in the SD granules and its interaction with the ceramic particles will affect the flowability (during spreading) and the chemical response of SD granules to the printed binder. The interaction between the polymer and water (solvent of binder) was investigated by washing the SD granules in water and performing the thermogravimetric analysis on the dried powder. TGA data of the washed and dried SD granules with PEG and PAA organic additive is shown in figures 4.3 and 4.4. The result shows that nearly all of PEG dissolved in water during washing while there was no loss of PAA organic by washing.

PEG, PVA as well as PAA are all hydrophilic polymers [76]. During spray drying, the polymer in the suspension is exposed to high temperatures (~100^0C). PEG and PVA do not exhibit any cross-linking behavior upon heating to 100^0C. Therefore, spray drying will not introduce any changes in their solubility behavior. According to Boucher [77], PAA may lead to cyclic anhydride formation upon heating thus reducing its solubility in water upon cooling. Existing literature also shows that the carboxylic acid group of PAA can chemisorb onto alumina surface by reacting with its hydroxyl group [78,79].

Diffuse Reflectance Infrared Fourier Transform Spectroscopy (DRIFTS) is used as a tool to determine the mechanism causing the insolubility of the PAA polymer within the SD alumina granules. DRIFTS analysis was performed on neat PAA polymer powder and ceramic powders containing adsorbed organic molecules. The samples were diluted with KBr powder sufficient enough to maximize the signal-to-noise ratio of acquired spectra. The dilution was between 70 to 90 wt% for all samples. DRIFTS sample preparation was performed in air just prior to analysis. DRIFTS spectra were acquired at a resolution of 4 cm^{-1} using 32 scans.

Figures 4.5 and 4.6 compare the transmission spectrum of a pure PAA film with that of a PAA film which was heated to 120 C to determine if the solubility characteristics of the film change due to the anhydride formation. Both the spectra show the presence of carboxylic peak centered around 1740 cm^{-1}. The spectrum of heat treated PAA film also shows the presence of anhydride peak centered at 1810 cm^{-1} [80]. However, the heat treated film dissolved readily in cold water. Therefore, anhydride formation in the PAA film is not the cause for the insolubility of organic within the SD granules. Figure 4.7 compares the transmission spectrum of PAA in a 2.0 wt% PAA/Alumina SD granule with that of pure PAA. The carboxylic peak is completely absent in the SD granule sample. Instead, a strong absorption band centered at 1576 cm^{-1} is quite apparent. This band has

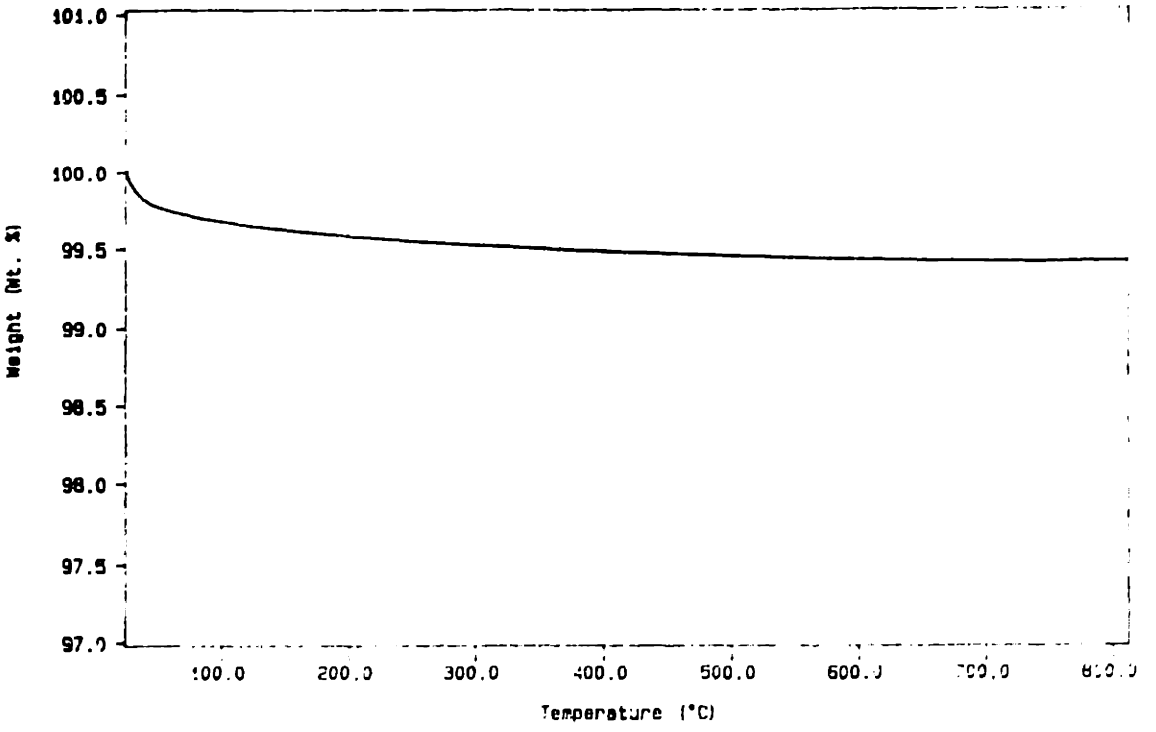

Figure 4.3: TGA of SDPEG/alumina granules after being washed in water and dried.

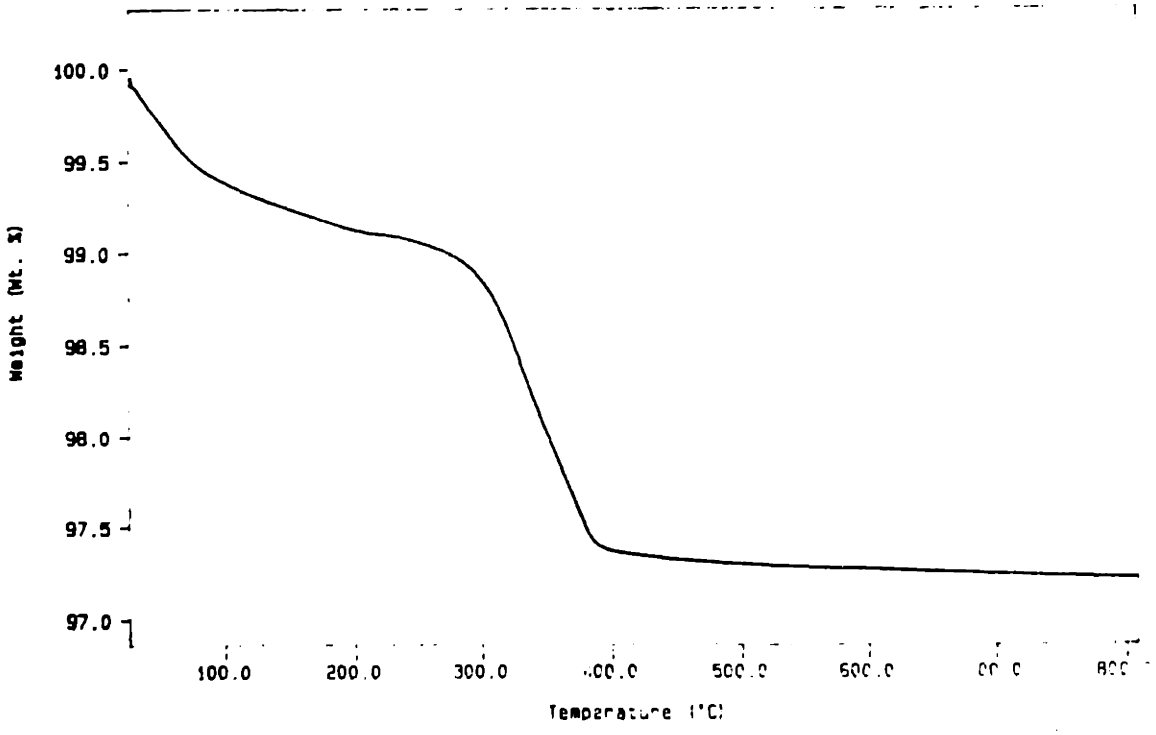

Figure 4.4: TGA of SDPAA/alumina granules after being washed in water and dried.

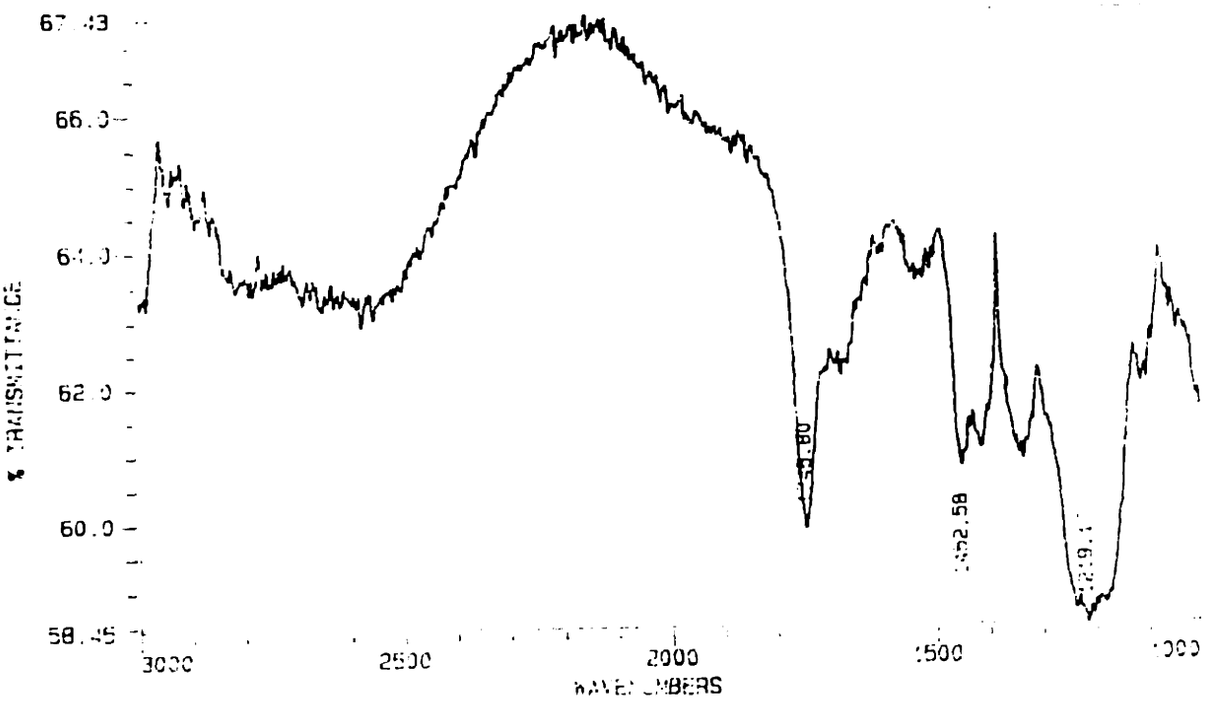

Figure 4.5: DRIFTS spectrum of neat PAA polymer.

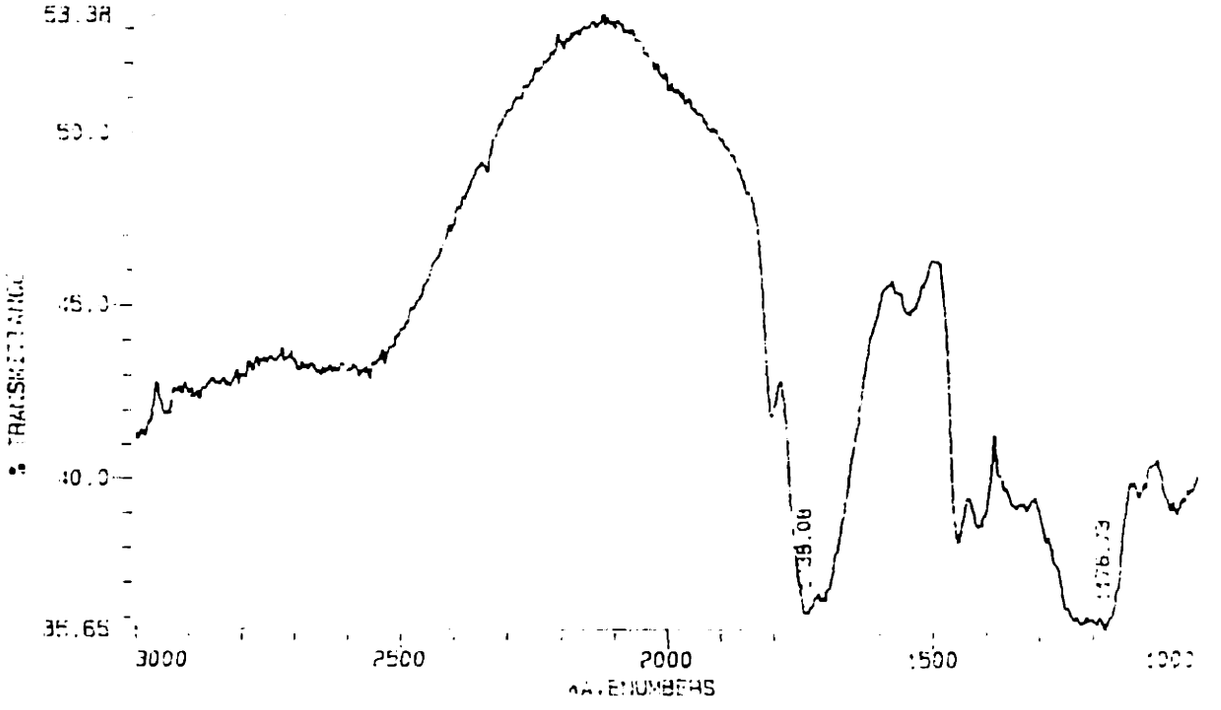

Figure 4.6: DRIFTS spectrum of PAA polymer heated to 120 C.

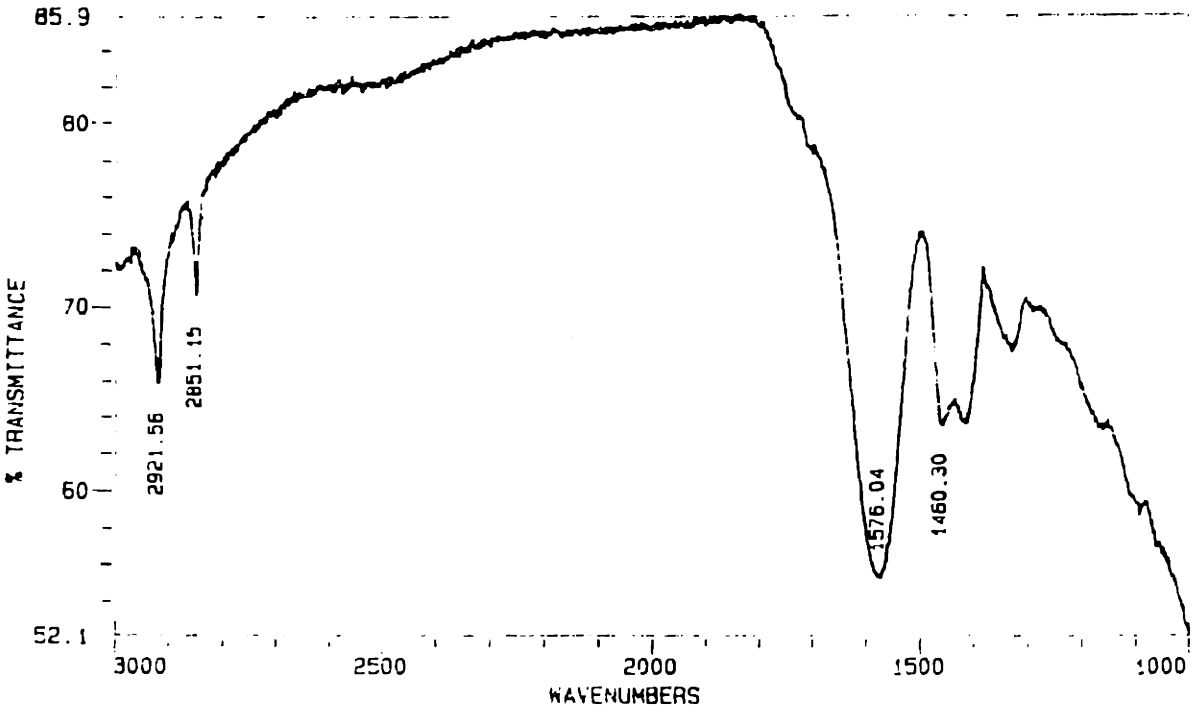

Figure 4.7: DRIFTS spectrum of SDPAA/alumina granules.

been observed before in alumina/PMMA composites and is attributed to the formation of metal carboxylates species at the alumina surface. This type of reaction between the carboxylic group of an ester and the hydroxyl group of alumina is well documented in literature [78,79]. Such a reaction is called ester saponification. This chemisorption can completely change the solubility characteristics of the organic additive in the SD granules. The spectrum for 2 wt% PAA SD alumina granules shows that almost all of the carboxylic group of PAA is being present as aluminum carboxylate. Calculations were performed to find out the amount of hydroxyl group on alumina surface and carboxylic groups in PAA for 2 wt% SDPAA/alumina sample. According to Higgins [81] the hydroxyl concentration on alpha alumina surface is 18 OH^-/nm^2. The surface area of alumina powder was measured by BET as 7.4 m^2/g. Therefore there are 2.15 * 10^{-4} moles OH^-/g of alumina. For 2 wt% PAA (d.w.b. of alumina), there are 2.8 * 10^{-4} moles $COOH^-/g$ of alumina. It is clear that if there is no steric barrier, nearly all of the PAA can potentially chemisorb onto the alumina surface.

4.3.2 Flowability

All the SD granules showed good flowability as is evident from the angle of repose measurements (Table 4.1), significantly better than the flowability of fine powder agglomerates (angle of repose ~ 38.3°) used in the press-rolling technique. Lower angle of repose values indicate better flowability. SD granules with PAA organic exhibited the lowest angle of repose and the best flowability behavior.

The flowability of the SD granules will be affected if they absorb moisture from the atmosphere. Control of humidity in large-scale manufacturing facilities is often impractical and therefore it makes sense to reduce the humidity sensitivity of the SD granule for more robust performance. Moisture sensitivity of the SD granules will be a strong function of the chemical nature of the organic additive. According to Whitman [82], both PVA and PEG binders absorb large amounts of moisture. PVA changes its T_g linearly from 42 C at 20% humidity (2% moisture adsorbed) to -10 C at 95 % humidity (16 % moisture adsorbed). This decrease in T_g to below room temperature as well as the cohesiveness introduced due to water can adversely affect the flowability of the SD granules and decrease the packing density as shown in the Table 4.1. On the other hand, PEG has a very low T_g (-65 C) to start with, and therefore does not get plasticized any further. Therefore, even though the flowability of SDPEG powder will be adversely affected by the presence of moisture, the change will be significantly less than PVA based ceramic granules.

Table 4.1: Physical properties of the spray dried granules.

Physical Properties	2 wt% PEG/Alumina	2 wt% PVA/Alumina	2 wt% PAA/Alumina
Packing density (% theoretical)	~ 35.1	~ 30.9	~ 33.3
Bulk density (% theoretical)	51.7%	50.4%	49.2%
Angle of Repose	20.1	21.5	16.8
Average Size, Std. Deviation (μm)	18.4 (7.4)	18.3 (7.6)	27.2 (13.4)
Intra-granular porosity (μm)	0.1	0.1	0.1
Molecular weight of binder	4600	9000-10,000	90,000
Glass transition temperature of binder	-65 C	74 C	106 C

PAA is completely chemisorbed onto alumina surface, therefore, it does not have any free polar carboxylic group to absorb moisture. SDPAA/alumina system is, therefore, least moisture sensitive as is confirmed by the low angle of repose data.

The powder bed surface made out of SD granules was very uniform and regular. No crater defects were formed during spreading. The packing density of a powder bed made out of SD granules is in the order of ~33 % as compared to the powder density of 40% obtained via the press-rolling approach. However, the good flowability of SD granules guarantees uniform packing density and microstructure within the spread powder layers.

4.3.3 Bulk density and pore size distribution

The bulk density and packing density of the SD granules are listed in Table 4.1. SDPEG granules have the highest bulk and packing densities. Packing density is affected by the bulk density and the packing behavior of the SD granules. Powders composed of granules containing large pores, donut shaped granules and irregular shaped granules with rough surface would result in low packing density. A typical fill density, reported in the literature, for a granulated powder is in the range of 25-35% [15, 73]. It is very important to identify the key factor causing the donut formation so that a right processing strategy can be formulated to correct the problem.

The droplets from the atomizer in the spray-dryer is heated with a blast of hot air. Initially, the solvent in the droplets evaporate rapidly from the surface. Evaporation retards the heating of the product. Soluble materials in the solvent are left behind to form a skin on the surface upon drying. As the drying proceeds, the liquid within the droplets must now diffuse to the surface to evaporate. The liquid must not only pass through the solid particles packed in the droplet, but also the film of soluble solids left behind as the skin on the surface. The skin therefore grows inward. The droplets do not rotate as they are projected through the heated air, therefore, one side always see hotter gas. Evaporation is faster on the hot side and the shell thickens more rapidly on this side. The trailing side has only a thin shell and the interior on this side tends to stay wet and fluid. As the liquid and solids migrate to the hot side, the thin side is drawn inward, resulting in the familiar hollow sphere with a dimple. The use of dispersants enhances this phenomenon. The donut formation can be minimized by using a) less dispersant, binder or other solubles in the slurry, (b) partially flocculated slurry and (c) slower drying, by employing lower gas temperatures [72,83].

Pore size distribution of a powder bed made out of SDPAA/alumina granule is shown in figure 4.8. The graph shows two distinct jump in the cumulative intrusion

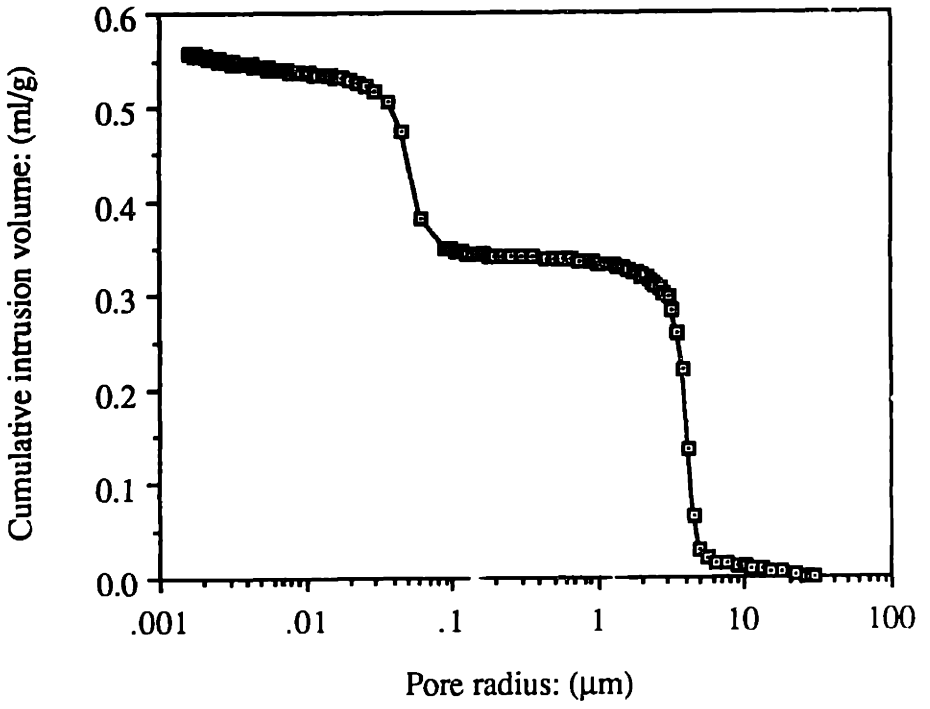

Figure 4.8: Pore size distribution of SD granule powder bed.

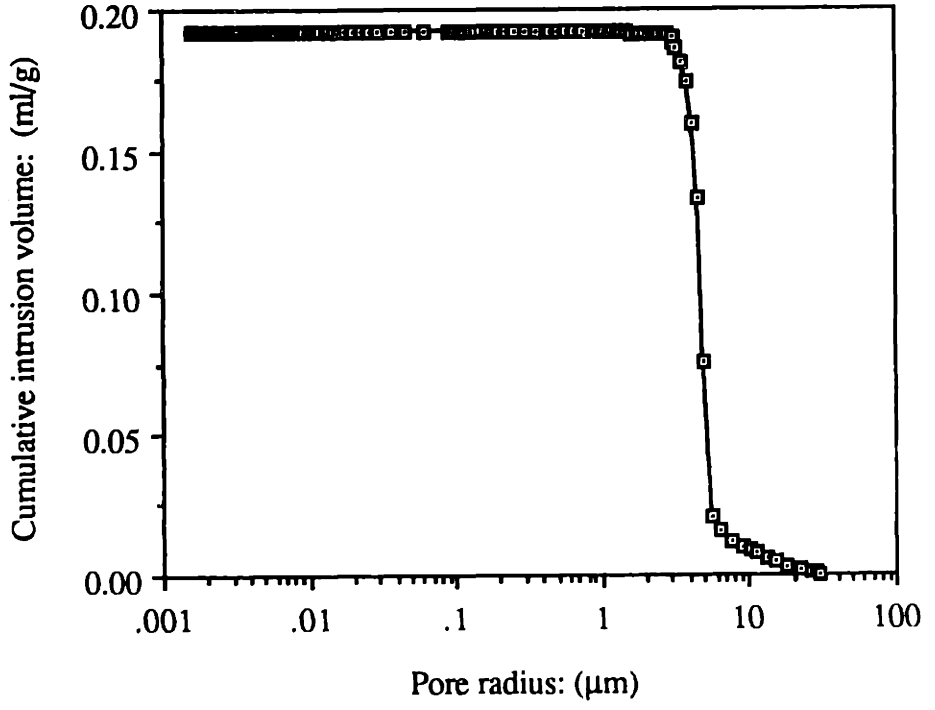

Figure 4.9: Pore size distribution of 30 μm dense spherical alumina powder bed.

volume axis. The first jump at ~ 6 - 8 μm corresponds to the average intergranuler pores between SD granules while the second jump at ~ 0.05 - 0.1 corresponds to the average intragranular pore within a SD granule. The pore size distribution of SD granule is compared with a powder bed composed of dense spherical alumina granule in figure 4.9. The graph shows only one jump corresponding to the intergranular pores. The significance of a combination of fine and coarse pores in the powder bed will be more evident in subsequent sections.

4.4 Distortion during printing

4.4.1 Possible mechanisms for shrinkage in 3DP process

Warpage can occur in any rapid prototyping technique that builds parts on a layer by layer basis, where the printed area undergoes shrinkage. The key materials components which control the part formation in 3DP are: printed binder, powder bed and their interaction . The interaction of a single droplet with the powder bed typically includes ejection of powder due to ballistic impact [84], a chemical reaction (dissolution and/or gelation) between the organic additives in the powder bed with the printed binder, migration of binder from the printed region to the surrounding powder [85] and rearrangement of particles by capillary forces upon drying of the printed solvent [74]. The resulting microstructural feature is termed a "primitive". The primitives are stitched together to form lines. Lines are subsequently knitted to form planes. Since, these features are formed sequentially, shrinkage during the build process will introduce differential strain within the part and will result in distortion. 3DP printed area can shrink due to:

1. Dissolution of the organic additives in the printed solvent and subsequent redistribution upon drying.
2. Forces created due to non-uniform drying of the printed solvent [51,53]. Excessive drying is possible from the top surface exposed to atmosphere, especially when the powder bed is composed of a lot of fine pores.
3. Migration and redistribution of liquid from the printed region to surrounding powder bed due to existing porosity can introduce differential stress as explained in the background section.
4. Shrinking forces exerted on particles by the drying of gelled binder [86].

The extent of warpage in typical 3DP parts for investment casting applications is fairly small, making it difficult to measure the effect of various processing variables on shrinkage. The use of SD granules as a model materials system ensures the enhancement of the phenomenon of warpage caused by either of the above mentioned mechanisms.

Organic dissolution of SD granules would result in higher shrinkages (~ 20-30 vol%) and fine intra-granuler porosity would enhance liquid migration within the powder bed, and also result in higher drying stresses. In addition, for the same shrinking stresses either due to drying or gelling, the rearrangement of spherical, lighter and highly flowable SD granules will be more pronounced than coarser regular sized particles.

4.4.2. Distortion due to chemical dissolution

4.4.2.1 Experimental methods

Single layers were built by printing water on powder-beds made out of SDPAA, SDPVA and SDPEG alumina granules. Single layers were also printed from debound SD granules. The organic of SD granules was burned out at 750 C. For comparison, single layers were also built out of 10 and 30 μm dense spherical and 30 μm platelet alumina particles. Each layer consisted of five independent bars; 6.25 cm long and 0.6 cm wide. Deionized water was used for printing as it eliminated the contribution to shrinkage due to the gelling of the printed binders. The bars were printed at 178μm line spacing with a fast axis speed of 165 cm/s. The flow-rate of water was ~1.2 cc/min. SEM was used to perform the microstructural analysis of the printed layer.

4.4.2.2. Results and discussion

Figure 4.10 shows the top surface of single layers created by printing water on powder beds made out of SD alumina granules containing PEG, PVA and PAA as binders respectively. It is clear that the layers made out of SD granules containing PEG and PVA warped but the one containing PAA did not exhibit any curling. SDPEG showed the most extensive warpage. Single layers made out of debound SD granules and dense spherical 30 μm alumina did not show any warpage (figures 4.11 and 4.12). Figure 4.13 shows the SEM micrographs of the top surface of the printed layers for the three SD systems. SD granules containing PEG shows the disintegration of granules, due to the dissolution of PEG in printed water, which results in complete elimination of inter-granular voids leading to large linear shrinkages (~ 7.9%, calculations on next page). PVA swells in the presence of cold water and results in the deformation of SD granules due to the capillary stresses upon drying and therefore eliminates the intergranular voids in SDPVA system. However, the individual granules still remain intact. This results in lesser shrinkage than PEG system and therefore less warpage. SDPAA system shows no effect of dissolution and swelling and therefore does not exhibit warpage. Single layers made out of debound SD granules and dense coarse particles did not have any organic additives and therefore did not show any warpage. None of the debound SD granule systems show any evidence

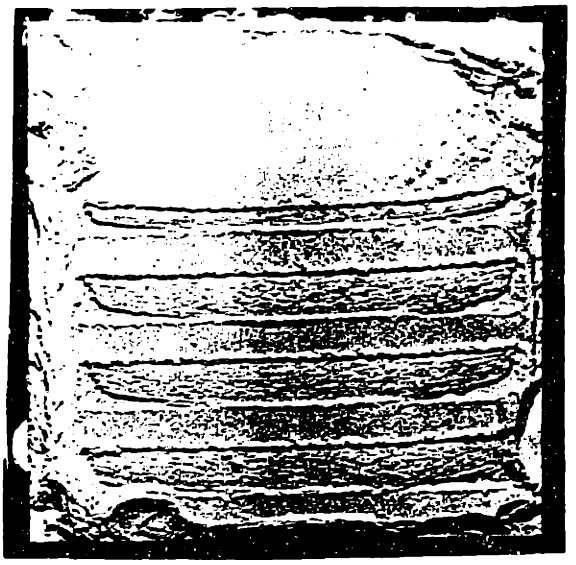

SDPEG/Alumina

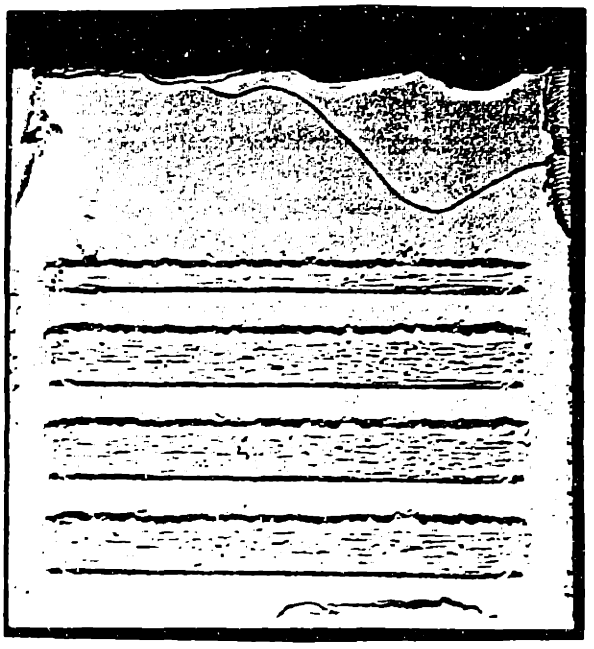

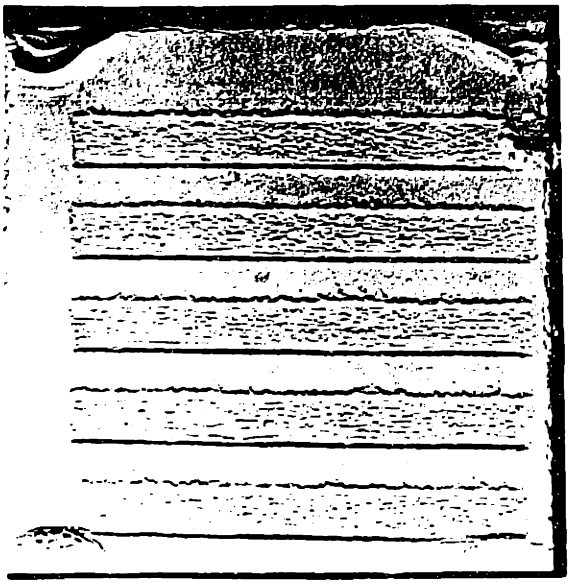

SDPVA/Alumina

SDPAA/Alumina

Figure 4.10: Photograph of single layers made by printing water on SDPEG, SDPVA and SDPAA alumina granules powder bed.

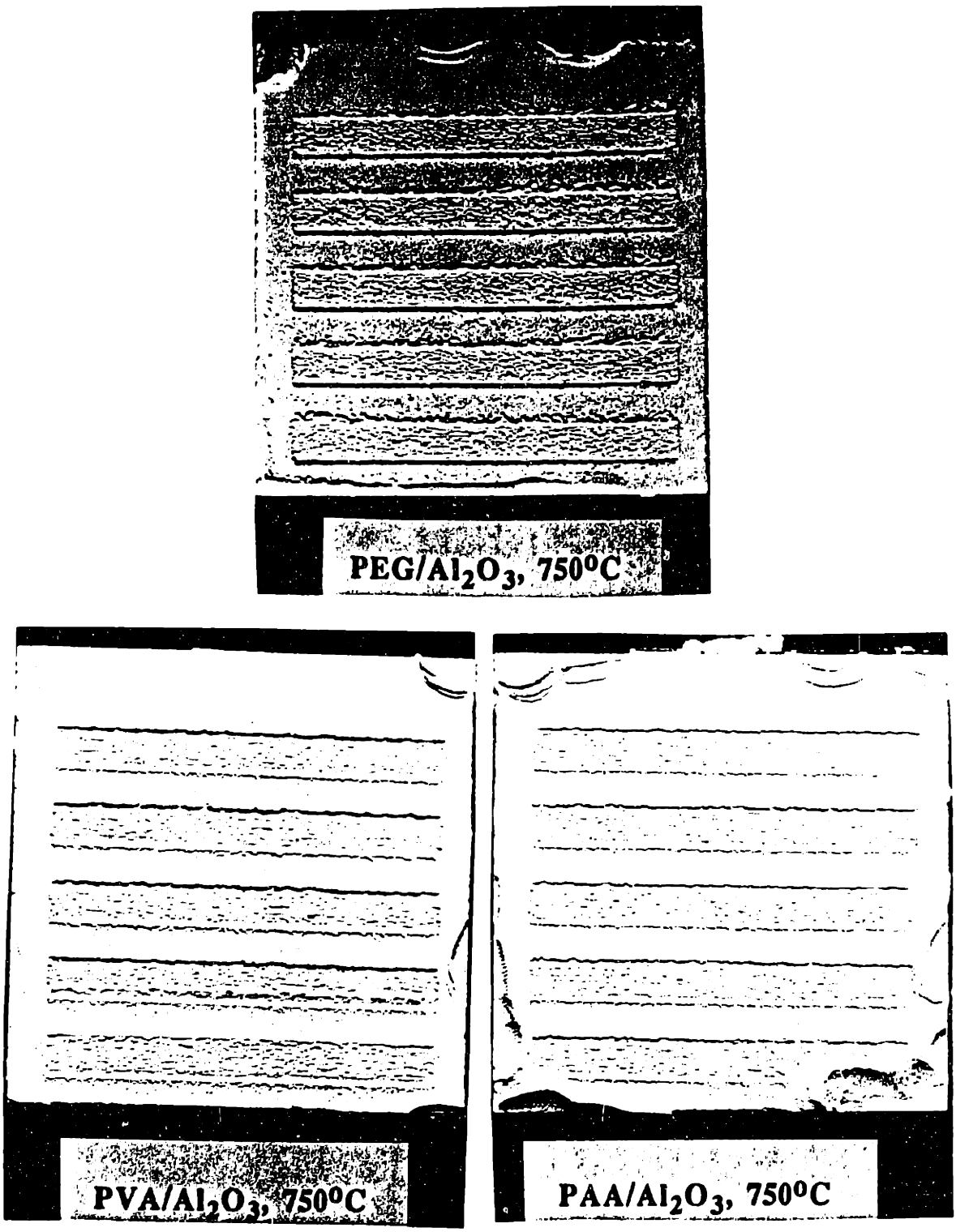

Figure 4.11: Photograph of single layers made by printing water on debound SDPEG, SDPVA and SDPAA alumina granules powder bed.

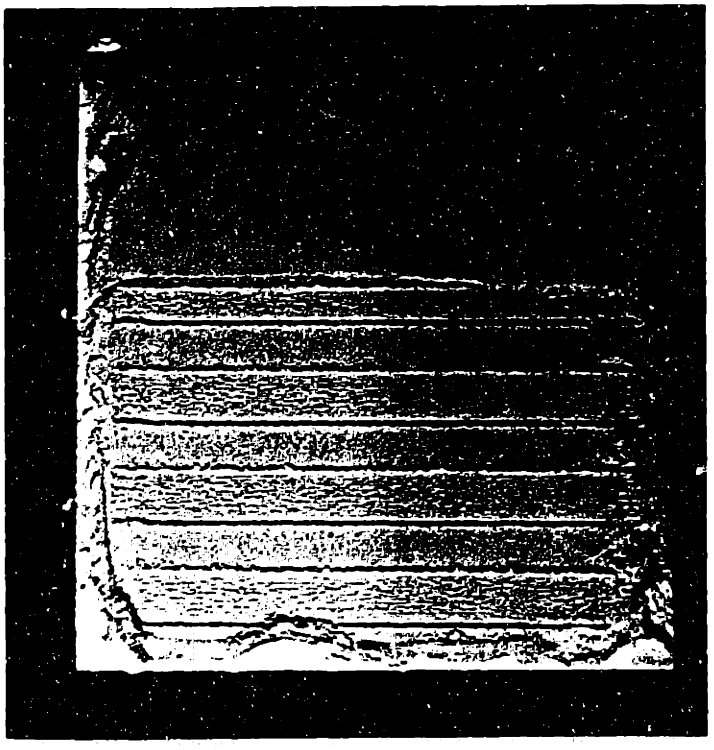

Figure 4.12: Photograph of single layers made by printing water on 30 μm dense spherical alumina powder bed.

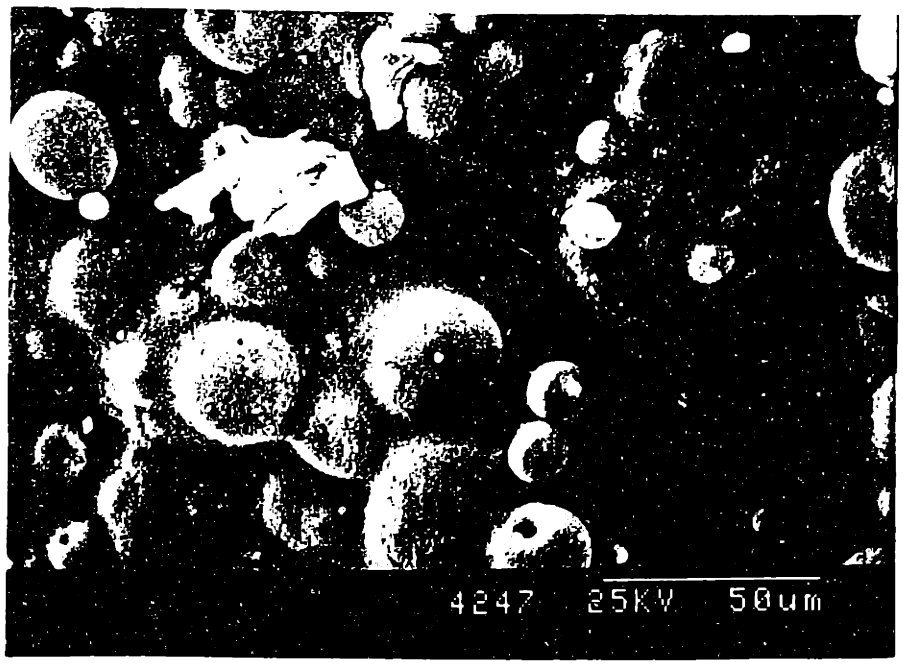

SDPEG/Alumina

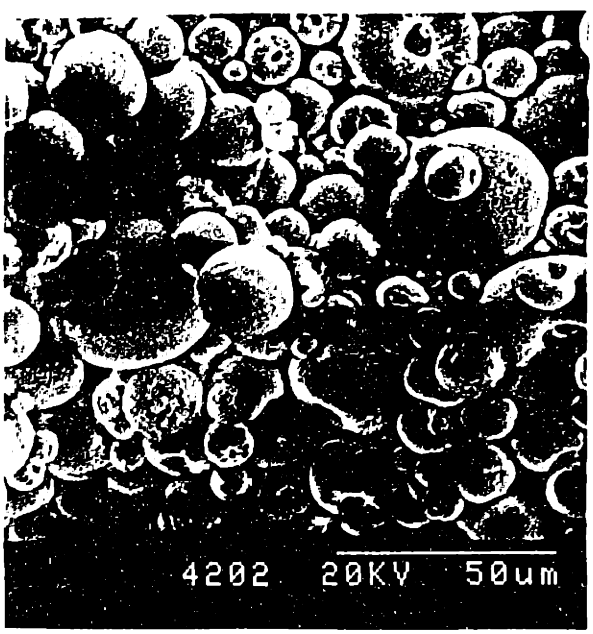

SDPVA/Alumina

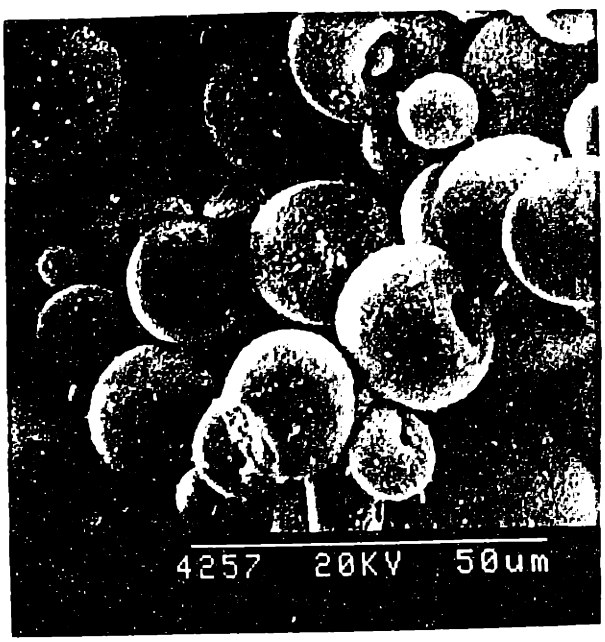

SDPAA/Alumina

Figure 4.13: SEM micrographs of the top surface of single layers made by printing water on SDPEG, SDPVA and SDPAA alumina granules powder bed.

of warpage. This experiment confirms that the shrinkage was exclusively due to the dissolution of the organic additive of the powder bed by the printed binder. Generally, organic additives are added to the powder to modify the physical properties of the powder-bed and/or to gel the printed binder effectively [85,86]. The present study indicates that their dissolution and redistribution can lead to shrinkage.

We can explain the extent and the direction of warpage using the shrinking layer model as explained in the background section. Unlike the simple model, where the entire layer shrinks simultaneously, in the current SD systems, lines constituting the layers shrank even before the entire layer was completed. This results in the warpage of single layers. The first printed line shrinks freely and shows no evidence of curling. However, the second printed line bonded to the first line, induces a net bending moment on the first line upon shrinkage. This results in the warpage of the parts in the direction of slow-axis, where the subsequent lines are being added to complete the layer, as is evident from figure 4.10.

The shrinkage of SDPEG system can be calculated by measuring the radius of curvature of the warped bar from the photomicrographs. Radius of an arc, 'R' can be measured by the following equation:

$$\frac{1}{R} = \frac{8h}{L^2 + h^2}$$

where 'L' is the length of the chord and 'h' is height of the normal from the chord onto the arc. R for SDPEG is measured as 114 mm from the photomicrographs. The following equation is used to calculate the length of the arc [87],

$$\bar{L} = \frac{2.\left(\pi - 2.\tan^{-1}L/2h\right)}{1/R}$$

Strain is calculated with the following equation:

$$\text{strain} = \frac{\bar{L} - L}{\bar{L}} * 100$$

The linear strain for SDPEG is calculated as 7.9%. The large shrinkage strain of individual lines explains the extensive warpage in the slow axis direction.

The photographs also illustrate that warpage reduces (radius of the arc increases) as the width of the part increases along the slow-axis. The radius 'R'of the warped layer can be approximated by an expression for a straight elastic beam subjected to constant bending moment as [88]:

$$R = EI/M$$

where M is the bending moment, I is the moment of inertia and E is the elastic modulus of the beam. The elastic modulus of a wet granular body changes during drying. It behaves

like a viso-elastic material during the earlier stages of drying. Once the body is dry, in the absence of organic, the body will behave like an elastic material. The above simplified formula is used to explain qualitatively the trend of curvatures observed in the SDPEG part as a function of width along the slow-axis.

A large radius of curvature implies less warpage. The shrinkage stress for every shrinking line is constant. The first line shrinks independently. The second shrinking line has to distort itself and line 1 and the relative shrinkage between the two results in warpage. However, as more and more lines are added, the shrinking lines still have the same shrinking stress but the stiffness of the part to which they get attached keeps increasing (Product of EI). Therefore for same bending moment (M), radius will increase and the parts will become flatter. Therefore, bending moment and thereby shrinking stresses, should be reduced in order to minimize the warpage.

The above equation cannot be used to determine the extent of elasticity of the powder bed, as the value of bending moment is unknown. Timoshenko [89] has derived another variation of the same equation, relating strain to the radius of curvature of a warped bimetallic strip. The equation is expressed as:

$$\frac{1}{R} = \frac{-\alpha\Delta T}{\left(\frac{h_1 + h_2}{2}\right) + \left(\frac{E_1 h_1^{\,3} + E_2 h_2^{\,3}}{6(h_1 + h_2)}\right)\left(\frac{1}{E_1 h_1} + \frac{1}{E_2 h_2}\right)}$$

where $\alpha\Delta T$ is the thermal strain, h_1 and h_2 are the thicknesses and E_1 and E_2 are the elastic modulii of the two metal plates of the bimetallic strip respectively. The strain in our case is measured experimentally as 7.9%. The elastic modulus of a powder bed (E^*) is calculated by Kendall's [90] equation:

$$E^* = 17.1\phi^4\left(\frac{E^2\sigma}{D}\right)^{1/3}$$

where E is the elastic modulus of the material, ϕ is the packing density, σ is the surface energy and D is the diameter of the particle. The elastic modulus of alumina is 380 GPa and the surface energy 0.58 J/m^2. The packing density of the SDPEG powder bed changes from 35% (measured initial spread packing density) to ~ 60% once the shrinkage is complete after drying (based on the SEM micrographs). The intial particle size of the powder bed is ~ 30 μm, but after printing the average particle size within the printed part is ~ 0.8 μm. The ratio of the elastic modulus of the printed SDPEG part to the loose powder bed is calculated as 28.91. The line widths are ~ 180 μm. Applying these values to the equation results in a calaculated value of R as 8.2 mm. This calculated value of R is significantly less than the corresponding measured value. Curvature is inversely

proportional to the radius of an arc. Therefore, the calculated value implies larger curvature than the actual measured value. The deviation between the calculated and measured value could arise from the assumptions used in the calculation. Part of the shrinkage can be consumed to deform the SD granules. Also, the wet body may behave more like visco-elastic mass, while the calculations assumed a purely elastic behavior. The calculations assume that all the shrinkage is effectively communicated between the shrinking and dried line, therefore, it predicts more warpage than the real situation.

4.4.3 Distortion due to liquid redistribution

4.4.3.1 Experimental procedure

Multi-layered bars were built by printing acrysol on powder-beds made out of SDPAA and debound SD granules. SD granules were debound at 450 C. SDPAA alumina system was chosen, as it does not disintegrate in water based acrysol binder. Three different concentrations of acrysol: 6, 15 and 36 vol% were used to build parts fromSDPAA granules. Parts were also made by printing deionized water and 7 vol% alumina slurry. The experiments consisted of printing 20 independent bars; 3.5 cm long and 0.6 cm wide. The bars were printed at 178 μm line spacing. Two different fast axis speeds were used: 165 and 101 cm/s. Three different binder flow-rates were employed: 0.8, 1.0 and 1.2 cc/min. SEM was used to perform the microstructural analysis of the printed parts. Warpage measurements of the printed parts were done with an optical microscope, as is described in chapter 3.

4.4.3.2 Results and discussions

Table 4.2 summarizes the extent of warpage observed in the printed part for various SD granules and binder systems. The warpage increases in all the SD granules-binder systems with an increase in saturation. The saturation in these systems were changed either by changing the fast axis speed or the flow-rate. The nature of the binder used for printing also influenced the extent of warpage. The parts made by printing 36 vol% acrysol warped significantly more than the parts made by 6 vol% acrysol. The parts printed with deionized water showed no warpage. The parts made by printing 7 vol% alumina slurry on debound granules warped but the parts made by the same powder bed did not warp when 6 vol% acrysol was used instead. The chemical nature of the granules also influenced the warpage behavior. SDPAA alumina granules printed with 6 vol% acrysol warped while the debound alumina granules printed with the same binder did not warp.

Table 4.2: Extent of warpage observed in the printed parts for various SD granules and binder systems

SD granule system	Packing density (%)	Binder system	Flowrate , Fast axis speed	Calculated intergranular saturation (%)	Extent of warpage
Debound SD Al_2O_3	33	7 vol% Alumina slurry	1.2 cc/min, 165 cm/sec	95.7^{S} (20.7)*	++
Debound SD Al_2O_3	33	7 vol% Alumina slurry	1.0 cc/min, 165 cm/sec	79.8 (04.8)	+
DeboundSD Al_2O_3	33	7 vol% Alumina slurry	0.8 cc/min, 165 cm/sec	63.9 (0.0)	0
SDPAA/Al_2O_3	33	7 vol% Alumina slurry	1.0 cc/min, 165 cm/sec	79.8 (04.8)	+
SDPAA/Al_2O_3	33	7 vol% Alumina slurry	0.8 cc/min, 165 cm/sec	63.9 (0.0)	0
SDPAA/Al_2O_3	33	6 vol% Acrysol	1.2 cc/min, 165 cm/sec	95.7 (20.7)	++
Debound SD Al_2O_3	33	6 vol% Acrysol	1.2 cc/min, 165 cm/sec	95.7 (20.7)	0
Debound SD Al_2O_3	33	6 vol% Acrysol	1.2 cc/min, 101 cm/sec	155.6 (80.6)	+
Debound SD Al_2O_3	33	Water	1.2 cc/min, 165 cm/sec	95.7 (20.7)	0
SDPAA/Al_2O_3	33	Water	1.2 cc/min, 165 cm/sec	95.7 (20.7)	0

$, intergranular saturation is calculated assuming that fine pores are not readily available to printed binder.

*, intergranular saturation is calculated assuming that printed binder readily occupies the intragranular volume.

In systems where we saw warpage, the first printed layer started to warp out through the powder bed after a fresh layer of powder was spread on top of the printed region. Warpage is a manifestation of shrinkage, therefore, it was hard to conceive that a powder bed with 68% physical packing density (measured packing density /measured bulk density of granules) will exhibit any shrinkage. The following section discusses the origin of shrinkage in the SD granule systems.

SD granules exhibit a tremendous amount of ejection (significantly more than the dense coarse powders) during printing. Extensive ejection of the SD alumina granules during printing is due to its high flowability and light weight. Excessive ejection can result in the loss of packing density of the powder bed. The loss in packing density was quantified by printing 15 vol% acrysol on a powder bed made out of SDPAA/alumina granules. The packing density of the spread powder bed was measured as 33.3% while that of the printed part was measured as 31.3%. The density of the printed part included the mass of the printed organic binder. The density of the sample after excluding the weight of the dry acrysol was 29.98%. Therefore, there is a loss of ~ 3.3% in packing density of the powder bed during printing. The granules are only ~ 50% dense, therefore, the physical packing density effectively reduces by ~6.6%. The loss of packing density opens up the powder bed and allows for possible shrinkage during drying. The next sections discuss the role of saturation and the nature of the printed binder on the warpage behavior of SD parts.

4.4.3.2.1 Effect of saturation on distortion

The warpage behavior of parts made by printing 7 vol% alumina on the debound SD granules reduced as the saturation was decreased. The saturation was decreased by decreasing the flow rate, in effect depositing lesser binder per unit length of the printed part. The parts made at a flow-rate of 0.8 cc/min and 1.0 cc/min were weak and difficult to handle, therefore, the warpage could not be quantified. The warpage of a part made at a flow-rate of 1.2 cc/min is shown in figure 4.14. Warpage behavior was similar for parts made by printing 6 vol% acrysol on debound granules. However, the saturation had to be increased in this system over conventional printing parameters, by decreasing the fast axis speed, to observe the warpage in the printed parts. The parts slumped due to high saturation upon subsequent printing. The printed parts, in this case, also showed binder bleeding. Two layer parts for this granules-binder sytsem were difficult to handle, therefore, the warpge could not be quantified. Yu [91] had reported no warpage when printing 20 vol% acrysol on dense spherical 30 μm alumina powder.

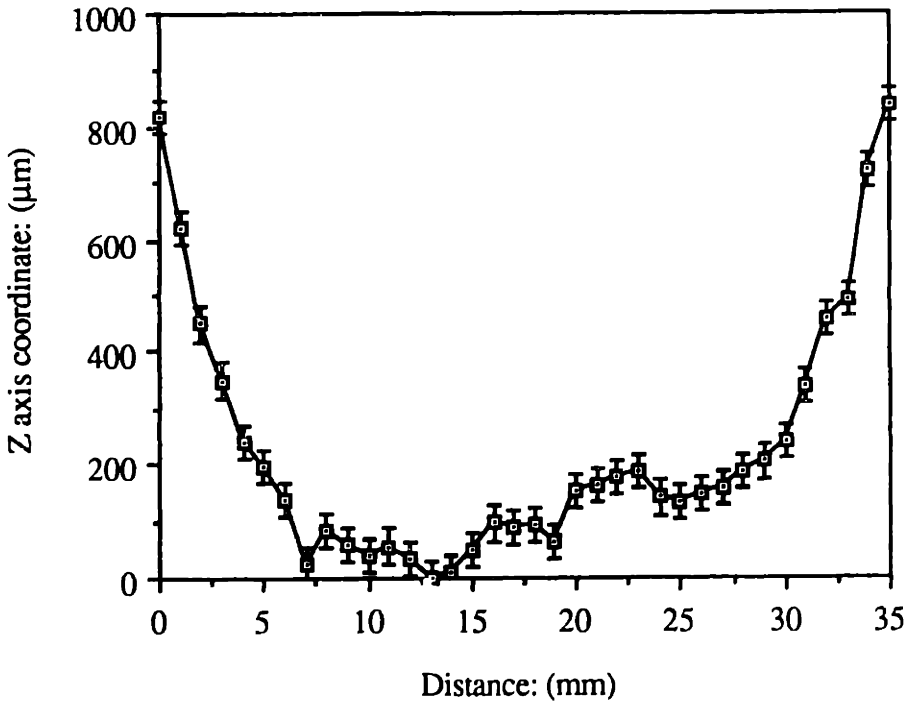

Figure 4.14: Warpage in parts made by printing 7 vol% alumina slurry on debound SD granules.

The powder bed created by SD granules has two distinct pore sizes; intergranular pores in the range of 6-8 μm while the intragranular pores are in the size range of 0.05 -0.1 μm. Liquid is attracted to the fine pores, while the big pores empty first, during drying [92,93]. Therefore, during printing multi-layered parts, there is a strong possibility of liquid redistribution within the SD powder bed. Lewis and Cima [94,95] have shown similar redistribution of thermoplastic binder due to pore size distribution during thermolysis of green tapes. Large pores connected to the surface emptied first while the smaller pores remained filled with binder.

Powder bed made from the SD granules is unique, as the liquid can migrate from big intergranular pores from the printed region to fine intragranular pores in the next spread layer, provided there is enough saturation. This phenomenon, henceforth, is referred to as 'inter-layer liquid migration'.

The drying rates (evaporation of water to atmosphere, henceforth called 'external drying') for water from wet fine ceramic granular bodies have been reported by Chiu as ~ 10^{-4} g/cm^2.sec. The drying rates due to interlayer liquid migration were calculated by using Darcy's and Carman Kozeny's equation. The permeability of porous bodies is expressed as [51] :

$$D = (1-d)^3 / 5(dSd_s)^2$$

where d is the relative density, $d = d_b/d_s$, d_b is the bulk density of the porous media and d_s is the skeleton density and S is the specific surface area. The specific surface area was measured by B.E.T. as 7.4 m^2/g. The permeability of a SD granule was calculated as $1.15 * 10^{-16}$ m^2. The flux of liquid sucked by the fine pores of the SD granules is calculated by Darcy's law. Darcy's law [51] is expressed as :

$$J = -D \Delta P_L / \eta_L$$

where J is the flux of liquid, ΔP_L is the gradient in pressure in the liquid, η_L is the viscosity of the liquid and D is the permeability of the porous media. The suction pressure exerted by the fine pores of the SD granules on water was calculated as 1.44 MPa, assuming a perfect wetting condition. The drying flux due to inter-layer liquid migration was calculated as 1.1 g/cm^2.sec. This calculation assumes that the SD granule is in contact with an intergranular region filled with water. The drying flux due to interlayer liquid migration is 4 orders of magnitude higher than that due to external drying. Interlayer liquid migration, therefore, produced an asymmetry in the build process. The anisotropic interlayer liquid redistribution introduced a compressive force on the top surface of the printed region and therefore resulted in the warpage of the printed region.

The anisotropic interlayer liquid redistribution can create warpage of the printed layer due to:

1. The compressive force produced in the spread powder layer. The liquid migrating from the printed layer into the spread powder layer can shrink the latter by introducing a capillary force between the SD granules.
2. The compressive force produced in the top portion of the printed layer. The high flux of interlayer liquid redistribution can result in a loss of liquid from the top portion of the printed parts, while the interior can stay saturated. The top portion of the printed part can, therefore, shrink with respect to the bottom surface. This would introduce a relative shrinkage within the printed layer and result in warpage.
3. Higher yield stress of the printed binder due to higher interlayer liquid migration flux. High drying flux is analogous to high strain rates. The polymer subjected to higher strain rates have lesser time to relax. The yield stress of the polymer increases with an increase in the strain rate. As the yield stress of the polymer binder is increased, it can support more stress during drying before yielding and therefore could result in higher shrinkage of the SD printed parts.

Another possible reason for the excessive stress in the SD granules system could be the high drying rate ('external drying') of the liquid from the high surface area of fine pores. The above hypothesis was evaluated by building parts in the presence of mist to reduce the external evaporation rate of water. The printed parts still exhibited the same warpage behavior. This confirms that stresses created due to 'interlayer liquid migration' is the main mechanism controlling the warpage in the SD granules parts. Powder beds made out of dense granules do not have these bimodal (big and small) pore distribution and therefore do not exhibit warpage like SD granules parts. Figure 4.15 shows schematically the mechanics of interlayer liquid migration and its effects on the distortion behavior of the SD parts during printing.

The extent of interlayer liquid migration will depend on the amount of liquid present in the intergranular pores. This is indicated by the intergranular saturation. There is no driving force (capillary pressure gradient) for the liquid to migrate from the fine intragranular pores of the printed region to the fine intragranular pores of the next spread dry powder layer. Saturation of the printed parts will depend on the packing density of the powder bed, wetting properties of SD granules-binder systems (whether fine pores are accessible to the printed binder or not) and also on the amount of the printed binder (flow-rate and fast axis speed).

Permeability is a strong function of the saturation of the wet body. The flow conductivity of the fluid within a wet body decreases as the saturation decreases. The fluid conductivity and permeability D_0 are at their maximum values for a fully saturated wet body. As saturation S_w decreases, an effective permeability D_{eff} must be defined to

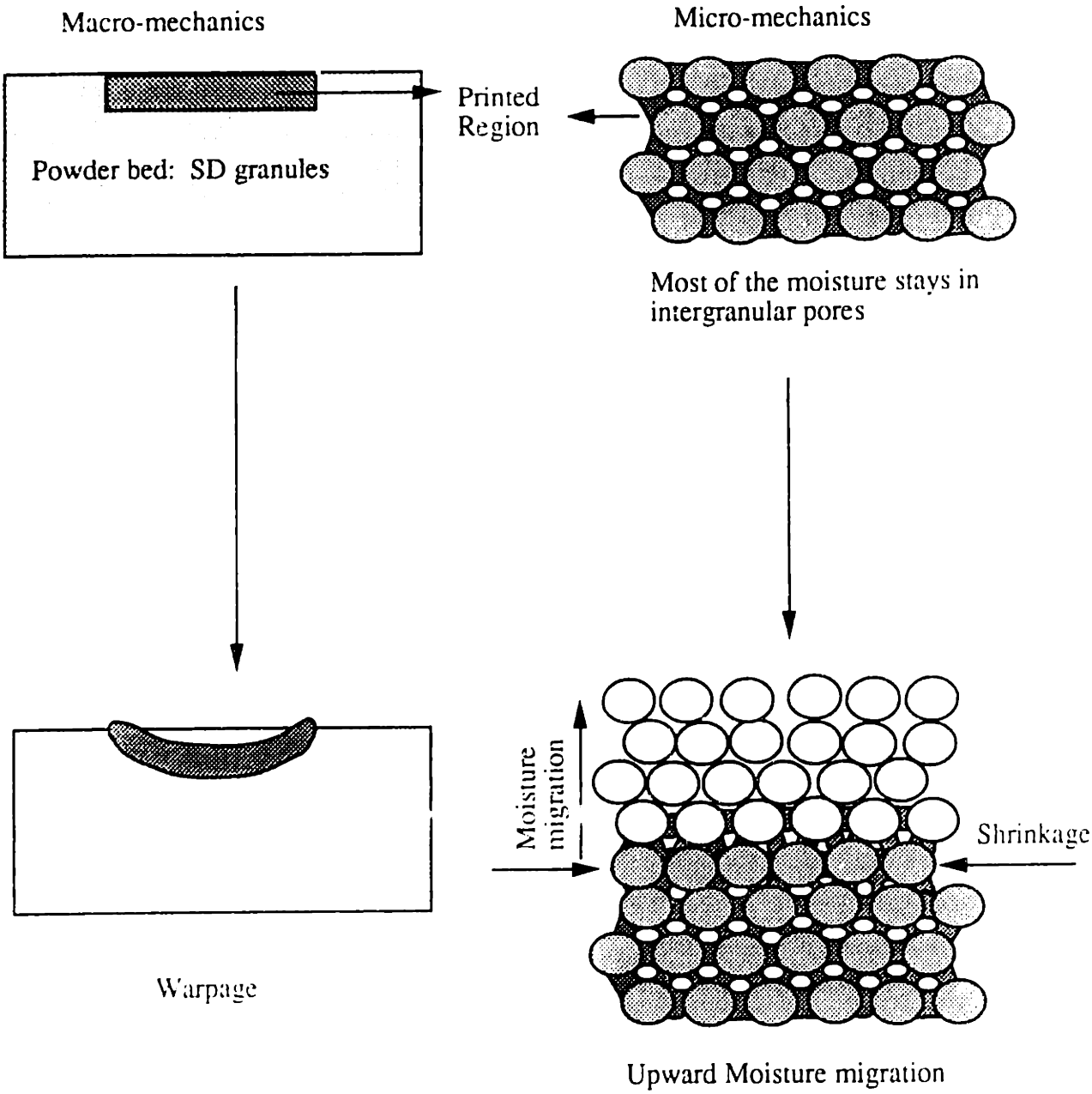

Figure 4.15: Micro and macro-mechanics of warpage due to interlayer liquid migration.

account for the associated decrease in the permeability relative to D_o. Corey and Scott [96] developed the following expression which relates D_o to D_{eff} in terms of P_c:

$$d_{eff} = \frac{D_{eff}}{D_o} = \left(\frac{P_{co}}{P_c}\right)^n$$

where P_{co} is the entry suction pressure at $S_w = 1$, and P_c is the entry suction pressure at a given S_w, and n is an integer whose value depends on the relationship between P_c and S_w.

Darcy's law is obeyed as long as the liquid phase is funicular (i.e. interconnected). If the liquid is pendular (i.e. isolated in pockets) it can only be transported by diffusion of the vapor. In a powder bed made out of the SD granules with bimodal pore size distribution, liquid redistribution will be extensive due to the capillary pressure gradients, provided the mobility of the liquid is sufficient.

Jacob Bear [97] has proposed that the suction pressure is a strong function of saturation along with the surface tension and the contact angle of fluid and the pore size of the porous body. He also suggests that there is a critical wetting fluid transportation saturation S_o at which the fluid mobility in the medium becomes zero. A fluid cannot migrate if the saturation is below S_o (0.2 to 0.25), i.e. the liquid cannot reach from one pore to another. This state is called 'pendular state'. The saturation at the transition from this state to the 'funicular state' (when liquid has finite mobility) is 0.3, but is variable depending on the pore geometry.

The above theory explains the observed decrease in warpage behavior with a decrease in saturation within the printed part. The 'inter-layer migration' decreases with a decrease in intergranular saturation. As a result, lesser warpage is observed in the printed parts. The saturation was changed by decreasing the flow-rate or fast axis speed. In these experiments, along with the decrease in the saturation, the green strength of the body also decreased due to lesser amount of binder deposited per unit volume of the powder bed. The difference in the amount of printed binder not only influences the saturation but can also change the shrinkage force during drying.

Another set of experiments were designed where the saturation of the printed part was changed by drying each layer after printing with a halogen lamp, before spreading the powder for next layer. These experiments evaluate the effect of saturation explicitely on the warpage behavior of SD granules. Same amount of binder was deposited in all the printed parts. Figure 4.16 shows the warpage observed in the debound SD parts printed with 7 vol% alumina with and without an intermediate drying step. The parts made with the intermediate drying step did not show any warpage. Figure 4.17 schematically illustrate the effect of intermediate drying on saturation and thereby the warpage behavior of SD granule parts.

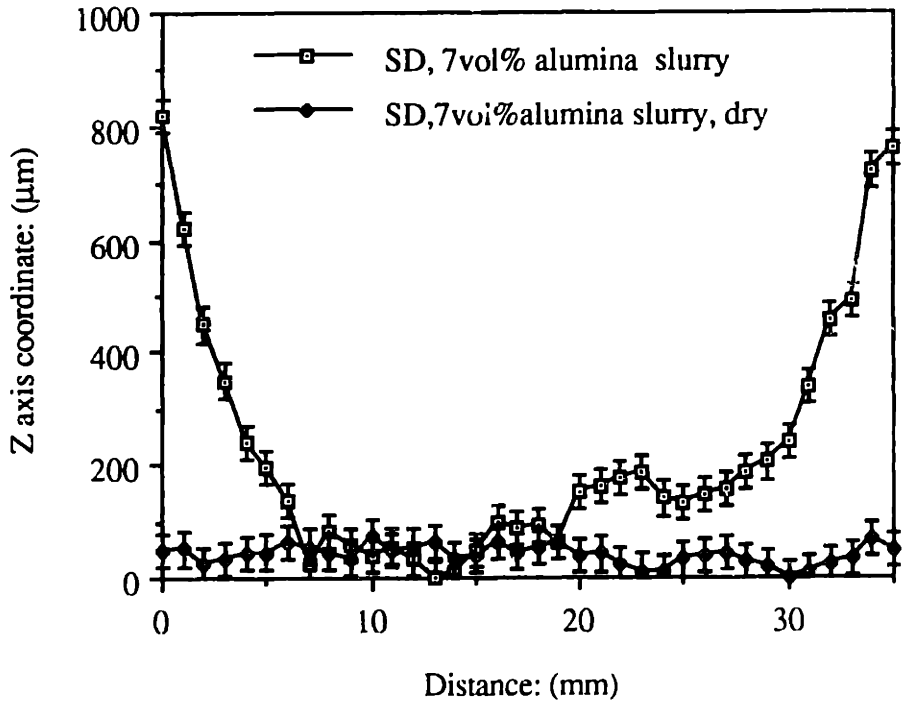

Figure 4.16: Effect of intermediate drying on warpage of SD bars.

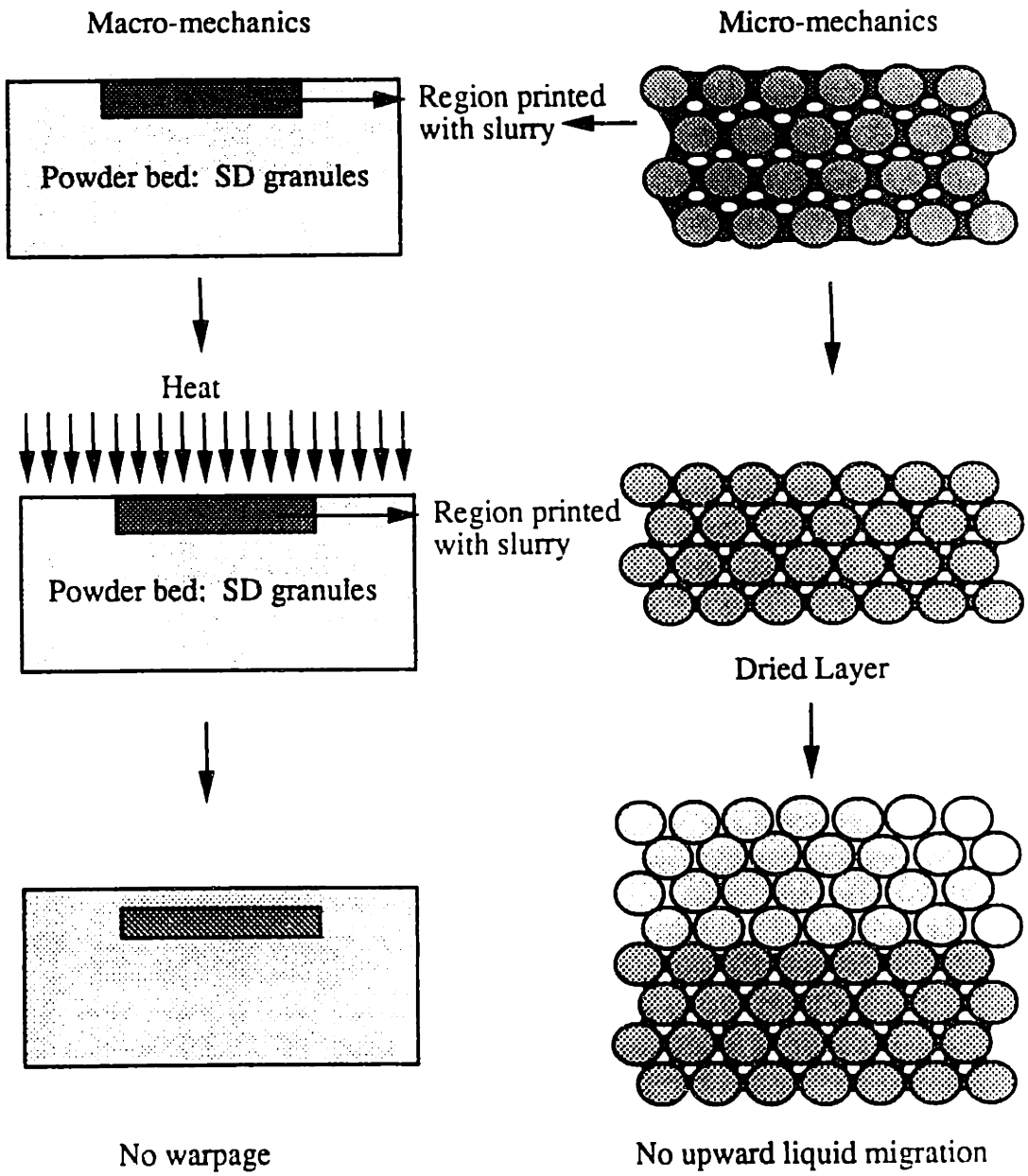

Figure 4.17: Schematic illustrating the effect of intermediate drying on the macro and micro-mechanics of warpage.

Gelling additives capable of absorbing water were added into the SD powder bed to lock the binder in the gel and subsequently prevent the interlayer liquid migration. SD granules parts containing gelling additives did not warp. This experiment is discussed in more details in section 4.5.2.2. The above experiments confirm the role of 'interlayer liquid migation' on the extensive warpage observed in the SD granules parts.

4.4.3.2.2 Effect of SD granules-binder interaction on distortion

The parts made by printing 6 vol% acrysol on SDPAA granules warped but the parts made by printing the same binder on debound alumina granules did not warp. Both the parts were printed at a flow-rate of 1.2 cc/min and a fast axis speed of 165 cm/sec. The results are shown in figure 4.18. Bredt [85] has measured the contact angle of water on alumina as 8.6°. The wetting properties of the debound alumina granules with water should be similar. The polar carboxylic groups present in SDPAA granules are almost completely chemisorbed onto the alumina surface (chapter 4) Therefore, the contact angle of SDPAA with water could be much higher than that of pure alumina.

The fine pores of the debound granules are readily accessible to the printed binder because of the low contact angle. Assuming that all the intragranular (fine pores) volume of debound SD granules is available to the printed liquid, the intergranular saturation of parts printed with a flow rate of 1.2 cc/min and a fast axis speed of 165 cm/sec is calculated as 0.21. This saturation is below the critical saturation for sufficient mobility and is described by the pendular stage (figure 4.19). The liquid in the pendular stage will not migrate upwards when the next powder layer is spread and the warpage is prevented. Excess binder was printed so as to increase the inter-granular saturation beyond critical saturation stage. Parts were built with the same binder and flowrate except the fast axis speed was decreased to 101 cm/sec. The printed intergranular saturation is calculated as 0.81. The parts warped in this case. Printing next few layers resulted in supersaturation within the newly printed layer due to upward moisture migration and resulted in slumping of the parts. The printed part also showed bleeding. Since two layer parts were difficult to handle, the warpage could not be quantified.

The parts made out of SDPAA granule warped when printed at a fast axis speed of 165 cm/sec. The fine pores of the SDPAA alumina granules are not readily available to the printed binder because of higher contact angle. Inter-granular saturation is calculated as 0.95, assuming that most of the printed binder is located within the inter-granular pores. High intergranular saturation lead to 'interlayer liquid migration' and resulted in warpage of the printed parts.

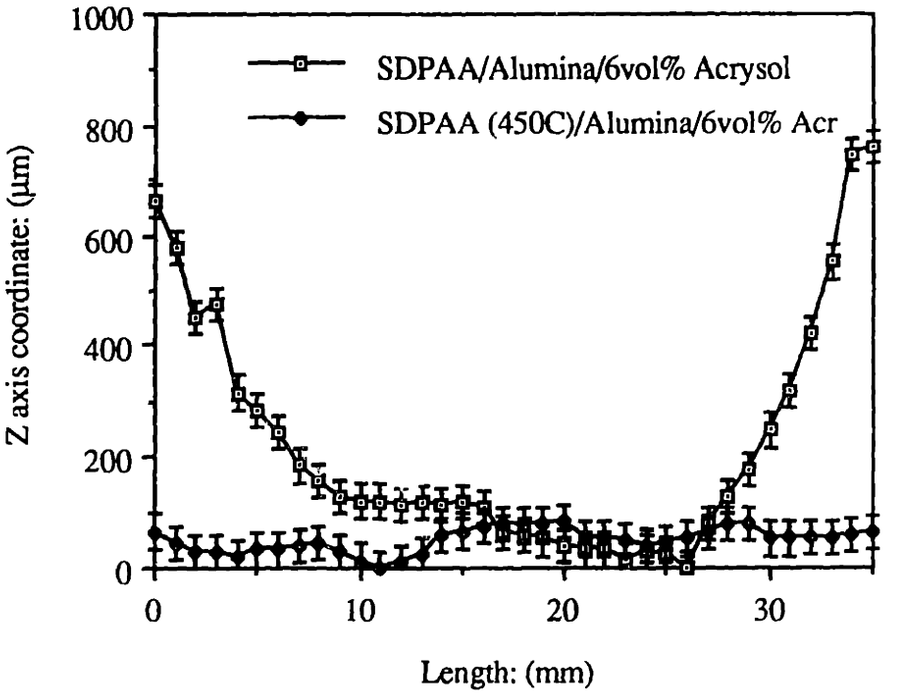

Figure 4.18: Warpage: Debound and non-debound granules.

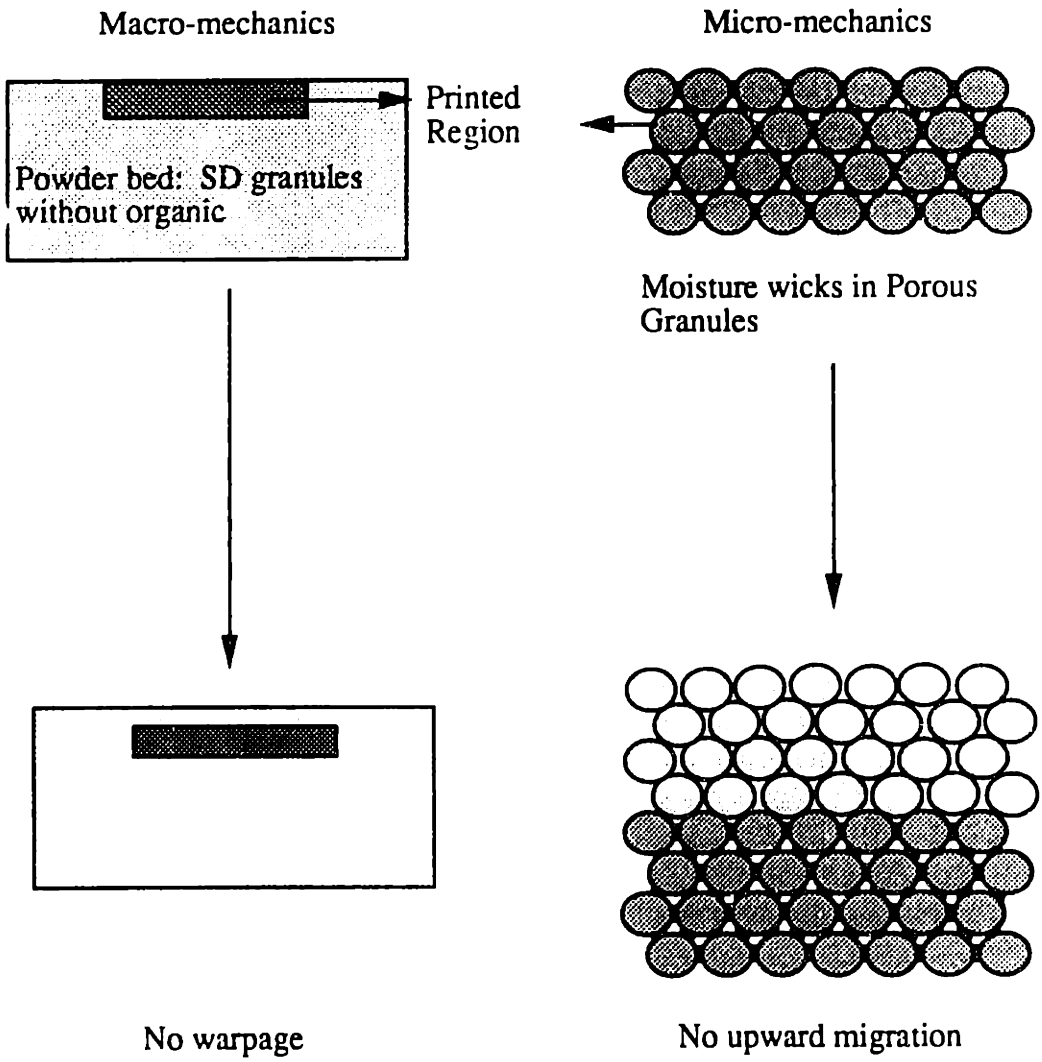

Figure 4.19: Micro and macro-mechanics of warpage behavior in parts made out of debound alumina granules/6 vol% acrysol system.

The green strength of the parts made by printing 6 vol% acrysol on SDPAA and debound granules was measured using a 4 point bend testing method. Printing was performed at a flow-rate of 1.2 cc/min and a fast axis speed of 165 cm/sec. The strength of the parts made with the SDPAA granules was measured as 0.84 MPa (Std dev 0.14 MPa), while those made out of debound granules as 0.27 MPa (std dev 0.03). The strength of the SD granules parts will depend on the amount of binder deposited at the neck region. Onada [98] has shown that the strength of a green ceramic body depends strongly on the amount, distribution and nature of the binder phase within the preform. The parts made out of debound granule will have less binder at the neck region, since the binder can readily go inside the granules, and as as a result would be weaker. The observed lower strength of the debound SD parts confirm our assumption that the fine pores in this system are readily available to the printed binder.

4.4.3.3.3 Effect of binder on distortion

The parts were built by printing 6, 15 and 36 vol% acrysol binder on the SDPAA/alumina granules. All the printed parts were printed at a flow-rate of 1.2 cc/min and a fast axis speed of 165 cm/sec. The parts printed with 36 vol% acrysol showed the most warpage. The maximum warpage occured at the two ends of the bars. The maximum warpage for 6 vol% acrysol parts was measured as 690 μm, for 15 vol% acrysol as 1484 μm while that for 36 vol% as 4370 μm (figure 4.20). This gives the ratio of warpage as 1: 2.1: 6.3. The capillary stress due to the printed binder is the same in all the above parts, as the binders have the same latex particle size and solvent. However, the cross-sectional area of the binder at the neck region between the SD granules, during drying, is the highest in the parts printed with 36 vol% acrysol. Therefore, the net 'shrinkage force' due to the printed binder on the spread powder is highest in parts built with 36 vol% acrysol. Higher shrinkage force would result in higher shrinkage of the powder bed. The ratio of binder concentration is 1: 2.5: 6.0 which is very close to the measured warpage ratio. Therefore, increase in the shrinkage force was found to be directly proportional to the ratio of acrysol (latex) binder concentration.

The extent of warpage was also found to be a strong function of the nature of the printed binder. Figure 4.21 shows the warpage behavior of SDPAA/alumina granules printed with water, 6 vol% acrysol and 7 vol% alumina. The binder flow-rate in all the three cases was ~1.2 cc/min and the fast axis speed was 165 cm/sec. The parts printed with water did not show any warpage while the parts printed with acrysol and alumina slurries warped. The parts printed with alumina slurries warped slightly more than the

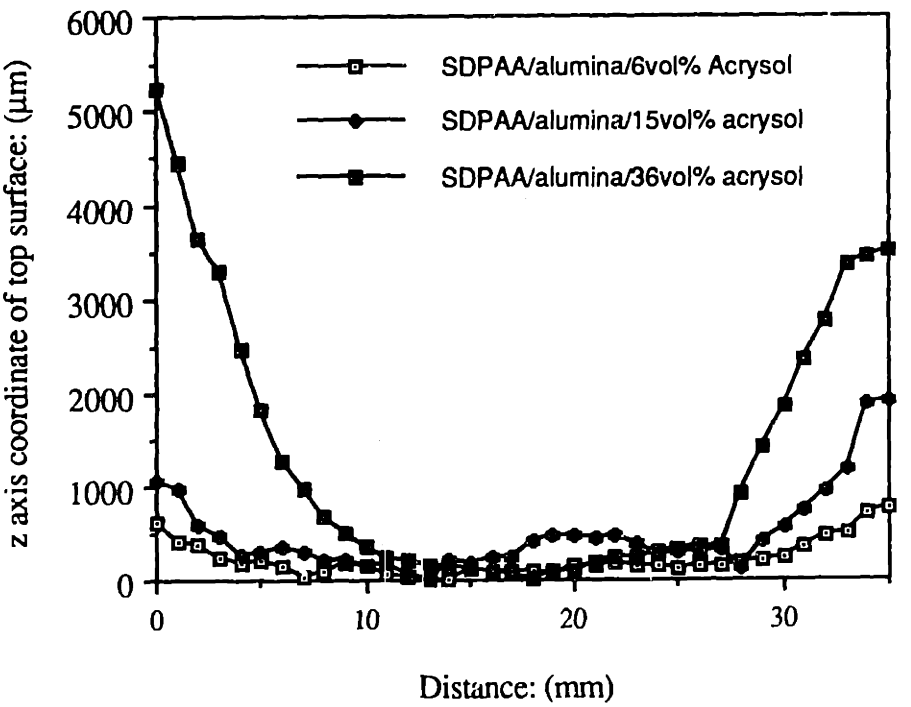

Figure 4.20: Warpage: Effect of concentration of the printed binder.

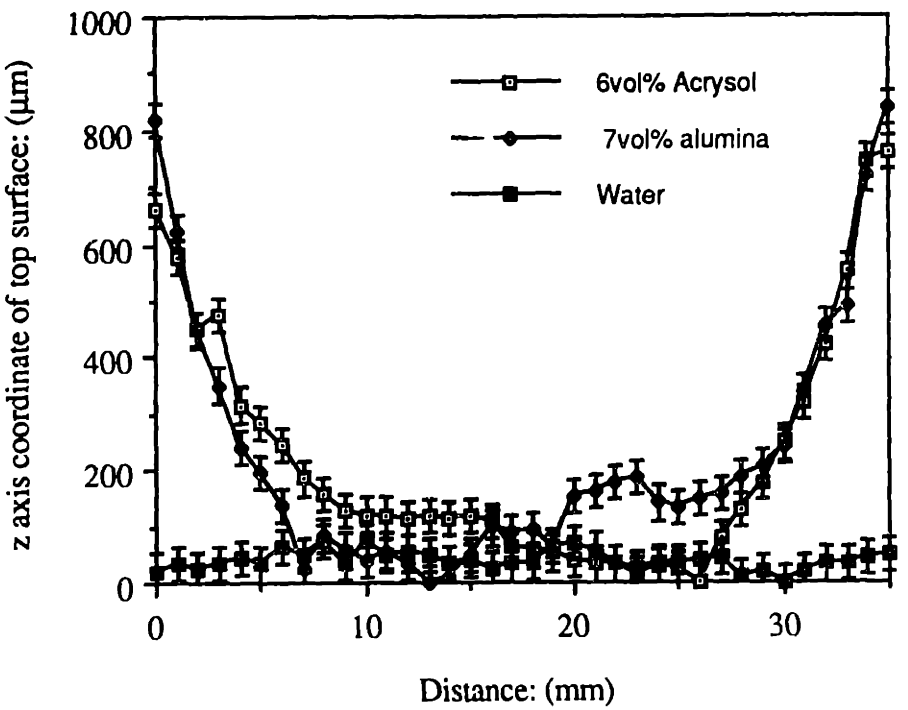

Figure 4.21: Warpage: Effect of nature of the printed binder.

part made by printing acrysol binder. The maximum stress in parts printed with water is due to the capillary pressure corresponding to the intergranular pores (6 μm), during drying. The drying stress is calculated as 24 KPa, assuming full saturation conditions. However, based on the actual printing parameters, the net intergranular saturation in the printed parts was 0.21. Therefore, the actual drying stress would be considerably less than 24 KPa. This stress level appears to be not enough to warp the SD granules parts.

Acrysol and alumina binder, on the other hand, contain sub-micron particles and could result in higher capillary stress in the binder necks between the SD granules than those based on the intergranular pores. Also, these binders can bond with the surface of granules and pull the powder layer closer, due to the shrinkage induced in the binder during drying. It is hard to compare the shrinkage behavior of acrysol with alumina slurries, as acrysol consists of latex spheres with a minimum film formation temperature of -10 C [99] while the alumina slurries consist of rigid non-deformable ceramic particles. The stress supported by the binder is a strong function of their elastic modulus [100] :

$$\sigma = \frac{E(\sigma)\varepsilon}{(1-\upsilon)}$$

Acrysol forms a film at room temperature, therefore, shrinkage force is capable of deforming its particles. Acrysol has a glass transition temperature of ~ 45 C which is lowered in the presence of water. Therefore, acrysol will have more viscous component than alumina. The alumina slurry network will be capable of supporting more stress than the acrysol binder based on the above equation. Therefore, more elastic stress can be stored and transferred between layers in alumina system as compared to acrysol. Alumina should result in more warpage since elastic stresses are responsible for relative shrinkage. However, unlike acrysol particles which can deform and form a film during drying, the rigid alumina particles deposited in the powder bed can also hinder the shrinkage process.

4.5 Strategies to avoid shrinkage

4.5.1 Avoid physical ejection or physical rearrangement during printing

4.5.1.1. Vacuum deposition of powder

The objective of this work is to use vacuum to increase the cohesiveness of the powder bed. The critical flow-rate of air around a single granule in order to prouce a drag force equivalent to the weight of the particle is calculated by Stoke's law [101] as 5.31 * 10^{-5} m/s. Our preliminary investigations showed that the SD granules powder bed become very cohesive when the vacuum is sucked from the bottom of the powder bed. A special piston plate was machined (Thanks to Jain!) as shown in figure 4.22 to suck vacuum through the powder bed on the proto machine. The piston plate consists of a

borosilicate filter mounted on an aluminum plate with openings at the bottom of the plate which can be connected to the vacuum pump to suck vacuum through the powder bed. It was found that layers could not be spread easily if the vacuum was on. Therefore, layers were spread with the vacuum turned off. After the powder layers are spread, vacuum is turned on before printing. Printing was performed with 6 vol% acrysol at a fast axis speed of 165 cm/sec on SDPAA powder bed. The very first printed layer showed ejection, though considerably less than the parts printed with no vacuum on. The extent of ejection increased as the thickness of the printed part increased. Drying of the printed layers did not improve the ejection problem. The bottom surface of the green part made with vacuum deposition appeared to be smoother than that obtained by the regular method (no vacuum).

The downward holding force on a granule due to the suction of air through the powder bed is calculated by Darcy's law as 10^{-8} N while the force imparted on a granule due to the binder droplet impact is calculated as 10^{-6} N. Since the incoming droplets have a higher energy then the force holding down the particles, ejection is inevitable. However, if the energy of the incoming droplets be decreased by using a DOD printing technique then the ejection can be potentially avoided. The major advantage of this technique is that the powder remains cohesive as long as the vaccum is on. Once the vacuum is turned off, the SD granules become highly flowable again. This attribute is extremely useful for powder removal stage.

4.5.1.2 Use of PEG/water mist to increase the cohesive strength of the powder bed

The parts made by the press-rolling technique did not warp during the build stage. Even though the packing density of the press-rolled powder bed is just 40%, the powder bed is highly cohesive and prevents rearrangement of the particles during printing and drying. The high cohesive strength of the powder bed, however, also makes the powder removal an extremely difficult job. We investigated the role of PEG mist to increase the cohesive strength of the powder bed made out of SDPAA/alumina granules. Solutions containing upto 10 wt% PEG (Mwt 4600) were sprayed on the SDPAA powder bed with a humidifier. The cohesive strength of the powder bed improved but was not good enough to prevent ejection. Ejection of powder will depend not only on the cohesive strength of the powder bed but also on the momentum of the incoming droplets. By incorporating low velocity droplets and appropriately modifying the strength of the powder bed, it should be possible to avoid the ejection and loss of packing density of SD granules powder bed during printing.

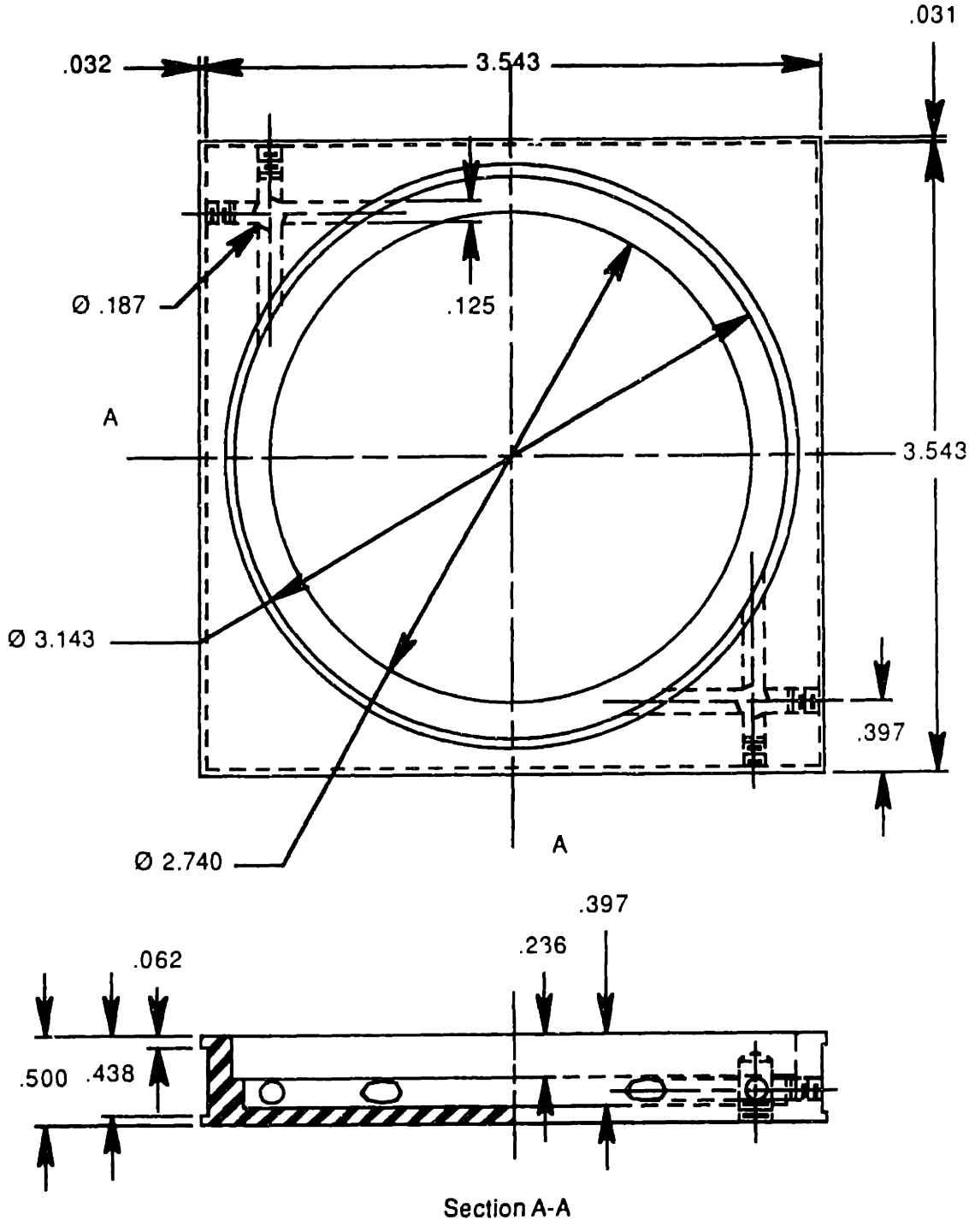

Figure 4.22: Schematic of bottom plate for vacuum piston (Jain).

4.5.2 Avoid moisture migration

4.5.2.1. Intermediate drying of printed layers.

In order to avoid the interlayer liquid migration process, printed layers were dried so that there is no moisture left in the printed layer to migrate upwards. Experiments were performed by printing 7 vol% alumina slurry on debound SD granules. The heating set-up consisted of a 1000 watt quartz halogen lamp and a variac was used to limit the voltage to half its specified voltage (120 V). The set-up was held above the powder bed for 2 minutes. The temperature of the powder bed was measured by a thermocouple as ~ 65 C. Printing was performed at a flow rate of 1.2 cc/min and fast axis speed of 165 cm/sec and 101 cm/sec. The measured warpage for a part printed with and without intermediate drying is shown in Figure 4.14. The part without an intermediate drying step shows warpage while the one with intermediate drying does not show warpage. The explanation for this observation is schematically shown in figure 4.15. Through the intermediate drying step, the moisture is removed from the printed layer before the next layer of SD granules is spread and the possibility of upward moisture migration is eliminated.

4.5.2.2 Adding gelling additives to the powder bed

The objective of this strategy was to lock the printed binder in the the form of a gel by incorporating polysaccharides additives in the powder bed. Carrageenan [102] is a naturally occurring family of polysaccharides extracted from the red seaweed and are used as gellants and thickeners in pharmaceutical, cosmetic and food industry. One of the variety of Carrageenan is Viscarin 109 with a higher levels of ester sulphates. It absorbs water at room temperature to produce a gel. 7 vol% alumina slurry was printed on a powder bed made out of debound SD granules containing 5 wt% (d.w.b. of powder) Viscarin 109. Viscarin powder was added to the SD granules and was mixed in the ball mill. The parts were printed at a binder flow-rate of 1.2 cc/min and a fast axis speed of 165 cm/sec. The parts did not show any warpage, indicating that the printed binder gets locked in Viscarin as a gel and does not participate in interlayer liquid migration. The distribution of the viscarin (mixed by dry milling) in the powder bed was found to be quite non-uniform and it can adversely affect the properties of the fired part. It is conceivable to incorporate the gelling additive in the SD granulation process to ensure the uniformity of their distribution.

4.5.2.3. Coating granules to seal the intragranular pores

The objective of this study is to coat the granules so that the fine pores are sealed and the SD granules behave like coarse spherical particles. As shown earlier, parts made

out of dense particles do not exhibit the unusual warpage behavior of the SD granules. One of the major challenges in developing this process is to keep the flowability of the SD granules intact i.e. coat the granules but still be able to avoid any neck formation between the granules (agglomeration of granules). The major disadvantage of this approach is the reduced amount of external matter that can be deposited by printing in SD granules powder bed, as the fine pores will no longer be available for absorbing printed binder.

We tried two different approaches to coat the SD granules. First approach consisted of spray drying SDPAA granules disperesed in dilute acrysol binder. The suspension concentration was chosen so as to capture one granule per droplet. Most of the granules were deposited on the walls of spray dryer.

The second approach consisted of mixing acrysol/alumina codispersion in a rotovap and gradually drying. The dried mass came out as big flakes and agglomerates of SD granules. Agglomeration of granules reduced the flowability of the powder. In both the approaches, the flowability of the powder was sacrificed as the SD granules bond with each other during the coating process.

4.5.3. Decrease the strength of the polymer binder

The strength and the elastic modulus of the polymer binder can be reduced by adding an appropriate plasticizer to the binder solution. As shown earlier, the amount of stress supported by the printed binder is directly proportional to its elastic modulus. Elastic modulus of the acrysol binder was reduced by plasticizing the binder with PEG (Mwt 1000). The binder formulation was changed form 6 vol% acrysol to 6 vol% acrysol plasticized with 25 wt% of PEG 1000 (d.w.b. of polymer). The warpage behavior of parts printed with regular and plasticized binder is shown in figure 4.23. The parts printed with the binder containing the plasticizer showed no warpage. However, the green strength of the parts also reduced. An optimal plasticizer amount will have to be designed for each system in order to eliminate warpage by this method without sacrificing too much of green strength.

4.6 Properties of the green parts

The packing density of the green part was measured as 31.3%. The printed part densified to 51.5% after being fired at 1650 C for 2hours (No isopressing). Figure 4.24 shows the SEM micrograph of the polished cross-section of the fired part. The micrograph clearly shows that the individual granules have densified. However, the big intergranular pores remained intact during the firing process. Individual layers are easily distinguishable in the printed part indicating the presence of interlayer defects.

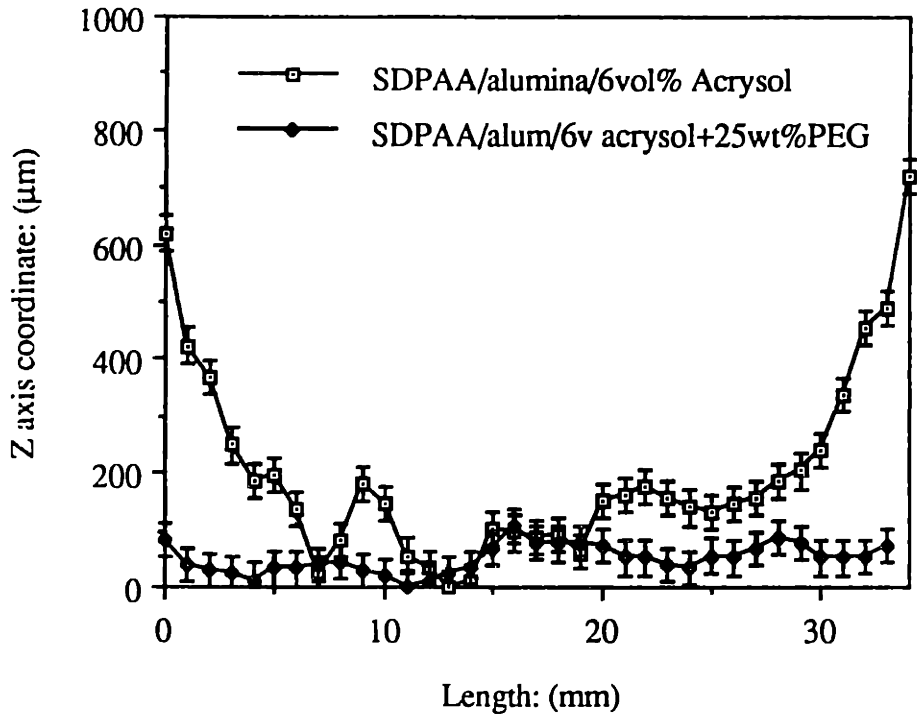

Figure 4.23: Effect of plasticizer in the binder on warpage of SDPAA/alumina parts.

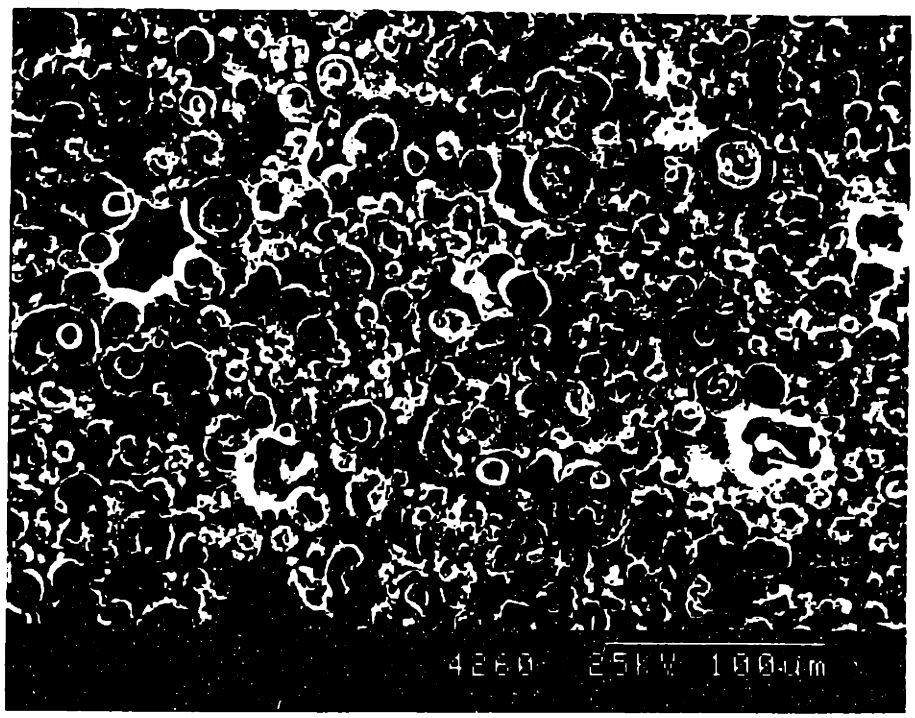

Figure 4.24: SEM of the polished fired cross-section of the SD part (No cipping).

4.7 Post processing of the green parts

The SD green bodies were densified with the help of isopressing. Figure 4.25 shows the variation in the packing density of the green body as a function of isopressing temperatures. All the parts were pressed at 40,000 psi for 10 minutes. Parts wipped at 80 C attained almost full density (>99%) upon firing at 1650 C.

Figure 4.26 shows the measured shrinkage of the SD granule parts along different directions between the green and the fired stage. The shrinkage exhibits anisotropic behavior with the maximum shrinkage along the z axis. However, low standard deviation values indicate highly reproducible shrinkage.

During wipping, there were no problems of shear distortion or z-axis warpage, indicating uniformity in the packing density of the powder bed (Figure 4.27 & 4.28). Powder removal was extremely easy. The uniformity of the powder bed helped not only to reduce the distortion problems but also to achieve superior mechanical properties. The 4 point bend strength of the fired SDPAA part was measured as 360 MPa as compared to 320 MPa for the fired press-rolled part . Also, the grain size of the SD parts were smaller (3.7 μm) and more uniform than those obtained by the press-rolled process (5.6 μm).

4.8 Conclusions

The uniformity of spread powder layers was improved significantly by the use of highly flowable SD granules over those obtained by the press-rolling process. The individual pores in the powder bed do not have any preferential orientation along the axis of the layer. Therefore, the basic microstructural unit in the SD granular powder bed is more isotropic than the press-rolled powder bed. The use of SD granules, however, did not eliminate interlayer defects. The parts made out of SD granules exhibited extensive warpage during the printing stage. The extensive shrinkage produced in the SD parts during printing stage creates an anisotropy in the build process; the new printed element undergoes a relative shrinkage with the existing printed region.

Two different factors were found to be responsible for introducing excessive shrinkage in the SD granule parts during printing stage. SD granules containing water soluble organic additive, such as poly ethylene glycol (PEG), disintegrated during printing and shrank upon drying to high packing density. The relative shrinkage between the two printed lines was measured as 7.9%. This shrinkage resulted in warpage of the printed layer, as the lines are built sequentially and bonded to each other .

Shrinkage due to SD granules dissolution was avoided by the use of SD granules containing 2 wt% polyacrylic acid (PAA) as an additive. PAA was shown to be

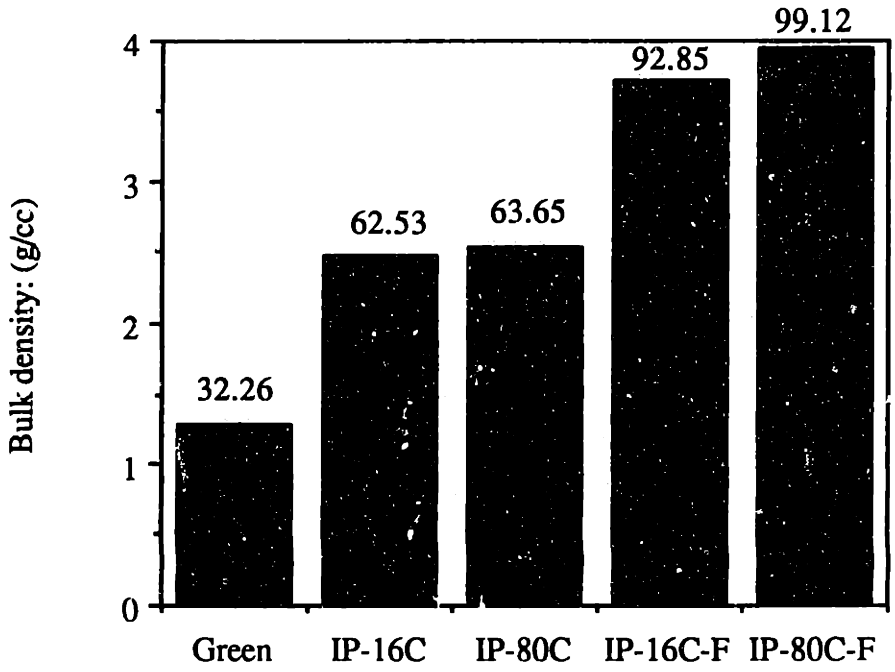

Figure 4.25: Packing density of isopressed and fired part as function of isopressing temperature.

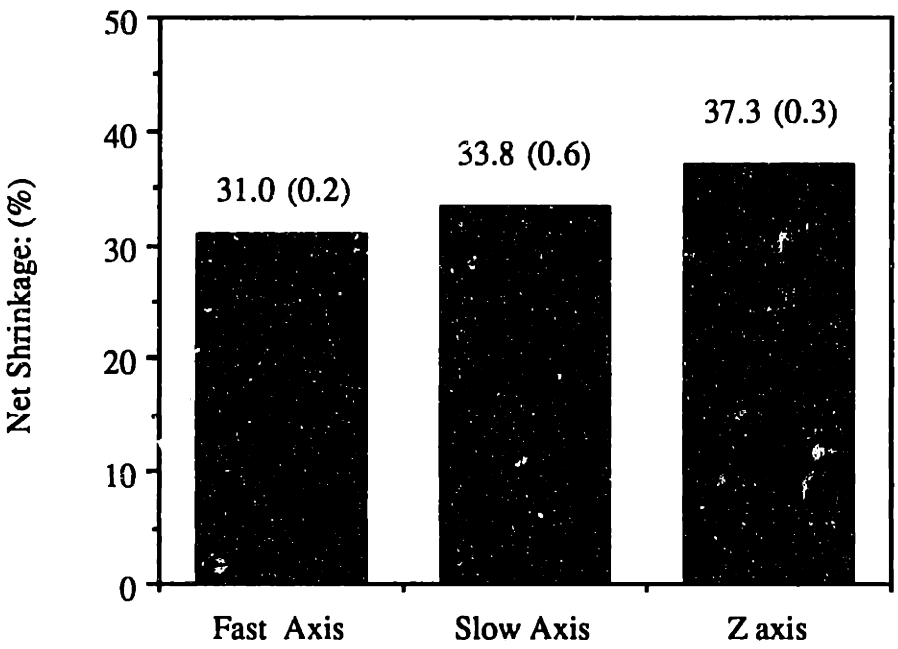

Figure 4.26: Shrinkage of the SD granule bars along different directions.

Figure 4.27: Optical micrograph of a SD part after wipping showing the absence of shear distortion.

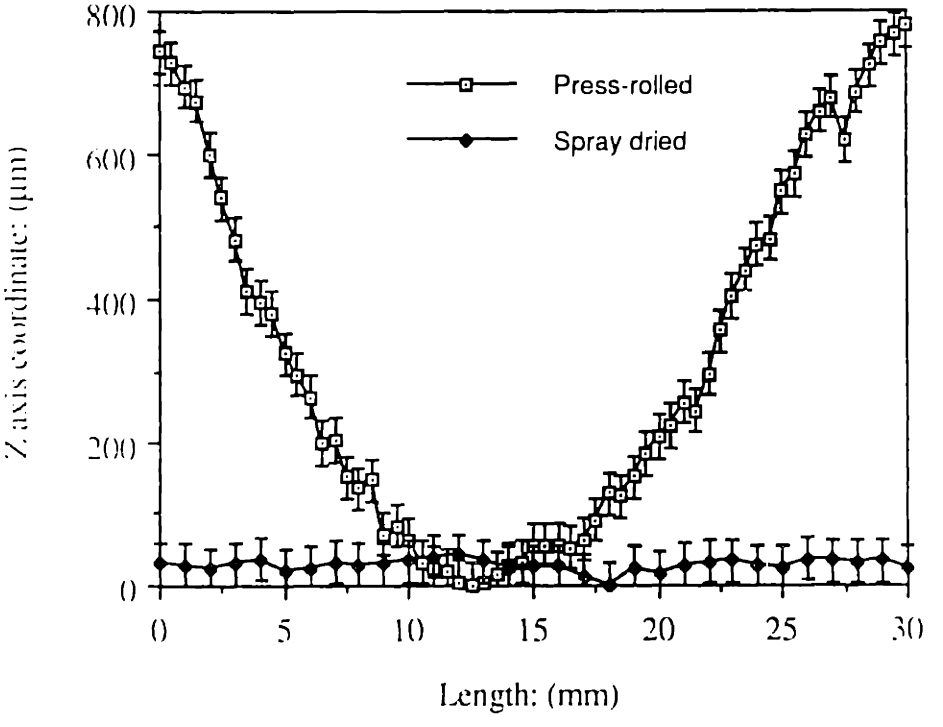

Figure 4.28: Measured z-axis warpage of a press-rolled and a SD bar after wipping.

completely chemisorbed to the alumina surface and as a result insoluble in water. Therefore, SDPAA granules did not disintegrate upon printing.

The parts made with SDPAA granules, however, warped when powder layers were spread on top of printed layers. Fine pores (~ 0.1 μm) in the spread layers can absorb liquid from the larger inter-granular pores (~ 6 μm) of the printed layers. Spreading of a new powder layer created an anisotropic liquid migration condition with respect to the printed layer below. This introduced an asymmetry in the build process. The mass flux of liquid migration due to intragranular (fine) pores of SD granules was calculated as 1.1 g/cm^2-s. The mass flux due to water evaporation to atmosphere, in comparison, is in the order of 10^{-4} g/cm^2-s. The anisotropic interlayer liquid redistribution introduced a compressive force on the top surface of the printed region and therefore resulted in warpage of the printed region. The extent of asymmetry and as a result warpage was shown to be strongly dependent on the saturation of the printed part and on the strength of the printed binder. Higher saturations and higher strength binders resulted in increased warpage.

The asymmetry in the build process due to interlayer liquid migration has been reduced by employing an intermediate drying of the printed layers with a heat lamp and/or plasticizing the binder. Heating of a printed layer with long wavelength light ensured uniform drying and avoided the anisotropic interlayer liquid migration during spreading of a subsequent powder layer. The addition of a plasticizer (PEG, Molecular weight 1000) decreased the strength of the acrysol binder and therefore reduced the warpage. The above strategies have been used to successfully fabricate complex shaped parts out of alumina and silicon nitride.

The parts made out of SD granules are ~30% dense and require an intermediate isopressing step to achieve the critical packing density, before they can be sintered to full density. Isopressing was shown to heal the interlayer defects, thereby improving the uniformity of the pressed parts. The SD parts did not exhibit distortion problems during the isopressing step, thus indicating uniform packing density.

CHAPTER 5
PRINTING SLURRIES ON SPRAY DRIED GRANULES

5.1 Introduction

The parts made by printing acrysol on the spray dried (SD) granules are ~ 30% dense. These printed parts require an additional densification step in the form of isopressing to increase the green density to ~ 60% before they can be sintered to full density upon firing. The benefits of making high green density parts directly by 3DP are several. High green density parts will not require the isopressing step. They will also result in low shrinkage. The objective of this research was to deposit matter in the form of colloidal suspension through an ink-jet printhead into the powder bed to increase the packing density of the printed part. This study will also help to identify the key issues involved in changing the composition of the powder bed on a local scale by printing colloidal suspension.

5.2 Process concept

The objective of this reserach is to deposit slurries through an ink-jet printhead in order to fill the big intergranular pores of the SD granule powder bed. The intergranular pores of the powder bed made out of SD granules are in size range of 6-8 μm and do not have the driving force to densify by pressureless sintering. The individual granules, however, densify completely during sintering, as the intragranular pores are in the range of 0.05-0.1 μm. The goal is, therefore, to fill the intergranular pores with submicron particles to increase the packing density of the green parts and reduce the big pores to submicron size for enhanced densification behavior during firing. The process concept is schematically shown in figure 5.1. The key process variable is the solids concentration required in the slurries to make 60% dense green parts out of SD granules powder bed. Figure 5.2 shows the calculated increase in the green density of a 30% dense SD powder bed as a function of the solids concentration in the printed slurry. This calculation assumes that the pores are filled to 100% saturation and the initial packing density of the powder bed is preserved during printing. It shows that alumina slurries containing 42 vol% solids will have to be printed into SD granules powder bed to make 60% dense green parts.

The development of this technique required the processing of SD granules and the printing of slurries through an ink jet printhead. Chapter 4 describes the manufacturing and properties of the SD granules. The printing of alumina slurries through a nozzle, at the time of this process development, was novel for the entire 3DP research group.

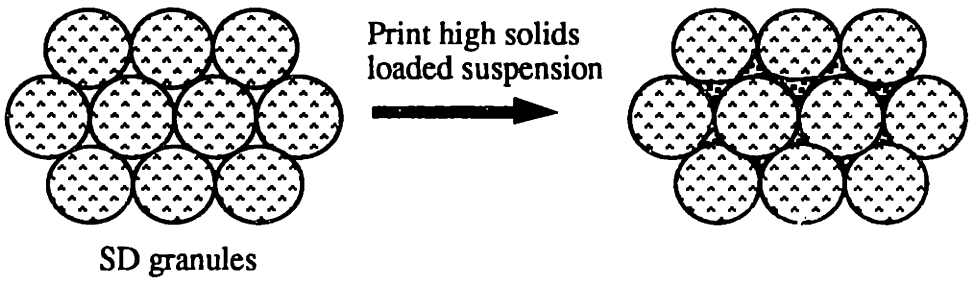

Figure 5.1: Schematic of building high green density part by printing slurries on SD granules powder bed.

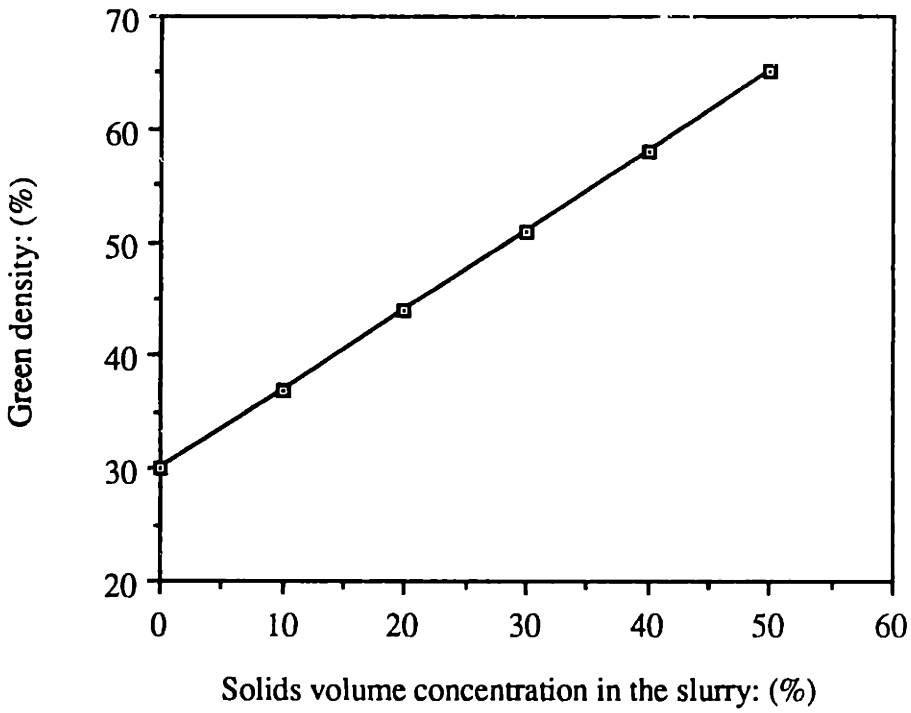

Figure 5.2: Calculated increase in the green density of a 30% dense SD powder bed as a function of the solids concentration in the printed slurry.

Colloidal silica [85] and latex emulsion [103] are used as binders for fabricating investment casting and tooling parts respectively. Both of these binder systems are used with minor chemical modifications to the pre-formulated materials received directly from the vendor. The printing of alumina slurries provided us with the opportunity of tailoring the properties of the binder in-house. The lessons learned in printing alumina suspension will be useful to print other colloidal suspensions, which are not commercially available.

The first section of this chapter describes the strategies necessary to print concentrated alumina suspension through a fine orifice. The latter half of the chapter then discusses the properties of the green parts made by printing alumina slurries into SD granules powder bed.

5.3 Printing slurries

The important processing steps necessary to print any binder by three dimensional printing technology involve: devising a setup to obtain a stable and consistent flow of suspension without losing too much solids during filtration, and determining the right printing parameters for producing uniform sized droplets. A stable flow rate will depend on the nature and the quality of the slurries and its interaction with the nozzle and the filters [85].

5.3.1 Slurry preparation

5.3.1.1 Requirements

The dispersion quality of slurries greatly affects its rheological properties: the flow of matter in response to the applied stress [104, 105]. The key requirement for printing in 3DP is that the material dispersed in the liquid system be stable with respect to the fluid delivery system. The binder must be stable and should not settle in the tubes while being pumped from the reservoir to the tip of the nozzle. It should be stable under moderate shear in the tubing and the filters, stable with the rinse solution, able to survive the brief but enormous deformation that occurs inside the nozzle.

The flow of a liquid through a straight capillary is given by Poisseule's law [101] which states that the applied pressure increases linearly with the increase in viscosity of the liquid for a constant flow-rate. It is necessary to keep the viscosity of the slurries low to obtain the required flowrate (~ 1.2 cc/min) at low pressure. Therefore, the slurry rheology should be controlled in order to avoid shear thickening behavior. Orifice size controls the size of the droplets and also the feature size. The binder printed through finer orifices potentially translate into better resolution. Currently, all the binders are printed

through 45 μm size orifice, therefore based on the empirical ratio [106], the size of the particles should be kept under 2.5 μm for a stable flow.

5.3.1.2 Preparation and characterization

The slurries were prepared by adding submicron sized alumina powder (Reynolds RC-172 DBM) in deionized water gradually. The pH of the slurries was continuously modified to 3.5 with 0.1 M nitric acid. The isoelectric point of alumina in water is ~ pH 7.5. The colloidal alumina suspension is very stable at pH 3.5 as it has a fairly large zeta potential ~ 60 mV. The Schulze Hardy [107] rule shows that the stability of a slurry is inversely proportional to the square of the charge on the counterion, present as impurities. Therefore, counterions with higher valency will tend to coagulate the slurry which is undesirable for printing purposes. The use of deionized water ensures absence of high valence counterions. The slurries were mixed on a ball mill for 24 hours. In order to remove the unbroken agglomerates, alumina suspensions were size-classified by a semi-continuous centrifugal classification technique, developed in Ceramics Processing Research Laboratory at MIT [108]. Table 5.1 lists the operating parameters for classifying alumina slurries. The resulting size-classified suspensions had ~ 7 vol% alumina particles concentration. The suspensions were further concentrated in a batch centrifuge. The pH of the suspensions was always maintained at 3.5.

The particle size distribution of the classified slurries is shown in figure 5.3. The average particle size of the slurries is 0.67 μm. The viscosity of 30 vol% alumina slurry was measured by a rotary viscometer as 9.4 mPa.s. The plot of viscosity vs shear rate as shown in figure 5.4 shows almost newtonian response, with very little dilatancy or shear-thickening.

5.3.2 Selection of nozzle

The second step in printing colloidal slurries was the selection of the right kind of nozzle. At the time, silica binder was being printed with nickel orifice Diconix system. Therefore, our first attempt involved printing slurries with nickel orifices.

5.3.2.1 Requirements

The key requirements of the nozzles are to withstand the rigors of the chemical suspension without any wear and also be chemically inert to the binder. The successful fulfillment of these requirements is essential to obtain a stable and a consistent flow of slurries through a nozzle.

Table 5.1: Operating parameters for classifying alumina slurries.

- Add 48 cc of concentrated nitric acid to 8000 cc of deionized water; shake
- Add 4400 g of alumina (RC172-DBM w/o MgO); shake
- Mill for 24 hours (no media)

Cut size (μm)	Flowrate (cc/min)	RPM
1.2	455	1500
0.8	375	2000

The viscosity of 30 vol% slurry was measured by rotary viscometer as 9.4 mPa.s (centipoise).

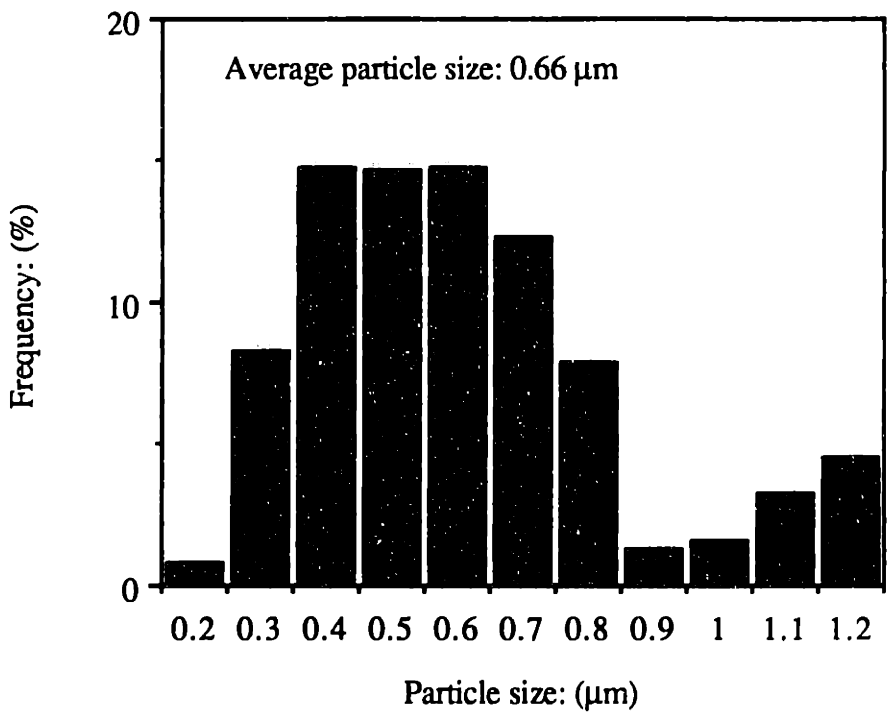

Figure 5.3: Particle size distribution of classified alumina slurries.

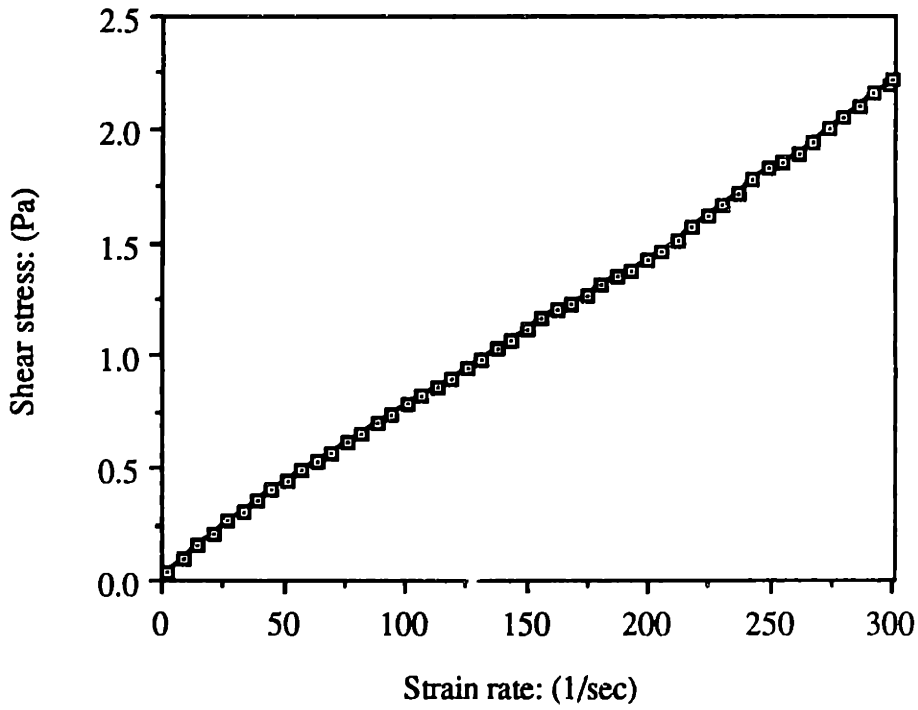

Figure 5.4: Shear stress vs strain rate plot for 30 vol% alumina slurries.

5.3.2.2 Results and discussions

The metals used in nozzle set-ups are susceptible to corrosion. Nickel and stainless steel are the most widely used materials in the manufacturing of printheads. These materials are most stable at a pH range of 9.5 - 10.5. Sapphire nozzles are also used as orifices in the printheads [109].

Nickel orifice plates were used to print alumina slurries. The diameter of the orifices weres measured before and after printing. The filtration assembly, at that time, was not optimal and consisted of only one 5 μm capsule filter. The flow-rate of the alumina slurries coming out of the nickel orifices was also measured with time.

The measured flow-rate data (figure 5.5) for printing 32.88 vol% alumina slurries shows an increase in the flow-rate with time. The experiment was stopped after 22 minutes and the nickel orifice was inspected under an optical microscope. Figure 5.6 shows the optical micrographs of the same orifice plate before and after printing alumina slurries. The increase in diameter of the orifice from 47.18 μm to 82.5 μm explains the increase in the flowrate as the printing progressed. The alumina slurries were electrostatically stabilized at pH 3.5, therefore, the increase in orifice diameter could have been either due to the ceramic particles (erosion) and/or due to the corrosive action of the acidic water. In order to measure the relative contribution of corrosion, deionized (DI) water at pH 3.5 was printed through the nickel orifice plates. Figure 5.7 shows the optical micrographs of the same nickel orifice before and after printing the acidic water. Figure clearly shows the increase in diameter of the orifice. Table 5.2 lists the erosion rates of nickel orifice plates while printing acidic water and alumina slurries. The erosion rates of nickel orifices while printing 32.88 vol% alumina slurry was measured as 1.61 μm/min while that for acidic water as 0.234 μm/min. Erosion is the dominant mechanism of wear while printing concentrated slurries. Ni orifices, therefore, can not be used with the binder system when the latter contains ceramic particles. The printing of alumina slurries requires a ceramic orifice to avoid erosion. Wire bonding alumina nozzles were subsequently used to print alumina slurries. The use of ceramic nozzles solved the erosion problem.

5.3.3 Filtration optimization

5.3.3.1 Requirements

The main challenge in ink-jet printing of high solids loaded suspensions is to obtain a consistent and a stable flow of binder without losing too much solid during filtration. The filter material should be chosen so that it is chemically stable against the

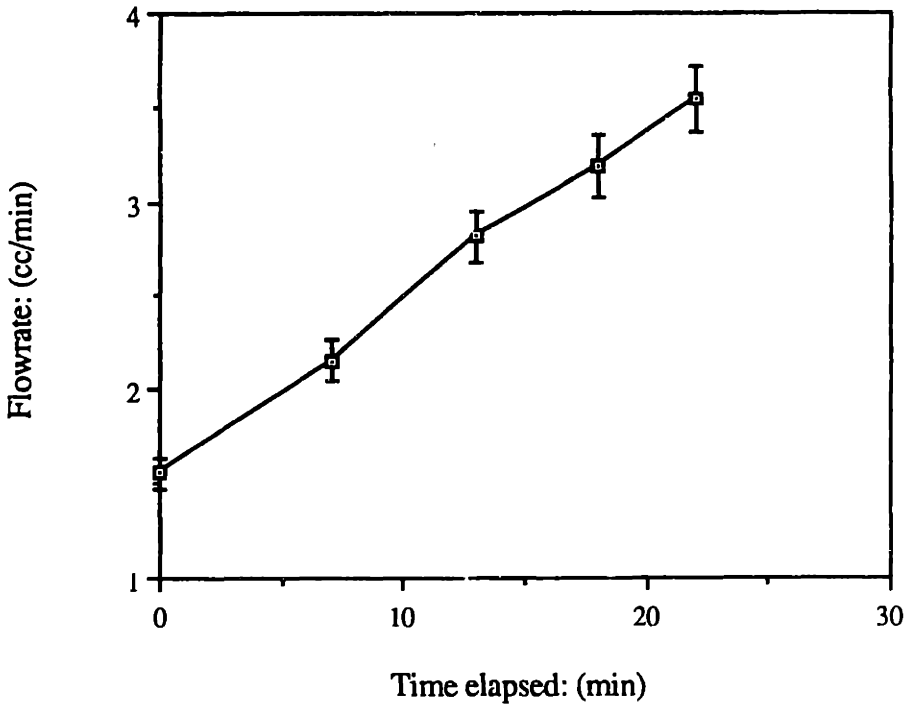

Figure 5.5: Measured flowrate of 32.88 vol% alumina slurry through a nickel orifice plate.

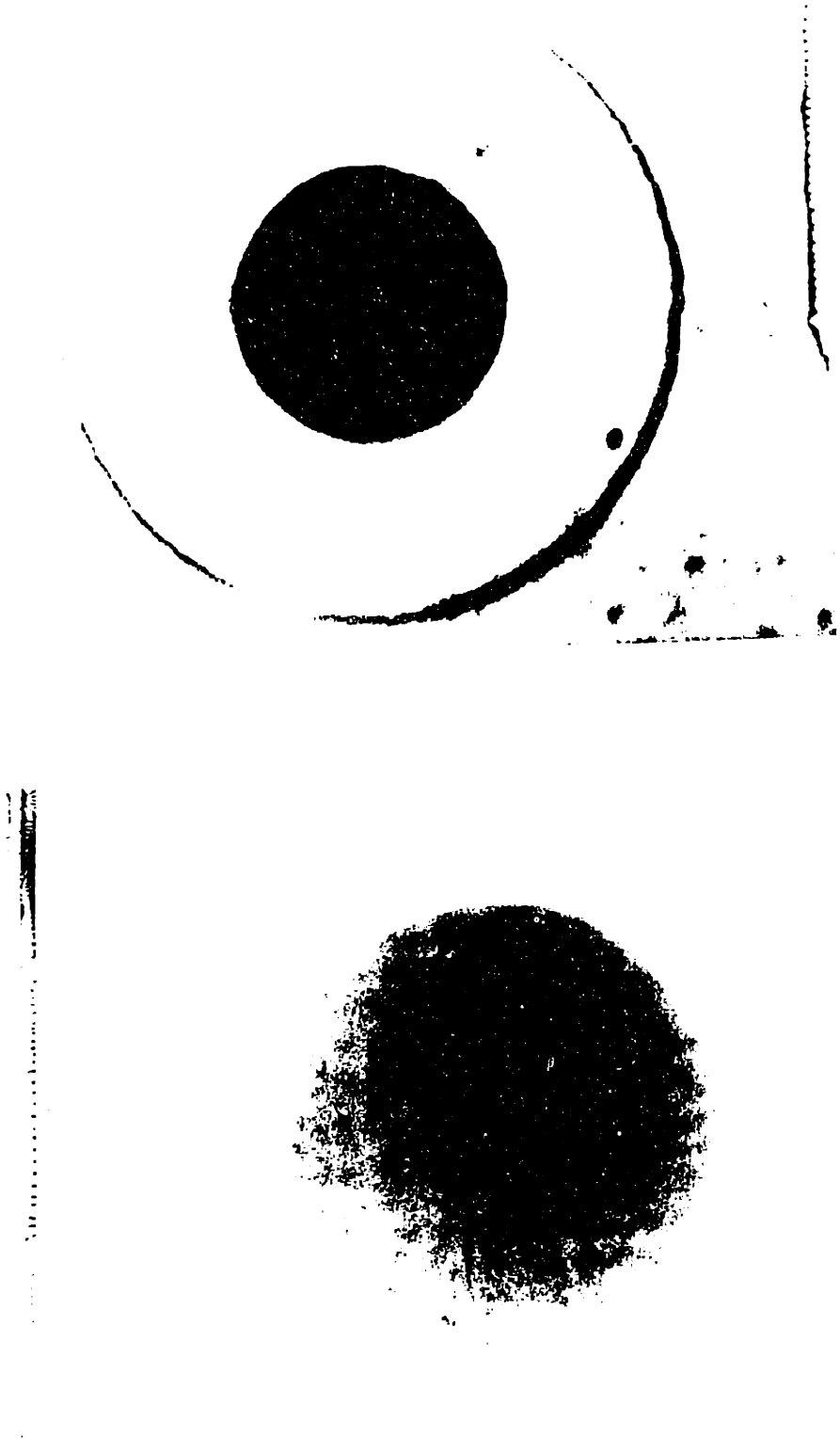

Figure 5.6: Ni orifice before and after printing 32.8 vol% alumina slurry.

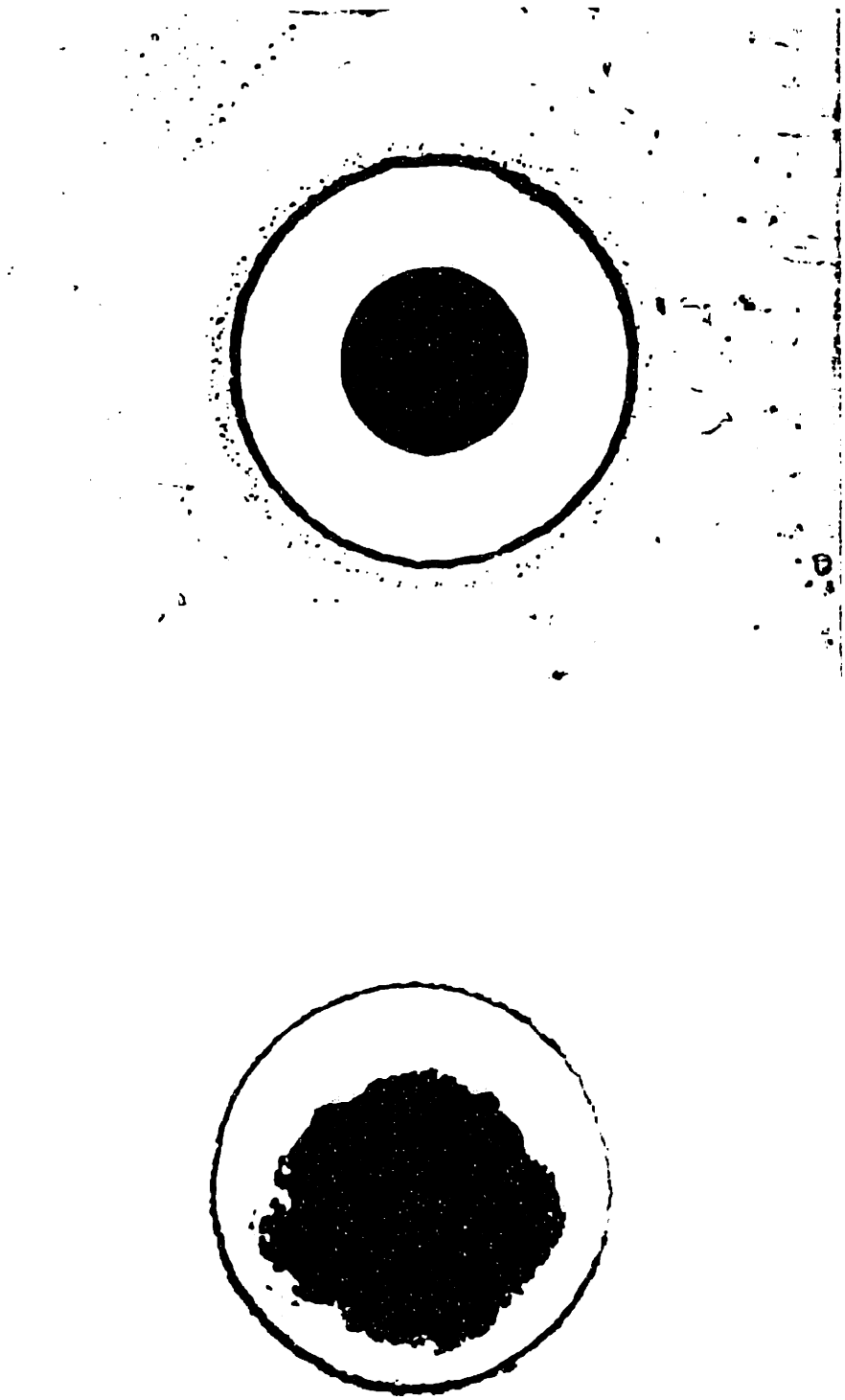

Figure 5.6: Ni orifice before and after printing water at pH 3.5.

Table 5.2: Erosion rate of nickel orifice plate with various binder systems.

Binder System	Ni orifice plate: Diameter (μm)		Printing Time (minutes)	Erosion rate (μm/minute)
	Before printing	After printing		
Water @ pH 3.5	48.75	78.0	125	0.234
Alumina slurry (32.88 vol%)	47.18	82.5	22	1.61

slurry. An uncompatible binder-filter system could change the pore size of the filter either due to the chemical leaching or the flocculation of the slurries.

5.3.3.2 Results and discussions

The alumina suspension were prepared by mixing alumina (RC172-DBM) with deionized water and were stabilized electrostatically at pH 3.5. The alumina suspensions were size-classified to remove the agglomerates. The filtration set-up was optimized to obtain a steady flow rate of the alumina suspensions. The filtration set-up consisted of two 5 μm capsule filters and a 15 μm on-line stainless filter connected in series. A 5 μm stainless disc filter was introduced in the hypodermic syringe holding the nozzle assembly to remove any big particles just before printing. The nozzle assembly consisted of an alumina nozzle mounted at the end of a hypodermic needle (bore ~ 8 mils) and also a pair of piezo-electric disks attached to the stem of the needle to ensure shorter break-off lengths and to produce uniform sized droplets. The filtration setup is shown in figure 5.8.

A typical printing cycle consisted of flushing the entire filtration assembly with deionized water. The nozzle assembly was then mounted and was run on water for ~ 15 minutes. This was followed by switching the flow from deionized water to alumina suspensions. Deionized water was replaced with acidic water (pH 3.5) for flushing purposes. The role of acidic water is multi-fold: first it helps in cleaning the dust particles from the system; second, it prevents the localized flocculation at the water /slurry interface when the flow is changed from water to slurry. Finally, acidic water may electrostatically charge the alumina nozzles and thereby help in repelling the similar charged alumina particles of the suspension away from the nozzle wall.

It was also observed that a gradual change in the concentration of the suspension through a nozzle developed into a better and more stable flow. The slurry was therefore introduced in the capsule filters filled with acidic water to allow for a gradual change in the concentration. Figure 5.9 shows the flow-rate and the concentration of 19.4 vol% classified suspensions printed through an alumina nozzle using the above processing scheme. This technique resulted in variable flow-rates, which is undesirable, because the concentration of the slurry through the nozzle constantly changed as a function of time. The solids concentration and viscosity of the suspension coming out of the nozzle increased with time. The applied gas pressure was constant, therefore, an increase in viscosity decreased the flow rate of the printed suspension. The time to achieve the steady state solids concentration was measured as ~300 minutes.

An on-line stainless filter with a volume of ~10 cc was used to provide the gradual change in concentration to reduce the time required to set up the steady concentration

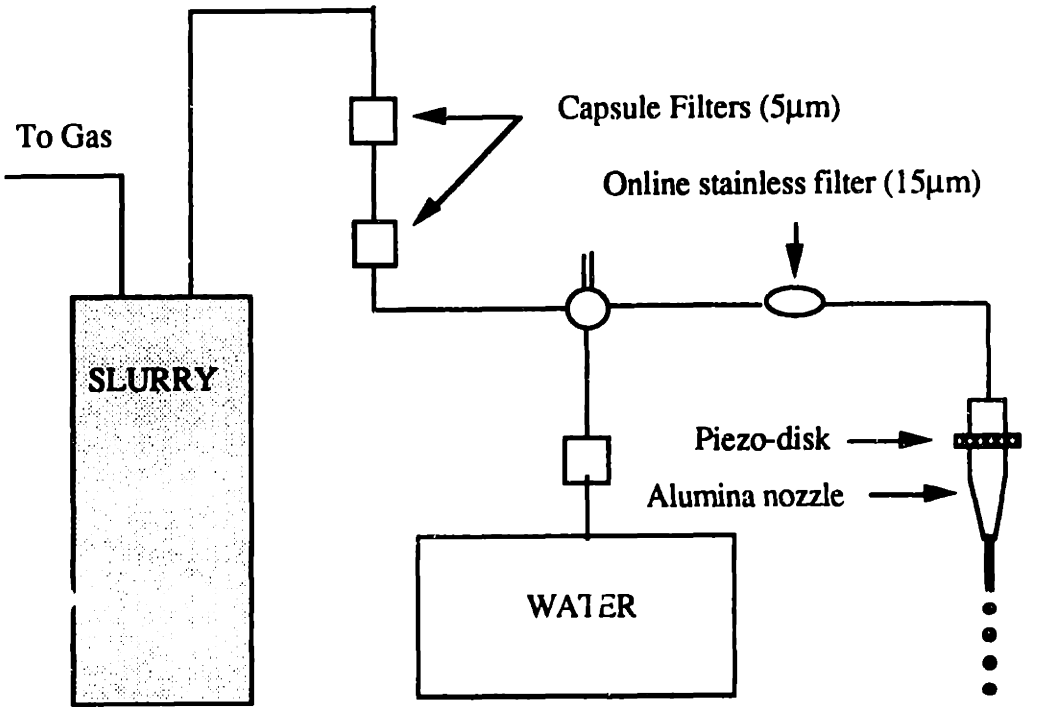

Figure 5.8: Schematic of the filtration set-up.

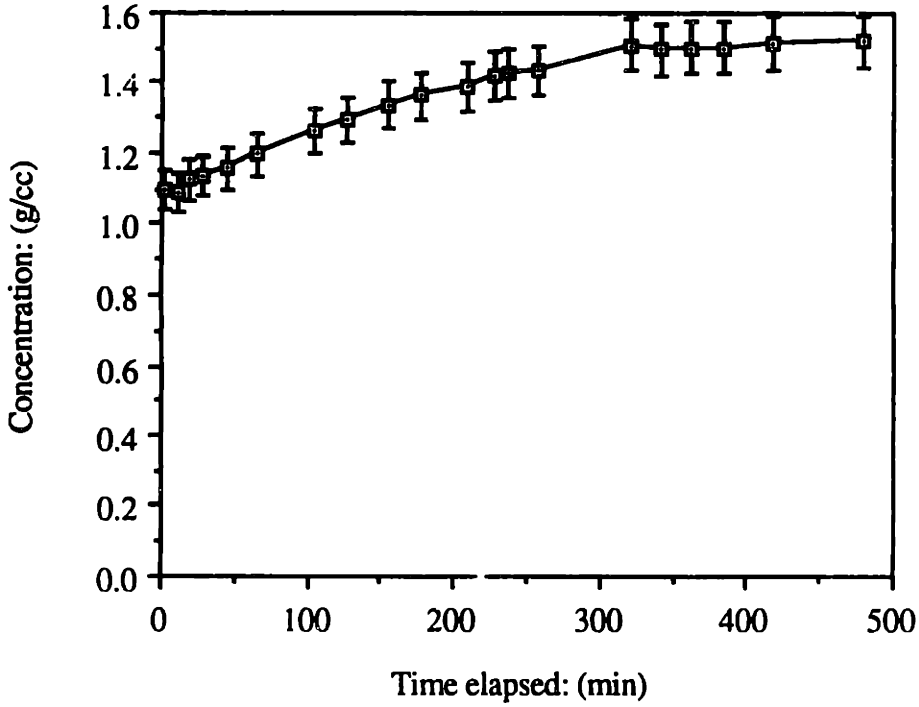

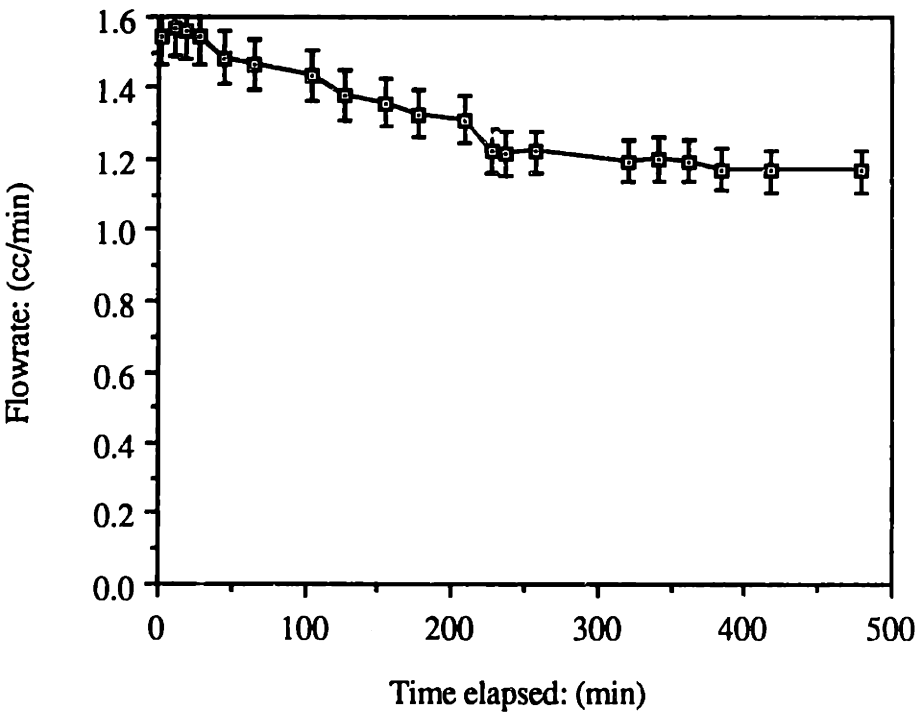

Figure 5.9: Measured concentration and flowrate profile for slurries introduced into filters filled with water.

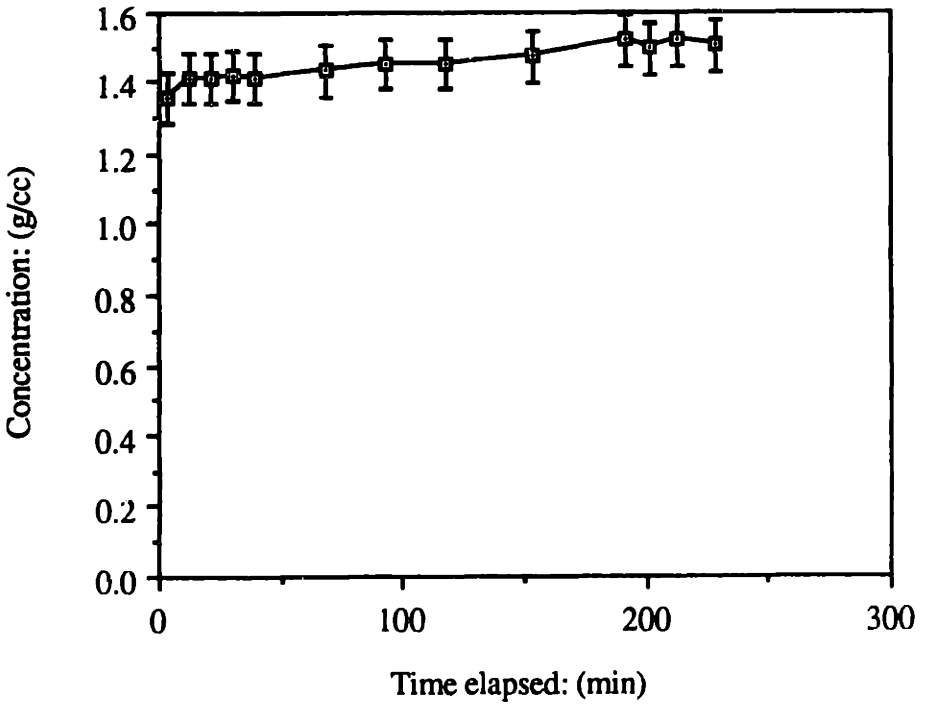

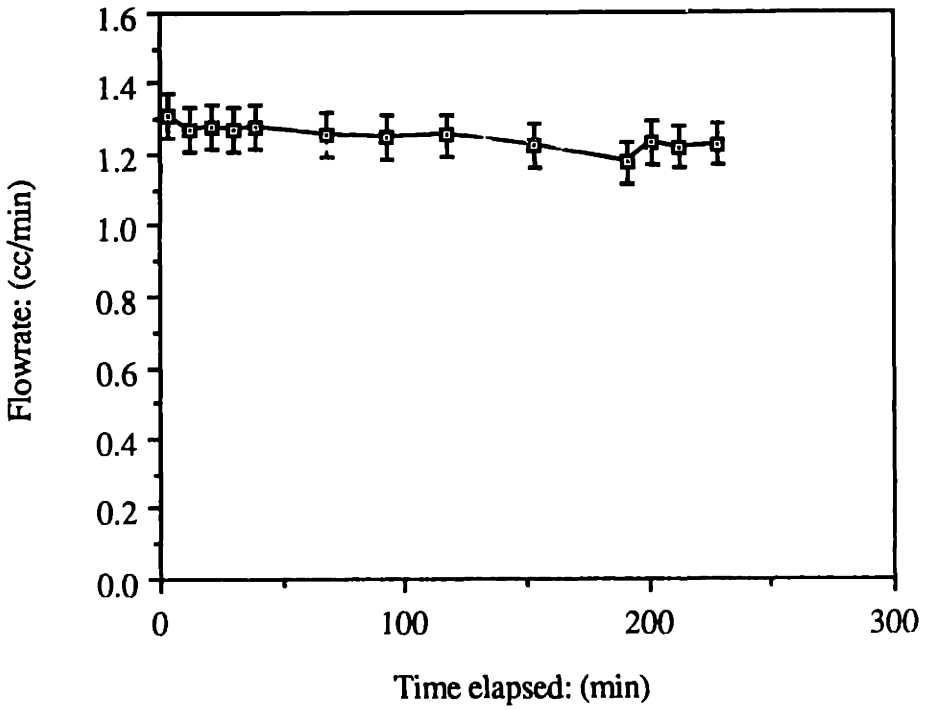

Figure 5.10: Measured concentration and flowrate profile for slurries introduced into empty filters (Filtration felt contains water).

profile. The new set-up allowed the concentrated slurries to be fed directly to an empty capsule filter. Figures 5.10 shows the concentration and the flow-rate profile of the alumina slurries when water was removed from the capsule filters and was filled with concentrated slurries just before printing. The time to reach the steady state concentration in this approach reduces to ~ 150 minutes. Removing water from the capsule filters reduced the time to achieve steady flow rate. However, this step did not completely remove the water from the capsule filter, as the felt material of the filter retained absorbed water. The alumina slurries were added to the capsule filter after removing water and was shaken to remove water from the felt. The diluted slurries were emptied out of the capsule filters. Fresh slurries were loaded into the washed filter. Figure 5.11 shows the concentration and flowrate profile of the alumina slurries when the capsule filters are washed with the slurries once. This strategy clearly shows a dramatic decrease in the time (~10 minutes) to achieve a steady concentration profile. The current scheme has been used to obtain a stable flow of suspensions, containing up to 40 vol% alumina particles, through a 45 micron alumina nozzle for up to 10 hours, when the supply was depleted.

5.3.4 Droplet formation characteristics of slurries

5.3.4.1 Requirements

The binder stream coming out of the nozzle is broken into regular and uniform sized droplets by applying periodic mechanical impulses to the jet through a piezo-electric disc attached to the nozzle assembly. The droplets are passed through a charging cell and then deflected as desired by controlling the voltage on the deflection plates. The key requirement for printing is that the liquid carrier for the suspensions should be conductive so that it can charged easily [85]. The suspensions should have the right surface tension and viscosity properties so as to result in uniform sized droplets. The stream breaks into more than one drop under most operating conditions for every period of the exciting signal. Amongst the several droplets formed, the one significantly larger than the rest is used for printing. The smaller droplets called satellites, detrimentally affect the printing process by disturbing desired drop charging or by flooding the charging cell and by causing a buildup on the deflection plate. The formation of the satellite droplets is explained by Pimbley and Lee [110] with a second order non-linear analysis of the drop formation problem as a result of spatial instability. The objective of this part of the research was to determine the operating conditions which will generate uniform sized primary droplets without any satellite droplets.

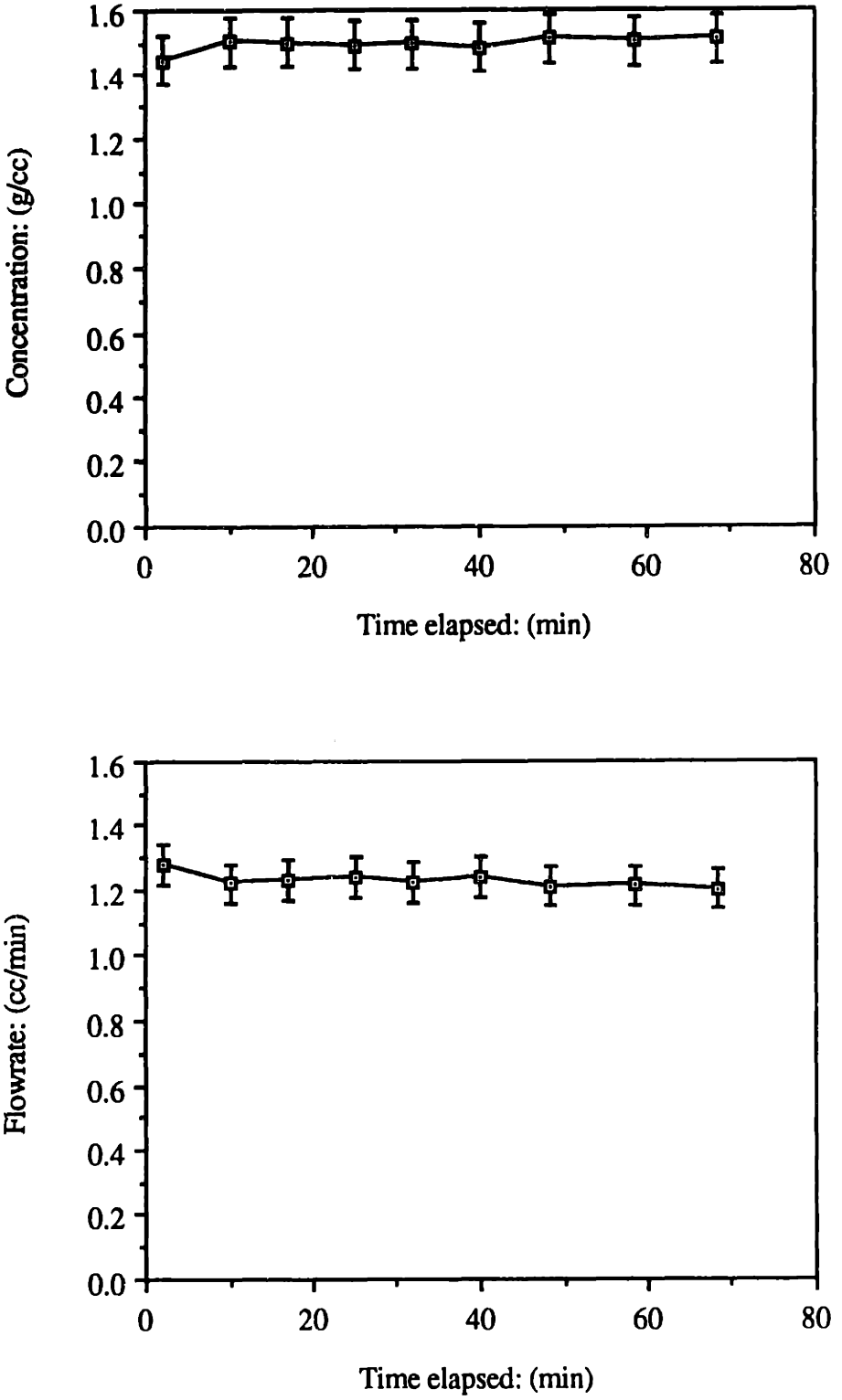

Figure 5.11: Measured concentration and flowrate profile for slurries introduced into filters which are washed with slurry once to get rid of the water from the felt.

5.3.4.2 Results and discussions

The droplet formation behavior of alumina suspensions, as a function of a variety of electric signals characteristics was investigated. Preliminary results showed that the normal print-head parameters were suitable for printing alumina suspensions also. Figure 5.12 shows the break-off lengths of 19.4 vol% alumina suspensions as a function of applied frequency and voltage to the piezo-electric disks. The set-up for measuring the break-off lengths included a video camera and a stroboscope operating at frequencies matched with the droplet formation rate. The break-off lengths shows a strong dependence to the frequency and the amplitude of the exciting voltage. The shortest break-off length was measured as 0.178 cm at 60 KHz with an exciting voltage amplitude of gain 2.5.

The break-off lengths are calculated using Rayleigh's [111] model expressed as:

$$L = 8.33\, U \left(\frac{\rho r^3}{\sigma}\right)^{1/2}$$

where L: Break-off length, r: radius of nozzle, σ: surface tension, U: jet velocity and ρ: density of the slurry. The values of various variables and measured break off lengths are listed in Table 5.3. The calculated break-off length is 0.168 cm which matches very well with the measured value of the break-off length.

The experimental results suggest that the vibration frequency has a dominant effect on the production of uniform droplets. The break-off length goes through a minimum with an increase in frequency at constant jet velocity. Similar observations have been reported by Cline [112] in their study of break-off measurements with water. The primary droplets at low frequencies were large and far apart with a long ligament between the droplets. The neck between the droplets became shorter with increasing frequency. The break-off length of the jet was minimum at a frequency of 60 KHz, and the droplets were quite regular in size. Lord Rayleigh [111] has shown that an inviscid liquid jet, in the absence of aerodynamic forces is most unstable under the action of a disturbance with a wavelength

$$\lambda(max) = 9.02\, r \qquad \text{----- (1)}$$

where r is the jet radius, λ(max) refers to the maximum instability. The wavelength can be computed using the following equation:

$$v = \lambda f \qquad \text{-------- (2)}$$

where f is the frequency of the applied waveform. The velocity of the binder through the ink-jet is measured as 13.62 m/sec while the frequency giving the lowest break-off length is measured as 60,000 Hz. Using equation 1, λ(max) is calculated as $2.02 * 10^{-4}$ m. Substituting the value of λ(max) in equation 2 gives the value of f (frequency) for

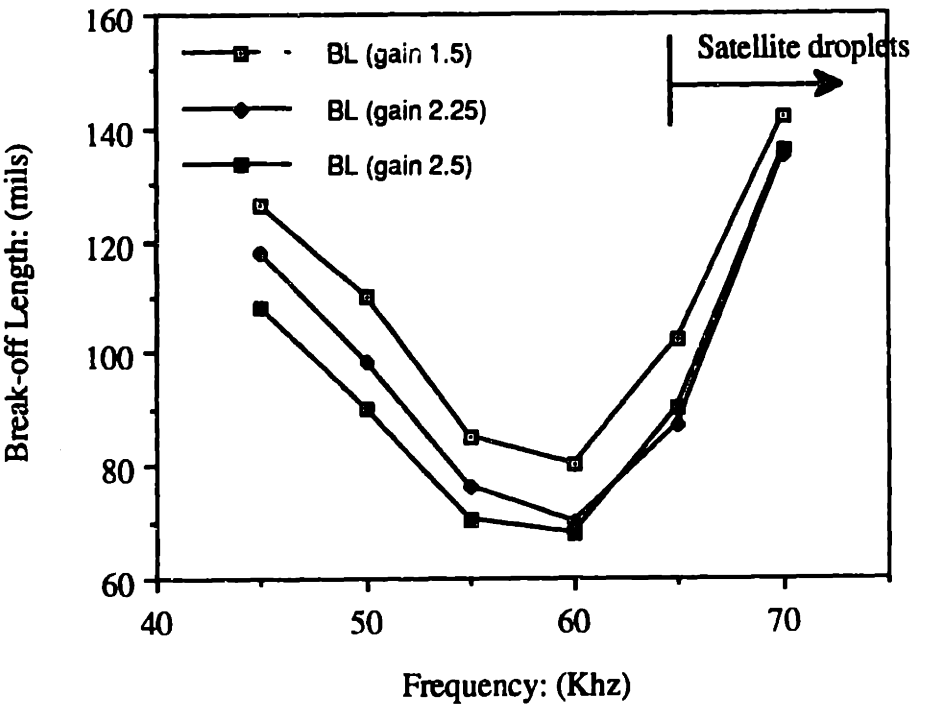

Figure 5.12: Break-off lengths as a function of applied frequency and amplitude for 19.4 vol% alumina slurry.

Table 5.3: Calculated break off length.

Experimental Variable	Value
Radius of the nozzle	45μm
Surface tension	72 dynes/cm
Flow-rate	1.3 cc/min
Density	1.39 g/cc
Velocity	13.62 m/sec
Calculated break-off length	0.168 cm

maximum instability as 67,110 Hz, which is very close to the measured frequency value for minimum breakoff values. As the frequency is increased above the critical value, the vibration has little effect on the disintegration and the jet disintegrates from the influence of the background vibration.

An increase in amplitude of vibration, for the same frequency, also reduced the break-off length. The theoretical expression relating the break-off length to the amplitude is given by [111, 113]:

$$\ln \alpha_1 - \ln \alpha_2 = -K (L_1 - L_2) \quad \text{--------(3)}$$

where L: break-off length, α: disturbance amplitude, and K is the ratio of amplification factor and jet velocity. The break-off length, therefore, decreases with increasing amplitude as shown by the measured values in our experiment.

5.4 Green body formation

5.4.1 Experimental procedure

Parts were made by printing 7 and 26 vol% alumina slurries on the debound alumina SD granules. The flow-rate of 7 vol% slurry was 1.2 cc/min while that of 26 vol% alumina slurry was 1.1 cc/min. Saturation was varied by printing at 65 and 40"/sec fast axis speed. Extensive powder ejection was observed during printing of 26 vol% alumina slurries. The printing of alumina slurries also exhibited excessive catcher buildup. The problem of caking on the catcher was more prominent while printing 26 vol% alumina slurries.

5.4.2 Properties of green parts

The printed green parts were fired at 950 C for 3 hours in order to develop sufficient strength for ease of handling. Porosimetry was performed on the parts printed at 40"/sec. The green density of the parts printed with 7 vol% was measured as 34.27%. Based on the mass balance, increase in the packing density should have been 4.36% over the spread packing density of the fired SD granules (33%) . Effectively, there is a net loss of 3 % in packing density due to excessive ejection during printing. The green density of the parts printed with 26 vol% alumina slurries was measured as 41.5%. The increase in packing density should have been 14.84% based on mass balance. The packing density of the green parts should have been 47.84% in the absence of ejection during printing. There is a net loss of 6.34% of packing density during printing with 26 vol% alumina slurries. The ejection was observed to be more severe when printing with 26 vol% alumina slurry. Fan [84] has showed that the amount of ejection will depend on the powder bed properties and the energy of the incoming droplets. The powder bed

characteristics were essentially the same for the two experiments, therefore, the difference in the ejection behavior is due to the difference in the energy of the incoming droplets. The mass of the droplet containing 26 vol% alumina is 1.47 times heavier than the droplet containing 7 vol% alumina. As a result, the powder bed printed with 26 vol% alumina suspension will eject more, under similar printing conditions.

Figure 5.13 shows the pore size distribution of the SD samples printed with 7 and 26 vol% alumina slurries. It clearly shows that the increase in solids concentration of the printed slurries reduces the amount of intergranular space. Figure 5.14 shows the SEM micrographs of the polished cross-section of the printed parts. The part printed with 26 vol% alumina slurry shows more intergranular pores filled with the printed slurry than the part made with 7 vol% alumina slurry. SEM micrographs of the parts printed with 26 vol% alumina slurry also show that the printed slurry does not uniformly penetrate completely through spread powder layers but instead segregates at the top half of the layer, creating a laminated structure. Segregation of the printed slurry created an anisotropy along the z-axis of the printed part. Figure 5.15 shows the polished cross-section of the parts made by printing 30 vol% alumina slurry on dense 30 μm platelet particles. The printed slurry does not show any segregation problem. Individual printed layers wer easily distinguishable in either case. The presence of interlayer defects would not allow to fabricate isotropic green components directly from the 3DP machine by this method.

An interaction of the printed droplet with the SD granules involves two competing phenomena: slip casting of the slurry on the SD granules (fine pores) vs infiltration of the slurry droplets into the SD powder bed. The time required by the water to infiltrate a SD granule is calculated by using Darcy's law and Carman-Kozeny equation. The permeability of SD granule is calculated by Carman-Kozeny equation as $1.15 * 10^{-16}$ m^2. The velocity of infiltration is calculated by Darcy's law. Capillary Pressure is calculated as $1.44 * 10^6$ N/m^2 for a wetting angle of $\theta = 0$ and pore radius of 0.1 μm. Darcy's law is then used to calculate the velocity of infiltration as 0.011 m/s. This translates into $1.35 * 10^{-3}$ seconds to infiltrate a 30 μm SD granule. Fan [84] has measured the time taken by a binder droplet to infiltrate a layer as to be the order of 1 millisecond by using high speed photography methods. Since the time constant for slip casting and infiltration of the printed droplet in a powder layer is in the same order, the printed binder segregates and results in non-uniform microstructure. The segregation of the alumina slurries can be minimized by printing dilute suspensions and/or or making the SD granules behave like solid granules. The slurry did not segregate when printed on dense particles. However, if the intragranular pores are not available for infiltration, then the maximum packing

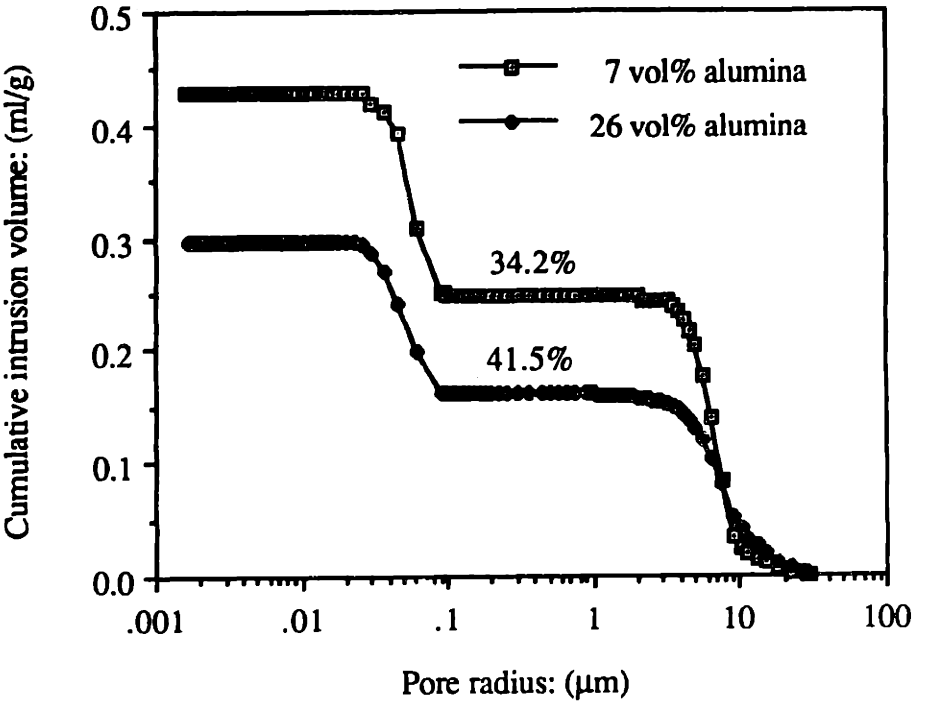

Figure 5.13: Cumulative intrusion volume of SD part printed with 7 and 26 vol% alumina slurry.

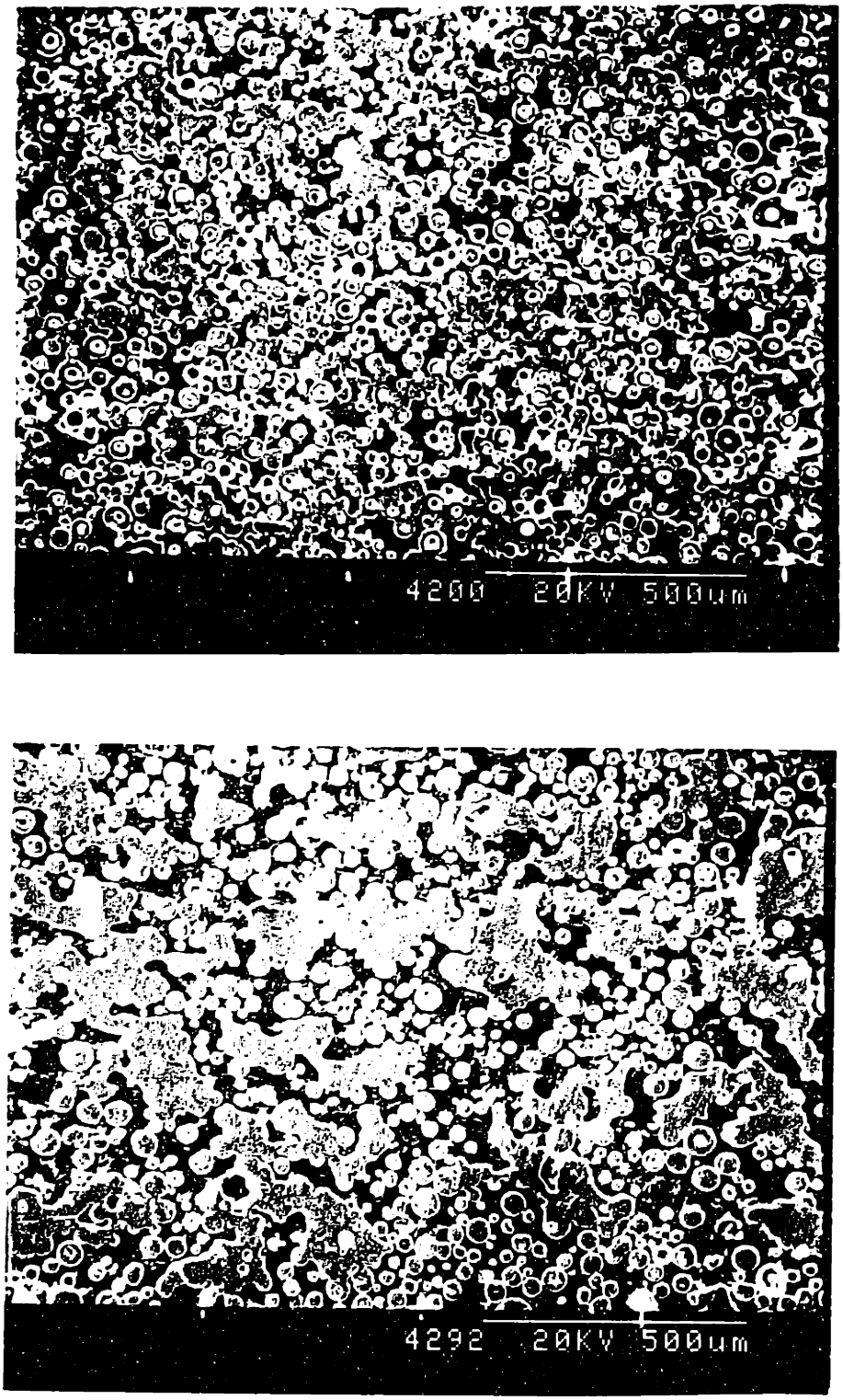

Figure 5.14: SEM micrograph of polished cross-sections of parts made by printing 7 and 26 vol% alumina slurry on SD granule powder bed.

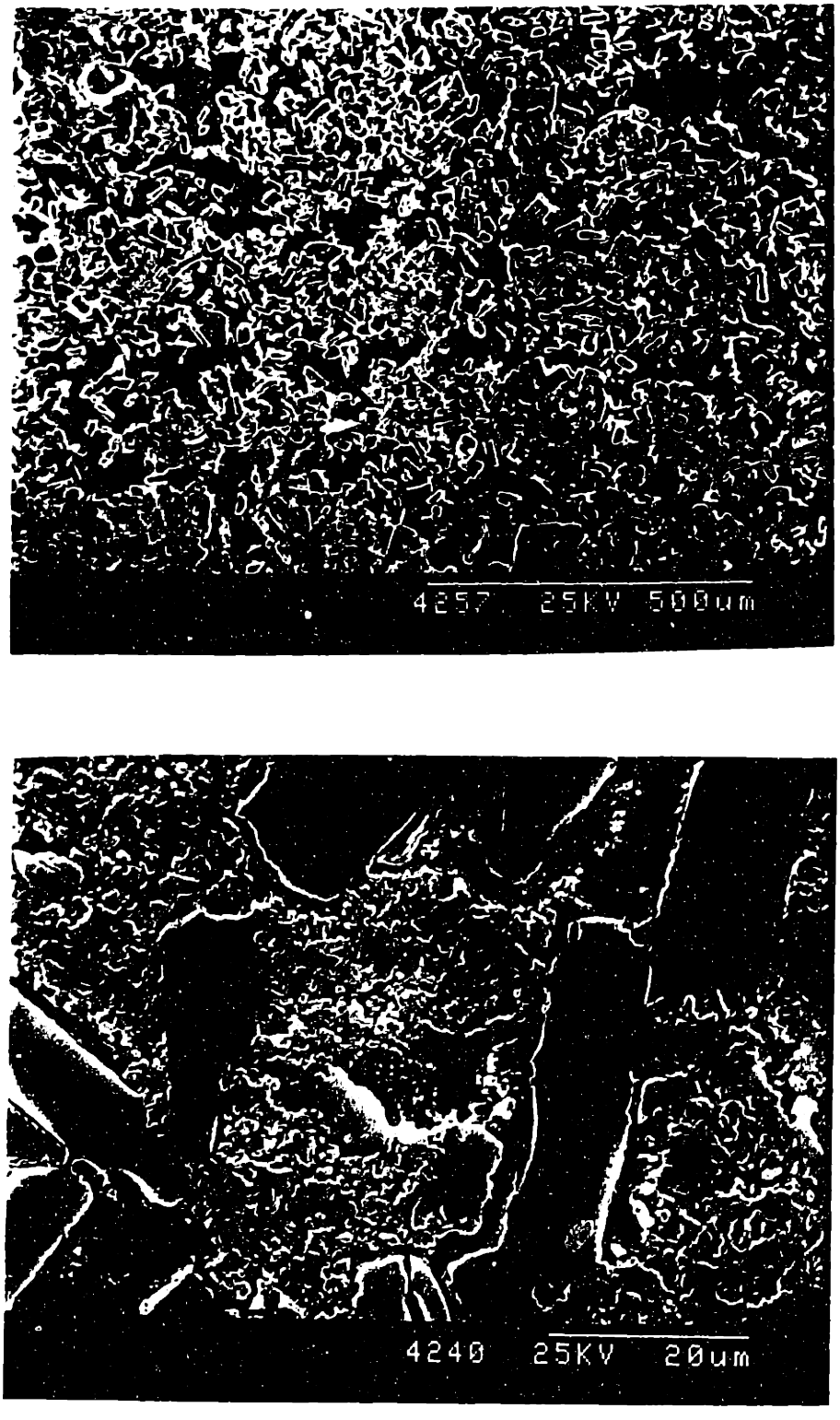

Figure 5.15: SEM micrograph of polished cross-sections of parts made by printing 30 vol% alumina slurry on 30 μm dense platelet alumina powder bed.

density of the powder bed can be improved to only 46% with similar assumptions as used in the beginning of the chapter, i.e. a maximum of 16 vol% of second phase can be added by printing.

5.5 Conclusions

Anisotropy was introduced in the SD green parts built with 26 vol% alumina slurry due to segregation of the printed slurries on the top half of a spread powder layer. Segregation of the printed slurries, therefore, created an anisotropy along the z-axis of the printed part. Such non-uniformity in microstructure was not observed in the parts made out of dense particles and is unacceptable for fabricating defect-free structural ceramic components. An interaction of the printed slurry droplet with SD granules powder bed was shown to involve two competing phenomena: slip casting of the slurry on the SD granules (intragranular pores) versus infiltration of the slurry droplet into the powder layer. The time required by water to infiltrate a SD granule was calculated as to be the order of 1 millisecond; this is comparable to the measured time taken by a slurry droplet to infiltrate a powder layer thickness. The anisotropy due to slurry segregation was reduced by printing dilute slurries (7 vol%) into SD granule powder bed. This method, however, did not minimize the formation of interlayer defects, inherent in the conventional 3DP process. The next two chapters discuss new strategies to fabricate high, uniform and isotropic green bodies directly from the 3DP machine.

CHAPTER 6
PRESS-COMPACTION

6.1 Introduction

We have already fabricated complex shaped distortion-free green fine ceramic parts by printing an organic binder on SD granules. These green bodies, however, have low packing density, typically in the range of 30%. The printed components also have interlayer defects which introduce an anisotropy along the z-axis. The printed parts require a densification step in the form of isopressing to increase their packing density to ~ 60% and to heal the interlayer defects. Giritlioglu [70] has modified the wet bag isopressing technique to isopress complex shapes by surrounding the printed parts with PEG powder, and dissolving the PEG in water after the compaction step. The PEG powder prevents the hollow sections of the printed parts from collapsing upon isopressing. The press-compaction process was developed to fabricate high, uniform and isotropic structural ceramic components directly from the 3DP machine.

6.2 Process concept

The use of SD granules dramatically improved the powder bed quality over that obtained by spreading fine powders. However, the low bulk density of the SD granules result in low packing density of the powder bed. One of the techniques to increase the packing density of the powder bed is to crush the agglomerates after spreading the powder layer, as is used in the dry-pressing industry. The press compaction technique will involve spreading SD granules and compacting it to high density by applying a pressure on the powder bed. The compaction of individual layers against the existing powder bed will minimize the interlayer defects. Binder will be subsequently printed to define a shape and then the whole cycle will be repeated. The printed part will be separated from the powder bed chemically.

One of the major disadvantages of dry-pressing is the cost and time it takes to design a tool die set for fabricating shapes. Moreover, it is economically unfeasible to make a die set for fabricating few parts. The shape of the part in the press compaction technique is defined by the printed binder and not by the die set. Pressing is used explicitly to increase the packing density of the powder bed only. Therefore, press-compaction retains the flexibility of 3DP to form shapes directly from the CAD files.

The second disadvantage of dry-pressing is the density gradient and the non-uniformity created in the part due to the friction between the powder and the die wall

which limits the L/D aspect ratio to 3:1. The pressure transmission through the compact in a uniaxial pressing is approximated by the following equation [15]:

$$P = P_o \exp\left(\frac{-4\mu\alpha L}{D}\right)$$

where P_0 is the mean applied pressure, P is the pressure transmitted at a depth of L, μ is the powder wall friction, α is defined as the ratio of radial to axial compaction stress at the die wall and L/D is the length to diameter ratio (aspect ratio) of a compact. The stress distribution within a compact is a strong function of factor $\mu\alpha L/D$. In the absence of wall friction, a uniform compaction pressure P_0 will exist through a compact [114].

$$\lim_{\mu\alpha L/D \to 0} P/P_0 = 1$$

Lower L/D values, for a given μ and α, will result in uniform packing density of the compact during pressing. Dimilia and Reed [115] report typical values of μ as 0.3 for unlubricated steel dies and α as 0.4 for SD granules containing PVA as a binder. Compacts with thicknesses of 180 μm and diameters of 2.54 cm (size of one inch die, in reality this number will be much larger than 1 inch) will have L/D ratio of 0.007. Putting these values in equation 1 results in a $P/P_0 = 0.991$. Therefore, compaction of thin layers will result in uniform density distribution within pressed parts.

An experiment was performed to evaluate the feasibility of printing on high green density pressed parts. It was found that the latex emulsion (as dilute as 3 vol% rhoplex), the binder of choice at that stage of the process development, formed a film on the surface of the pressed compact, as shown in Figure 6.1. The process concept was then modified to incorporate a low pressure step to make a powder bed with big intergranular pores necessary for the binder to infiltrate. Compaction to high density (elimination of intergranular pores) is accomplished after printing. The press compaction process is shown schematically in figure 6.2. More details of the process are provided in subsequent sections.

In order to evaluate the critical issues involved in press compaction process, a die setup was needed to allow us to do repeated compaction of the granular layers to make multilayered parts without any difficulty. Section 6.3 describes the design strategy to build such a die setup. The overall press compaction process can be divided into: powder deposition stage, printing and part retrieval stage. The subsequent sections discuss the critical issues involved under each of these categories.

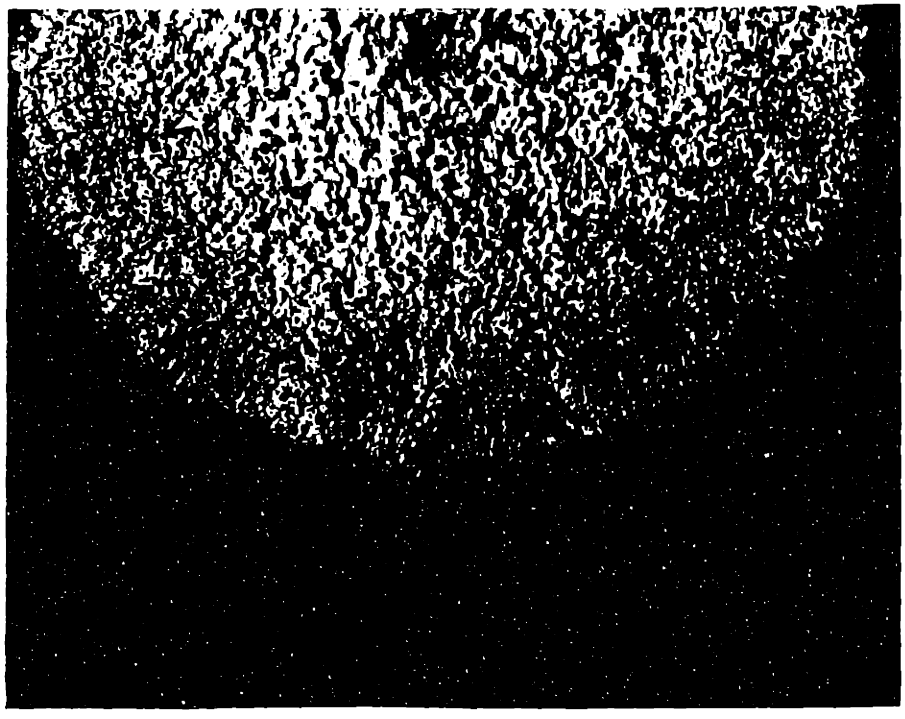

Figure 6.1: Latex binder droplet on top of ~55% dense SDPAA/alumina compact.

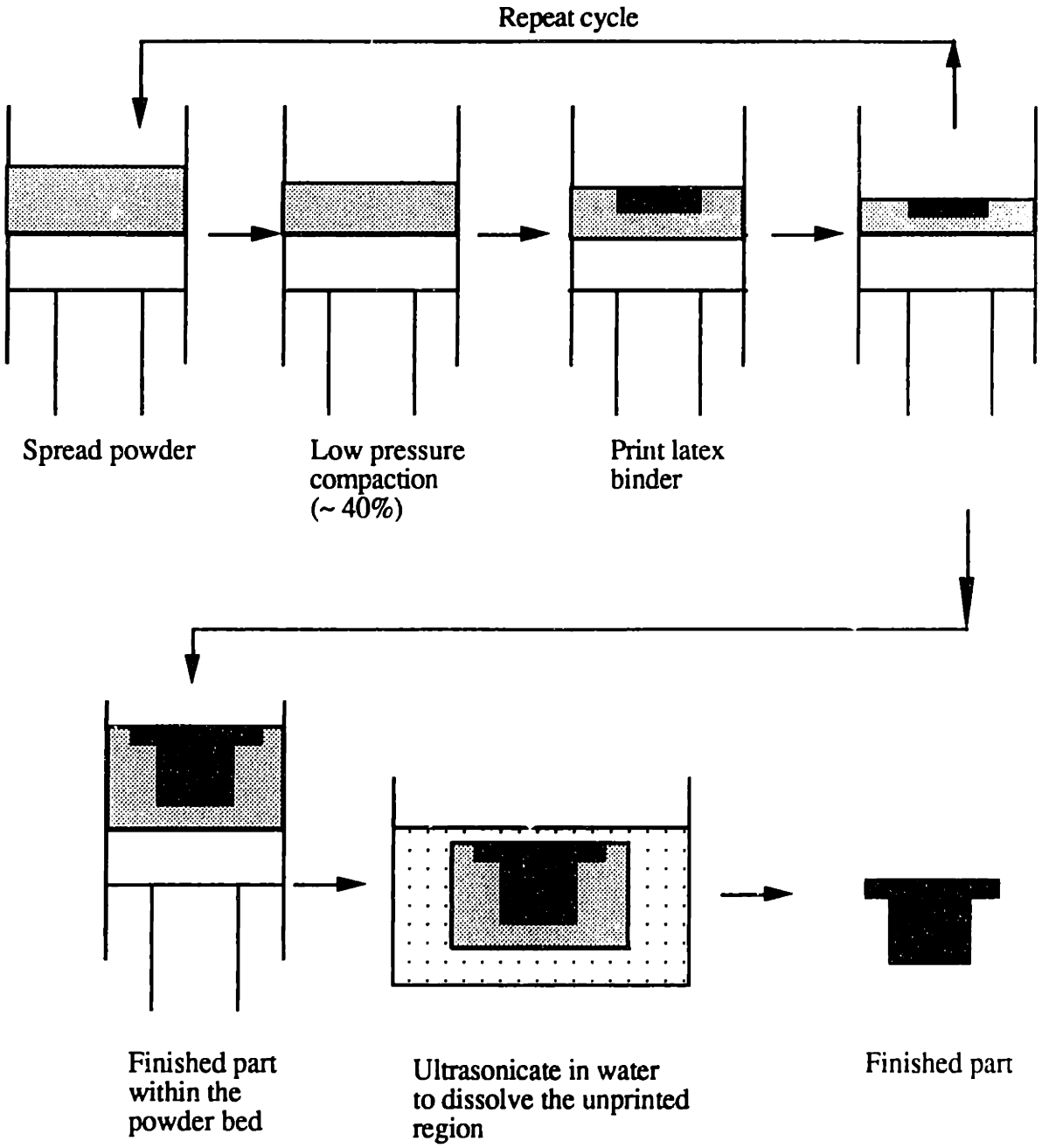

Figure 6.2: Schematic of the press-compaction technique.

6.3 Design of set-up to do repeated pressing operation

Manual dry pressing dies can not be easily used to build multi-layered parts. The clearance between the ram and the die wall is usually low and a small particle can get trapped between the wall and the ram to lock it up. Therefore, a typical manual dry pressing process involves cleaning the die set after every pressing operation. A new die set-up fabrication was necessary to avoid the particles getting trapped between the ram and die wall to do repeated spreading and compaction of the powder easily.

Similar problems were observed by Herald Tureck [116] while he was designing the piston for spreading powder in the 3DP process. His solutions included increasing the width of the gap between the piston and the walls to more than the individual particle size, so that the individual particles cannot get wedged in that open slot and provide excessive friction. Also, he used a felt seal to prevent the powder from trickling down through the slot and getting sandwiched between the piston and the cylinder walls. Similar strategy was incorporated in the press-compaction set-up, as shown in figure 6.3.

A slot was cut in the ram and was wrapped with a felt to provide a good seal between the piston and the cylinder die walls. The felt material is a ceramic tape called 'Ultra temp 390' made by Cotronics. The top surface had a clearance of 254 μm, much bigger than the individual granule size (~ 30 μm), so that the particles can fall through that slot and do not get wedged between the die and the ram. The felt provides the seal with the die walls. The setup was used successfully to make multi-layered parts.

The second major technical issue was the sticking of the powder onto the ram surface after low pressure application, resulting in defects on the surface of the powder bed. This problem was solved by attaching Teflon (VWR) tape (with an adhesive backing) to the surface of the ram. The low friction of the powder against the teflon surface solved the powder sticking problem.

6.4 Powder bed properties

The first step to make this process successful is to optimize pressing parameters to make defect-free, uniform and high packing density powder beds. The powder deposition stage requires an application of pressure to deform SD granules. We studied the compaction response of the powder bed as a function of the SD granules characteristics and the applied pressure. Two different binder systems, PEG (T_g~-67 C) and PAA (T_g ~106 C) were used to modify the properties of the SD granules. The details of SD granules preparation and their properties can be found in sections 4.2 and 4.3 of chapter 4.

The application of pressure and the nature of SD granules control the packing density of the powder bed. In addition to the packing density of the individual layers,

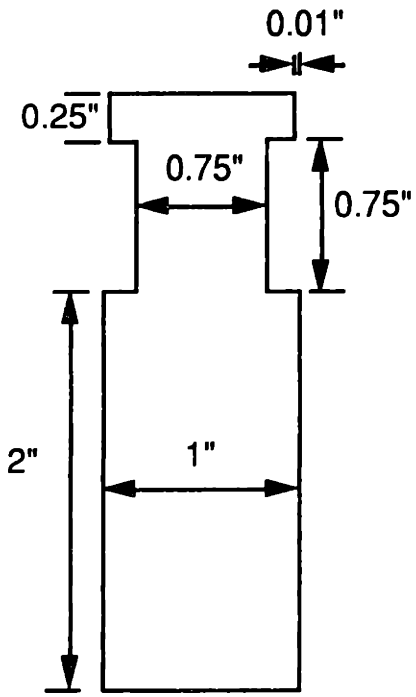

Figure 6.3: Schematic of the ram design.

another issue was whether pressing of any spread powder layer will affect the packing density of the already compacted layers. Section 6.4.2 investigates the quality of inter-layer stitching as a function of the applied pressure and the SD granules properties. Finally, the pore size distribution of the green compacts as a function of the applied pressure is investigated to determine the optimal conditions for printing binder and final packing density of the printed parts.

6.4.1 Packing density of powder bed

Packing density of the powder bed will strongly depend on the compaction behavior of SD granules as a function of the applied pressure. Therefore, it is important to understand the role of various factors affecting the compaction behavior of SD granules.

Compaction of SD granules is a very well studied field and has been reported by several researchers [117, 118, 119,120,121]. Organic binders are added to the SD granules to increase their deformability during compaction. The extent of deformation is controlled by the amount and nature of the organic phase. Binders with lower glass transition temperatures deform at lower pressures, i.e. they have lower granule yield points. The compaction temperature should be above the T_g of the binder in order to ensure plastic compaction behavior. The binder will behave as stiff material below the T_g. Plasticizers can be added to the binder in order to decrease the T_g or bring it down to below room temperature, but it will also reduce the strength of the binder and therefore the strength of the pressed compact. Nies and Messing [119, 120] showed that softer and more deformable granules result in more reproducible packing and lesser springback due to stress relaxation of the softer systems during pressing.

The compaction experiments included pouring the SD granules into the die followed by gentlly tapping the die wall from outside to ensure a uniform distribution of the powder within the die. The pressing was performed in a Carver dry-press.

Figure 6.4 shows the compact density as a function of the applied pressure for SDPAA and SDPEG/ alumina granules. This plot is popularly known as compaction diagram and the pressure axis is plotted in a logarithmic scale. The figure shows that for the same pressure, SDPEG densifies to a higher density than SDPAA. It is not surprising, as PEG has a lower glass transition temperature than PAA.

Reed et al. [15] have proposed three stages of compaction based upon the compaction diagram. A slight densification above the fill density (D_f) may occur in stage I, owing to the sliding and the rearrangement of SD granules. The interstices among granules are much larger than the average pores within the granules. The granules deform or fracture in stage II, reducing the volume of the relatively large interstices. The apparent

yield pressure (P_y) of the granules is less than 1 MPA when the binder system is soft and ductile. Denser granules with a poorly plasticized binder system resist deformation and a higher pressure is needed to compact these to an equivalent density. The densification in stage II may be approximated by the following equation [15]:

$$D_c = D_f + m \ln (P_a/P_y)$$

where D_c is the compact density at an applied pressure P_a and m is the compaction constant that depends on the deformability and the packing of the granules. Stage III begins when most of the large pores among deformed granules have disappeared, and the higher applied pressure causes the sliding and rearrangement of particles or fracture fragments within the granules into a denser packing configuration. Interfaces between smaller and softer granules begin to be eliminated in Stage II, and groups merge into a homogenous mass. Interstices between large granules or harder granules and within large granules often persist into Stage III.

The yield strength of SDPEG/alumina system was measured from the compaction diagram as 0.095 MPa while that of SDPAA/alumina as 0.408 MPA. The yield strength of the SDPAA/alumina granules is, therefore, 4.3 times higher than that of SDPEG granules. The value of 'm' indicates the ease of deformation of the granule. Higher 'm' values mean higher rates of densification for the same applied pressure conditions. The value of 'm' for SDPEG was calculated as 0.004 and that for SDPAA as 0.00038. The drastic difference between the compaction behavior between the two SD granule systems can be easily explained by the difference in their glass transition temperatures. All the pressing experiments were conducted at room temperature (~20C) which is considerably higher than the Tg of PEG (-67 C) but lower than the glass transition temperature of PAA (Tg ~ 106C). SDPEG /alumina compacts achieved a density of ~60% at a pressure of 2546 psi while SDPAA/alumina granules densified to ~56% even after pressed at 19098 psi.

The packing densities of multi-layer compacts were also measured. Figure 6.5 shows the plot of compact densities for single and multi-layered parts. The density of the multi-layered parts is the same as that of the single layer, implying that the subsequent pressing step did not affect the packing density of the previously compacted layer. If the applied pressure stays constant for all the pressing steps, then the maximum pressure experienced by the previously compacted layer will be less than the applied stress. A fraction of the applied stress will be lost in overcoming the friction between the die wall and the powder, therefore, densification of the previous layers will not be affected. However, if the applied force is increased by mistake, then if we are in the position on

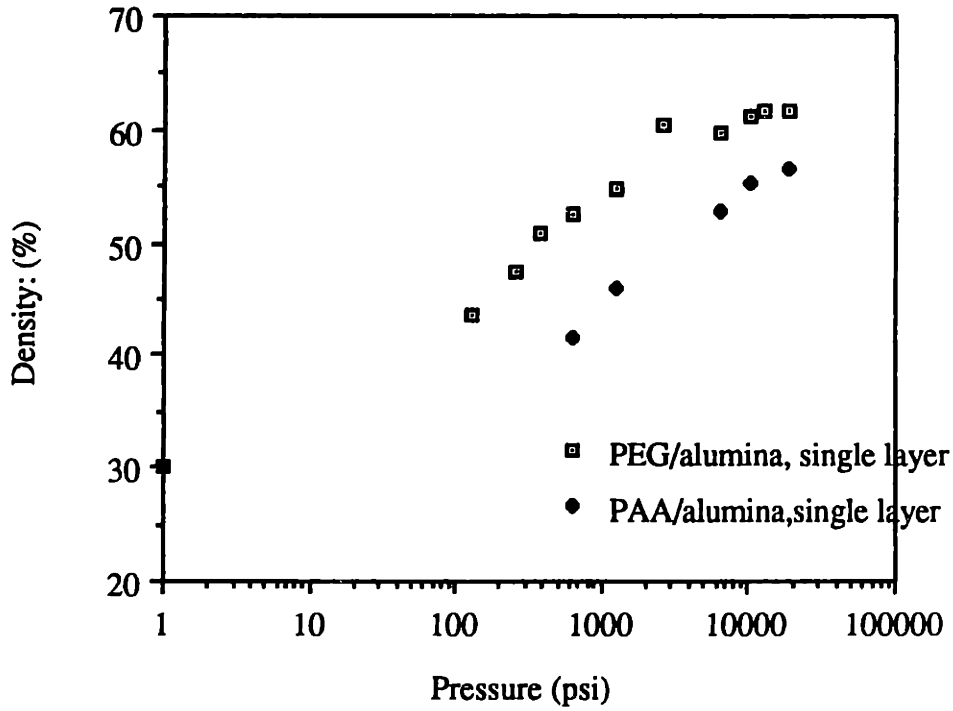

Figure 6.4: Packing density of single layers

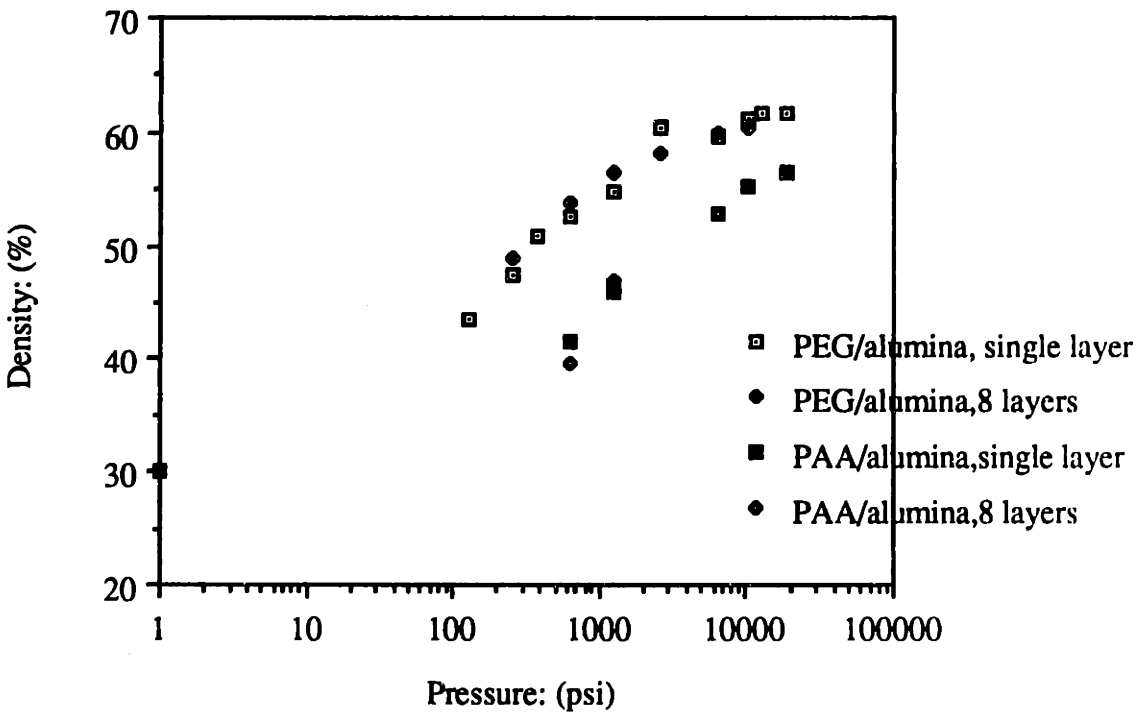

Figure 6.5: Packing density of single and multiple layers.

compaction diagram where the density profile is flat (as is the case of SDPEG granules), the packing density will not change even with the additional pressure.

6.4.2 Inter-layer stitching

The ease of SD granules deformability is also seen on the interlayer stitching behavior. Softer granules tend to deform and weld better than the harder agglomerates. The higher granule strength of SDPAA/alumina reflects in poor welding between the granules. This becomes evident from figure 6.6 which shows the polished cross-section of compacts made out of SDPEG and SDPAA/alumina as a function of the applied pressure. The compacts made out of hard granules at low pressure show inter layer stitching problems in the form of lamination defects. The compacts made out of SDPEG (soft granules) do not show inter-layer defects. Similar observations have been reported by Verma [122] who investigated the welding behavior of various SD granules as a function of the nature of organic additives. However, the lamination defects of SDPAA are healed after being compacted at high pressures as shown in figure 6.7. Therefore, press-compaction process helps to eliminate the interlayer defects and produces isotropic green compacts.

6.4.3 Pore size distribution of the powder bed

Figure 6.8 and 6.9 show the pore size distribution of the compacts made out of SDPEG and SDPAA/alumina as a function of the applied stress. It is clear that in both cases, as the applied pressure is increased, the intergranular pores disappear gradually. SDPEG shows the disappearance of intergranular pores at a lower pressure than SDPAA. The removal of big intergranular pores improves the sinterability of the compacts. The presence of big intergranular pores at intermediate pressures is necessary to print latex emulsion during the printing stage, as will be shown in the next section.

6.4.4 Fired density and shrinkage

SDPEG compacts pressed at 2546 psi (packing density ~60%) and SDPAA pressed at 6367 (~53%) psi were both fired at 1650 C for 2 hours. The fired densities were measured by mercury porosimeter as 96.8% and 94.3% which translate into 14.7% and 17.5% linear shrinkage respectively. As shown in the pressing equation in section 6.2, there should not be any density gradients in the compacts when the layer thickness is small. The uniformity of the packing density is confirmed by firing press-compacted samples. The parts, after firing, stayed flat implying that the density profile within the compacts is fairly uniform.

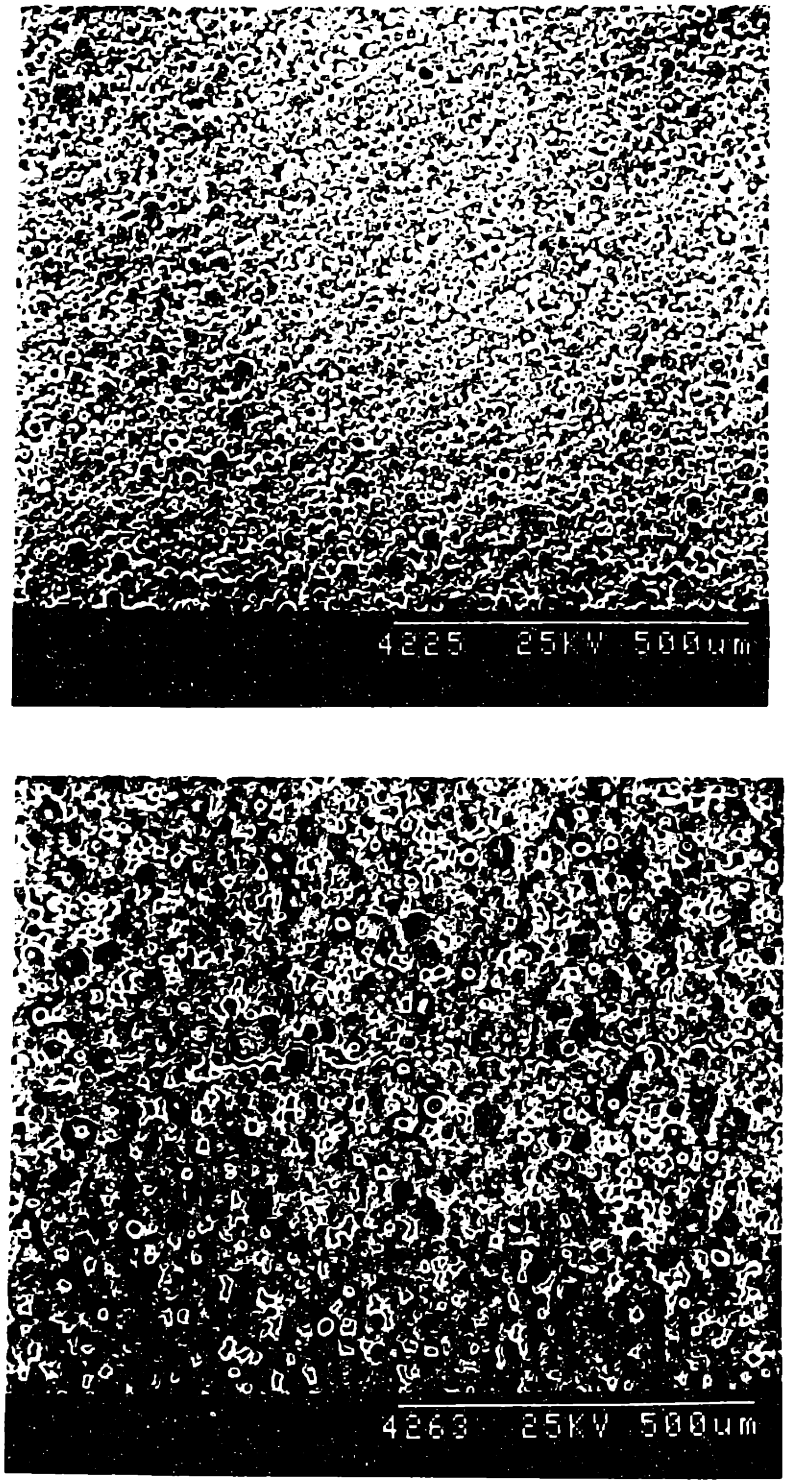

Figure 6.6: SEM micrographs showing the cross-sections of PEG/alumina pressed at 127 psi and PAA/alumina pressed at 637 psi. Both the samples were fired to 1500^0C for 4 hours.

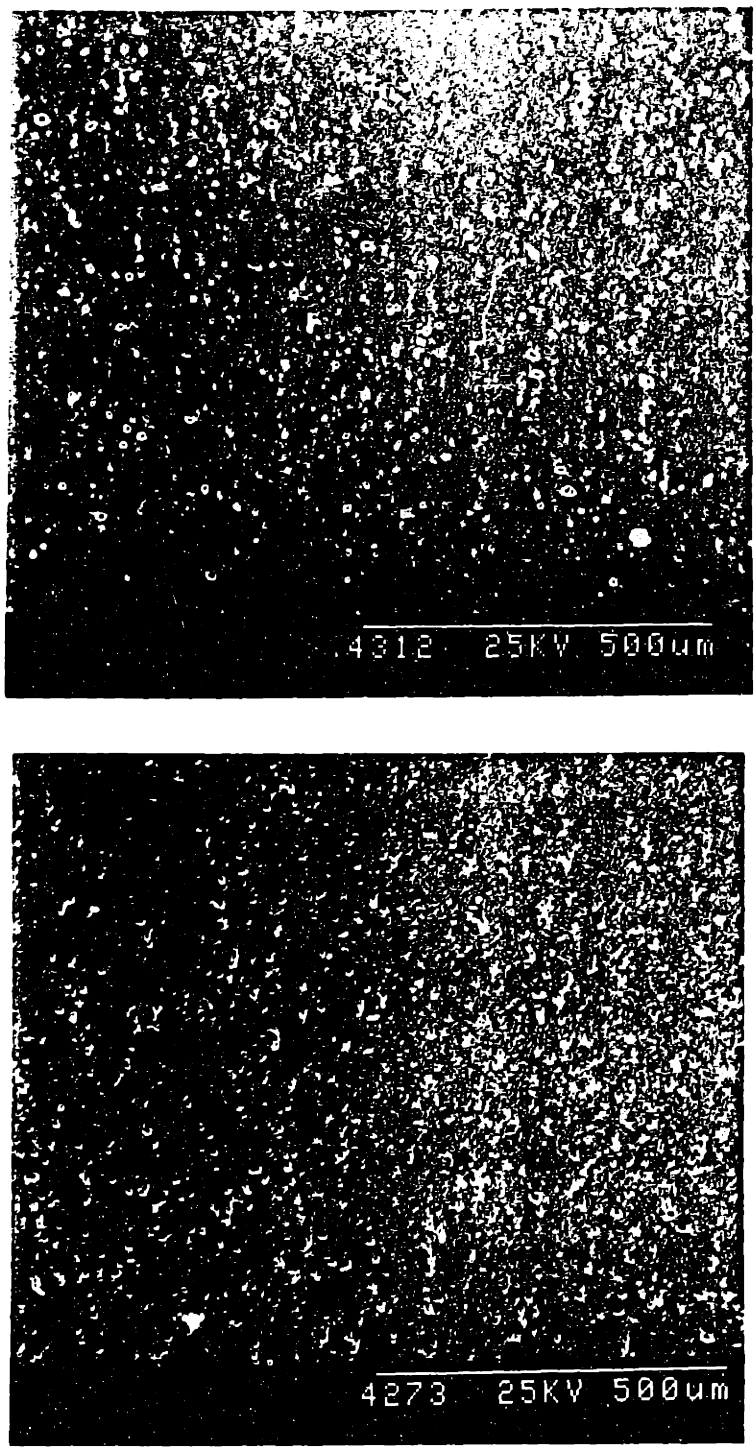

Figure 6.7: SEM micrographs showing the cross-sections of PEG/alumina pressed at 2546 psi and PAA/alumina pressed at 6367 psi. Both the samples were fired to 1500^{0}C for 4 hours.

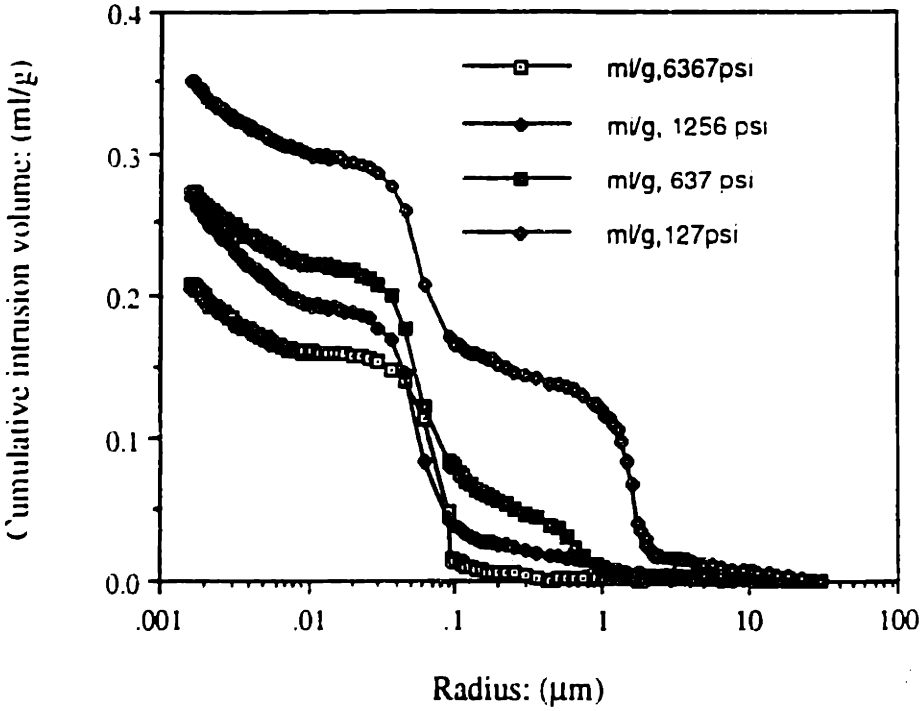

Figure 6.8: Pore size distribution of SDPEG/alumina granules as a function of pressure.

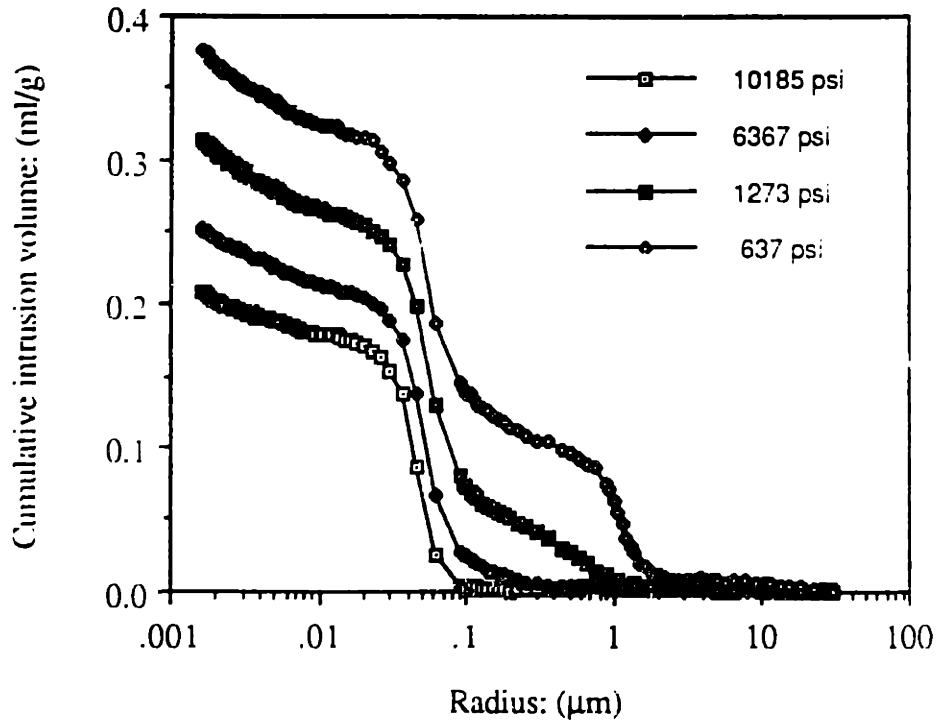

Figure 6.9: Pore size distribution of SDPAA/alumina granules as a function of pressure.

6.5 Printing stage

6.5.1 Selection of binder and powder bed packing density for printing

The penetration characteristics of the printed binder was investigated as a function of the packing density of the powder bed. The preforms pressed at various pressures were tested for binder infiltration. Droplets made out of 6 vol% Rhoplex containing Alizarin Red S monohydrate dye (Aldrich Chemicals 11996-2) were placed on the surface of the compact. There were two criteria for selection of the pressure for making the low density compact: the pressure at which the compact survived the ejection pressure and also provided sufficient binder infiltration without any film formation on the surface. This pressure was found to be 637 psi for SDPAA/alumina granules. SDPEG/alumina reacts with the aqueous latex emulsion and created infiltration problems even for compacts pressed at low pressures. The extent of infiltration was measured as between 300 - 350 μm for SDPAA compacts from the sample cross-sections. The dimensions of the die and the compaction profile was used to determine the right amount of powder for a 200 μm thick powder layer after the low pressure compaction. The amount of powder for SDPAA was calculated as 0.17 g/layer.

6.5.2 Shape change of the printed region upon further compaction

The printed layers in the press-compaction technique is densified with a high pressure step. This section will investigate the effect of high pressure compaction on the shape of the printed region. The parts fabricated by dry-pressing powder in a constrained die, undergo all the shrinkage in the direction of the z-axis. The cross-section of the parts remain the same during dry-pressing.

6.5.2.1 Experimental procedure

Rhoplex binder (6 vol%), containing red dye, was used for printing to distinguish the printed region from the rest of the powder bed. The printed region on the powder bed appeared pink. This approach was used to measure the size of the printed region right after printing as well as after the high pressure densification step. The printed region was dried before pressing to high density. The printed region was defined with a mask containing a circular opening. The diameter of the circular opening was 7.0 mm. The vertical distance between the opening and the powder surface was 20.25 mm. The fast axis speed was 127 cm/sec and the flow-rate of the binder was 1.4 cc/min. The dimensions of the printed area were measured with a vernier calliper.

6.5.2.2 Results and discussions

The downward velocity of the binder stream is 14.67 m/sec while the horizontal velocity of the fast axis is 1.27 m/sec. The effective position of the stream during printing process is 4.9^0 off vertical direction. The vertical distance between the mask and the powder bed and the printed region is 20.25 mm. The binder stream printing at an angle to the cirular opening actually prints the region bigger than the diameter of the opening along the fast axis direction. The printed region, as a result, appears as an ellipse (figure 6.10). The major and minor axes of the elliptical printed region right after printing and also after the high pressure compaction step was measured with a vernier calliper and is shown in Table 6.1. The powder bed was dried after printing before the high pressure compaction step. The printed region did not change shape after the high pressure compaction.

6.6 Part retrieval stage

The key requirement of the part retrieval stage is to dissolve away the unprinted region without affecting the printed area. The parts were built by printing Rhoplex HA-16 on powder beds made out of SDPAA/alumina granules.

6.6.1 Selection of cleaning solution

Since PAA is chemisorbed onto alumina, it does not dissolve in water as shown in chapter 4. However, a strong base such as KOH can be used to leach out the chemisorbed PAA . The effectiveness of the cleaning solution was evaluated by washing SDPAA/alumina compacts in KOH solution at pH 10 and 13. SDPAA/alumina compacts were found to disintegrate in cleaning solution at pH 13. The disintegration process was almost negligible in cleaning solution at pH 10. FTIR is used to check the effectiveness of the two different KOH solutions to remove the chemisorbed carboxylate group from the surface of alumina. Figures 6.11 & 6.12 show the FTIR spectrum of SDPAA washed in two different pH solutions. The washing was performed for 2 hours. It is clear that the SDPAA washed at pH 10 still has a strong carboxylate peak centered at 1576 cm^{-1}. However, SDPAA washed at pH 13 lost most of the carboxylate group upon washing. Rhoplex after being crosslinked does not dissolve in KOH solution at pH 13. This was tested by measuring the weight of a film of Rhoplex before and after sonicating the film in KOH solution and subsequently drying. There was no change in the weight of the Rhoplex film.

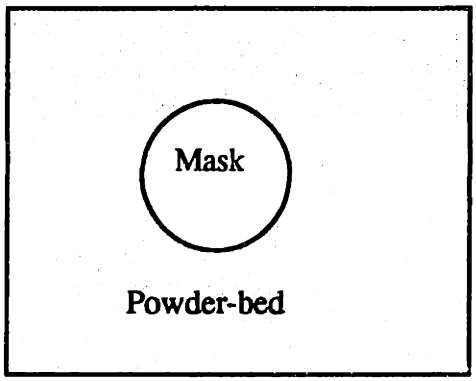

Mask was kept at a distance of 20.25 mm from the powder surface

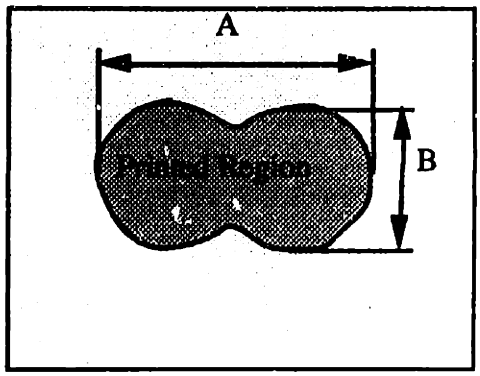

Shift error created distortion in the printed region

Figure 6.10: Effect of shift error on the shape ofthe printed region.

Table 6.1: Measured major and minor axis of the elliptical printed region right after printing and after high pressure compaction.

Printing Parameters: fast axis speed 127 cm/s, flowrate 1.4 cc/min

Axes	Calculated printed region size (mm)	Measured printed region size before the high pressure compaction (mm)	Measured printed region size after the high pressure compaction (mm)
A	~ 10.63	~ 10.87	~ 10.90
B	~ 7.13	~ 7.12	~ 7.10

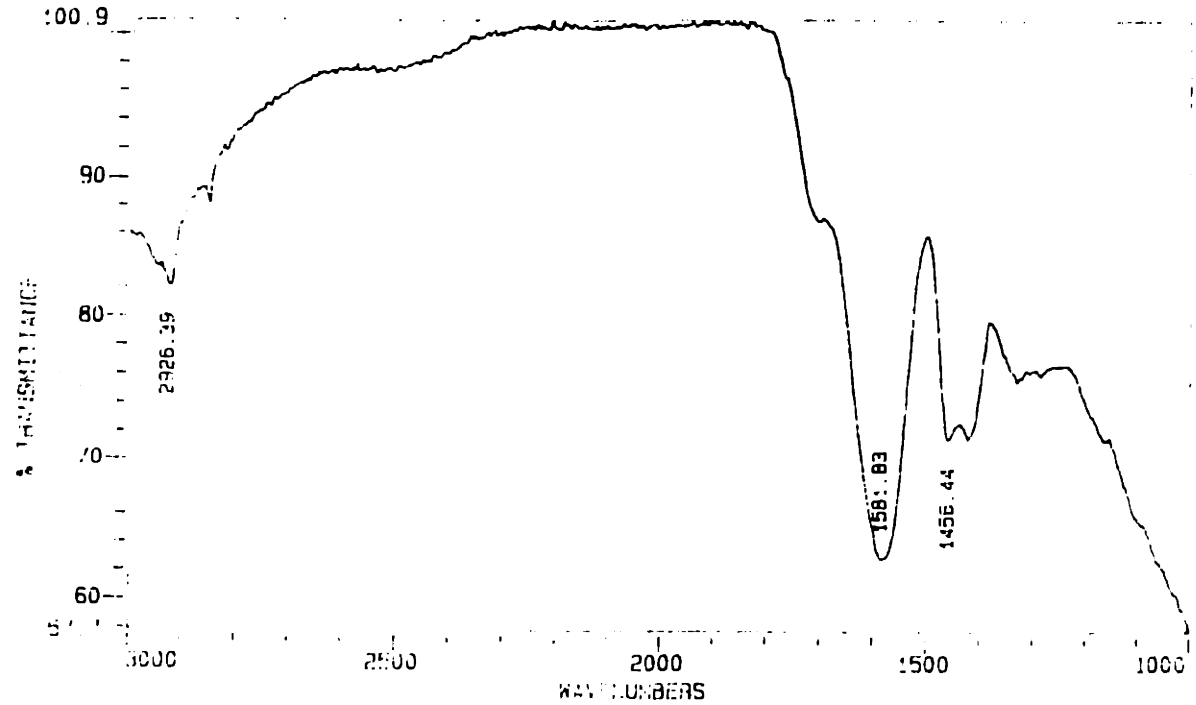

Figure 6.11: FTIR of SDPAA powder after being washed in KOH solution at pH 10 for 3 hours.

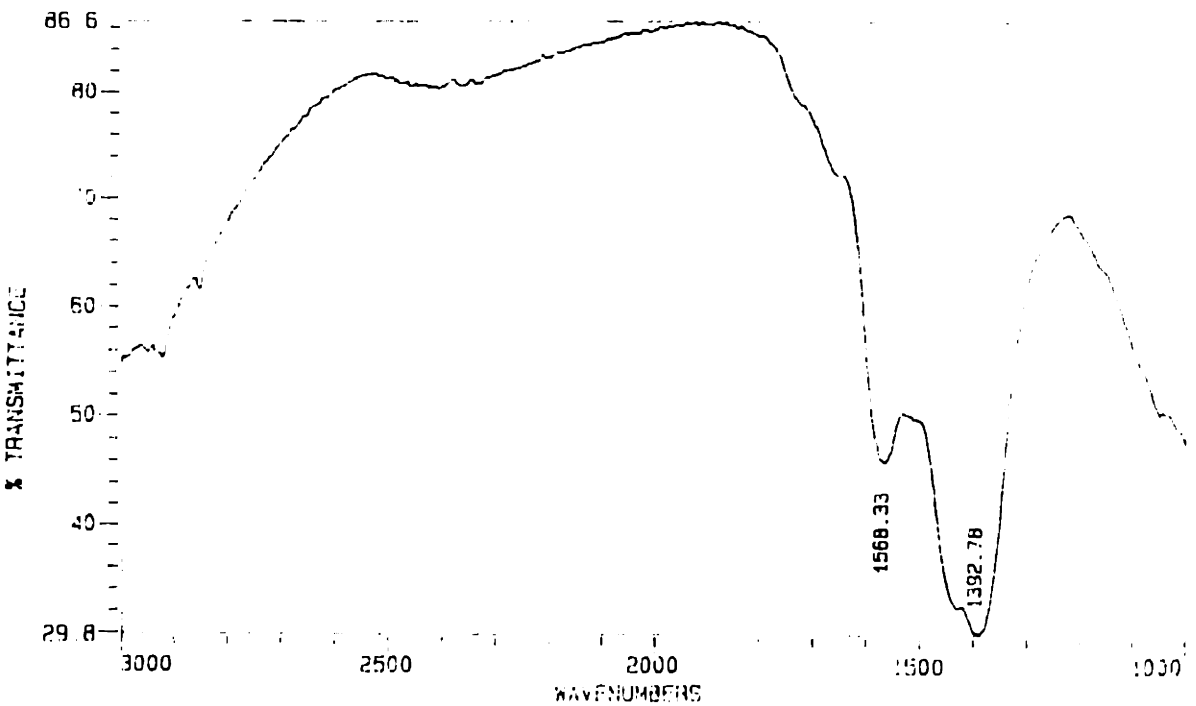

Figure 6.12: FTIR of SDPAA powder after being washed in KOH solution at pH 13 for 3 hours.

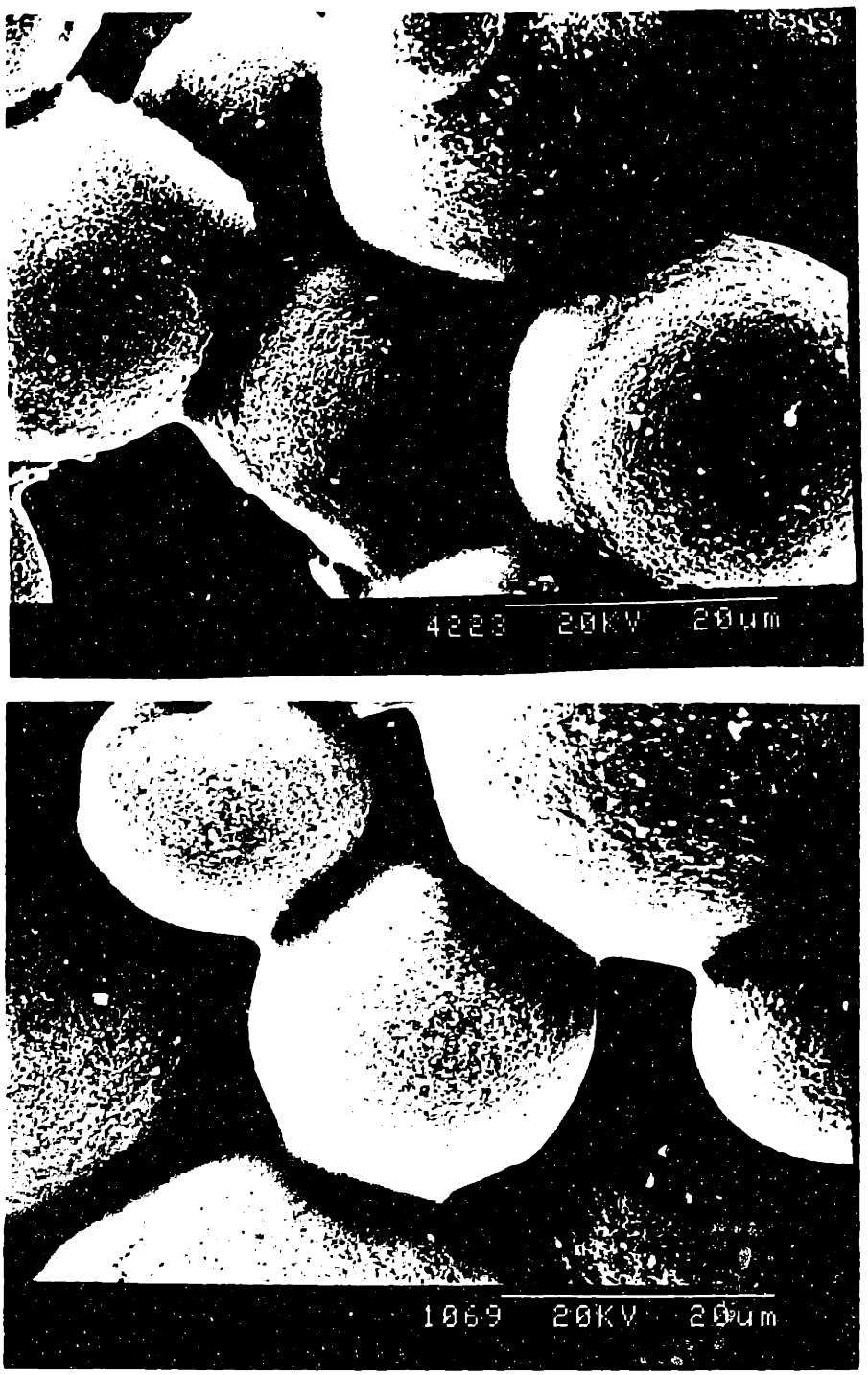

Figure 6.13: SEM micrograph showing the top surface of SD alumina powder bed printed with 30 vol% rhoplex once and twice respectively.

6.6.2 Part retrieval: observations and analysis

The parts were built by printing 6 vol% Rhoplex HA-16 binder on SDPAA/alumina powder beds. It was observed that the printed parts disintegrated in the cleaning solution along with the powder bed. The printed binder segregates at the neck region during the printing step. The binder distribution within the printed part will be preserved during the subsequent high densification step. This microstructure allows the uncoated sides of SD granules to dissolve away in KOH solution during the cleaning process.

Parts were printed with 30 vol% Rhoplex on an uncompacted powder bed to simulate the distribution of the printed binder within the press-compacted powder bed. The flow rate ofthe binder was 1.3 cc/min and the fast axis speed was 50 inches per second. The amount of deposited polymer was varied by printing the binder once and twice on the same layer. The printed parts with 32.7 % and 49% polymer (volume fraction of the polymer as a fraction of the total solid contents in the printed parts) were built. Figure 6.13 shows the SEM micrographs of the top surface of the printed parts. It is clear that even with such high amounts of polymer deposition, the complete coverage of the SD granules is not accomplished. Unlike the latex emulsions, the current polymer binder solutions are capable of infiltrating the high packing density powder compact directly. This will ensure a more uniform distribution of the printed binder in the printed part, as the printing can be accomplished directly after the high pressure densification step. But now we also have a better way of making high green density powder beds through a wet deposition approach (Chapter 7). One of the major advantages of the wet deposition process is the absence of the compaction step . High pressures on a big area will translate into large absolute loads and can make machine design quite a challenge.

6.7 Conclusions

Press-compaction process was successfully used to fabricate high, uniform and isotropic powder beds out of fine structural ceramic powders. The use of latex emulsion as a binder at the time of this process development required the presence of large intergranular pores. The printed binder was shown to segregate at the neck regions between the SD granules during printing. The binder distribution was preserved during the subsequent high pressure compaction step. The non-uniform microstructure allowed the uncoated side of the SD granules within the printed region to dissolve away in the cleaning solution. This resulted in the disintegration of the printed parts during the part retrieval step. Chapter 7 describes a novel wet deposition approach of fabricating high and isotropic green fine ceramic components directly by 3DP.

CHAPTER 7
SPRAY DEPOSITION

7.1 Introduction

Our efforts so far had been to improve the flowability of the fine powder in the dry state to create uniform and defect-free powder layers with the conventional 3DP spreading set-up. High flowability of fine powder was successfully accomplished with the use of spray dried (SD) granules. The SD printed parts have low packing density and interlayer defects. Isopressing is required to increase the packing density and heal the interlaminar defects to form isotropic components.

Conventional forming methods, such as casting, employ wet slurry processing to fabricate high and uniform packing density parts out of fine powders. Conventional 3DP process has so far employed only dry methods for spreading powders. Michaels [123] had tried to deposit metal powders in thin layers by spreading pseudoplastic metal paste with a doctor's blade (repeated tape casting). This approach was not successful as the wet paste slip-casted against the previously deposited layers, resulting in an uneven powder layer surface.

The main objective of this research is to develop a new process capable of fabricating a high, uniform and isotropic green density (GD) preforms directly from a 3DP machine, using a wet deposition approach. In addition to the benefits of high and uniform packing density green parts, wet processing can also be used to deposit thinner layers (~10 μm). A 10 μm thick layer cannot be spread with the conventional dry spreading methods. The deposition of thinner layers via wet processing technique can potentially be used to improve the surface finish of the printed parts.

This study is conducted to evaluate the feasibility of the overall concept and set up the stage for more extensive future research.

The first section of this chapter describes the criteria for depositing crack free granular films form alumina slurries. The second section discusses the methods of depositing slurries on repeated layer basis and describes the properties of the powder bed. The latter half of the chapter discusses issues involved in printing and retrieving printed parts out of the powder bed generated by the wet deposition technique.

7.2 Criteria for making crack-free powder bed

A wet deposition process will involve depositing slurries, followed by drying, to create the powder bed from fine powder. Drying of wet granular films often causes the formation of cracks unless large amounts of organic are added. Crack formation is related

to the dispersion formulation and the drying conditions. The tendency towards cracking is measured by the critical cracking thickness (CCT) above which a drying film cracks. Cracking will not occur unless the energy required to form a crack is less than the energy gained in relieving the strain in the film. The factors controlling the stress generated in the granular film, during drying, has been systematically investigated by Chiu and Cima [124].

Biaxial stresses can develop in a drying film either due to the moisture gradient across the thickness of the film or due to the constraint imposed by the substrate. Both these mechanisms can induce differential shrinkage between the top and bottom of the film and can produce stress that can result in cracking. The determination of the right mechanism is necessary to select the correct processing strategy to avoid cracking.

The development of moisture gradient in a drying body depends on the free surface evaporation rate and the ability of the green body to redistribute liquid internally. If the redistribution rate is slow compared to the evaporation rate, a sharp moisture gradient will develop parallel to the drying surface. The driving force responsible for the redistribution of liquid during drying is a result of capillary pressure gradient associated with different pore size in the packed powder bed. This pressure gradient when equated with that created by viscous flow gives the scale over which the saturation gradients will occur [32, 50, 124]:

$$\frac{h}{d} = \frac{\Delta\phi\, \varepsilon^3\, \gamma}{18\, K\, G\, \nu\, (1-\varepsilon)^2}$$

where ν is the kinematic viscosity, G is the mass flux for surface evaporation, d is the particle diameter, γ is the surface tension, ε is the void fraction of the green body, $\Delta\phi$ is the geometric factor based on differences in particle packing, K is the tortuosity factor, and h is the length scale for capillary flow. $\Delta\phi$ is approximately equal to 8 for a randomly packed structure. The void fraction was experimentally measured for isopropanol/alumina powder bed as 0.5. The external drying rate was measured by spreading isopropanol (IPA) slurries on a flat plate and measuring the weight loss upon drying. The evaporative flux was measured as $2.2 * 10^{-4}$ Kg/(m^2.s). The kinematic viscosity of IPA is $2.85 * 10^{-5}$ m^2/s. The surface tension of IPA is 21.7 dynes/cm. The value of 'h' is calculated as 0.12 m which is 3 orders of magnitude larger than the thickness of the deposited film (90 μm typically). Therefore, stresses will not be created by moisture gradient when a granular film is dried.

A biaxial stress can also develop in the drying film due to the dimensional constraint imposed by the substrate. Chiu and Cima have shown that crack free films as

thick as 2 mm could be made on a smooth substrate like teflon and Hg (non-constraining substrate). They have proved that stresses are generated due to constraint imposed by the substrate and not by the moisture gradient for drying of thin wet granular film. They have also shown that the drying rate does not change the CCT when the stresses are generated due to the constraint imposed by the substrate. Therefore, higher drying rates could be employed in 3DP to reduce the drying time of a wet layer. Chiu [50] has also reported that there are no residual stress in the granular films formed from RC-172 alumina slurries, after the drying is complete. The biaxial stress is relieved by the particle rearrangement during drying.

The CCT (h_c) is a function of the magnitude of the biaxial stress (σ) and the fracture resistance (K_c) of the film material. The mechanics of cracking of thin films on rigid substrates is given by Hu [125] as:

$$h_c = \left(\frac{K_c}{1.4\,\sigma} \right)^2$$

Therefore, CCT can be increased by decreasing the biaxial stress and/or increasing the fracture resistance of the granular films. The drying stress will be as high as the capillary stress. The film stress, therfore, can be decreased by decreasing the surface tension of the suspension and increasing the particle size. The fracture resistance of the granular films can be modified by adding organic. Chiu experimentally measured the CCT of a granular film as a function of PVA added to the electrostatically stabilized alumina slurry. The graph is shown in figure 7.1. Without any PVA, the CCT is reported as 65 μm. The CCT increases linearly with the PVA binder content in the slurry which indicates that the fracture resistance of the film is proportional to the square root of the binder content.

7.3 Methods for wet deposition of fine powder

Approach 1: Approximately 90 micron thick dispersed slurry layers consisting of 30 vol% solids was spread with a doctor's blade on alumina and glass substrates. The spread layer was air-dried. Assuming a 60 vol% particle packing density upon drying, the thickness of the dried layer was measured as ~ 45μm. The slurry for spreading second layer slip casted against the dried powder layer. Spreading of the second layer was also difficult as it kept peeling off portions of the first layer. The net result was an uneven powder bed surface; the position on the powder bed where the slurry was placed first results in thicker sections.

Approach 2: Spreading of the slurry on a porous gypsum mold eliminated the peeling of previous layers during the repeated slurries spreading operation. However, it did not

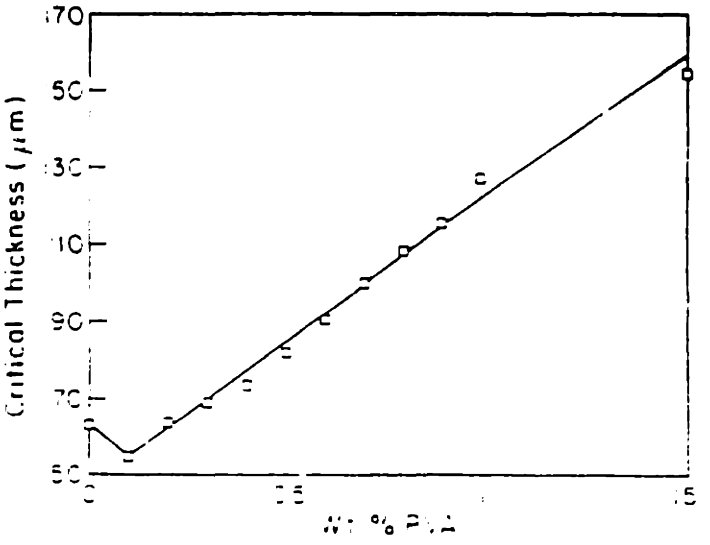

Figure 7.1: CCT of alumina granular film as a function of wt% PVA. (Chiu)

solve the problem of slip casting of the wet slurry on the dried surface. Slip casting leads to relatively thicker films on areas where the wet slip is first placed on the dry surface. However, the entire dried body peeled off the gypsum substrate after spreading and drying of three layers. The film peeled off even when the gypsum mold surface was made rough with an emery paper. Spreading was also done on borosilicate filters with a median pore size of 10 μm to avoid the peeling problem. The first few layers infiltrated the filter pores which are bigger than the average particle size of the alumina slurries. The dried film, in this case, did not peel off from the substrate upon drying. The infiltrated portion of the film probably provides a constraining force against peeling. Rapid slip casting of the wet slurries on dried layers, before spreading, is a major bottleneck in obtaining uniform layers by repeated tape/slip casting approach.

Approach 3: Slurry was sprayed on a porous borosilicate substrate with an air-brush to avoid slip casting problem during spreading. This approach resulted in fairly uniform surface. The process is described in more details in the powder bed generation section (7.5).

7.4 Process-concept

The overall 'spray deposition' process is conceptually demonstrated in figure 7.2. The first part of the process is to make slurries out of the desired ceramic material. The slurries are then sprayed onto a substrate and dried to create a powder bed. An organic binder is then printed on the powder bed to define a printed area. This process is repeated until the entire part is built. The printed part is subsequently chemically extracted from the rest of the powder bed. There are three critical stages in the spray deposition process:

1. Powder bed generation
2. Printing stage
3. Part retrieval stage

The next few sections will describe the critical processing issues involved in each of these stages.

7.5 Powder bed generation

Cracking of the powder bed during drying was observed as one of the major processing problems during the initial investigation of the spray deposition process. The critical processing issues and strategies to make multi-layered crack free powder bed is discussed in section 7.5.1. The powder bed should not only be crack free, but should also have a high and uniform packing density and no lamination defects. The pore size and

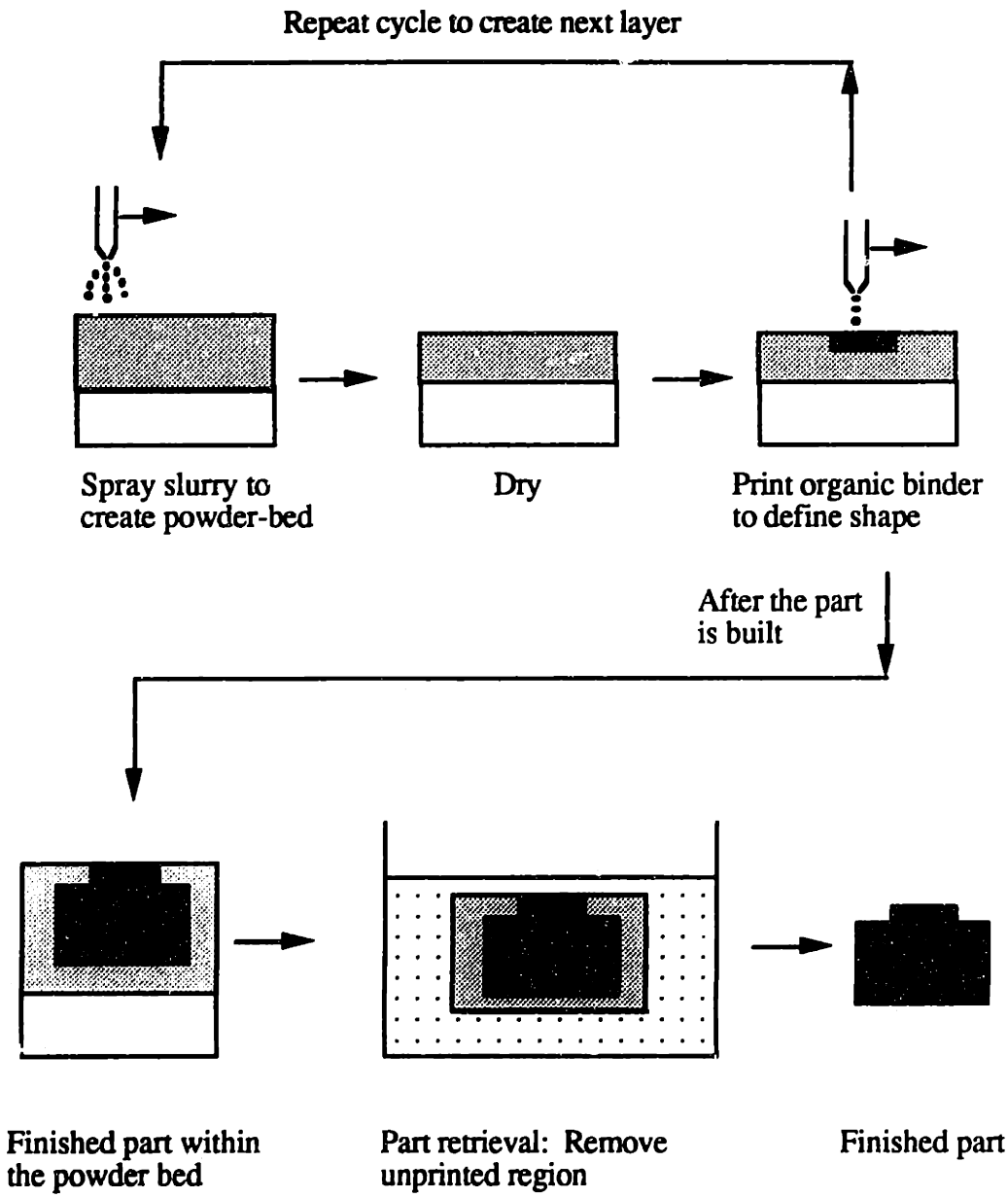

Figure 7.2: Schematic of the spray deposition process.

permeability of the powder bed will dictate the selection of the right kind of organic binder for printing. These issues are discussed in subsequent sections.

7.5.1 Repeated layer formation by spraying slurry (Control of CCT)

The initial investigations were conducted with a manual spray deposition set-up. The set-up consisted of a two nozzle Pasche air-spray brush. One of the nozzle is used for feeding the slurry while pressurized air is forced through the other. The pressurized air impinges on the slurry stream and converts it into spray. An air pressure of 20 psi was used for all the spraying experiments. Deposition of slurries was accomplished by manually rastering the sprayer on top of the porous borosilicate substrate at an approximate pitch of 10 to 20 mm, approximately at a scan speed of 50 cm/sec. The working distance, defined as the distance between the tip of the air brush to the top surface of the substrate, typically ranged from 5 to 12 cm. The manual setup was devised to establish the key processing variables necessary for the design of the automated setup.

Critical cracking thickness (CCT) is influenced by the presence of an organic additive and the variables affecting the drying stress. The spray deposition process involves an additional variable whereby the initially deposited layer may get partially dispersed by the freshly sprayed layer. Therefore, even though each deposited layer could be less than the CCT, the partial dispersion of the earlier layers could make the effective layer thickness above the CCT and result in cracking.

According to Chiu [124], CCT for pure alumina film is ~ 65 μm which can be increased to ~ 150 μm by adding just 0.15 wt% PVA binder to the ceramic slurries. The preliminary experiments were conducted by spraying 10 vol% alumina slurry containing 0.15 wt% PVA (d.w.b. of ceramic powder) on borosilicate filters. The build rate was calculated by measuring the increase in weight of the substrate after spraying and using the packing density and cross-sectional area of the substrate to approximate the average thickness of the deposited layer. The deposition rate varied between 30 to 60 μm per spray. The variation in the build rate is due to the continuous change in the liquid level in the container and/or change in the spray nozzle tip condition due to drying of the slurry while the spray is turned off between depositing subsequent layers. It is hard to control the thickness of the film uniformly across the entire substrate manually,therefore, the thickness of the films at some places can be larger than the average measured values.

The drying temperature was found to dramatically change the solubility of the PVA [126]. A drying temperature of 195 C resulted in crack free powder beds. However, the powder bed was found to be insoluble in water. This drying temperature ensured that a newly deposited layer did not disperse the earlier deposited dry layer. Therefore, cracking

of the film is avoided as long as the thickness of the sprayed layer is below CCT. A lower drying temperature such as 80 C maintains the solubility of PVA in water but was found to be more prone to cracking. An intermediate drying temperature of 120 C was found to be optimal for making crack free powder bed with reasonable water solubility characteristics. The extent of dispersion of the existing dry powder bed in the freshly sprayed layer will dictate the upper limit of film thickness which can be deposited with any slurry system. The amount of moisture during the powder bed generation process should be controlled so as to keep the net effective thickness of the wet layer (freshly deposited + redispersed portion of the dry powder bed) under CCT in order to build crack free powder bed. It is hard to control the thickness accurately with the manual set-up, therefore, this experiment was conducted with the automatic set-up where sprayed layers can be deposited more reproducibly.

The drying stresses of the alumina slurries were lowered by using isopropanol (IPA: lower surface tension) as a solvent. Para hydroxy benzoic acid (p-HBA) was used as a dispersant [127]. The lower surface tension (21.7 dynes/cm) of IPA reduces the drying stress and therefore should increase the CCT of IPA based alumina films. Layers deposited with the IPA slurry were found to be less prone to cracking as compared to water based slurry. IPA based alumina spray droplets exhibited drying behavior before getting deposited on the substrate (evidence in the later sections) resulting in lesser saturation within the sprayed layer. According to Chiu [50], the maximum stress in a granular film, during drying, occurs just below 100 % saturation. The drying of the droplets on flight would result in reduced saturation levels in the deposited layer and correspondingly the drying stresses will reduce and the CCT will increase. The extent of drying for aqueous and IPA based slurry is discussed later in this section.

Figure 7.3 shows the DRIFTS spectrum of the dried alumina/HBA granular film. It clearly shows that all the carboxylic functional group of HBA is chemisorbed on to the alumina surface as aluminum carboxylate. The carboxylate peak is present at 1620 cm^{-1} while the carboxylic peak (1760 cm^{-1}) is almost non-existent. This chemisorption makes the alumina granular film insoluble in IPA. As shown earlier, if the sprayed layer does not disperse the previously deposited layer, the chances of cracking reduces dramatically as long as the individual deposited layer thickness is kept under the CCT.

The amount of HBA for monolayer coverage, assuming no steric hindrance, was calculated as 2.9 wt%. The hydroxyl concentration on alpha-alumina surface is ~18 OH^-/nm^2. In order to estimate the steric factor, the molecular diameter of HBA was calculated as 4.35 Å. This corresponds to 5.28 HBA/nm^2. Higgins [81] also reported that only 68% of monolayer coverage was accomplished with PMMA/Alumina system. Assuming

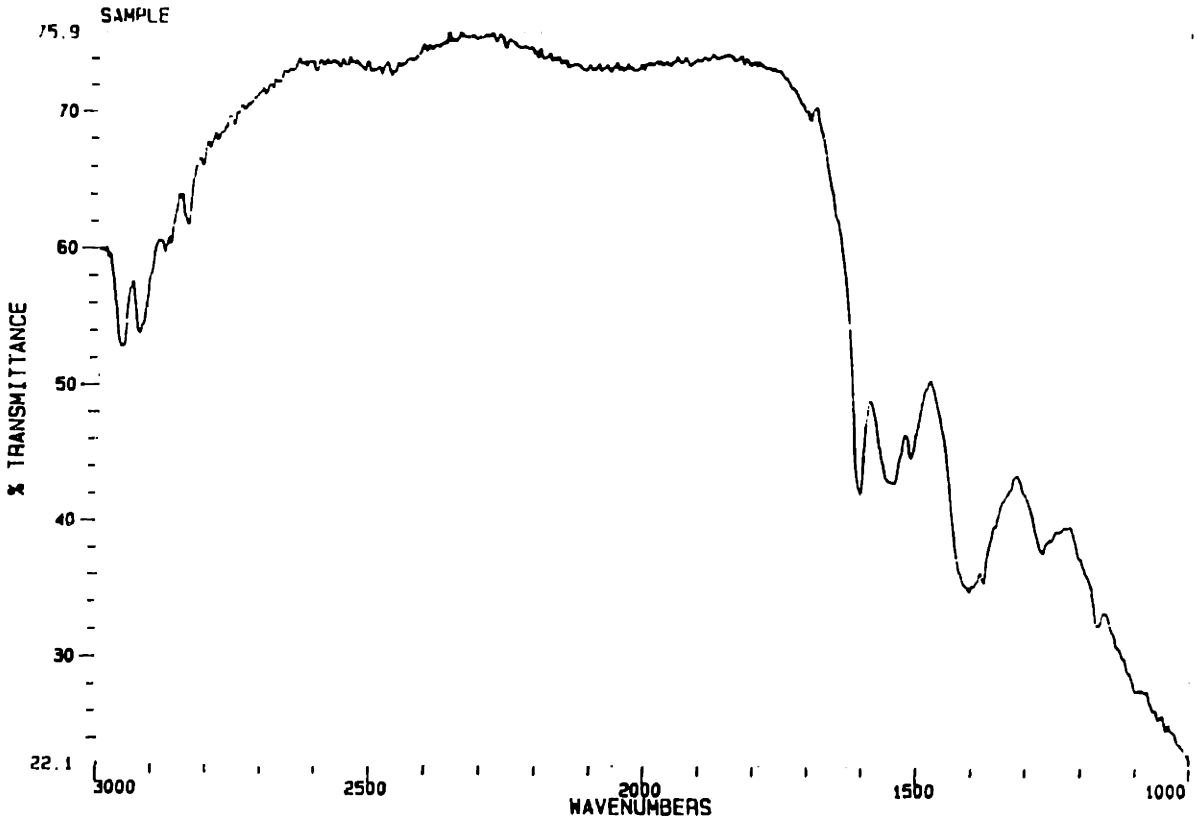

Figure 7.3: DRIFTS spectrum of 0.5 wt% HBA/alumina powder bed.

similar coverage, there will be 3.6 HBA/nm^2. As there are 18 OH^-/nm^2 on alumina surface, effectively there will be 1 HBA (carboxylic)/5 OH^-. Therefore, the amount of HBA needed for monolayer coverage is 0.59 wt%.

The powder bed prepared from IPA/HBA/alumina slurry had lower cohesive strength than that obtained by spraying aqueous alumina slurry. This observation is routinely observed in ball milling process where alcohol is used as a solvent for mixing powders to obtain lower cohesive strength agglomerates upon drying. Water cracks the HBA/alumina powder bed into several small pieces which can easily be washed away.

It was shown earlier that the flow-rate of the spray set-up, working distance and as a result uniformity of the thickness is very difficult to control with the manual set-up. A lot of these concerns can be addressed very easily by mounting a spray set-up on a mechanical x-y stage. The mechanical stage will guarantee constant working distance and uniformity of deposition, once parameters for consistent flow-rate are established.

The automated set-up is shown in figure 7.4. It consists of an airbrush mounted on a x-y stage of a vector machine. Variable flow rate during deposition stage will result in variable thickness which is not desirable. Therefore it is necessary to establish parameters to achieve constant flow rate. The slurry was fed from a reservoir in the preliminary experiments. The slurry level constantly changed during the spraying process. Periodically the slurry was added to the reservoir. Figure 7.5 shows the measured flow-rate as a function of time. The jumps in the flow-rate are a result of different hydrostatic heads. The slurry tank was pressurized by air to eliminate the head variation. It was also discovered that during the spraying process, spray droplets bounced back due to their impact with the catcher and coated the spray nozzle. This affected the nozzle openings for the slurries as well as for the pressurized air and influenced the flow of the slurry coming out of the nozzle. The spray-back problem was avoided by mounting the spray nozzle at 45 degree to push the spray direction away from the nozzle. The flow rate was measured after incorporating these corrections in the design. The flow rate became fairly constant as shown in the figure 7.6.

The pitch between spray rasters will control the amount of slurry deposited per layer. The objective is to deposit an amount sufficient to build a crack free uniform thickness powder layer. At a spray pitch of 1 mm, striations or beach marks were noticed on the powder bed. The flow-rate of the spray was ~ 0.2g/second. The striations disappeared when the spray pitch was increased to 1.5 mm with a repeat fill pattern.

Another important variable in the design of the automated setup is the working distance between the tip of the spray and the substrate. The powder bed built at a working distance of 26 mm exhibited cracking problem. Cracking problem was solved when the

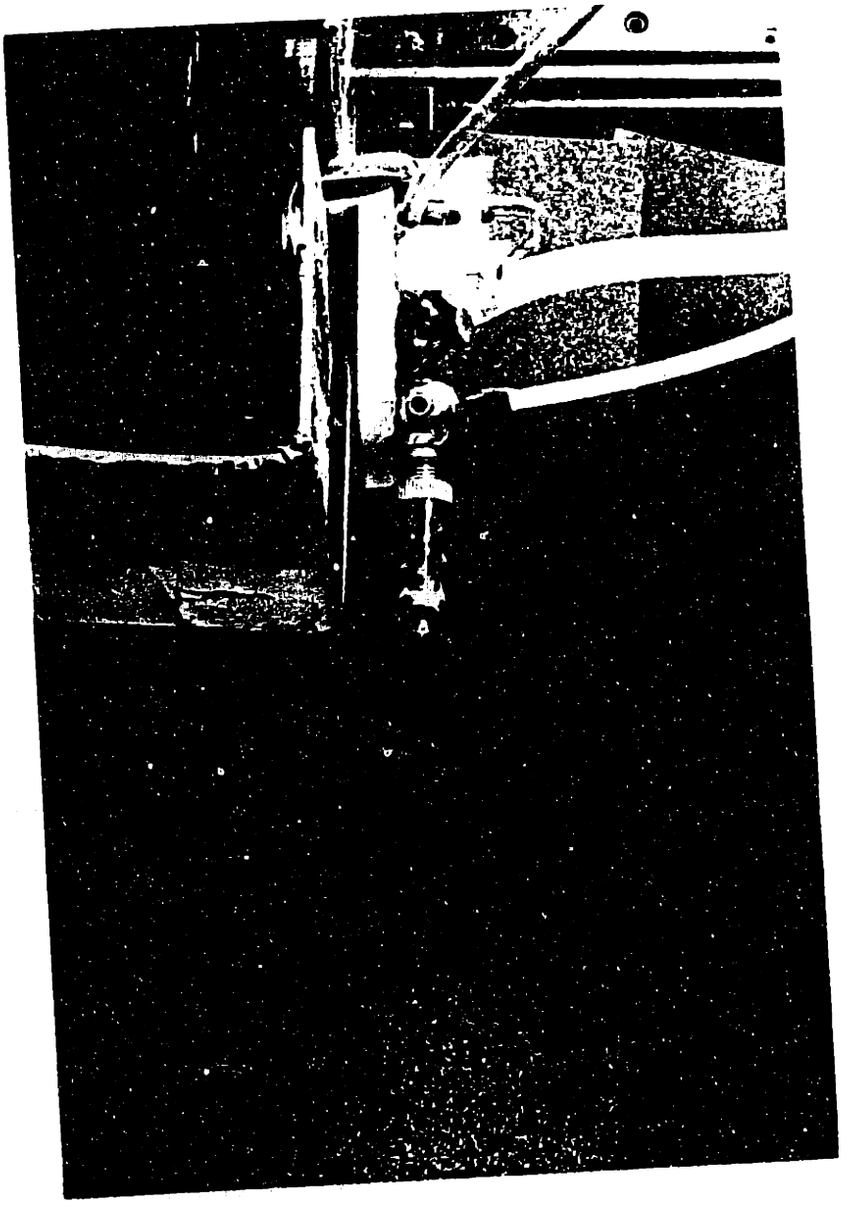

Figure 7.4: Spray machine set-up.

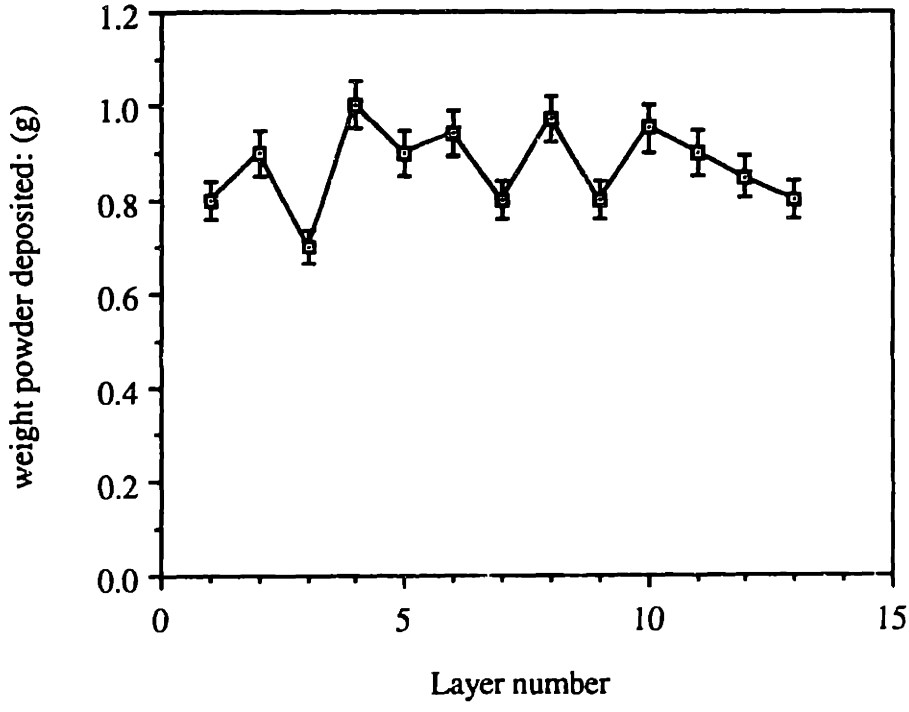

Figure 7.5: Spray flow-rate when the slurry is gravity fed.

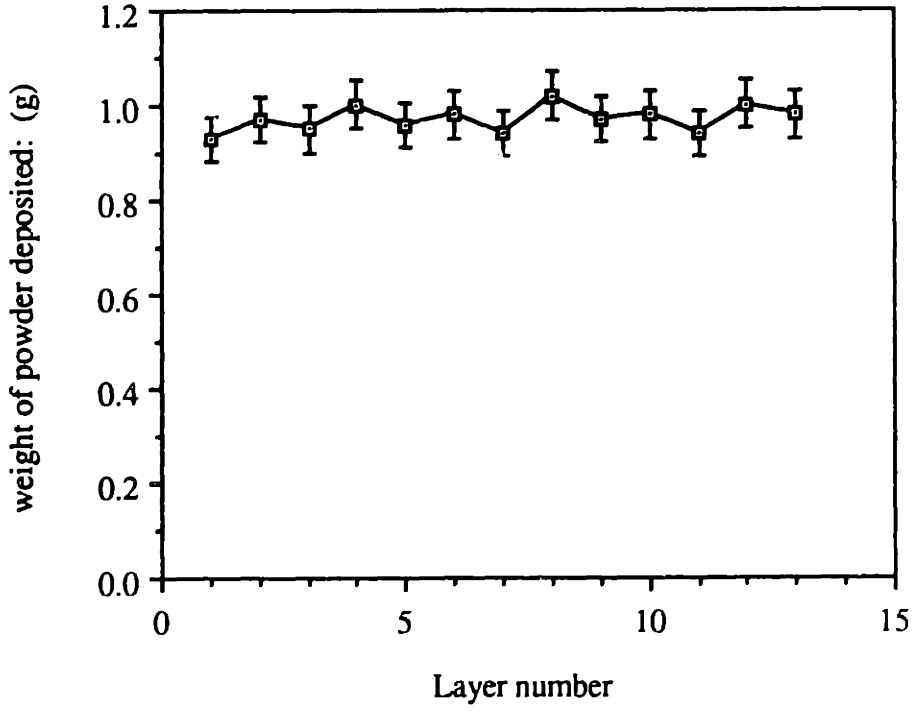

Figure 7.6: Spray flow-rate when the slurry tank is pressurized.

working distance was increased to 40 mm. IPA slurry droplets have a high vapor pressure and when mixed intimately with the air in the spray brush can dry to different extents, depending upon the flight distance before getting deposited on the substrate. The extent of drying of the droplets will affect the properties of the powder bed.

Single spray passes were performed on glass slides at working distances of 26 and 40 mm at two different fast axis speeds of 26.5 cm/sec and 51 cm/sec to prove the concept of drying of droplets. The width of the spray pattern deposited on the glass slide for various conditions are shown in table 7.1. It is clear that at a lower working distance, the width changes as more slurry is deposited at lower speeds indicating that the deposited matter is wet and can spread depending on the wetting parameters. The width of the sprayed pattern stayed constant in case of higher working distance, irrespective of the fast axis speed, implying that the deposited layers were dry enough to resist any spreading. The extent of drying not only affects the cracking behavior of the powder bed but it also affects its packing density as will be shown in the subsequent section.

Chiu [50] has experimentally measured the drying stress in a wet granular film as a function of saturation. Figure 7.7 shows the drying stress for a 60 μm thick granular films with an average particle size of 0.4 μm. The drying rate was $7.2 * 10^{-6}$ kg/m^2.s. The drying stress reaches a maximum value just below 100% saturation and then decreases monotonically as a function of saturation. By controlling the extent of drying during spraying, it will be possible to reduce the degree of saturation and thereby the drying stress. This will help to avoid high drying stress and as a result will reduce the cracking problem duringthe powder deposition stage.

Grau [128] has quantified the extent of drying obtained by spraying an aqueous and IPA based alumina slurry. The aqueous slurry was electrostatically stabilized with nitric acid at pH 3 and had a solids concentration of 25 vol%. The IPA based slurry was sterically stabilized with 0.5 wt% HBA (d.w.b. alumina) and had a concentration of 10 vol%. A flowrate of 0.2 g/sec was used in both the experiments. The extent of drying was calculated by measuring the weight of the deposited wet layer right after deposition and the dry weight. The extent of saturation was calculated by:

% saturation = (1- dry weight /wet weight) 100

A 25 volume percent aqueous alumina slurry is 43 weight percent water, and a 10 volume percent IPA slurry is 64 weight percent IPA. Drying was measured for the airbrush held in a fixed position over the substrate and for a normal spraying operation where the airbrush is rastered across the substrate evenly. The former condition allows to determine the extent of on-flight drying while the latter shows the drying due to the surface area effect. The data is shown in table 7.2. The aqueous system showed a loss of only 2-3

Table 7.1: Width of single spray pass as a function of fast axis speed and working distance.

	Working distance (mm)			
	22		40	
Fast axis speed (cm/sec)	51	25.5	51	25.5
Width of single spray pass (mm)	9.5	15.5	15	15.5

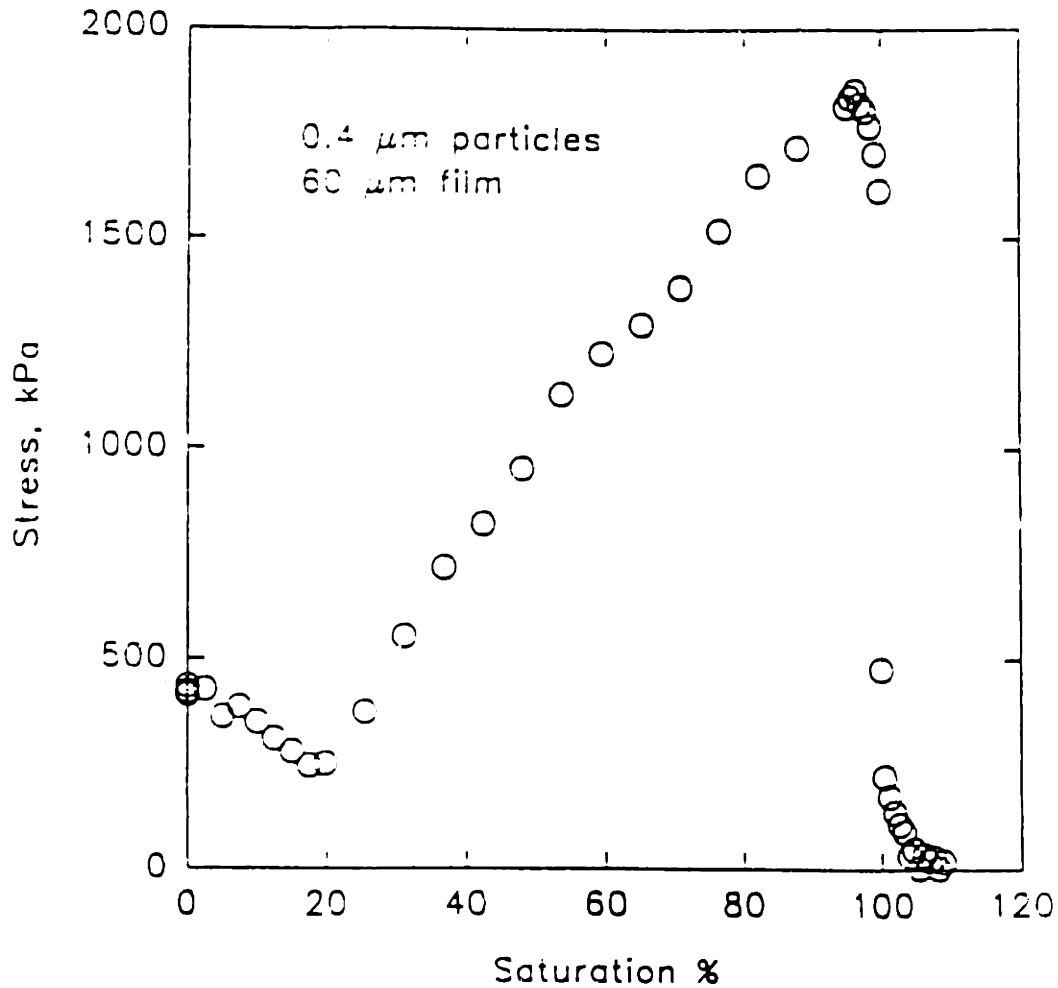

Figure 7.7: Measured drying stress of a 60 μm wet granular film as a function of saturation. The average particle size was 0.4 μm and drying rate was 7.2 * 10^{-6} kg/m^2.s. (Chiu)

Table 7.2: Saturation and the extent of drying for aqueous and non-aqueous slurry as a function of working distance. (Grau)

Working distance (cm)	Saturation and (weight loss) (wt%) Airbrush position fixed	Saturation and (weight loss) (wt%) Airbrush rastered
Aqueous alumina slurry (weight of water = 43 wt%)		
3.8	40.8 (2.2)	--
15.3	40.0 (3.0)	27 (16)
IPA/HBA/alumina slurry (weight of IPA = 64wt%)		
3.8	46.8 (17.2)	38.25 (25.75)
15.3	31.1 (32.9)	2.3 (61.7)

wt% water on-flight for both 3.8 and and 15.3 cm working distance. IPA based slurry, however, showed a lot more on-flight drying. The IPA/alumina slurry lost 30 wt% IPA (~ 50% of IPA present in the slurry) on-flight before getting deposited on the powder bed.

The extent of drying increases for both aqueous and non-aqueous slurry systems when the airbrush is rastered. The higher extent of drying in IPA based system ensure lesser drying stress as the saturation of the film is very low. In addition, higher drying rates result in lower packing density and larger average pore size(discussed in the next section) further reducing the drying stress. All the above factors help to reduce the cracking problem in IPA/alumina system. Grau [128] is currently conducting experiments to optimize the extent of drying to build high packing density crack free powder beds out of aqueous alumina slurries.

7.5.2 Packing density

Packing density of the powder bed is very critical in determining the absolute shrinkage during firing. A low packing density powder bed with low cohesive strength is prone to shrinkage and warpage, as shown in the earlier chapters. Therefore, a high packing density is a very desirable attribute in the powder bed not only to minimize sintering temperature but also to minimize the distortion during the build process. The powder bed should also be easily dispersible for a successful part retrieval stage.

The density of the powder bed prepared by spraying 10 vol% IPA/Al_2O_3 containing 0.5 wt% HBA is measured by the porosimeter as 49.2% and that of the powder bed made by spraying water/Al_2O_3 containing 0.15 wt% PVA as 57.8%. The difference in the packing density for the two solvent systems could be either due to the quality of the dispersion and/or due to the different extent of drying of the droplets during the spray deposition process. The effect of the quality of dispersion on the packing density is very well documented in the literature [129-132]. Flocculated slurries pack to lower packing density while the dispersed slurries pack to higher density. In the last section, it was shown that the spray droplets dry during the deposition stage. The extent of drying depends on the vapor pressure of the solvent. Droplets made out of high vapor pressure solvents, such as IPA, were found to dry at a faster rate. The drying of the spray droplets can prevent rearrangement or merging between the droplets adversely affecting the packing density of the powder bed.

The quality of dispersion were evaluated by making green bodies out of the two slurry systems and the measuring the packing density with a porosimeter. Two different methods were used to prepare the green bodies. Method 1 included centrifuging (accelerated sedimentation) the slurry at 1500 g's, separating the clear supernatant from the

Table 7.3: Packing density of compacts prepared from various slurry systems.

Slurry system	Packing density of oven dried slurry cake g/cc, (% Th. density)	Packing density of spray deposited powder bed (% Th. density)
IPA/Al_2O_3	1.625 (40.82%)	
IPA/Al_2O_3/HNO_3 (pH ~3.5)	1.585 (39.82%)	
IPA/0.2 wt% HBA/Al_2O_3	1.778 (44.68%)	
IPA/0.2 wt% HBA/Al_2O_3 (cetrifuged at 1500 g's)	1.81 (45.47%)	
IPA/0.5 wt% HBA/Al_2O_3 (80C)	2.18 (54.77%)	49.2%
Water/0.15 wt% PVA/Al_2O_3 (pH ~ 3.5)	2.28 (57.3%)	57.8%

wet cake and drying the green body in an oven at 80 C. Method 2 involved placing the slurry in an aluminum dish and drying it in an oven at 80 C. Both these methods resulted in almost identical packing density for IPA/0.2 wt% HBA/Al_2O_3 slurry system as shown in table 7.3 . Method 2 was subsequently used to make the green bodies for rest of the slurry systems. Table 7.3 shows the measured packing density of compacts made out of various slurry systems.

The packing density of the compact increased as the amount of HBA was increased in IPA/Al_2O_3 system. It was reported earlier that 0.59 wt% of HBA is needed to form a monolayer coverage of alumina. Therefore, increase in HBA up to 0.5 wt% improves the quality of the slurry and result in increased packing density. The packing density of a green body obtained by drying IPA/0.5 wt% HBA/Al_2O_3 (10 vol%) slurry was measured as 54.77%. This is significantly higher than the density measured (49.2%) for powder bed obtained by spraying the same slurry. The packing density of oven dried and spray deposited powder bed made out of water/Al_2O_3 (10 vol%) slurry containing 0.15 wt% PVA were found to be identical. The difference in the packing density can be explained easily by the difference in the extent of drying observed during spraying an aqueous and IPA based alumina slurries. IPA/alumina droplets exhibit higher on-flight drying rates (last section). The drying of droplets could lead to inadequate merging of droplets upon hitting the substrate and result in lower packing density of the powder bed.

Uniformity of the packing density within a powder bed was evaluated by firing pieces of powder bed and checking the extent of distortion. The fired cross-sections of the powder bed appear to be straight after firing, implying fairly uniform packing density in the compact.

7.5.3 Inter-layer stitching

The inter-layer stitching (lamination) behavior was evaluated by firing the pieces to 1650 C and then examining the polished cross-sections. Figure 7.8 shows the cross-section of HBA/alumina powder bed. SEM micrographs clearly show that there are no interlayer defects in the powder bed. Spray deposition process, therefore, can be used to fabricate high and isotropic powder beds directly out of fine powders.

7.5.4 Permeability of the powder bed

The pore size distribution of the spray-deposited powder bed was measured on a porosimeter. Figure 7.9 shows the pore size distribution for both PVA/alumina and HBA/alumina powder bed. Both the powder beds have pore sizes in the submicron range. Though perfect for sintering, the submicron pores create new challenges for printing, as is

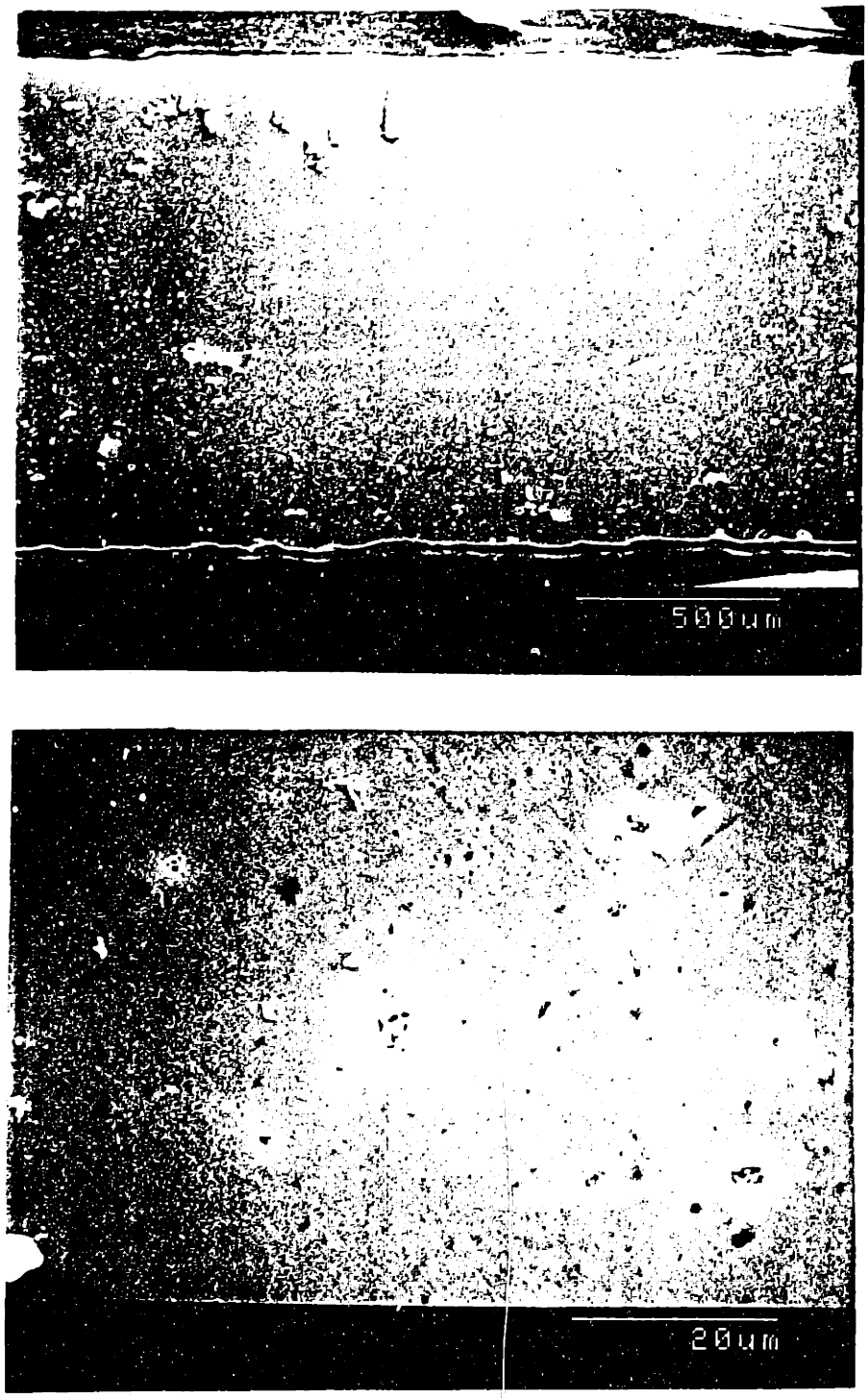

Figure 7.8: SEM micrograph of the polished cross-section of HBA/alumina powder bed. The powder bed was fired at 1650 C for 2 hours.

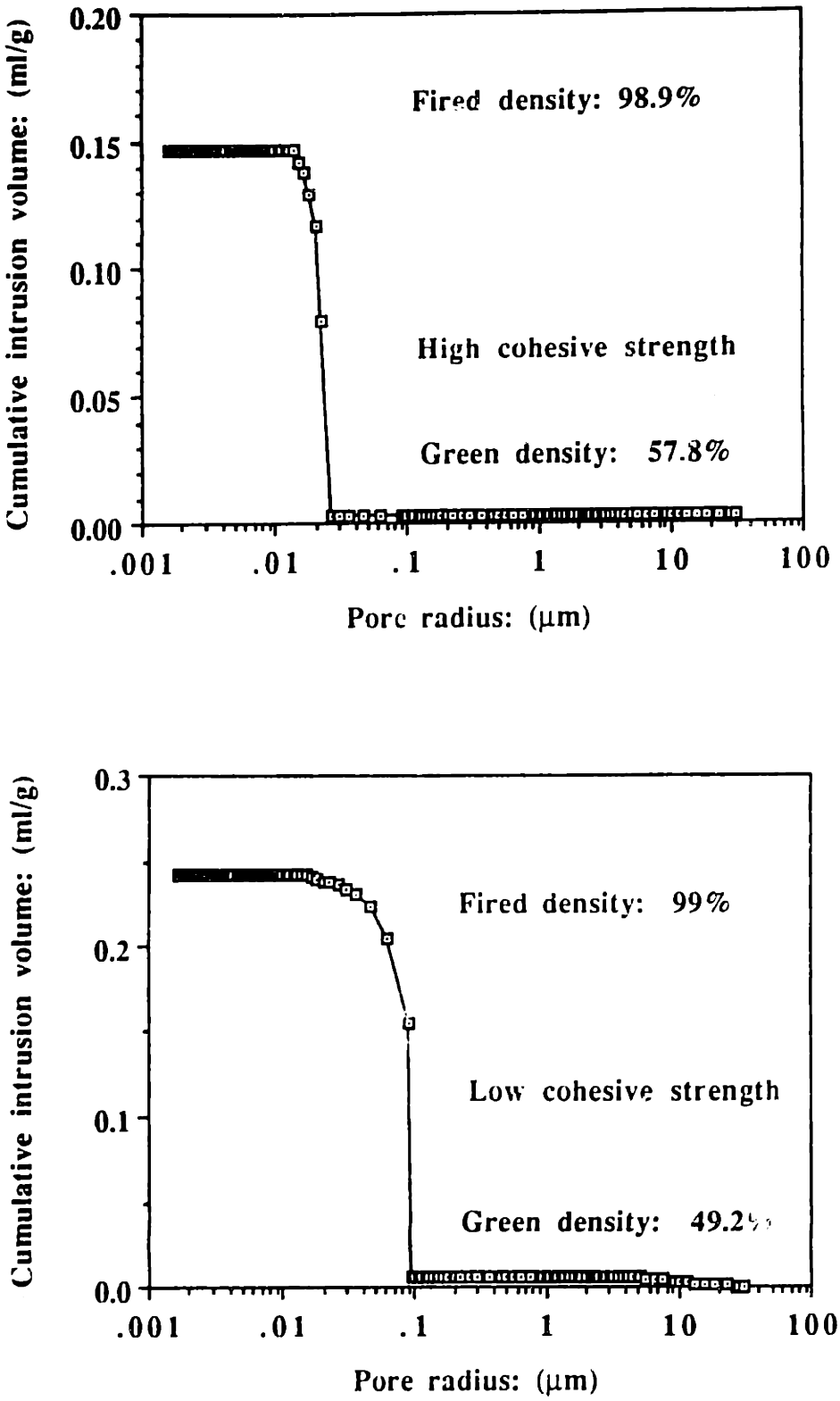

Figure 7.9: Pore size distribution of PVA/alumina and HBA/alumina powder bed.

described in the next section. Sufficient permeability in the powder bed, as is indicated by the open porosity of the powder bed, is a necessary pre-requisite for printing. An excess amount of organic additive in the initial slurry can plug the pores and may reduce the extent of infiltration of the printed binder in the powder bed.

7.6 Printing

Latex emulsions were the first binder system investigated for printing on spray deposited powder bed. However, droplets of acrysol with concentration as low as 3 vol% formed a film on the surface instead of infiltrating the powder bed. Thus, latex binder systems are not appropriate for printing on spray deposited powder beds. It will be shown in the subsequent sections that the polymer solution binders infiltrate the spray deposited powder bed easily. The selected binder should print through the nozzle and infiltrate the powder bed easily. Our first study was conducted with PVA alumina powder bed and super glue (methyl cyano-acrylate) as a binder to determine any additional issues involved in the printing process.

7.6.1 Identification of critical process variables using aqueous PVA/alumina powder bed and superglue (Methyl cyano-acrylate)

7.6.1.1 Printing of binder and infiltration stage: Observations and analysis

Crack free powder bed have been made by spray-depositing PVA/alumina slurries. It was shown that the PVA/alumina powder bed dried at 120 C show reasonable dispersion characteristics in water. Methyl cyano-acrylate does not dissolve in water. Our objective was to make the printed region insoluble by printing methyl cyano-acrylates into the PVA/alumina powder bed.

Methyl cyano-acrylates [133] are unique among many classes of adhesives as they are the only single component, instant bonding adhesives that cure at ambient conditions without requiring an external energy source. This characteristic coupled with an ability to bond a variety of diverse and dissimilar substrates has made them the ideal adhesives for numerous bonding applications. The reactivity of cyanoacrylates is directly traceable to the presence of two strong electron withdrawing groups (designated X and Y)

$$CH_2=C-XY$$

where X= CN (nitrile) and Y= COOR (alkoxy carbonyl). These groups make the double bond highly susceptible to attack by weak bases such as water. Cyanoacrylate monomers are highly reactive compounds and will polymerize via anionic and/or free radical mechanisms. The anionic reaction route is by far the predominant mechanism and can be initiated by even small amounts of a weak base such as water. Exposure to extended high

temperatures, ultraviolet light, or heat in the presence of peroxides can cause free radical polymerization to be initiated.

Super glue, permabond 910 (National Starch and Chemical company, NJ), with a mean viscosity of 100 centipoise was used as a binder. As received cyano-acrylate did not infiltrate the porous spray deposited PVA/alumina powder bed due to its high viscosity. The as-received cyano-acrylates were diluted in acetone and different concentrations were prepared. It was found out that 15 wt% cyanoacrylate solution in acetone infiltrates the PVA powder bed without forming a film on the surface and was therefore used as our first binder system.

Methyl cyano-acrylate polymerizes very quickly in presence of water and therefore cannot be printed easily. The anionic cure of cyanoacrylates proceeds as a result of basic catalyst, therefore, acids should be considered as stabilizers. Acids of either the Lewis or protonic types have been used successfully to reduce the kinetics of polymerization. Strong protonic acids such as aliphatic and aromatic sulfonic acids and mineral acids have been used in low levels as stabilizers. Carboxylic and anhydrides have also been used as stabilizers but generally are less effective than the stronger acids. Toluene-sulphonic acid was used to stabilize the monomer. Two batches of 15 wt% cyano-acrylate in acetone were prepared with 10 and 100 ppm toluene sulphonic acid respectively. The batch with 10 ppm stabilizer polymerized within 2 hours (turned opaque) while the one containing 100 ppm stayed stable for over two days. It gradually became more translucent with time. These solutions were printed successfully through the vector machine using teflon tubing, 7 μm online stainless filter and alumina nozzle.

7.6.1.2 Binder and powder bed interaction: observations and analysis

Toluene sulphonic acid dramatically slows down the kinetics of polymerization of cyano-acrylates. However, exposure to strong base such as ammonia enhances the polymerization rate. The stabilized cyano-acrylate was polymerized with ammonia in a petri dish. The polymer did not dissolve in water.

15 wt% permabond 910 in acetone with 100 ppm stabilizer was used as a binder and was printed at a fast axis speed of 150 cm/sec and a flow-rate 1.2 cc/min. Eight layers were printed at an average layer thickness of 116.8 μm (deviation 12.3 μm) (layer thickness was measured by weighing the borosilicate filter before and after spraying and assuming a uniform 60% dense powder layer over the entire filter cross-sectional area). Layer thicknesses were built at a rate of ~ 20 μm/ spray. The part was heated at 50 C for 30 seconds after printing to evaporate acetone and then exposed to ammonia gas for 30 sec in order to gel the cyano-acrylates. Saturation was controlled by choosing three different

line spacing: 100 (theoretical 284% super saturation, in reality 100% is the maximum saturation)), 200 (142%, super saturation) and 400 (71%) μm.

The first printed layer looked alright as the printed binder can spread out to any thickness in order to achieve an equilibrium saturation. Subsequent spraying of alumina slurry showed the earlier printed region. The sprayed slurry over the printed region stayed wet while the unprinted powder bed stayed dry upon subsequent spraying operation. The second sprayed layer was wettest right above the printed parts made with 100 μm line spacing. The slurry sprayed to create the next powder layer exhibited cracking problem right above this printed region. The contact angle of water on cyanoacrylte was measured as 90^0. Due to the high contact angle, water based slurry did not spread very well on the printed surface and at local spots could have exceeded the CCT and therefore resulted in cracking. The rest of the part (printed at 200 and 400 μm line spacing) was built up to 8 layers. The printed layer could be seen after the first spraying operation even when the line spacing was 200 and 400 μm. However, this problem appeared to diminish upon subsequent spraying operations. The printed part buried in the powder bed was exposed to ammonia for 10 hours after the build stage. The printed region turned yellow upon exposure to ammonia gas. The high cohesive strength of the aqueous powder bed eliminated the warpage problems during printing.

The printed part could not be retrieved from the powder bed. The printed part had 4.3 vol% binder. Details of part retrieval are discussed in the next section. One of the hypothesis was the absence of an adequate amount of the printed binder in the part to allow for sufficient distinction between the printed and the unprinted region. The amount of binder in the printed parts was increased by using Permabond 910-FS binder, with a viscosity of 3 centipoise. Toluene sulphonic acid (100 ppm) was used to stabilize the binder. Binder solution consisted of 84 wt% 910-FS cyano-acrylate in acetone. The average powder layer thickness was 145.66 μm (deviation 6.71 μm). The saturation was controlled by printing at 200 (114% saturation), 300 (76%) and 400 (57%) μm line spacing.

The first printed layer looked alright. There were non-wetting problems over the printed region during subsequent spraying operations. The wet spots over the printed region were more noticeable as compared to the printing accomplished with 15 wt% cyano- solution. Printing with the concentrated binder solution resulted in higher amounts of cyanoacrylate deposited in the printed region. The second sprayed layer showed cracking problem right over the region printed with 200μm line spacing. Similar problem was also observed for the powder bed sprayed over the printed region with 300 μm line spacing during spraying for layer 3. The part printed with 400μm line spacing showed

less of this problem. The part was built up to layer 8 and then treated with ammonia for 7 hours. The printed part had 19.2 vol% cyano-acrylate binder but did not appear to be stronger than the powder bed.

Acid strength and their levels are important variables in choosing a stabilizer. High levels of acid can overstabilize and make polymerization or cure speed of the adhesives quite sluggish and can contribute quite significantly to a rapid deterioration in adhesive performance. The water in combination with strong acid stabilizer, can cause hydrolysis of monomer, forming carboxylic acids which drastically retard the cure speed and therefore can affect the strength of the polymer. Therefore, it is possible that the presence of toluene sulphonic acid, though essential for printing, can adversely affect the properties of the printed region.

7.6.1.3 Lessons learned

1. Optimum wetting and viscosity characteristics of the binder solution is essential for infiltration. These requirements are valid for the infiltration of any porous bodies and is very well documented. Washburn equation quantifies this relationship.
2. The selection of compatible solvents and binder system is necessary to perform repeated spraying over the printed region. This requirement is unique to spray deposition technique. Large thickness variation will be found in the dried granular films if the slurries make a high contact angle with the printed region and as a result could crack.
3. Sufficient strength difference between the printed region and the powder bed will have to be created for easy part retrieval process. PVA/alumina powder bed are fairly cohesive. Weaker powder bed can be created by changing the surface tension of the solvent by using IPA based slurry. It was shown earlier that IPA/HBA/alumina powder bed could be made easily without any cracking. The objective should be to reduce the cohesive strength of the powder bed without sacrificing the packing density.

7.6.2 IPA/HBA/Alumina powder bed

7.6.2.1 Selection of binder

7.6.2.1.1. Monomer approach

This approach can be used to deposit a large amount of binder in the printed region. Infiltration of the porous bodies with monomers is fairly easy, as their viscosity is typically very low. The powder bed, in this approach, will be printed with the monomer and then will be polymerized in-situ. One of the problems with this approach is the additional time required for the polymerization step which might add to the overall cycle time.

Methyl methacrylate (MMA) monomer was the first binder system which was investigated for printing on HBA/alumina powder bed. Benzoyl peroxide was used as the initiator. Excessive monomer evaporation was found to be a problem during thermal polymerization step. The presence of oxygen is documented as an inhibitor to the polymerization of MMA. Ultraviolet (UV) curable monomer system were used to avoid the monomer evaporation problem. The inhibitive action of oxygen on the polymerization step is addressed by incorporating a free radical oxygen scavenger to the monomer solution [134-137].

Photomer 4017 (Henkel corporation) is made up of 1,6 -Hexanediol diacrylate (HDDA) and cures readily with UV. It has a viscosity of 10 cps at 25 C and exhibits a moderate shrinkage profile (14.4%) upon curing. Darocur 4265 (Ciba Geigy) was used as an initiator. It consists of equal amounts of 2-hydroxy-2-methyl-1-phenyl-1-propanone and Diphenyl (2,4,6-trimethylbenzoyl)-phosphine oxides (TPO). These photoinitiators allow the polymerization of HDDA with UV in air. Oxygen molecules are known to terminate the polymerization reaction of methacrylate monomers. The propanone photoinitiator act as oxygen scavenger and therefore help the polymerization reaction in air [34].

Monomer solutions containing 2 wt% photoinitiator were polymerized with a 100 W UV lamp, mostly emitting long wavelength UV radiations. The monomer solutions polymerized in 10 minutes to a fairly strong polymer. The polymer did not dissolve in water.

Single droplets of the monomer solutions were placed on a powder bed prepared by spraying 10 vol% Alumina in IPA containing 0.5 wt% para- Hydroxy Benzoic Acid (P-HBA) as a dispersant. The droplet infiltrated the powder bed. The powder bed was exposed to UV lamp for 10 minutes. Two different qualitative tests were conducted to determine the polymerization behavior of the monomer. First, powder could be brushed off the printed region as well as the unprinted powder-bed with the same ease. In comparison, single droplet primitives made with 8 wt% PMMA/acetone solution appeared fairly strong and did not exhibit powdery behavior. Second test consisted of retrieving the primitive by washing the powder bed with water. The primitive behaved very much like the powder bed i.e. it cracked and became soggy and could not be distinguished from the powder bed.

The powder bed after being exposed to UV light was also heated to 60 C for 5 minutes to help the polymerization step. This process also did not help the polymerization step. Also, UV exposure for longer times (90 minutes) did not show any improvement in the strength of the printed part.

Since the powder bed contained 0.5wt% HBA, there was a possibility that it might affect the polymerization step. This hypothesis was evaluated by dissolving 0.5 wt% p-HBA in Photomer 4017 containing 2 wt% photoinitiator and then exposing to UV light. The solution polymerized and resulted in a water insoluble polymer. In conclusion, scattering of the radiation by powder bed inhibited polymerization of infiltrated monomer. Similar observations have been reported by researchers in the stereolithography field [34].

7.6.2.1.2 Solution approach

The viscosity of a polymer solution is a strong function of the chemical nature of the polymer, its molecular weight and the concentration of the polymer in the solvent. The polymers solutions have been successfully printed by Wu and Borland [138] for building polymer parts. Poly methyl methacrylate (PMMA) does not dissolve in water and was therefore chosen as a binder to make the printed region on the HBA/alumina powder bed insoluble [139]. HBA/alumina powder cracked easily with water. 8 wt% PMMA (Mol wt 25,000)/acetone solution infiltrated this new powder bed and was selected for printing. Higher polymer concentrations formed films on the powder surface.

8 wt% PMMA/acetone solution was printed on the HBA/alumina powder bed. The flow-rate of the binder was 1.2 cc/min and the fast axis speed was 150 cm/sec. The parts were printed at 100, 150, 200, 300 and 400 μm line spacing in two separate runs. The very first layer warped after printing. The parts were printed along the substrate length.

The binder was diluted to 4 wt% to reduce the warpage (lessons learned from the SD granules system). The parts printed at 100, 150 and 200 μm line spacing warped with dilute solutions also. However, the parts printed at 300, 400 and 600 μm line spacing stayed flat. The parts were printed along the entire substrate length. Three layered parts were constructed with latter printing condition. Each subsequent deposited powder layer was 150 μm thick. The part retrieval was not easy as the printed part did not have enough strength.

A plasticizer, dibutyl phthalate, was also used to reduce warpage. The plasticizer reduces the strength of the binder and decreases the warpage problem. The decrease in warpage comes at the expense of the strength of the printed binder due to the plasticizer, which in turn adversely affects the strength of the printed part.

Repeated printing of 8 wt% and 4 wt% PMMA solution was performed in the hope of increasing the amount of polymer within the printed part and thereby increasing the part strength. Figure 7.10 shows the polished fired cross-sections of the parts built by printing 8 wt% PMMA/acetone solution once and thrice, every powder layer, on the HBA/alumina

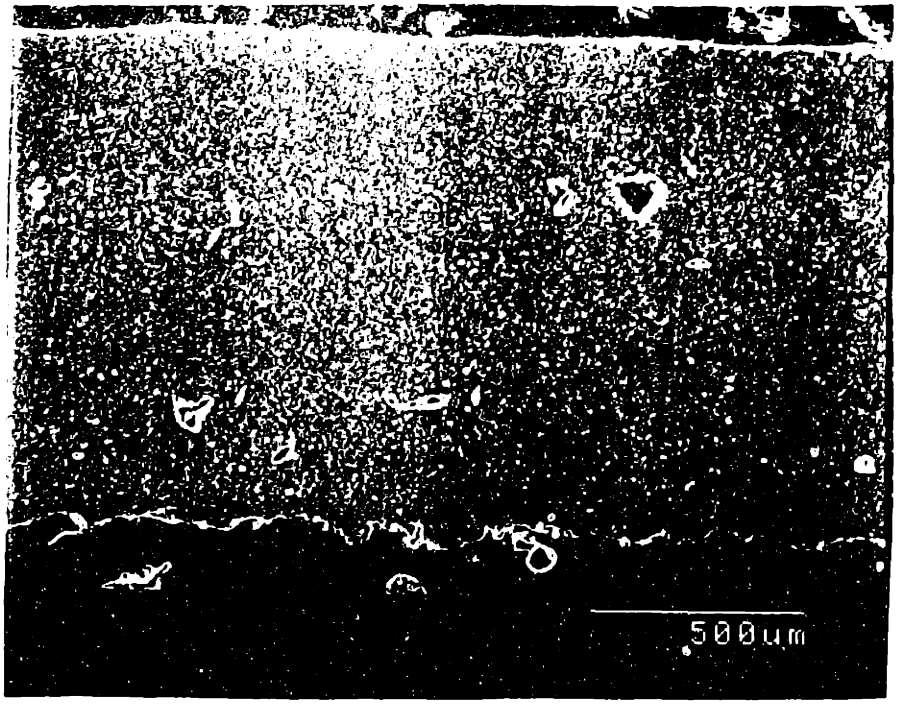

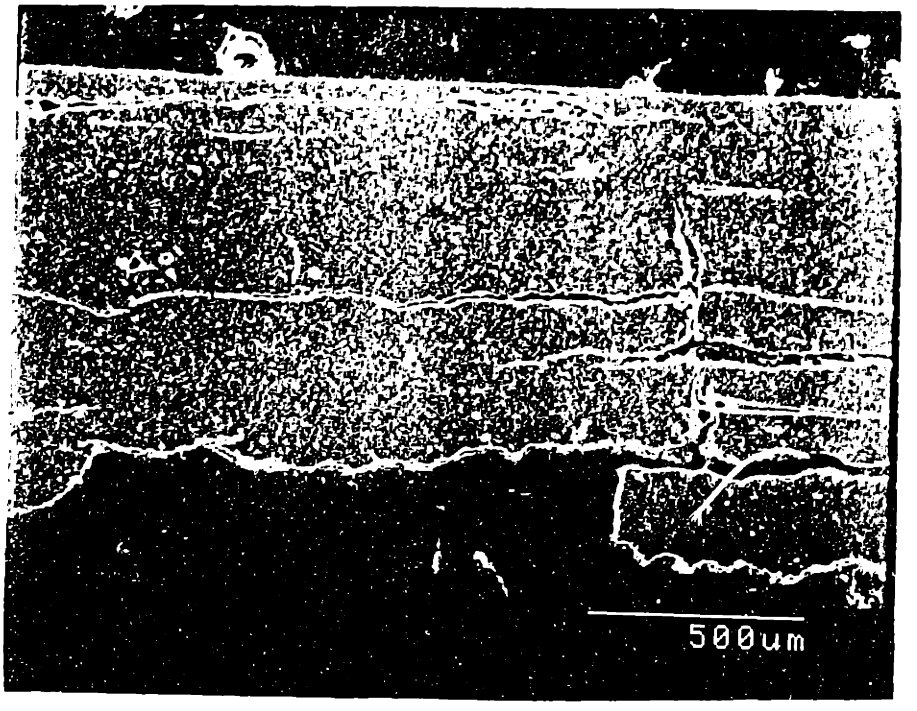

Figure 7.10: SEM micrograph of cross-section of parts made by printing 8 wt% PMMA/acetone solution on HBA/alumina powder bed once and three times per layer. The parts were fired at 1650 C for 2 hours.

powder bed. The repeated printing leads to the segregation of the polymer on top of the deposited layer and result in delamination. Therefore, repeated printing of the binder solutions is not the right strategy to increase the amount of printed binder in the printed part.

7.6.2.1.3 Lessons learned

1. The printed binder should infiltrate the powder bed. The polymer left on the surface will result in lamination defects. In this case, the next sprayed layer will also not spread uniformly over the printed region.
2. The distribution and strength of the binder along with the packing density and cohesive strength of the powder bed will determine the warpage behavior of the printed region. The powder bed with higher packing density and higher cohesive strength (PVA/alumina) did not warp while the HBA/alumina powder bed with lower packing density and lower cohesive strength warped. The warpage problem can be solved by reducing the strength of the printed polymer but it also simultaneously reduces the strength of the printed part. Unlike dry powder processing, where shrinkages are produced only during printing step, in case of wet processing, shrinkages are produced during powder deposition process also. If the part warps and is detached from the rest of the powder bed, subsequent spraying will enhance the warpage as the sprayed slurry undergoes a lot of shrinkage from 10 vol% to 50 vol% during deposition stage. Therefore, high packing density is a very desirable attribute in the powder bed.

7.7 Part retrieval stage

7.7.1 Initial observations and analysis

The first binder system, methyl cyano-acrylate printed on PVA/alumina powder bed created problems during part retrieval stage. The powder bed had a fairly high cohesive strength and the printed region had very similar strength (for reasons cited in the earlier sections) as the powder bed, therefore the printed part could not be retrieved. The strength of the powder bed was reduced by using IPA/HBA/alumina slurry. Unfortunately, along with the decrease in the strength of the powder bed, the packing density was also sacrificed. A high concentration polymer solution binder, though desirable for increasing the strength of the printed region, could not be used, as it resulted in warpage during printing. The warpage problem was solved by reducing the strength of the printed binder either by reducing the concentration of the polymer in the solution binder (4 wt%) or by adding plasticizer (dibutyl phthalate) to the solution binder. Both

these strategies helped to eliminate the warpage problem, but also simultaneously reduced the strength of the printed region, making part retrieval process a difficult operation.

The part retrieval process involved submerging the powder bed along with the printed region in a container full of water. Cracking was observed to initiate in the powder bed and in some cases extended through the printed part during the cleaning process. It was necessary to establish the underlying mechanism causing the cracking problem so that appropriate strategies can be devised to avoid cracking of the printed part during cleaning process.

The low strength of the IPA powder bed allowed us to retrieve printed parts when extreme care was taken during part retrieval process. The retrieved printed part had low wet strength. The broken pieces of HBA/alumina powder bed do not redisperse easily in water. The carboxylic group of HBA reacts with the hydroxyl group of alumina to form aluminum carboxylate (Fig) reducing their redispersibility in water. Redispersion of the powder bed in water was found to improve with an ultrasonicator. However, the printed part also disintegrate under the ultrasonic action. HBA chemisorbs onto alumina surface and therefore shield PMMA from forming a chemical bond with alumina.

A powder bed with a high packing density with easily redispersible characteristics is desirable for a successful part retrieval stage. Lower packing density powder beds such as Alumina/HBA also have low cohesive strength and create problems of warpage when a strong binder solution is printed into them. Subsequent sections describe our strategies to optimize the properties of the powder bed for easy part retrieval. The powder bed properties were tailored to allow for easy redispersion in water and to form a strong bond with the powder bed.

The next section systematically investigates the underlying mechanisms controlling the cracking of the powder beds. The understanding of the mechanisms is then used to design strategies to prevent violent cracking during the cleaning process.

7.7.2 Theory of cracking during part retrieval stage

One of the possible reasons for cracking of the powder bed during cleaning step can be explained by a theory proposed by Heertjes et.al [140]. They studied the disintegration behavior of rutile agglomerates submerged in various solvent systems and reported the excess pressure generated by the entrapped air within the agglomerate as a main mechanism of explosion. They also reported that the chances of explosion are higher if the wetting velocity of liquid is higher and also if the pore size distribution is narrower.

There are two key components in Heertjes model: First, excess pressure generated in the powder bed which will depend on the surface tension of the cleaning solution, the

Table 7.4: Disintegration behavior of the powder bed during part retrieval process

Powder bed systems	Immersion in water (In air)	Evacuation of powder bed and subsequent immersion in water
Alumina, Pure IPA, no HBA	Disintegration with explosion. The broken pieces do not disperse in water upon shaking. water remains clear.	Intact powder bed. In some cases, the powder bed breaks into couple of big pieces but in none of the cases did the powder bed disintegrate with explosion.
Alumina, IPA, pH modified with HNO_3, No HBA	Explodes but breaks into few pieces. The broken pieces disperse in water. water turns milky	Intact powder bed. In some cases, the powder bed breaks into couple of big pieces but in none of the cases did the powder bed disintegrate with explosion.
Alumina (0.1 wt% HBA)	Disintegration with explosion. The broken pieces do not disperse in water upon shaking. water remains clear.	
Alumina (0.5 wt% HBA)	Disintegration with explosion. The broken pieces do not disperse in water upon shaking. water remains clear.	The powder bed did not explode but broke into several more pieces than the bed made out of pure IPA/alumina powder bed.
Alumina, water containing 0.15 wt% PVA (80 % hydrolyzed), 20 % acetates which will chemisorb onto alumina surface	Compact stayed intact	
Alumina, water containing 0.15 wt% PEG	Compact disintegrated, no violent explosion. The broken pieces disperse in water. Water turns milky	

contact angle of the solvent with the powder bed and the pore size. The second element is the strength of the powder bed; if the strength of the powder bed is higher than the stress generated due to air entrapment, then the cracking of powder bed can be prevented.

Experiments were performed with a variety of powder beds made out of different organic and solvents. All the compacts were immersed in a dish full of water. Experiments were also conducted by firstevacuating the samples before immersing them under water. The observations are summarized in table 7.4. It was found that the IPA based powder bed,with lower cohesive strength, exploded violently when immersed in a bath of water. However, the same experiments when conducted under vacuum eliminated the violent explosion. In some cases, the powder bed did break into two or three pieces as compared to hundreds of pieces during the regular cleaning process. Stronger powder beds such as those made out of PVA/alumina heated to 190 C (where the PVA becomes insoluble in water) did not show any explosion problem. The mechanism of infiltration of the liquid in a porous powder bed is modeled in the next section.

When the powder bed is submerged in water, the geometrical situation (figure 7.11) at the beginning is that of a dry powder bed surrounded by the liquid. The powder bed contains a bundle of interconnected capillaries. If air is entrapped in the powder bed, the air can only escape from the powder bed when the capillaries differ in size and the larger openings are situated at the outer surface. In the absence of air, a liquid will enter a capillary spontaneously if $\theta < 90^0$. However, the powder bed is normally filled with air, therefore, entry of the liquid would cause an increase in pressure of the air. Complete wetting is impossible in such a case even when $\theta < 90^0$. If the diameter of the pores at the outer surface of the powder bed is slightly different in size then the penetration of the liquid can be modeled as following:

The liquid penetrates via the narrow capillary into the powder bed. The air is forced out of the powder bed through the large opening, because this requires a minimal excess pressure (figure 7.12). The capillary pressure, ΔP_{cap}, sucking the liquid into the capillary is expressed as :

$$\Delta P_{cap} = 2\gamma_{lv}\cos\theta r^{-1}$$

The force K_{cap}:

$$K_{cap} = \Delta P_{cap}\pi r^2 = \gamma_{lv}\cos\theta 2\pi r$$

The excess pressure in the bubble at the other end varies, because the radius of the bubble is not constant. The radius of the bubble is infinite before wetting. The radius decreases during wetting until a minimum value is reached. This minimum radius is as big as the radius of the opening from which the bubble is growing. Thereafter, the radius increases again until the bubble escapes from the capillary. Then another bubble is formed.

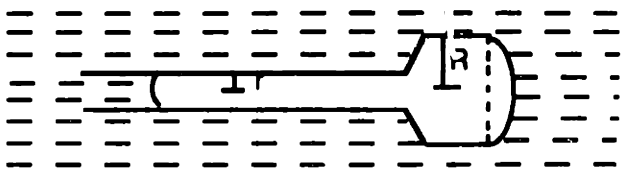

Figure 7.11: Penetration of liquid in a capillary of non-uniform size.

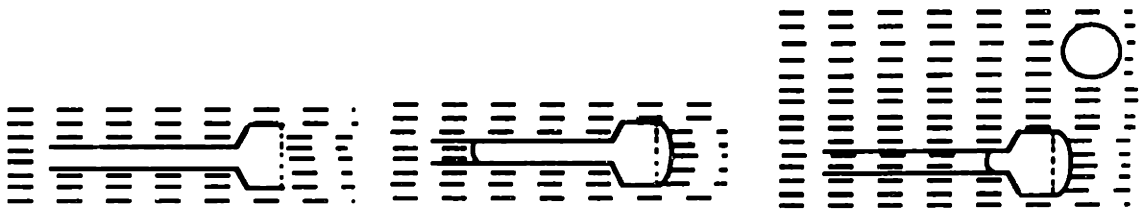

Figure 7.12: Three stages in the escape of air from a capillary of non-uniform size.

The excess pressure in the bubble is at its maximum when the radius of the bubble has reached its minimum value. If the radius of the large opening of the capillary is R, the maximum excess pressure is :

$$\Delta P = 2\gamma_{lv}R^{-1}$$

This excess pressure gives a force, K_p, acting against the liquid front entering the fine capillary expressed as:

$$K_p = 2\gamma_{lv}R^{-1}\pi r^2$$

The condition for wetting process to occur requires K_{cap} to be larger than K_p :

$$\gamma_{lv}\cos\theta 2\pi r > 2\gamma_{lv}R^{-1}\pi r^2$$

or

$$\cos\theta > r/R$$

From the above equation it follows that the wetting of an aggregate filled with air not only depends on the surface properties of the solid and liquid, but also on the pore structure of the powder bed.

If all the pores in the aggregate are of equal size (as is the case of spray deposited powder bed), upon immersion, liquid will gush inside the powder bed from all the directions and would result in excess pressure in the equilibrium state given by:

$$\Delta P = \frac{2\gamma_{LV}\cos\theta}{r}$$

This equation is used to calculate the excess pressure generated in the powder bed and the printed parts when immersed in water. The average pore size of an HBA/alumina powder bed is 0.1 μm. The part is printed with PMMA. Bredt [85] has measured the contact angle of water on alumina as 8.6° and with PMMA as 50°. Therefore, an excess pressure of 1.42 MPa will be generated in the powder bed. The printed region has a lower contact angle with respect to water therefore an excess pressure of 0.92 MPa is generated in the printed part. The presence of PMMA also increases the strength of the printed part over that of the powder bed. In effect, higher excess pressure and lower strength of the powder bed compared to the printed region, explain the observation that powder bed cracks first when immersed in water. However, as the size of the crack increases, lesser stress is required to continue its growth. If the printed part does not have enough strength, the crack instead of defelecting at the powder bed-printed region interface, will break the printed part. Therefore, in order to avoid the cracking of the printed part, not only should the violent cracking be reduced, but the strength of the printed part should also be increased.

The excess pressure can be reduced by reducing the surface tension of the cleaning liquid, increasing the contact angle of the liquid with the solid and increasing the pore size.

Another way to avoid the excess pressure is to partially submerge the powder bed in the liquid. In this case, the air can leave the powder bed without bubble formation, because the openings above the liquid are in connection with the surrounding air.

We reduced the cracking problem by allowing the water to wick up from the bottom of the part so that air can escape from the top. This strategy eliminated the violent cracking problem. The presence of non-soluble polymers in the printed region like PMMA reduces the wetting angle and as a result reduces the excess pressure. If there is no wetting in the printed region, the excess pressure due to the compression of the air is completely avoided and the cracking problem in the printed region is eliminated.

7.7.3 Strategies to improve the part retrieval process

There are two key elements of the part retrieval process: first, powder bed should redisperse easily in the cleaning solution. Second, the printed part should have sufficient strength so as to resist the dispersive forces due to the cleaning solutions. Researchers have thoroughly investigated the dispersion mechanism of the fine powders in liquid. Fine powders tend to agglomerate due to Van der Waal's force. An understanding of the factors that help to redisperse the porous fine powder agglomerates in liquid can be utilized to design our powder bed. The factors preventing the redispersion can be used as guidelines to tailor the printed region.

Fine particle agglomerates require sonication or mechanical energy to break before they can be well dispersed. The particles are held together with VDW and mechanical (frictional) forces in soft agglomerates. Sonication is usually sufficient to redisperse the soft agglomerates in presence of an appropriate dispersing media. However, when the agglomerates are hard, i.e. when the particles are chemically bonded, then the sonication energy may not be sufficient to break the agglomerates [141]. The chemically bonded hard agglomerates are separated from the dispersion by sedimentation. We want our powder bed to behave like soft agglomerates and the printed region like hard agglomerates. The powder bed should be engineered so as to have only VDW and frictional forces. The printed binder should be chemically bond to the surface of the particles and provide a network of particle to particle interaction strong enough to resist the dispersive forces during the cleaning operation.

Powder bed was made by spraying an electrostatically dispersed 10 vol% aqueous alumina slurry (pH ~ 3.5). The powder bed did not have any organic in the form of dispersant and therefore was held purely by VDW and frictional forces. As a result, the powder bed exhibited excellent redispersible characteristics in water. The powder bed was constructed manually at a rate of ~ 30 μm/spray. The sprayed powder bed had a packing

density of 54.2 %. A 10 wt% PAA solution (Molecular weight: 5000) in water was used as the binder. The flow-rate was 1.2 cc/min and the fast axis speed was 150 cm/sec. Layer thickness was ~ 90 μm and line spacing was 250 μm. The printed parts were removed by partially submerging the powder bed in water. Once the whole powder bed was saturated, the powder bed was covered with water and sonicated. The unprinted powder bed dispersed in water leaving behind the printed part. The printed part is shown in figure 7.13 .

DRIFTS spectrum (figure 7.14) of the printed part shows part of the -COOH group of the printed polymer chemisorbed onto the alumina from the powder bed as carboxylates. The presence of carboxylates makes the polymer insoluble, as shown in chapter 4. Thermogravimetric analysis (TGA) of the printed part is shown in figure 7.15. Figure 7.16 shows the TGA of the printed part after being washed for more than 20 hours and subsequently dried. The TGA data shows that most of the printed polymer remain unaffected during the washing process. The alumina surface is basic and the carboxylic acid chemically reacts with the surface to make a water insoluble aluminum carboxylate at the surface. Therefore, essentially, the printed region behave as 'one big hard agglomerate' i.e. particles are bonded together with a chemical bond. This allows the printed part to be distinguished easily during the cleaning process.

7.8 Properties of the printed green parts

The density of the parts made by printing PMMA/acetone containing 50wt% dibutyl phthalate (d.w.b of PMMA) solution on IPA/alumina powder bed was measured by porosimeter as 49.1% dense. The parts were debound at 450 C to burn out the organic. The fired part densified to >99%. The linear shrinkage was measured as 20.26%. Fired cross-sections of the printed part is shown in figure 7.10.

The density of the parts made by printing PAA solution into aqueous powder bed was measured as 56%. The part was sintered at 1650 C for 2 hours. The fired density of the printed part was measured as 96%. The linear shrinkage of the part during firing is ~ 16.5%.

7.9 Conclusions

The packing density of a crack free powder bed created by spraying electrostatically stabilized alumina slurry was measured as ~56%. The powder beds prepared by spray deposition develop a fairly high cohesive strength during drying. The high packing density and cohesive strength of the powder bed eliminated the shrinkage during printing. Therefore, no warpage was observed in the printed part. The

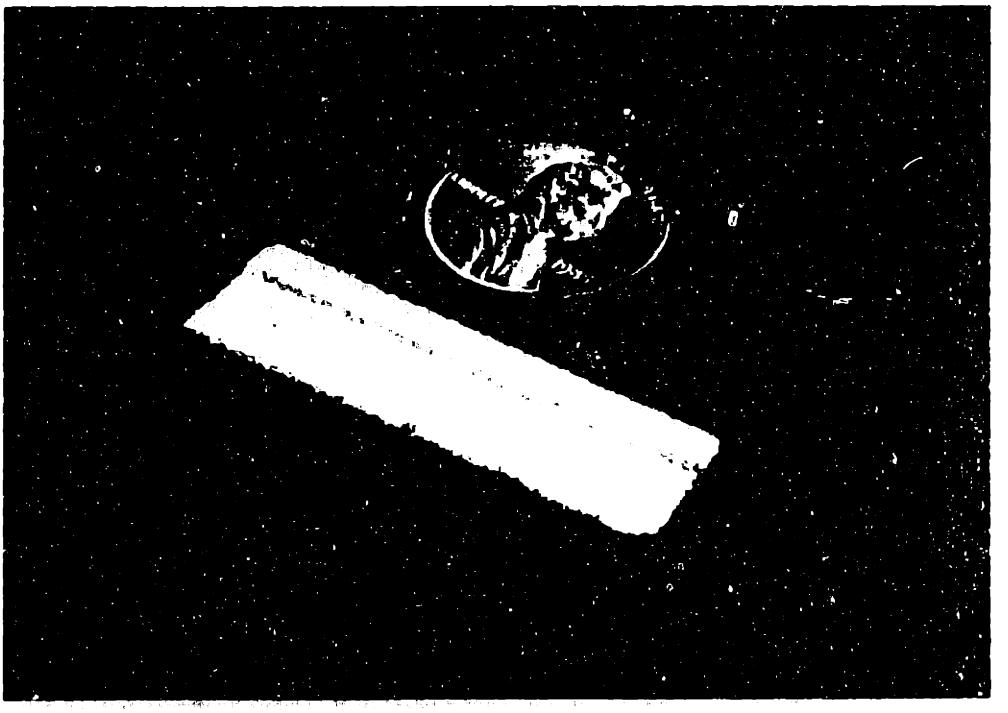

Figure 7.13: A part made by printing 10 wt% PAA solution on aqueous powder bed.

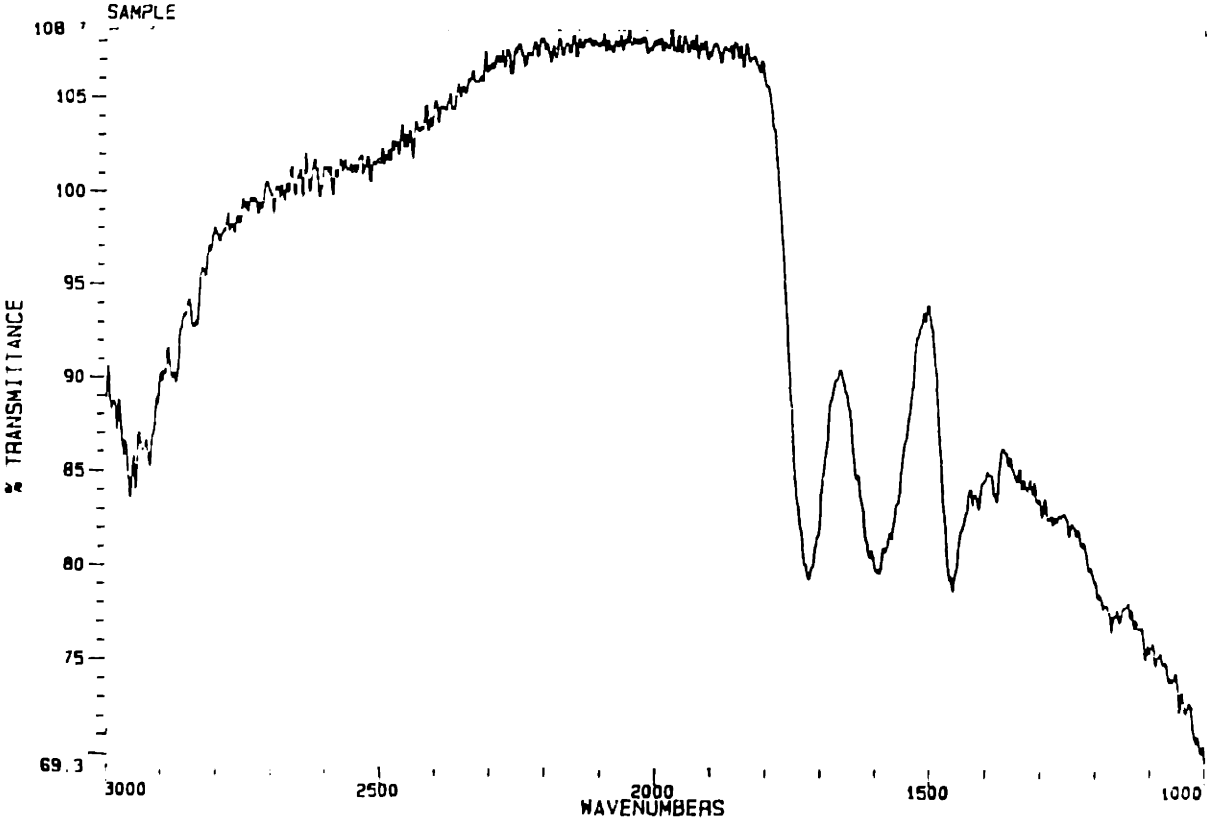

Figure 7.14: DRIFTS spectrum of parts made by printing 10 wt% PAA solution on aqueous powder bed.

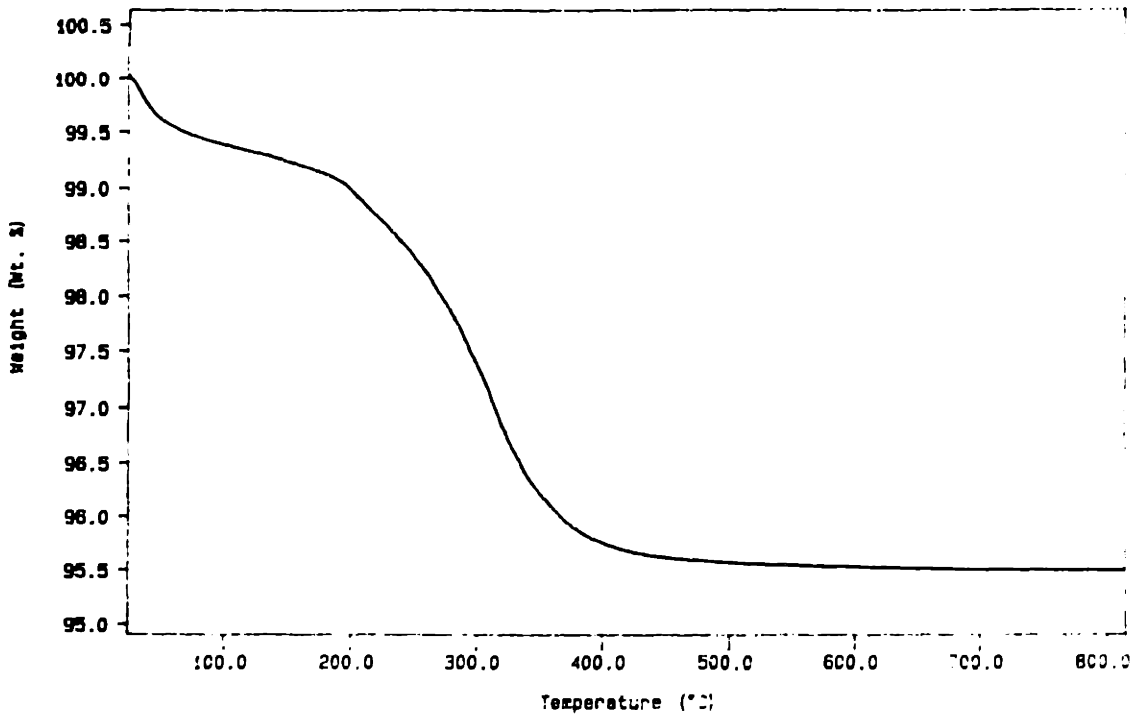

Figure 7.15: TGA of parts made by printing 10 wt% PAA solution on aqueous powder bed.

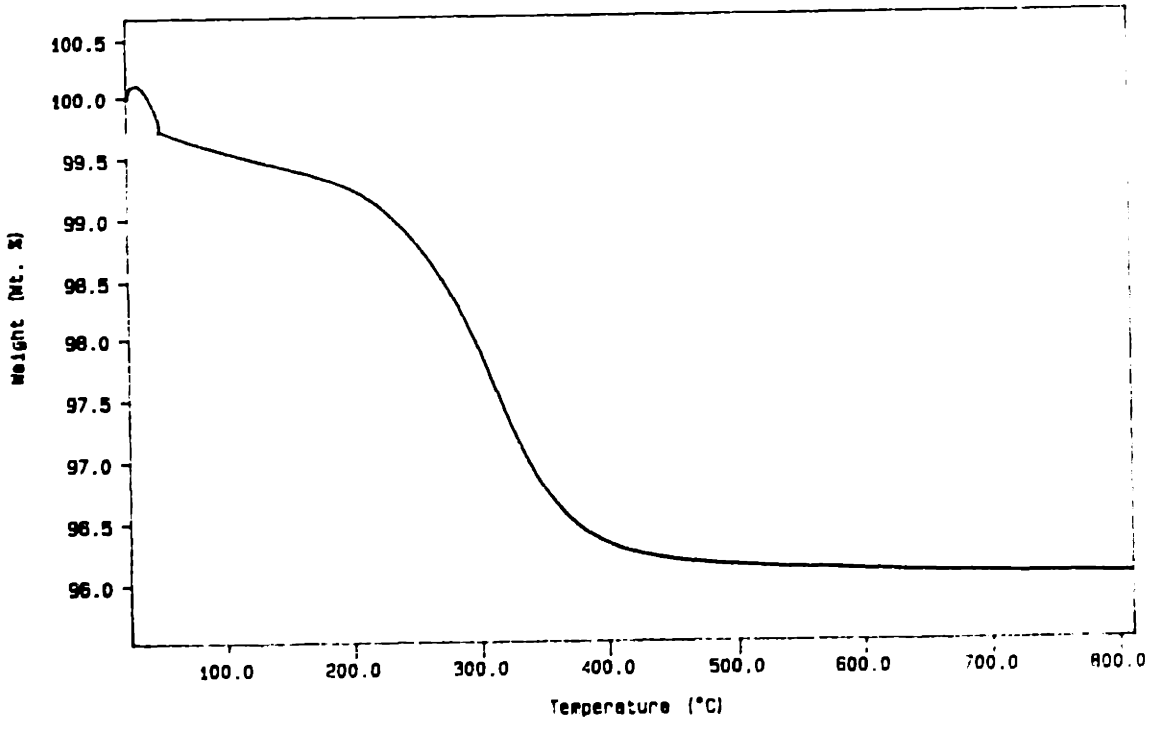

Figure 7.16: TGA of parts made by printing 10 wt% PAA solution on aqueous powder bed after being washed for 20 hours and dried.

concentration of polymer binder solutions were selected to avoid segregation of the printed binder within the powder layer. The individual printed layers were dried to avoid the anisotropy created due to interlayer liquid migration. The printed part does not show any interlayer defects. Therefore, the spray deposition process eliminates the anisotropy due to inter-laminar defects along the z-axis. Thus, a highly isotropic and uniform packing density parts can be made with the 3DP spray deposition process.

The high cohesive strength of the powder bed, however, made the conventional method of removing powder, such as brushing, ineffective to retrieve the printed part from the sprayed powder bed. A chemical method has been developed to disperse the alumina powder bed and leave the printed part intact. The use of electrostatically stabilized alumina slurries for powder bed allowed for an easy redispersion in water during the cleaning process. The printed binder was chosen so as to chemically bond with the surface of the particles and provide a strong printed part insoluble in water. Alumina was successfully chemically bonded with a polyacrylic acid (PAA) binder. The result of this research work has been successfully used to fabricate 56% dense structural ceramic parts directly by 3DP, which achieved almost full density upon firing.

Bibliography

1. G. Geiger, "Powder Synthesis and Shape Forming of Advanced Ceramic," Am. Cer. Soc. Bull., vol. 74, 8, 62-65, August 1995.

2. W. D. Kingery, "Ceramic Fabrication Processes," M. I. T. press, 1963.

3. I. J. McColm and N. J . Clark, "Forming, Shaping and Working of High Performance Ceramics," Chapman and Hall, NY, 1988.

4. V. Pujari, "Robust Forming Needs for the Commercialization of Advanced Ceramics," 97the Annual ACERS meeting, Cincinnati, 1995.

5. T. Wohlers, 'Make Fiction Fact fast," Manufacturing Engg., 44-49, March 1991.

6. E. Sprow, " Rapid prototyping: Beyond the Wet Look," Manufacturing Engg., 58-64, November 1992.

7. S. Ashley, " Prototyping with Advanced Tools," Mechanical Engg., 48-55, June 1994.

8. H. L. Marcus and D. Bourell, "Solid Free Fabrication Finds New Applications,' Advanced Materials and Process, 28-35, 9, 1993.

9. E. Sachs, M. Cima, J. Cornie et al, "Three Dimensional Printing: Rapid Tooling and Prototypes Directly from CAD Representation," Solid Freeform Fabrication Symposium Proceedings, Univ. of Texas, 27-47, 1990.

10. E. Sachs, M. Cima, P. Williams and D. Brancazio, "Rapid Tooling and Prototyping by Three Dimensional Printing," Trans.NAMRI/SME, 41-45, 1990.

11. M. J. Cima, Internal communications.

12. F. F. Lange, "Processing Related Fracture Origins: II, Agglomerate Motion and Cracklike Internal Surfaces Caused by Differential Sintering," J. Am. Cer. Soc., 66(6), 398-406, 1983.

13. J. W. Holloran, "Role of Powder Agglomerates in Ceramics Processing," In "Forming of ceramics", Advances in ceramics , volume 9, Ed J. Mangels and G. Messing, Am. Cer. Soc., 67-75, 1984.

14. H. Rumpf and H. Schubert, "Adhesion Forces in Agglomeration Forces," in "Ceramics Processing Before Firing," edited by G. Onada and L. Hench, John Wiley & Sons, 357-376, 1978.

15. J. S. Reed, " Introduction to the Principles of Ceramic Processing," John Wiley and Sons, NY 1989.

16. O. J. Whitmore, "Particle Compaction," in "Ceramics Processing Before Firing," edited by G. Onada and L. Hench, John Wiley & Sons, 343-357, 1978.

17. J. S. Reed and R. B. Runk, " Dry Pressing,", in Treatise on Materials Science and engineering, vol. 9: Ceramic fabrication Processes, Academic Press, NY, 71-93, 1976.

18. J. S. Reed, "Critical Issues and Future Direction in Powder Forming Processes," Ceramic Powder Science, II B, edited G. Messing, E. Fuler and H. Hausner, Am. Cer Soc., 1987.

19. A. Hendry, "Processing of Engineering Ceramics," Powder Metallurgy, 20-22,.

20. B. J. McEntire, "Tooling design for Wet Isostatic Pressing," In "Forming of ceramics", Advances in ceramics , volume 9, Ed J. Mangels and G. Messing, Am. Cer. Soc., 16-31, 1984.

21. J. E. Funk, "Slip Casting and Casters," In "Forming of Ceramics", Advances in ceramics , volume 9, Ed J. Mangels and G. Messing, Am. Cer. Soc., 76-85, 1984.

22. T. J. Fennelly and J. S. Reed, "Mechanics of Pressure Slip Casting," J. Am. Cer. Soc., 55 (5), 264-68,1972.

23. F. Lange and K. Miller, "Pressure Filtration: Consolidation Kinetics and Mechanics," Am. Cer. Soc. Bull., 66 (10), 1498-1504, 1987.

24. D. S. Adcock and I. C. Mcdowall, "The Mechanism of Filter Pressing and Slip Casting," J. Am. Cer. Soc., 40 (10), 355-362, 1957.

25. M. J. Edrisinghe and J.R.G. Evans, "Review: Fabrication of Engineering Ceramics by Injection Molding. I. Materials Selection," Int. J. High technology Ceramics, 2, 1-31, 1986.

26. M. J. Edrisinghe and J.R.G. Evans, "Review: Fabrication of Engineering Ceramics by Injection Molding. II. Techniques," Int. J. High technology Ceramics, 2, 249-278, 1986.

27. T. J. Whalen and C.F. Johnson, "Injection Molding of Ceramics," Am. Cer. Soc Bull., 60(2), 216-220, 1981.

28. M. A. Strivens, "Injection Molding of Ceramic Insulating Materials,' Am. Cer. Soc Bull., 42 (1), 13-19, 1963.

29. J. A. Mangels and W. Trela,"Ceramic Components by Injection Molding," In "Forming of ceramics", Advances in ceramics , volume 9, Ed J. Mangels and G. Messing, Am. Cer. Soc., 220-233, 1984.

30. V. V. Stanciu, "Tooling for Ceramic Injection Molding," In "Forming of ceramics", Advances in ceramics , volume 9, Ed J. Mangels and G. Messing, Am. Cer. Soc., 239-240, 1984.

31. A. Johnson, E. Carlstrom, L. Hermansson and R. Carlsson, "Rate controlled Thermal Extraction of Organic Binders from Injection Molded Bodies," In "Forming of ceramics", Advances in ceramics , volume 9, Ed J. Mangels and G. Messing, Am. Cer. Soc., 241-245, 1984.

32. J. A. Lewis, "Binder Distribution Processes in Ceramic Green Tapes During Thermolysis," Ph.D. Dissertation, M.I.T., Materials Science and Engineering, 1991.

33. P. F. Jacobs,"Fundamentals of Stereolithography," SME, 1992.

34. M. Griffith, "Stereolithography of Ceramics," Ph.D. Dissertation, University of Michigan, Materials Science and Engineering, 1995.

35. U. Lakshminarayan, S. Ogrydiziak and H. l. Marcus, "Selective Laser Sintering of Ceramic Materials," Solid Freeform Fabrication Symposium Proceedings, Univ. of Texas, 16-26, 1990.

36. D. L. Bourell, H. L. Marcus, J. W Barlow and J.J. Beaman, "Selective Laser Sintering of metals and Ceramics," Int. J. Powder Met., vol28, no.4, 369-381, 1992.

37. M. Cima, A. Lauder, S. Khanuja and E. Sachs, "Microstructural Elements of Components Derived from 3D Printing," Solid Freeform Fabrication Symposium Proceedings, Univ. of Texas, 1992.

38. M. Cima and E. Sachs, "Three Dimensional Printing: Form , Materials, and Performance," Solid Freeform Fabrication Symposium Proceedings, Univ. of Texas, 187-194, 1991.

39. A. Lauder, M. Cima, E. Sachs and T. Fan, "Three Dimensional Printing: Surface Finish and Microstructure of Rapid Prototyping Components," in Proceedings, "Synthesis and Processing of Ceramics," MRS, 331-336, 1991.

40. M. J. Cima, E. Sachs, L. G. Cima, J. Yoo, S. Khanuja, S. W. Borland, B. Wu and R. Giordano, "Computer-Derived Microstructures by 3D Printing: Bio and structural Materials," in Proceedings of the SFF symposium, Univ of Texas, 1994.

41. D. Nammour, " Fabrication of Glass-Ceramic Components via 3DP," M.S. Thesis, M. I. T., Materials Science and Engineering, 1995.

42. J. Yoo, M.J. Cima, S. Khanuja, and E. Sachs, "Structural Ceramic Components by 3D Printing," in proceedings of the SFF, 40-50, 1993.

43. S. Michaels, E. M. Sachs, M. J. Cima, "Metal Parts Generation by Three Dimensional Printing," proceedings of SFF symposium, edited by J. J. Beamen, H. Marcus, D. L. Bourell, J. W. Barlow, and T. Crawford, University of Texas, 187-94,1992.

44. M. Feygin, "LOM goes into Production," Second International Conference on Rapid Prototyping, p 351-357, 1991.

45. M. Feygin, "Apparatus and Method for Forming an Integral Object from Laminations," U. S. patent no. 4,752, 352, 1988.

46. C. Griffin, J. Daufenbach and S. Mcmillan, "Desktop Manufacturing: LOM vs Pressing," Am. Cer. Soc. Bull., vol 73, 8, 109-113, 1994.

47. K. E. Richardson, "Production of Wax Models by the Ballistic Particle manufacturing Process," Second International Conference on Rapid Prototyping, 15-22, 1991.

48. S. S. Crump, "Fused Deposition Modeling: Putting Rapid back in Prototyping," Second International Conference on Rapid Prototyping, 358-361, 1991.

49. M. Hasatani and Y. Itaya, "Effect of Drying on Quality Control in Ceramic Production," in "Drying," edited by A. S. Majumdar, Elsevier, 1181-1198, 1992.

50. R. Chiu, "Drying of Granular Ceramic Films," Ph.D. Thesis, Materials Science and Engineering, MIT, 1991.

51. G. W. Scherer, "Theory of Drying," J. Am. Cer. Soc., 73 (10), 3-14, 1990.

52. C. J. Brinker and G. W. Scherer, "Sol Gel Science: The Physics and Chemsitry of Sol-Gel Processing," Academic press, NY, 1990.

53. A. R. Cooper, "Quantitative Theory of Cracking and Warping during the Drying of Clay Bodies," in "Ceramics Processing Before Firing," edited by G. Onada and L. Hench, John Wiley & Sons, 261-276, 1978.

54. F. H. Norton, "The Flow of Ceramic Bodies at Elevated Temperatures," J. Am. Cer. Soc., 15, 126, 1936.

55. C. Herring, "Effect of Change of Scale on Sintering Phenomenon," J. Appl Phys., 21 (4), 301-303, 1950.

56. D. Richerson, "Modern Ceramic Engineering," Marcel dekker Inc., NY, 1982.

57. W. D. Kingery, " Introduction to Ceramics," 2nd edition, John Wiley and Sons, NY, 1976.

58. S. J. Bennison and M. P. Harmer, "Effect of MgO Solute on the Kinetics of Grain Growth in Alumina," J. Am. Cer. Soc., 66 (5), C90-C92, 1983.

59. J. E. Burke, "Role of Grain Boundaries in Sintering," J. Am. Cer. Soc., 40 (3), 80-85, 1957.

60. J. S. Reed, T. Carbone, and C. Scott, "Some Effects of Aggregates and Agglomerates in the Fabrication of Fine Grained Ceramics," in 'Processing of crystalline ceramics,' ed. by H. Palmour, R. F. Davis, and T. M. Hare, Plenum press, NY, 171-180, 1977.

61. C. Greskowich, "Effect of Green Density on the Initial Sintering of Alumina," Phys. sintering, 4, 33-46, 1972.

62. C. A. Bruch, "Sintering Kinetics for the High Density Alumina Process," Am. Cer. Soc. Bull., 41, 12, 799-806, 1962.

63. A. Roosen and H.K. Bowen,"Influence of Various Consolidation Techniques on the Green Microstructure and Sintering Behavior of Alumina Powders,"J. Am. Cer. soc., 71 (1), 970-977, 1988.

64. 12. T. Yeh and M. D. Sacks,"Effect of Particle Size Distribution on the Sintering of Alumina," J. Am. Cer. Soc. 71(12), C 484-487, 1988.

65. J. Zhao and M.P Harmer, "Effect of Pore Distribution on Microstructure Devlopment: III Model Experiments" J. Am. Cer. Soc., 75 (4), 830-43, 1992.

66. G. Y. Onada, Jr., "Green body Characteristics and their Relationship to Finished Microstructure, " in Ceramic Microstructures-'76, edited by R. M. Fulrath and J. Pask, Westview Press, Colorado, 163-181, 1976.

67. J. Cesarano, I. A. Aksay and A. Bleier, "Stability of Aqueous Alumina Suspension with Poly(methacrylic) Acid Polyelectrolyte, " J. Am. Cer. Soc., 71 (4), 1988, 250-255.

68. D. H. Napper, "Polymeric Stabilization of Colloidal Dispersion," Academic Press, NY, 1983.

69. Th. F. Tadros, "The Effect of Polymers on Dispersion Properties," Academic Press, NY, 1982.

70. B. Giritlioglu, "The effect of print style on mechanical and microstructural properties of structural ceramic parts via three dimensional printing," M.S. thesis, Materials science and engg, MIT, 1995.

71. W. Bang, internal communications.

72. S. J. Lukasiewicz, "Spray Drying Ceramic Powders,' J. Am. Cer. Soc, 72 (4), 617-24, 1989.

73. K. Masters, "Spray Drying Handbook," 4th edition, John Wiley and Sons, NY, 1985.

74. A. Lauder, "Microstructure and Particle Arrangement In Three Dimensional Printing," M.S. thesis, Materials science and engineering, 1992.

75. F. W. Billmeyer, "Textbook of Polymer Science," 3rd edition, John Wiley and Sons, NY, 1984.

76. P. Molyneux, "Water soluble Synthetic Polymers: Properties and Behavior," CRC press, 1983.

77. E. A. Boucher, "Reaction Kinetics of Polymer Substituents: Neighboring-Substituents Effects in Pairing Reactions," J. Chem. Soc. Faraday Trans 1, 68, 2281, 1972.

78. K. Konstadinidis, B. Thakkar, A. Chakraborty, L.W. potts, R. Tannenbaum amd M. Tirrell, "Segment Level Chemsitry and Chain Conformation in the Reactive Adsorption of Poly(methyl methacrylate) on Aluminum Oxide Surfaces," Langmuir, 8, 1307-1317, 1992.

79. R. J. Higgins, "The Chemsitry of Carbon Retention during Non-oxidative Binder Removal from Ceramic Green Ware, " Sc.D. dissertation, Materials Science and Engineering, 1989.

80. J. R. Dyer, "Applications of Absorption Spectroscopy of Organic Compounds," Prentice-Hall, NJ, 1965.

81. R. Higgins, W. Rhine, M. J. Cima, H. K. Bowen and W. Farneth, "Ceramic Surface Reactions and Carbon Retention during Non-oxidative Binder Removal: Alumina/poly(methyl methacrylate) at 20 -700 C," J. Am. Cer Soc, 77 (9) 2243-53, 1994.

82. D. W. Whitman, D. I. Cumbers and X. K. Wu, "Humidity Senstivity of Dry-Press Binders," Am. Cer. Soc Bull., 74 (8), 76-79, 1995.

83. F. V. Shaw, "Spray drying: A Traditional Process for Advanced Applications," Am. Cer. bull., 69 (9), 1990.

84. T. Fan, internal communications.

85. J. Bredt, "Binder Stability and Powder-Binder Interaction in Three Dimensional Printing," Ph. D. dissertation, M.I.T., Mechanical engineering, 1995.

86. J. Charnnarong, internal communications.

87. Y. Tang,"Removal of Organic Binder form Multilayer Ceramic Structures," Ph.D. dissertation, Materials Science and Engineering 1994.

88. A. Higdon , "Mechanics of Materials," John Wiley & Sons, Inc. NY, 1976.

89. S. Timoshenko, "Mechanics of Materials,"

90. K. Kendall, "Agglomerate Strength," Powder metallurgy, 31 (1), 28-31, 1988.

91. Richard Yu, "Development of Co-Dispersion Binder for the Three Dimensional Printing Process to Facilitate Handling of Ceramic Casting Shells in the Green Strength," M.S. thesis, Mechanical engineering, 1994.

92. A. E. Scheidegger, "The Physics of Flow through Porous Media," 3d ed., University of Toronto press, Toronto, Canada, 1974.

93. F. A. L. Dullien, "Porous Media-Fluid Transport and Pore Structure," Academic press, NY 1979.

94. J. A. Lewis and M. J. Cima, "Mass Transfer Processes during Multicomponent Binder Thermolysis," Mat. Res. Soc. Symp., vol. 249, 363-370, 1992.

95. M. J. Cima, J. A. Lewis and A. Devoe, "Binder Distribution in Ceramic Greenwrae during Binder Thermolysis," J. Am. Cer. Soc. 72 (7) 1192-99, 1989.

96. V. H. Scott and A. T. Corey, "Pressure Distribution during Steady Flow in Unsaturated Sands, " Soil Sci. Proc., 270-74, 1961.

97. J. Bear, "Dynamics of Fluid in Porous Media," Dover edition, 1988.

98. G. Y. Onada, "Theoritical Strength of Dried Green Bodies with Organic Binder," J. Am.Cer. Soc., 236-239, 59 (5).

99. Acrysol WS-24, Rohm and Haas Co., PA.

100. S. G. Croll, "The Origin of Residual Internal Stress in Sovent-Cast Thermoplastic Coatings," J. Appl. Polym. Sci., vol. 23, 847-858, 1979.

101. G. H. Geiger and D. R. Poirier, " Transport Phenomenon in Metallurgy," Addison Wesley, 1973.

102. Carrageenan Products, FMC Corporation, Food Ingredients division, PA.

103. S. Michaels, "Production of Metals Parts Using the Three Dimensional Printing Process," M.S. thesis, Mech E., MIT, 1993.

104. J. W. Goodwin, "Rheology of Ceramic Materials, " Am. Cer. Soc. Bull., 69 (10), 1694-98, 1990.

105. M. E. Woods and I. M. Krieger, "Rheological Studies on Dispersions of Uniform Colloidal Spheres," J. Colloid Interface Sci., 34 (1), 91-99, 1970.

106. M. Galla, "Process Development for Three Dimensional Printing of Metal Slurries," M.S. thesis, Materials Science and engineering, 1994.

107. P. Hiemenz, "Principles of Colloid and Surface chemistry,' Dekker, 431,1977.

108. P. Nahass, R. Pober and H.K. Bowen, "Semi-continuous Classification of Ceramic Powders," CPRL Report no. 76, 1987.

109. Bird Precision, Waltham, MA.

110. W. H. Pimbley and H.C. Lee, "Satellite Droplet Formation in a Liquid Jet," IBM Journal of research and development, vol. 21, no.1 , jan 1977, 21-31.

111. R. Rajgopalan and C. Tien, "Production of Mono-Dispersed Drops by Forced Vibration of a Liquid Jet," The Canadian Jornal of Chem. ENgg. vol. 51, june 1973, 272-79.

112. H.E. Cline and T.R. Anthony,"The Effect of Harmonics on the Capillary Instability of Liquid Jets," J. Appl. Phys. 49 (6), 1978, 3203-3208.

113. S. A. Curry, H. portig, "Scale model of an Ink-Jet," IBM J. Res. Div. 21 (1), 10-20, 1977.

114. R. A. Thompson, "Mechanics of Powder Pressing: 1, Model for Powder Densification," Am. Cer. Bull., 60 (2), 237-243, 1981.

115. R. Dimilia and J. S. Reed, "Stress Transmission during the Compaction of a Spray Dried Powder in a Steel Die," J. Am. Cer. Soc., 66 (9), 667-672, 1983.

116. H. Tureck, "Design of a Powder Cylinder with Floating Piston for Three Dimensional Printing," M.S. Thesis, Mechanical engineering, 1992.

117. S. J. Lukasiewicz and J. S. Reed, "Character and Compaction Response of Spray-Dried Agglomerates," Am. Cer. Bull., 57(9), 798-805, 1978.

118. R. Dimilia and J. S. Reed, "Dependence of Compaction on the Glass Transition of the Binder Phase," Am. Cer. Bull., 62(4), 484-488, 1983.

119. C. W. Nies and G. L. Messing, "Effect of Glass-Transition Temperature of Polyethylene Glycol-Plasticized Polyvinyl Alcohol on Granule Compaction," J. Am. cer. Soc., 67(4), 301-304, 1984.

120. R. Dimilia and J. S. Reed, "Effect of Humidity on the Pressing Characteristics of Spray-dried Alumina," Advances in ceramics vol 9, forming of ceramics, 38-46, 1984.

121. C. W.Nies and G. L. Messing, "Binder Hardness and plasticity in granule compaction," Advances in ceramics vol 9, forming of ceramics, 58-66, 1984.

122. W. J. Walker, J. S.Reed and S. K. Verma, "Polyethylene Glycol Binders for Ceramics Produced by Compaction of Spray-dried Granules, " Carbowax company literature.

123. S. Michaels, internal communications.

124. R. C. Chiu, T. J. Garino and M. J. Cima, "Drying of Granular Ceramic Films: I, Effect of Processing Variables on Cracking Behavior," J. Am. Cer. Soc. 76 (9), 2257-64, 1993.

125. M. S. Hu, M. D. Thouless, A. G. Evans, "Decohesion of Thin films from Brittle Substrates," Acta Metall., 36 (5), 1301-1307, 1988.

126. C. A. Finch, " Poly Vinyl Alcohol-developments," John Wiley & Sons, NY 1992.

127. R. L. Pober, E. A. Barringer, M. V. Parish, "Dispersion and Packing of Narrow Size Distribution Ceramic Powders," CPRL # 20, 1982.

128. J. Grau, internal communications.

129. F. F. Lange, "Approach to Reliable Powder Processing," Ceramic powder science II B, edited by G. Messing, E. Fuller, H. Hausner, Am. Cer. Soc.,1069-1083, 1987.

130. I. A. Aksay, "Microstructure Control through Colloidal Consolidation," in the Proceedings of the advances in ceramics Symposium, Am. Cer. Soc., 9, 94-104, 1984.

131. A. Roosen, S. Sumita, and H. K. Bowen, "Powders, Interfaces, and Processing: Alumina as a case study," Materials Sci. Research, vol. 21, Role of Interfaces, edited by J. Pask and A. G. Evans, Plenum Press, NY, 1987.

132. B. V. Velamakanni, J. C. Chang, F. F. Lange, and D. S. pearson, "New method for Efficient Colloidal Particle Packing via Modulation of Repulsive Lubricating Hydration Forces, " Langmuir, 6(7), 1323-25, 1990.

133. I. Skeist, "Handbook of Adhesives," 3rd edition, Van Nostrand Reinhold, NY, 1990.

134. A. Reiser, "Photoreactive polymers: The science and technology of resists," John Wiley & Sons, NY, 1989.

135. N. Allen, " Photopolymerisation and Photoimaging Science and Technology," Elesevier Applied Science, NY, 1989.

136. C. E. Hoyle, " Radiation Curing of Polymeric Materials," Am. Chem. Society, 1989.

137. M. W. Ranney, "Specialized Curing Methods for Coatings and Plastics," Noyes data corp., NJ, 1977.

138.. B. M. Wu, S. W. Borland, R. A. Giordano, L. G. Cima, E. M. Sachs and M. J. Cima, "Solid Freeform Fabrication of Drug Delivery Devices," Accepted for publication in the J. of Controlled Release.

139. O. Fuchs, "Solvents and Non-solvents for polymers," in Polymer Handbook, ed. by J. Bhandrup and E. H. Immergut, John Wiley and Sons, 1989.

140. P. M. Heertjes and W. C. Witvoet, "Some Aspects of the Wetting of Powders,' Powder Technology, 3, 339-343, 1970.

141. G. D. Parfitt, "Dispersion of Powders in Liquids," 2nd edition, John Wiley and Sons, NY, 1973.